Exact Steering in Control Moment Gyroscope Systems

Sajjad Asghar

Submitted for the Degree of

Doctor of Philosophy

from the

University of Surrey

Department of Mathematics

and

Surrey Space Centre,

Faculty of Engineering and Physical Sciences

University of Surrey

Guildford, Surrey GU2 7XH, U.K.

October 15, 2008

Abstract

Single Gimbal Control Moment Gyroscopes (CMGs) are thought to be efficient actuators for the attitude control of the new generation of small and agile satellites. CMGs belong to a class of actuators known as momentum exchange devices. This thesis presents a detailed formulation of three-axis attitude dynamics and control of a satellite equipped with a cluster of n momentum exchange devices (which include CMGs and reaction wheels). The exact steering problem is formulated for a simple twin CMG system employed for single axis control. An analytical approach is developed which enables us to find values of feedback gains such that exact steering can use the full momentum capacity of the CMG system while just avoiding singularity. Incorporation of an explicit gimbal rate constraint in the proposed analytic approach of the exact steering problem is shown to yield near time-optimal control. A variable feedback gains approach for twin CMGs' exact steering is also developed. The exact steering problem is also formulated for the four CMG pyramid system employed for three-axis control of satellites. The satellite-CMG model is reduced to a nonlinear damped pendulum model for an eigenaxis rest-rest manoeuvre. This simplified model is then used to find the values of the feedback gains which correspond to using the full momentum capability of the CMG cluster. We propose an exact steering law based on using generalised-inverses (not the Moore-Penrose inverse) of a Jacobian matrix. This can avoid elliptic singularities and thus is able to use almost the full momentum capacity of the CMG cluster. The proposed steering logic brings the gimbal angles back to the initial zero state. We also propose a new singularity escaping steering law by selectively introducing robustness to the generalised-inverse based steering law in singular direction only. This steering law escapes elliptic singularities with high pointing accuracy and it is shown to outperform the Generalised Singularity Robust Steering Law both in speed of singularity escape and pointing accuracy. Finally, we propose and develop a generic form of inverse free steering law, which is derived using the Liapunov method. Special case of this proposed steering law can escape elliptic singularities. But it is not able to bring gimbal angles back to the initial zero state after completion of the manoeuvre. It also produces small tumbling motions during reorientation manoeuvres.

TO MY PARENTS, ALI ASGHAR KHAN AND ZUBAIDA KHATOON
FOR THEIR LOVE, AFFECTION AND PRAYERS
AND
TO MY WIFE SAADIA AND CHILDREN HASSAN AND RASHAEL
FOR THEIR LOVE AND PATIENCE

Acknowledgements

I would like to express my deep gratitude to my Supervisors: Professor Mark Roberts and Dr. Phil Palmer for guiding and encouraging me during this research work. Their full support and patience throughout the period of study have helped me a lot in bringing my work to completion. I would like to thank Dr. Vaios J. Lappas for his support and encouragement. Many thanks are due to Professor Sir Martin Sweetings for his encouragement after each monthly report. Next, I would like to express my gratitude to my sponsor: Ministry of Science and Technology, Government of Pakistan for funding my PhD studies abroad.

Many thanks are due to my friends especially Dr. Himat Mir for providing me a good company during my stay in Guildford. Finally, the love and support of my family is certainly a great source of encouragement and I would like to thank my family: my parents; my wife and children; and my brothers Waqar and Mudassar; and also my sisters Saira and Ayesha.

Contents

List of Figures

List of Tables

Nomenclature

$\mathcal{F}_B = \{\hat{\boldsymbol{b}}_x, \hat{\boldsymbol{b}}_y, \hat{\boldsymbol{b}}_z\}$	Frame fixed to satellite's body
$\mathcal{F}_A = \{\hat{\boldsymbol{a}}_x, \hat{\boldsymbol{a}}_y, \hat{\boldsymbol{a}}_z\}$	Reference frame for attitude motion
$\mathcal{F}_{A'}, \mathcal{F}_{A''}$	Intermediate frames of Euler angle rotations
$[\theta_x, \theta_y, \theta_z]$	Euler angles, roll, pitch and yaw respectively
$[q_0, q_1, q_2, q_3]$	Quaternion
$[q_{0f}, q_{1f}, q_{2f}, q_{3f}]$	Reference quaternion
$[q_{0e}, q_{1e}, q_{2e}, q_{3e}]$	Error quaternion
$\boldsymbol{e} = [e_x, e_y, e_z]$	Euler axis of rotation
θ	Rotation angle of satellite about Euler axis $\boldsymbol{e}$
$\boldsymbol{C}_x, \boldsymbol{C}_y, \boldsymbol{C}_z$	Matrices representing the rotation about x, y and z-axes respectively
$\boldsymbol{C}$	Transformation matrix from reference frame to body frame
$\{\hat{\mathbf{i}}, \hat{\mathbf{j}}, \hat{\mathbf{k}}\}$	Standard unit vectors of x, y and z-axes respectively
ω	Angular velocity of satellite expressed in its body frame
ω_f	Reference angular velocity
$\boldsymbol{\Omega}$	Kinematic matrix relating angular velocity to Euler angle rates
n_o	Mean orbital motion
n	Number of Momentum Exchange Devices in the array
$\mathcal{F}_{Gi} = \{\hat{\boldsymbol{g}}_{xi}, \hat{\boldsymbol{g}}_{yi}, \hat{\boldsymbol{g}}_{zi}\}$	Frame associated to ith Momentum Exchange Device
$\boldsymbol{C}_i$	Transformation matrix from body frame to ith device frame
β_i	Array configuration angle for ith device
δ_i	Gimbal angle for ith device
Ω_i	Spin rate of the wheel of ith device
$\boldsymbol{J}_i$	Inertia matrix of ith device expressed in its own frame
$\boldsymbol{I}_s$	Inertia matrix of satellite without rotating devices
$\boldsymbol{I}$	Total inertia matrix of satellite
$\boldsymbol{h}_i$	Angular momentum of ith device expressed in body frame
$\boldsymbol{h}$	Total angular momentum of the array expressed in body frame
$\boldsymbol{H}$	Total angular momentum of satellite equipped with array of momentum exchange devices expressed is body frame

$\boldsymbol{D}_o$	Matrix mapping the spinning rate of wheels to angular momentum vector
$\boldsymbol{B} = [\boldsymbol{b}_1 \boldsymbol{b}_2 \cdots \boldsymbol{b}_n]$	Matrix mapping the gimbal rates to gimbal angular momentum
$\boldsymbol{D}_1$	Matrix mapping the gimbal rates to torque vector or Jacobian matrix
$\boldsymbol{D}_2$	Matrix mapping the gimbal rates to torque due to directional change of gimbal angular momentum caused by angular motion of vehicle
$\boldsymbol{D}_3$	Matrix mapping the gimbal rates to torque due to variation in total inertia of the rotating vehicle
$\boldsymbol{D}_4$	Matrix mapping the gimbal rates to torque due to devices' product of inertia
$\boldsymbol{D}_5$	Matrix mapping the gimbal rates to torque due to variation in total inertia of vehicle with reference motion
$\boldsymbol{T}_{ext}$	External torque
$\boldsymbol{K}_1, \boldsymbol{K}_2$	Feedback gain matrices
k_1, k_2	Feedback gains
$_\omega$	Feedback gains
	Commanded torque
V	Liapunov function
$\boldsymbol{G}$	Inverse matrix of Jacobian matrix
$\boldsymbol{s}$	Singular direction
$\boldsymbol{h}_i^s$	Singular angular momentum of ith CMG in array
σ_i	Sign of singular angular momentum of ith CMG in array
$\mathbf{1}$	Identity matrix
$\boldsymbol{W}$	Weight matrix used in steering laws
$\boldsymbol{W}_1, \boldsymbol{W}_2$	Weight matrices used in Generalised Variable Speed Singularity Robust (GVSSR) Steering law
$\boldsymbol{\Lambda}$	Matrix used in GVSSR Steering law
$\boldsymbol{W}_\Omega^0, \boldsymbol{W}_\delta$	Weight matrices used in Variable Speed Steering law
$\boldsymbol{\Gamma}$	Vector containing spin rates and gimbal angles of devices
λ	Weighting factor used in steering laws
τ_{er}	Error torque
h_{cmg}	Angular momentum of a CMG unit
ω_m	Maximum slew rate
α	Gimbal rate saturation limit

ω_n	Desired natural frequency of closed-loop system
ζ	Desired damping ratio of closed-loop system
ϕ	Phase angle of closed-loop system
τ_o	Output torque
T_1	Switching time of controller
M	Amplitude of slew angle
N	Damped harmonic frequency
L	Time lead or lag
Φ_1, Φ_2	Phase angles
t_f	Manoeuvre time
m, n	Real numbers in variable gain steering law
δ_s	Switching value of gimbal angle in variable gain steering law
η	Angular variable to represent norm of momentum in certain direction
h_e^{max}	Maximum value of angular momentum in direction $\boldsymbol{e}$
ω_e^{max}	Maximum slew rate capability in direction $\boldsymbol{e}$
ω_{nL}	Natural frequency for linear closed-loop system
θ_L	Solution of damped harmonic oscillator equation
$\boldsymbol{F}$	Vector function
$\boldsymbol{A}$	Matrix used in Generalised Inverse Steering Law
η^s	Singularity of matrix $\boldsymbol{A}$
m	Singularity index
λ_s	Singularity escaping parameter (SEP)
κ_s	Maximum value of SEP
σ_s	Spread of SEP
λ	Singularity avoiding parameter (SAP)
κ	Maximum value of SAP
σ	Spread of SAP
$\boldsymbol{E}$	Matrix used in Singularity Escaping Steering law and also used in Generalised Singularity Robust (GSR)
$\boldsymbol{M}$	A positive definite matrix

Chapter 1

Introduction

1.1 Background

The common devices used in spacecraft attitude control systems as actuators (or torque producing devices) can be divided into two distinct groups:

1. Inertial control devices;

2. Non-inertial control devices or momentum exchange devices.

The inertial control devices change the overall angular momentum of the satellite. This group includes magnetic attitude control, reaction jets or thrusters and solar radiation based attitude control. The magnetic attitude control uses magnetic-dipole to provide a continuous and smooth control. However, the level of torque is generally very low $(1 - 10\mathrm{mNm})$ and insufficient to produce fast attitude manoeuvres. Also, it generates a control torque perpendicular to the local geomagnetic field vector which varies with altitude and inclination of the orbit. Due to this limitation, it is not suitable for three-axis control and is mainly used in momentum de-saturation.

Reaction jets/thrusters provide torques of constant amplitude and modulated time duration. Their output is neither smooth nor linear. They can also excite structural vibrations. Thrusters are mainly used for fast/course attitude control.

Torque obtained from solar pressure is not sufficient for using it in attitude manoeuvring since the level of torques that can be produced are of the order of $10 - 20\mu\mathrm{Nm}$.

Solar torques are sometimes used in geostationary satellite to counteract the parasitic solar disturbances acting on the spacecraft and provide active nutation damping to momentum bias-controlled satellites. Solar control is feasible for satellite in which solar panel can be rotated with respect to spacecraft body, as in the case of geostationary satellites.

Contrary to these actuators, momentum exchange devices transfer angular momentum to satellites without changing the angular momentum of overall system. The examples of this class of the actuators are reaction and momentum wheels, single and double gimbal Control Moment Gyros (CMGs) and variable speed CMGs. All these devices contain a rotating flywheels. Reaction wheels are the simplest and least expensive momentum exchange actuators. Typically a reaction wheel system consists of a spin rotor, whose axis is fixed to spacecraft. To generate a torque about spin axis, the speed of the wheel is either increased or decreased, which is nominally held at zero. Reaction wheels provide continuous and smooth control with the lowest possible parasitic torques. The level of torque of reaction wheel is the order of $0.05 - 2\mathrm{Nm}$. Due to small torque capability of reaction wheels, they are not suitable for fast attitude maneuvers. Moreover, varying wheel speed can excite structural vibrations.

Single Gimbal Control Moment Gyros (SGCMGs) are torque efficient actuators. They have been used in attitude control systems of spacecrafts and satellites. A SGCMG contains a spinning wheel with large angular momentum. The wheel is gimballed about an axis known as the gimbal axis. And this axis is perpendicular to the spin axis of the wheel and fixed with respect to spacecraft body. Directional change in angular momentum of the wheel produces a control torque orthogonal to both rotor spin and gimbal axes. Single gimbal CMG can achieve torque level of $200\mathrm{Nm}$ due to torque amplification property. Due to this property of single gimbal CMGs, they can provide greater agility than reaction or momentum wheels. As a result CMGs are thought to be ideal actuators for missions with rapid slew rates and high pointing accuracy requirements. The main disadvantage of single gimbal CMG clusters is the existence of associated singular gimbal states or non-torque producing gimbal states referred to as singularities. CMGs are also used in momentum management of large spacecrafts. The single gimbal CMGs were used in spacecrafts like High Energy Astronomical Observa-

tory (HEAO) and the Large Space Telescope (LST). Similarly, in large spacecrafts like Skylab and MIR space station, CMGs were used for attitude control and momentum management. Now miniature CMGs are replacing reactions wheels in new generation of low altitude Earth-imaging small satellites with significantly high agility and pointing accuracy requirements.

The Double Gimbal CMG (DGCMG) consists of a rotor suspended inside two gimbals able to be oriented on sphere along any direction. Double gimbal CMGs are mechanically complex and do not have torque amplification property. However, gimbal steering problem is simpler for DGCMG. The double gimbal CMG are now being used in space shuttle and International Space Station.

A variable speed CMG is the single gimbal CMG where variation in wheel speed is allowed to improve the singularity avoidance property of the CMG cluster and to achieve the power control. In power management case, CMG wheels are spun up to store the energy and are then spun down to release the stored energy as per requirement. The use of variable speed CMG clusters has been studied for both attitude control case and for simultaneous control of attitude and power case. This simutaneous control case is also known as Combined Energy and Attitude Control (CEAC).

Here we shall focus our study on SGCMG systems and it will be referred as CMG in rest of the discussion. The attitude control system using a CMG cluster requires a gimbal steering law to generate gimbal angle trajectories corresponding to the commanded torque. We know that singular states of a cluster of CMGs are those sets of gimbal angles for which it does not produce any torque. Therefore, a steering law must have ability to avoid or pass or escape the singularity while minimally affecting the overall performance of closed-loop system. Usually for a full three-axis control cluster of four identical CMGs is used. A four CMGs cluster provides an extra degree of freedom, which can be used to produce null motion in order to avoid singularity. Null motion is the motion of gimbals which produces no torque. An optimal arrangement of four CMGs is pyramid with skew angle 54.73^o, as it has almost spherical momentum envelope. In four CMG systems internal singularities pose a serious problem by restricting the available momentum space. In the development of steering laws researchers have

used different strategies for coping with internal singularities. These strategies mainly include avoiding, passing, escaping and excluding the singularities. However, development of an efficient steering law for a CMG cluster is still a major area of the research. In the literature available on the study of CMG systems, various steering laws have been proposed. All of them have their own advantages and disadvantages. Most of these steering methods are based on tangent approach which computes some inverse of the Jacobian matrix relating gimbal rate command to commanded torque. The most common steering methods include Moore-Penrose steering law, Singularity robust steering law, Generalised singularity robust steering law, Exact steering law operating in constraint work space and Singular direction avoiding steering law. Similarly steering laws using the variable speed CMGs are also proposed for attitude control only.

We summarize some important shortcomings of these steering methods in order to make the scope of our research work clear. It is noticed that there is no exact steering law which is able to use full momentum envelope. There is no singularity escaping law which can ensure high pointing accuracy. There are no inverse free steering law which is simple but effective and able to escape elliptic singularity. These questions provided prime motivation for this research.

1.2 Motivation

With the advent of small or so-called mini-CMGs, a new generation of small agile satellites are now thought to be viable option for Earth observation and space exploration missions. For their torque amplification property, CMGs are considered to be ideal actuators for missions where fast slew rate is required. However, singularities associated with single gimbal CMG clusters can have serious consequences for overall performance of attitude control system if the steering law is not efficient enough. The motivation of this research is to study the problem of CMG steering in the face of singularity for the simplest case of twin CMG system and a complex case of four CMG pyramid systems. The focus of this research is to develop novel CMG steering techniques which are able to overcome some of the performance related limitations of existing steering laws.

The prime reason of understanding a twin CMG system is that it has been used in BILSAT (see in Fig. (1.1)) a 120kg Turkish mini-satellite built by Surrey Space Centre. BILSAT is in sun synchronous low earth orbit at 686 km and its mission includes full imaging of Turkey, stereoscopic imaging of selected targets and developing a digital elevation map of Turkey. It has four reaction wheels for attitude control and a twin CMG system as experimental payload to control pitch axis. Attitude control system of BILSAT is capable of full three axis control, off-nadir pointing to reduce the revisit time and pitch manoeuvre of ± 30 deg for stereoscopic imaging. The mini-CMG unit designed and developed at Surrey Satellite Technology Limited (SSTL) for BILSAT application can be seen in Fig. (1.2).

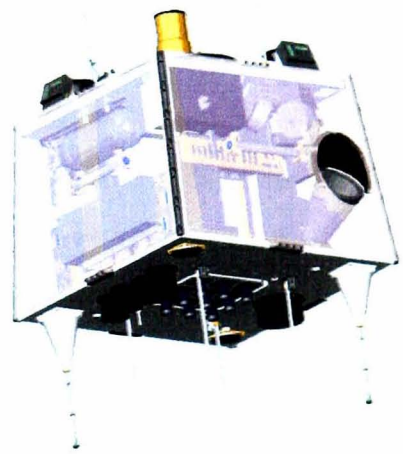

Figure 1.1: Computer image of BILSAT (courtesy of SSTL).

We consider the simplest form of twin type system made up of two single gimbal CMGs driven in opposite directions. Such system does not require matrix inversion for gimbal steering. Therefore, exact steering problem becomes a lot simpler and easier to understand. The study of such simple twin CMG system is thought to be helpful in finding some simple conditions on selection of feedback gains such that an exact steering law can exploit full momentum capacity of the CMG cluster. A four CMG pyramid type system employed for three-axis control of a satellite forms a highly nonlinear system. It has to be explored that how one can use full momentum capacity of a four CMG pyramid cluster through proper choice of feedback gains in some form of exact steering

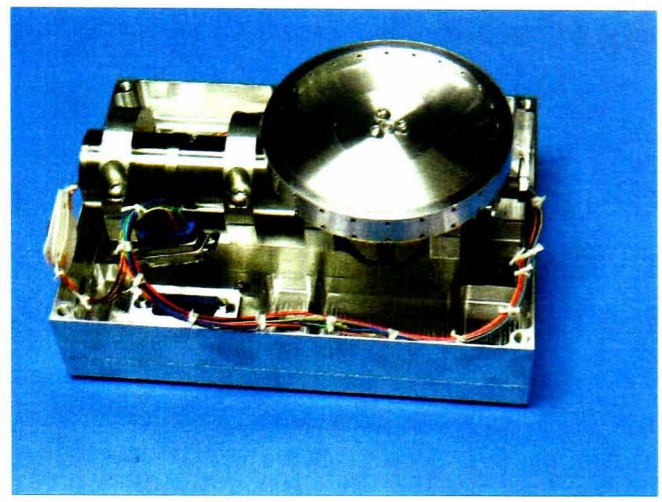

Figure 1.2: Photograph of BILSAT's mini-CMG unit (courtesy of SSTL).

law. The four CMG pyramid system is minimally redundant system. And the existence of internal singularities (elliptic) in pyramid systems can restrict the available momentum space for a number of existing steering laws. Although the six CMG system can provide a larger momentum space including no internal singularities (elliptic), but this system is too heavy and complicated as compared to a four CMG system. Therefore, it was deemed necessary to develop a new exact steering law which can avoid elliptic singularity in order to use full momentum space. By definition an Exact Steering Law is not singularity robust, so it can not escape an initial elliptic singularity. The existing singularity escaping steering law namely Generalised Singularity Robust (GSR) produces pointing error while escaping elliptic singularity. Therefore, there is need for a steering method which can escape elliptic singularity with high pointing accuracy. The concept of inverse free steering has attracted attention of many researchers while they were attempting a singularity free solution. However, the results of such attempts were not always simple e.g. one of such approach required training of neural networks in somewhat cumbersome framework. Therefore, a quest for simpler but effective inverse free steering approach remained there.

1.3 Aims and Objectives

The aim of this research is to develop new exact steering laws for a cluster of CMGs which can effectively avoid and/or escape singularities in order to use full extent of

momentum capability of a cluster. To achieve this aim the following objectives were setout.

- To study and explore the selection of feedback gains such that an exact steering law can use full momentum capacity of a CMG cluster under various constraints like slew rate limit, gimbal rate limit and singularity avoidance.

- Existing steering laws based on inversion of Jacobian matrix generally have problem in exploiting full momentum capability of a CMG cluster due to internal singularity (elliptic). Our second objective is to develop a new exact steering technique which can avoid elliptic singularity in order to use full momentum capacity.

- To develop a new singularity escaping steering law with high pointing accuracy.

- A singularity-free steering can be stated as the ultimate goal of CMG steering problem. Our final objective is to develop some simple but effective inverse-free steering law in order to achieve singularity-free steering.

1.4 Achievements

In this thesis following achievements are made:

- An analytical formulation is developed to calculate feedback gains to be used in the exact steering law for twin CMG systems such that singularity is avoided while using the full momentum capability. This formulation has been developed for both free and constrained gimbal rates.

- We have also developed a simple but effective variable feedback gains steering technique for twin CMG systems.

- The idea of feedback gains' formulation has been extended to a three-axis control problem of a satellite equipped with a four CMG pyramid system such that the exact steering law (proposed by us) can use full momentum capability of the CMG cluster by avoiding elliptic singularity.

- An exact steering law based on generalised-inverse is proposed and developed for a cluster of CMGs which can avoid elliptic singularity to be able to use almost full momentum capability. Another important feature of proposed steering is that it can bring gimbal configuration back to initial zero state at the end of a manoeuvre.

- A new singularity escaping steering law is proposed and developed which has been shown to escape the elliptic singularity far too quickly and has much higher pointing accuracy as compared to Generalised Singularity Robust Law. Therefore, this proposed law is suitable for fast-tracking manoeuvres.

- A new Inverse-free steering law is proposed and developed. The proposed steering law is much simpler and effective. Stability proof of the proposed steering law using Liapunov stability theory is also presented. Its modified form has been shown to escape elliptic singularity.

The steering laws developed in this thesis have novelty at their heart and potential to tackle the singularity in one way or the other.

1.5 Novelty of Research

Given the scope of the mini-CMG clusters as the attitude actuator in new generation of Earth-imaging small agile satellites, the research work presented in this thesis has the following novel contributions to the research area of the CMG steering laws:

- The proposed feedback gains formulation for twin CMG system based on phase-portrait analysis improves the understanding of the selection of feedback gains to be used in exact steering law subjected to various constraints namely slew rate limit, gimbal rate limit and singularity avoidance.

- The proposed variable gains exact steering law contributes in the area of adaptive steering law for twin CMG systems. For this case a new feedback formulation based on phase-portrait analysis is developed and a simple form of singularity index is used to vary the gains.

- A three-axis control problem using four CMG system is reduced to a non-linear damped pendulum problem by applying Euler's eigenaxis theorem. Then extension of proposed feedback gains' formulation to this problem is made possible by introducing a new angular variable representing angular momentum.

- The concept of steering law based on generalised-inverse rather than pseudo-inverse of Jacobian matrix is novel and it is first time proposed and successfully used by the author.

- We have proposed and developed a novel singularity robust steering law which is also based on generalised-inverse of Jacobian matrix. In order to make generalised-inverse singularity robust, this method introduces a minimal perturbation only in singular direction. This steering law can escape elliptic singularity very quickly with high pointing accuracy.

- The form of inverse-free steering law developed in this thesis is new and it is much simpler but effective.

1.6 Overview of this Thesis

In this section, an overview of this thesis is presented. In chapter 2, literature regarding attitude control of satellites using CMG systems is reviewed with special emphasis on CMG steering laws.

In chapter 3, mathematical model of a spacecraft using momentum exchange devices is derived. A quaternion feedback law for such system is also derived for a general class of manoeuvre using Liapunov approach. This elaborate attitude dynamic and control formulation is then simplified to discuss special cases of momentum wheel, constant speed CMGs and variable speed CMGs.

In chapter 4, we have discussed a single axis rest-to-rest manoeuvre for a satellite equipped with twin CMG system. The proposed formulation of feedback gains based on a simple analysis makes exact steering possible such that full momentum capacity of a twin CMG system is used by just avoiding singularity. When some explicit gimbal rate limit is incorporated in the proposed feedback gain formulation then resulting

manoeuvre has shown to become near-time-optimal. This chapter also includes the discussion on a new proposed idea of variable gains for single axis control of satellite using twin CMG systems.

In chapter 5, we discuss the exact steering in four CMG pyramid systems. Proposed feedback gains' formulation developed in chapter 4 is extended to a three-axis control problem. For four CMGs steering a new generalised-inverse based steering law is proposed in order to avoid elliptic singularity. This law gives exact steering while using almost full momentum capacity of the CMG cluster.

In chapter 6, we have discussed singularity robustness of generalised-inverse based steering law. In simulation results proposed method has been shown to outperform the Generalised Singularity Robust (GSR) method.

In chapter 7, a new inverse free steering law is proposed. This chapter includes a Liapunov proof of stability of proposed steering law and simulation results demonstrating the effectiveness of this method for a reorienting manoeuvre of the satellite.

Chapter 2

Literature Review

2.1 Reorientation of Satellites

In some satellite applications the primary mission tasks involve performing attitude manoeuvres during their life-span. The most common examples of such satellites are earth observation satellites and space telescope. The attitude or reorientation manoeuvre of a satellite requires a feedback control law to generate a commanded torque. The attitude control problem of satellites has been studied extensively. In this section, we shall review various attitude control laws developed for reorientation manoeuvres of satellites.

2.1.1 Nonlinear Attitude Control

The rotational motion of a rigid satellite is governed by Euler equations. Due to nonlinear nature of Euler equations, attitude kinematic equations and external torques, the attitude control problem is nonlinear for general large angle manoeuvres of satellites. Attitude dynamics can be linearized for small angle single axis manoeuvres and then a linear control law can be obtained by using linear control theory. In this subsection, however, we discuss a set of papers presenting nonlinear attitude control techniques.

Many researchers have attempted to find an approximate solution to attitude dynamics/control problem. For example, Longuski [82] presented an approximate solution to Euler's equations and Euler angles for a near-symmetric satellite. One step further,

Chowdhry et al [25, 26] studied the open-loop control of angular velocity by assuming that there was no direct control over one of the angular velocity components. Then a perturbation approach was used to vary control availability and parametric dependence of the solution was found.

A polynomial form of feedback law to perform a nonlinear slew manoeuvre was proposed by Carrington and Junkins [22]. The coefficients of polynomial were determined by iteratively solving successive increasingly nonlinear systems. Dwyer [35] used the nonlinear rigid-body model for an asymmetric spacecraft to study the feedback control under minimum energy constraint for large angle manoeuvre. In Ref. [36], Dwyer considers a nonlinear coordinate transformation for large angle reorientation problem of spacecraft to obtain a transformed equivalent linear system. Linear closed-loop control methods are used to solve the transformed system, and the resulting solution is put through the inverse transformation to obtain a solution of the nonlinear system. It was shown that optimal command can be carried out exactly in the transformed system.

In another class of nonlinear attitude control, a three-axes feedback law uses quaternion error vector and angular velocity vector with suitable gain matrices. Wie et al. [136] developed a quaternion feedback regulator to perform eigenaxis rotations. That regulator included gyroscopic coupling term to cancel it from closed-loop system's equation. The quaternion feedback law for three-axis control has been used in this thesis to perform an eigenaxis manoeuvre. In an earlier work, Wie and Barba [132] proposed three distinct forms of quaternion error feedback laws for three axis reorientation manoeuvres. The stability proof of quaternion feedback control has been provided in Ref. [128]. Cristi et al. [32] provided a quaternion feedback control which is globally stable and needs no knowledge of the spacecraft inertia matrix. This is an excellent property for control of a modular space station. Most of these papers discuss nonlinear attitude control techniques for large angle manoeuvre of rigid satellites without mentioning or modeling means of control actuation. In principle, these control strategies can be considered valid for any type of actuators but in practice the type of the actuator puts some extra constraints on dynamic variables (slew rate and control torque) and/or on feedback gains to be used in a feedback law. For example, Wie and Lu [135] incorporated the slew rate and control torque constraints in the quaternion feedback control. Wie et

al. [131] developed a nonlinear feedback attitude controller for an agile spacecraft that required a rapid re-targeting and fast transient settling. This feedback law uses variable limiter on quaternion error and it is subjected to various physical constraint like actuator saturation, slew rate limit and bandwidth limit. This technique was tested for an agile imaging satellite equipped with four CMG system in low Earth orbit. It appeared to have worked successfully in pointing the line of sight toward multiple targets on the ground, which shows a rapid multi-target acquisition and pointing capability of this control law. However, we think that there can be an alternative approach of incorporating the actuator's capability in the feedback law. This alternative approach constrains the feedback gains rather than constraining the control torque or putting variable limiter on quaternion error for a CMG based attitude control.

2.1.2 Optimal Control

The time-optimal attitude manoeuvre seeks to minimize the time required to rotate the satellite from some initial to final orientation. Maximum principle of the optimal control theory is used to formulate an optimal control problem. In the formulation, total manoeuvre time is used as performance index to be minimized subjected to the dynamic constraints given by nonlinear attitude model (Euler equations and quaternion kinematic equations) of a rigid satellite. The resulting formulation forms a two-point boundary value problem. In general, this problem has no known analytical or numerical solution unless solved for specific examples. For a single axis rotation about a principal axis a time-optimal control results in a bang-bang solution. Control command for the bang-bang solution remains saturated in either direction for the entire manoeuvre with at most one switch. And the switching time of the control command is determined by computing a mathematically defined switching function in order to find the instant when it changes its sign. That instant is the required switching time for bang-bang control command. A three-axis time-optimal attitude control has at least three independent control inputs. Therefore, in multi-input time-optimal control at least one input remains saturated all the time and the task of the optimization scheme is to compute the switching times of these inputs.

The problem of time-optimal manoeuvre has been studied by many researchers. Scrivener

and Thompson [103] presented a survey of the major contributions in this area. The early work on optimal control was only able to generate suboptimal solutions due to various assumptions to simplify the complexity and avoid the impracticality of control implementation [57]. In formulation of the time-optimal attitude manoeuvre problem, Vadali et al [121] have shown that the quaternion constraint leads to transversality condition requiring the co-state to be orthogonal to the quaternion vector. In a further development, Vadali [119] has shown that in time-optimal control, the control profile is independent of constraint multiplier. Vadali and Junkins [122] used an optimal control technique to achieve optimal momentum transfer. Then in Ref. [123] they analyzed the Liapunov stability of a simple spacecraft configuration for the closed-loop control of rest-to-rest and tracking manoeuvres.

Iwens [49] developed a quasi-time-optimal control for a reorientation manoeuvre of spacecraft equipped with a CMG system. This work had considered the eigenaxis manoeuvre as a time-optimal manoeuvre. A bang-bang control was used to generate angular velocity profile and a feedback controller was used to track these open-loop profiles. Li and Bainum [75, 76] assumed that the time-optimal solution lies close to eigenaxis rotation for developing a near-time optimal iterative technique of finding control profile and minimum time for the manoeuvre. Etter [38] presented a technique of achieving a time-optimal rotation about an eigenaxis of an asymmetric spacecraft. Billimoria and Wie [14] made a significant contribution by demonstrating that for a three axis constraint control eigenaxis manoeuvre in general is not time-optimal. The time-optimal control is bang-bang in all three axes and results in a significant nutational component. The task of optimization is to find switching times from switching functions for each axis. These ideas were applied by Byers and Vadali [21] to formulate a method to compute solutions for the time-optimal control switch times in the reorientation manoeuvres. In Ref. [20] a near-time-optimal manoeuvre was considered and different optimization methods for computing switching times were discussed. Junkins and Turner [53] presented methods for optimizing reorientation manoeuvres based on several different objective functions. In Ref. [117] stability analysis of attitude control problem was performed and optimality results were also discussed. Vadali and Krishnan [125] developed a control strategy which involved an open-loop control law using

a parametric optimization scheme for reorientation of ground based test article. The gimbal angle commands generated by feed-forward control were then tracked by feedback controller. They have compared the theoretical and experimental results, which are in agreement apparently. In Ref. [120] a near-time-optimal manoeuvre for large spacecrafts was discussed and experimental results were also presented. Skaar and Kraige [108] developed a near-optimal control algorithm for a general three-axes manoeuvre which used an open-loop optimal power criteria.

2.1.3 Attitude Control: Other Related Issues

The control law formulation for attitude control of satellites discussed above does not assume any specific actuation system but some of those use general features of the actuation systems. In this thesis the attitude control problem has been formulated specific to single gimbal CMG systems. The feedback law assumes a fully actuated satellite. However, a nonlinear tracking controller for an under-actuated spacecraft can be found in Ref. [13]. Similarly, attitude stabilization of a satellite using only two momentum wheels was considered in Ref. [58]. Generally, attitude dynamics/control formulation assumes its decoupling from orbital motion unless stated otherwise. For example, one can see Lian et al [77] which discussed coupling of attitude and orbital motions of satellites through gravity gradient torque. They have shown the controllability of orbital motion by controlling the attitude with reaction wheels or gas jets.

2.2 Control Moment Gyros

Research on CMG systems started in mid 1960s for their potential use in large spacecrafts such as "Skylab". At that time, computational power of available on-board computer did not allow matrix inversion calculations. So a twin CMG system was a candidate with their gimbals driven in the opposite directions [63]. However, a double gimbal CMG system consisting of three units was used in the Skylab with an approximated inverse calculation involving only a transposed Jacobian [27, 29]. Liska [80] discussed the use of double gimbal CMGs for high accuracy attitude control. Ground test facilities for double gimbal CMGs, such as a platform supported by a spherical air bearing, were developed [54]. Since then study of double gimbal CMG has matured and they

are now being used in space shuttle and International Space Station. The use of single gimbal CMGs in spacecrafts like High Energy Astronomical Observatory (HEAO) and the Large Space Telescope (LST) has brought extensive study of such systems. For HEAO a roof type configuration was also a candidate for its simpler mathematical formulation.

The use of single gimbal CMGs in the attitude control of spacecrafts was first proposed by Jacot and Liska [50]. In their treatment they omitted inertia of gimbal axis and used conservation of angular momentum approach. Colburn and White [28] discussed the computational aspects of using CMGs in attitude control of spacecrafts. The early work on CMG based control of satellites can be found in Ref. [3, 31, 79]. They had discussed basic issues like CMG selection, design criteria and precision pointing control using CMGs. In large spacecrafts like Skylab and MIR space station, CMGs were used for attitude control and momentum management. The use of CMGs in space station applications has been studied in Singh and Bossart [107] and Bishop et al. [15]. They had separately developed highly linearized and axis decoupled feedback laws for CMG based control. However, these laws are not suitable for large angle reorientations or high angular rates. Another study was done for applications to space station, which combined CMGs and RWs for integration of attitude control and power storage.

2.3 Applications of CMGs in Small Satellites

Single gimbal CMGs are generally used in spacecraft missions with high agility requirement. But these devices were never used in small commercial satellites until recently. With the advent of small and inexpensive mini-CMGs, a new generation of small satellites can have significantly improved capability in terms of agility and pointing accuracy, which was not possible with reaction wheels. Therefore, the low altitude imaging satellites can have high image acquisition rate. Hence, mini-CMGs provide a low cost and power-efficient solution to attitude control problem of small agile satellites, see Ref. [19, 23, 33, 45, 68, 69, 70, 71, 95, 97].

Blondin [16] discussed the use of small CMGs in space missions. Roser and Sghedoni [95] gave their proposal for designing mini-CMGs for future missions of ESA and

CNES. They presented a comparison of CMG systems with reaction wheel systems. Defendini [33] presented usage of mini-CMGs for agile satellite missions of Astrium France. Busseuil et al. [19] described the mini-CMG being developed in Alcatel, as well as development of their new steering law. Their proposed steering law is based on off-line calculations of gimbal angles necessary to perform a commanded manoeuvre. The resolution of mini-CMGs improves with the speed of rotor. But exiting mechanical bearing technology can not support very high speed of rotors as it allows physical contact which causes wear and prevents high rotational speed. On the other hand, magnetic bearings support the rotor without physical contact and therefore, are suitable for new generation of mini-CMGs with high accuracy requirement. Magnetic bearing improves the resolution of a CMG by a factor of 5. With this technology momentum wheels can be designed to operate at a high speed of 12000rpm. Salenc and Roser [97] also developed mini-CMGs for small satellite applications. They proposed a combination of three existing steering techniques to avoid singularities.

Surrey Satellite Technology Limited (SSTL) has been investigating and testing the mini-CMGs as an alternative to reaction/momentum wheels in advanced Attitude Determination and Control Subsystems (ADCS) for its missions [68, 69, 70, 71]. SSTL has developed a Turkish micro-satellite BILSAT-1, for Earth imaging, which is equipped with a twin CMG system as an experimental payload [18]. In orbit performance of this system has also been checked.

2.4 Other Applications

Theory of a redundant CMG system has a direct application in the control of a redundant manipulator and vice versa. For example, in Ref. [9, 10] singularity analysis of the redundant manipulator have been studied. This is very similar to CMG singularity problem. In Ref. [11], they presented a comparison of a CMG system and a manipulator in terms of inverse kinematic problem and existence of singular states. Therefore, many aspects of the CMG based control are analogous to the control of multi-joint manipulator.

Recently, in Ref. [113], the CMG system has been used for the first time in attitude

control of autonomous underwater vehicle (AUV). A CMG system is employed for an active three-axis attitude control and stabilization in a zero-G class underwater robot. The effectiveness of this control strategy has been demonstrated through series of experiments. In another development, Lim and Moerder [78] have studied the use of CMGs for attitude control of fixed-wing aircraft. They have also explored the interplay between conventional aerodynamic and CMG based attitude control.

2.5 The Singularity Problem

Despite many advantages of using a CMG system, associated singularities pose a serious problem for attitude control system. In a singular state, gimbal configuration is such that Jacobian matrix loses its rank and spacecraft loses control authority in a particular direction, which is clearly undesirable. It was observed through various simulations that singularity problem can not be ignored and some sort of singularity avoiding control was required for this type of system. To visualize the singularities of a CMG cluster in all possible directions corresponding singular momentum surfaces are drawn in three-dimensional angular momentum space. These convoluted momentum surfaces constitute a momentum envelope. The outer surface of momentum envelope represents the maximum momentum capability of CMG cluster in all directions, which also corresponds to saturation singularities. The inner convoluted surfaces in the momentum envelope represent the internal singularities. In a redundant CMG system gimbal configuration can be changed without changing the angular momentum of the CMG cluster. Such gimbal motion does not produce any torque, therefore, it is called null motion. Singularity avoidance by adding null motion has been studied. It was found that saturation singularities could not be avoided by adding null motion. Based on singularity avoidance by null motion criterion, internal singularities were categorized as hyperbolic (escapable) and elliptic (inescapable) singularities. The singular surfaces which correspond to hyperbolic singularities are passable, whereas those which correspond to elliptic or saturation singularities are not passable. Thus the passibility of a singular surface determines the nature of the singularity. The convoluted nature of these singular surfaces prevents their simple anticipation and avoidance in steering laws. Elliptic singularities are especially problematic as they significantly reduce the available

angular momentum. Therefore, an effective steering law is needed such that elliptic singularities are avoided where it is possible, or rapidly escaped while minimizing their effect on attitude control.

Singularity problem has been studied extensively by many researchers. Here we present a brief review of some important contributions regarding different aspects of singularity problem. Margulies and Aubrun [83] presented an elegant geometric representation and analysis of singularities associated with a CMG cluster. For a cluster of n CMGs, they had shown, there exist 2^n singular gimbal states for any direction. The geometric description of singular surfaces was used to explain the nature and passibility of singularities in a CMG system. They had analyzed the Moore-Penrose pseudo-inverse solution as a candidate for torque producing gimbal motion and null motion with view of avoiding singularity. There exist $n-3$ parameters family of null motion for a cluster of n CMGs. Classification of singularities based on null motion is also discussed. Moreover, it is also discussed that null motion can be added to torque-producing motion for achieving singularity avoidance. Bedrossian [9, 10] studied the singularities associated with redundant manipulators. His work involved classification of singularities. Tokar [115] gave description of the singular surfaces in terms of shapes, sizes and the workspace (useful region of the momentum envelope). In another work, he discussed the consideration of incorporating gimbal angle limits [114]. Then in a next paper, he discussed passibility of singular surfaces [116]. His conclusion was that a system with no less than six units would provide an adequately large workspace including no impassable surfaces. After this work, a six units symmetric system was designed for Russian space station MIR [37]. Kurokawa [66] formulated passibility of singular surfaces in terms of the geometric theory given by Margulies and Aubrun [83]. Then, Kurokawa and Yajima [65] clarified the existence of impassable surfaces in the roof-type system. In Ref. [34, 60, 130, 133] different aspects of singularity problem have been discussed, which include nature of singularities, singular momentum surfaces and null motion. Surface theory of differential geometry was employed to re-examine geometric properties of singular surfaces. The problem was illustrated for different CMG arrangement examples. Meffe and Stocking [84] presented topological mapping of singular surfaces for typical single gimbal CMG configurations. This study explains

construction, superposition and intersection of multiple singular surfaces. They have demonstrated the use of these concepts in CMG sizing and selection of the geometry of a CMG array.

2.6 A Survey of Existing Steering Laws

In this section, we present a survey of various steering laws and issues related to CMG based attitude control. Intensive efforts have been made to develop some efficient CMG steering technique. One may find a wide variety of steering techniques in the literature on CMGs. The main issues discussed in the papers are steering problem, singularity avoidance/escape, null motion, singularity robust steering, optimal steering, effect of disturbances on CMG steering and variable speed CMG steering for combined attitude/power control. It is worth mentioning that the steering methods obtained for CMG are applicable to robot manipulator control. In the following subsection, these issues will be tackled one by one.

2.6.1 The Steering Problem and Singularity Avoidance

Different aspects of CMG steering problem have been discussed by many researchers. O'Conner and Morine [87] proposed for the first time that gimbal rates rather than torque should be used as command input. They argued that friction on gimbal bearing was large enough to dismiss the torque as candidate input command. Perhaps the most important aspect of the steering problem is singularity avoidance/escape, as exactness and effectiveness of a steering method depend on its effective singularity avoidance/passing. However, a steering method avoiding/transiting one type of singularity, in general, may not be able to avoid/transit other type of singularity. The reason for this is the usage of gradient approach for deriving these steering laws, which considers the passibility problem as a local problem [30, 44]. The common example of gradient approach is Moore-Penrose inverse steering law. But, Baker and Wampler [6] have shown that local techniques do not guarantee singularity avoidance. A global steering method was proposed in Ref. [90]. This method used global optimization which considered passibility as a global problem. But such optimization techniques are computationally intensive and can not be used in real-time applications. Kurokawa [61]

stated that no steering law can follow an arbitrary command inside certain wide region of the workspace. And workspace must be reduced to obtain an exact control to exclude singularities. He achieved this exact control by applying a gimbal motion constraint to exclude elliptic singularities from the workspace [62]. But, such attempts of excluding singularity results in significantly reduced the available momentum space. It would mean over-sizing of the CMG system or in other words wastage of resources. However, Wu [138] has proved the existence of nonsingular gimbal angle paths for redundant CMG systems.

Cornick [30] has analyzed CMG steering for six CMG cluster. Two steering logics were proposed, one was direct method and other was called indirect method. Both methods computed location of singular states and used null motion to avoid these singularities.

Although, Tokar [116] suggested that a system needs at least six units in order to provide adequately large momentum space including no impassable surfaces. Even then the use of gradient method in roof type system may result in discontinuity [141]. Therefore, most of the steering laws were studied for pyramid type system containing four units (see Fig. 5.3), as six units system was considered too large and too complicated. Recently, Kurokawa [64] has used geometric view and analysis to survey singularity avoiding aspect of different steering laws. He concluded that no perfect steering law exists, especially for pyramid-type systems.

In summary, CMG steering has mainly two common strategies to cope with problem of singularity. In first case, CMGs are over-designed to exclude singularities from workspace which is a wastage of resources. Whereas in second case approximate singularity avoiding/passing algorithms are used at the expense of control accuracy.

2.6.2 Singularity Robust Steering and Null Motions

In a singularity robust steering, system can pass through singularity with some compromise on performance of attitude control system. Singularity Robust (SR) Steering Law is a common example of this class of steering laws. The SR steering law was originally developed for control of manipulator [85] and later it was used in CMG steering problem [11]. The SR solution is obtained by suitably changing the Moore-Penrose

solution in the vicinity of singularities. As a result SR technique computes an approximate finite solution of gimbal rates in the vicinity of singularities by allowing torque errors. However, this technique minimizes both gimbal rates and torque errors. The singularity robust (SR) steering law does not avoid singularity but it transit through singularity, therefore, this steering law is not able to use full momentum capability of CMG systems. The main disadvantages of SR technique can be summarised as: it has tendency of driving the CMG system to an elliptic singularity; it may cause a gimbal lock while passing through the singularity for excessive control effort; it restricts the available momentum space due to transit through elliptic singularity.

Bedrossian et al. [8, 11, 12] presented a method of addition of null motion to torque producing motion in order to avoid singularity. In Ref. [11] a non-directional null motion is added to SR inverse and compared with Moore-Penrose inverse solutions. Addition of null motion locally increases the CMG gain, a measure of farness from the singularity. This results in avoidance of elliptic singularity with penalty of large gimbal rates and torque errors.

The SR steering law was modified by Wie et al [128, 134] to form a Generalised Singularity Robust (GSR) steering law which was capable of escaping elliptic singularities. The modification is done by adding deterministic dither signal in off-diagonal terms of SR logic. Although this modified law is capable of using larger momentum space but it generates a pointing error. Therefore, this logic is not intended for missions in which exact attitude tracking is required. Wie [129] has further generalised the GSR steering law by including a weight matrix. It has been shown that a de-saturation manoeuvre is possible with this steering law provided weight matrix is chosen properly. However, the selection of the weight matrix, which makes de-saturation possible, is not obvious. The GSR steering law can not bring gimbal angles configuration back to initial state at the end of the manoeuvre rather null motion is added to it to perform this task. The performance of GSR steering law has also been tested for a CMG system with gimbal angle constraint of $\pm 180\text{deg}$ in Ref. [67]. Here null motion is added to GSR steering law to prevent gimbal angles from going to the $\pm 180\text{deg}$.

Ford and Hall [41, 42] presented a steering law which avoids singular direction. In this

law, the pseudo-inverse of Jacobian matrix is computed from its singular value decomposition (SVD). And pseudo-inverse is made singularity robust by modifying inverse of the smallest singular value. Wu and Chou [137] proposed a method of detecting the avoidable singularities. This method computes the eigenvalues of a matrix which is Jacobian of null vector. If real part of even one eigenvalue is positive then singularity is avoidable.

Oh and Vadali [88] formulated the complete equations of motion for large angle rotational motion of spacecraft equipped with a CMG cluster. The formulation included moment of inertias of spinning wheels and gimbal axes of the CMG units. They also presented some candidate feedback laws based on Liapunov stability approach. In one approach, they used variable gain matrix in order to avoid singularity. They proposed gimbal acceleration steering logic for the case where gimbal inertias are included.

2.6.3 Optimal and Feed-Forward Steering Methods

This class of steering law, generally, uses some optimization techniques for generating gimbal angle commands corresponding to a specified manoeuvre with a clearly defined objective function and constraints. The optimization is performed off-line and a feedback law is used to track these commands. Paradiso [90] developed a method for global avoidance of singularities in a feed-forward steering law. This technique involves a gimbal path planing using global optimization to achieve singularity avoidance. Hoelcher and Vadali [47] proposed open-loop and feedback control laws which minimize control effort and maneuver time and also avoid singular states of the CMG clusters. Vadali and Krishnan [125] narrowed the focus exclusively to avoiding singularities by parameterizing the gimbal rates as polynomial functions of time and optimizing the parameters with respect to a singularity avoidance objective function. A feed-forward law is used to generate suboptimal gimbal angle commands, which are then tracked by a feedback controller. But due to off-line computation this steering technique may not be suitable for on-board applications. Going one step further, Vadali et al. [124] developed a method for determining a family of initial or preferred gimbal angles which would avoid singularities during the manoeuvre. These preferred angles are found by back integration of the gyro torque equation from a desired final condition.

A null motion based scheme is also developed to position gimbals at preferred angles at end of the manoeuvre. Avazini [5] developed a control strategy which involved a feed-forward command generation by an inverse simulation method that uses local optimization to determine a singularity avoiding steering law. Then a feedback controller is developed and used to track the generated trajectories. Fleming and Ross [40] used the time-optimal control strategy for a reorientation manoeuvre of spacecraft equipped with four CMG pyramid system. This is a computationally intensive strategy which results in apparent singularity avoidance because of generating preferred initial gimbal state as a result of optimization. It does not require an explicit computation of inverse of Jacobian matrix.

2.6.4 Inverse-Free Steering Methods

Krishnan and Vadali [59] introduced an inverse-free technique to steer a CMG cluster, which uses transpose of Jacobian matrix. It uses radial basis function to parameterize nonlinear terms in attitude controller. They have discussed validity of this law using Liapunov's stability argument. This law generates finite gimbal rates while passing through singularity. But this steering law can not use full momentum capability as slew rate or momentum saturates at elliptic singularity. In another approach of inverse free steering, Avazini [4] formulated gimbal angle commands for a desired manoeuvre. This approach uses static inversion of kinematic relation between gimbal angles and angular velocity of spacecraft. Then formulated gimbal commands are tracked. The resulting steering technique does not avoid elliptic singularity, therefore, available momentum capability can not be fully utilized. Suzuki [111, 112] developed robust attitude control for a ground test facility using CMG system. Recently, Pechev [91] has developed a control strategy for attitude control using CMGs. This method determines the gimbal rate commands which minimizes H-infinity norm of torque errors in all three directions. Results show that it escapes elliptic singularity with some pointing error.

2.6.5 Effects of Disturbances

In some studies, external disturbance torques were also considered to analyze more realistic situations. Heilberg [45] gave description of disturbance sources for space-

crafts using single gimbal CMGs for pointing control. They have designed a filter to mitigate these disturbances. Furthermore, Heilberg et al. [46] developed mathematical model for spacecraft equipped with CMG cluster, which includes unbalanced forces on the momentum wheel and unbalance moment caused by other sources. Rokui and Kalaycioglu [94] used feedback linearization technique to control satellites equipped with single gimbal CMGs. Skelton [109] developed mixed control strategies based on Liapunov and feedback linearization. It uses single gimbal CMGs for course large angle slew manoeuvre and momentum wheels for precise control and reduction of error caused by initial conditions. One source of pointing error is the limit cycle caused by friction in gimbal motor [104]. Researchers have tried to resolve this issue by improving the motor control and canceling the disturbance torque by employing the reaction wheels [96]. Paradiso [89] has presented a study which combines CMGs and reaction wheels for an effective control. However, this problem has not been yet fully resolved. The attitude control of a flexible spacecraft using CMG system has been studied in Ref. [56]. The issue of singularity avoidance in the presence flexible modes has been discussed. The issues related to different disturbances, briefly discussed in this subsection, are beyond the scope of this thesis.

2.6.6 Variable-Speed CMG Steering Laws

Optimal control of a spacecraft equipped with a cluster of variable speed CMGs was developed by Liu et al [81] in one of the earliest work. The singularity avoidance by using variable speed CMG was considered by Schaub and Junkins [98, 100, 101, 102]. They developed a variable speed CMG steering law and null motion for attitude control. However, their method generates excessive variations in the wheel speed which is beyond the torque capability of available wheel motors. In Ref. [72] we have proposed a variable speed CMG steering technique for passing through singularities with good pointing accuracy as well as small wheel speed variations. This technique uses Generalised Singularity Robust (GSR) law for CMG mode and reaction wheel mode of VSCMGs is only used for compensating attitude drift caused by GSR method. In Ref. [74] a game theoretic approach is used to minimize gimbal rates under an inequality constraint condition for singularity avoidance. In simulation results they have used preferred initial gimbal angles so effectiveness of singularity avoidance of their

method can not be judged. Ref. [73] has developed an optimal steering strategy for CMGs/VSCMGs which avoids singularity by varying the wheel speed.

2.6.7 Combined Power and Attitude Control

Fly-wheel based system providing both energy and attitude control was proposed in Ref. [39, 43, 118]. Variable speed CMGs can also be used for combined attitude and power tracking [93, 126, 139, 140]. Varatharajoo and Fasoulas [126] discussed the feasibility of combined attitude and power control strategy on small satellites using momentum wheels. Whereas, Yoon and Tsiotras [139] presented an integrated approach of attitude and power control for spacecrafts using VSCMGs. They also presented indirect adaptive control for spacecrafts with uncertain inertia properties. They further studied the singularity problem of VSCMG clusters used for attitude tracking with and without power tracking requirement in Ref. [140]. They managed to develop a criterion to determine usable momentum workspace for this method. This workspace can be used in CMG sizing for specific mission requirements. Ref. [92] has presented the optimal sizing of miniature variable speed CMGs for combined power and attitude control. The optimization of design uses nonlinear programming technique. The variable speed CMG steering is beyond the scope of this thesis and this discussion is included only for the sack of completeness.

2.7 Summary

In this chapter, we have reviewed some major issues related to CMG based attitude control problem. We have discussed the development of quaternion error feedback law and time-optimal control law for rigid body's rotational motion. Different applications of CMGs are also discussed. A brief review and explanation of singularity problem has been presented. Then we have discussed merits and demerits of various existing steering laws and strategies.

In next chapter, we shall develop mathematical model of rotational motion of a satellite equipped with CMGs (or momentum exchange devices). The attitude feedback law will also be developed. Issues related to CMG based control will be further explained.

Chapter 3

Rigid Body Dynamics with Momentum Exchange Devices

3.1 Introduction

In this chapter, we have formulated the attitude dynamics and control of a rigid spacecraft equipped with momentum exchange devices. The detailed discussion of the attitude dynamics and control problem can be found in many references [24, 48, 51, 52, 55, 86, 106, 128]. The formulation of attitude control problem involves definition of attitude variables of spacecraft body with respect to a suitable reference frame, attitude kinematic equations, dynamic equations and attitude control law. A detailed description of different attitude representations and their respective kinematic relations can be found in Ref. [99, 105]. Here we have described Euler angles and quaternion based attitude kinematics.

We have formulated a detailed mathematical model of rigid body dynamics of a satellite equipped with momentum exchange devices. Our formulation attempts to generalise the mathematical model developed by Oh and Vadali [88]. They have presented attitude dynamic model for a rigid spacecraft equipped with a cluster of constant-speed CMGs with diagonal inertia matrices. Whereas we have developed a model for rigid spacecraft equipped with momentum exchange devices which include reaction wheels, momentum wheels, constant speed CMGs and variable speed CMGs. Moreover, initially we have not assumed that inertia matrix of each device is diagonal rather we

have introduced this assumption later in the derivation after developing generalised relations. Then Liapunov stability theory is used to find a stabilizing attitude control law for a generic attitude model. Finally, special features of attitude dynamics and control of using reaction/momentum wheels, constant speed CMGs and variable speed CMGs are discussed.

3.2 Attitude Representation

The attitude of a rigid spacecraft is the orientation of the body fixed frame $\mathcal{F}_B$ with respect to a reference frame $\mathcal{F}_A$. The choice of axis system $\mathcal{F}_A$ depends on the tasks of a satellite. In earth-orbiting satellites, orbit reference frame is chosen as a reference system to determine the attitude. The origin of this frame moves with c. g. of satellite. The X-axis points toward direction of motion of satellite in the orbital plane. The Z-axis points toward center of the earth in the orbital plane. And the Y-axis completes the right-handed axis system. Therefore, the attitude of satellites in Earth orbits is, in general, measured with respect to this orbit reference frame.

The attitude of a rigid body can be described in various ways namely Euler angles, Rodrigues parameters, modified Rodrigues parameters and the quaternion parametrization. Euler angles and Rodrigues parameters are three parameters representations whereas quaternion is a four parameters representation. The three parameters representations always exhibit singular orientations whereas the four parameters representation is singularity free. In this chapter, we shall present some necessary details of Euler angles and quaternion representation and more details can be found in number of books on attitude dynamics [24, 48, 52, 55, 98, 106, 127, 128].

3.2.1 Euler Angles

Three Euler angles are used to represent the attitude of a rigid body in space. A general rotation in terms of Euler angles is defined as successive angular rotations about three different axes of rotated intermediate frames. For a set of Euler angles $\boldsymbol{\theta} = [\theta_x, \theta_y, \theta_z]^T$ the sequence of three successive rotations can be written as

$$\mathcal{F}_A \xrightarrow{\theta_z} \mathcal{F}_{A'} \xrightarrow{\theta_y} \mathcal{F}_{A''} \xrightarrow{\theta_x} \mathcal{F}_B$$

Here $\mathcal{F}_{A'}$ and $\mathcal{F}_{A''}$ are intermediate frames. The basic rotation matrices are defined as follows: Rotation about z-axis of reference frame $\mathcal{F}_A$ is

$$\boldsymbol{C}_z(\theta_z) = \begin{bmatrix} \cos\theta_z & \sin\theta_z & 0 \\ -\sin\theta_z & \cos\theta_z & 0 \\ 0 & 0 & 1 \end{bmatrix}. \tag{3.2.1}$$

Rotation about y-axis of reference frame $\mathcal{F}_{A'}$ is

$$\boldsymbol{C}_y(\theta_y) = \begin{bmatrix} \cos\theta_y & 0 & -\sin\theta_y \\ 0 & 1 & 0 \\ \sin\theta_y & 0 & \cos\theta_z \end{bmatrix}. \tag{3.2.2}$$

Rotation about x-axis of reference frame $\mathcal{F}_{A''}$ is

$$\boldsymbol{C}_x(\theta_x) = \begin{bmatrix} 1 & 0 & 0 \\ 0 & \cos\theta_x & \sin\theta_x \\ 0 & -\sin\theta_x & \cos\theta_x \end{bmatrix}. \tag{3.2.3}$$

The overall transformation matrix or direction cosine matrix from $\mathcal{F}_A$ to $\mathcal{F}_B$ is

$$\boldsymbol{C}(\theta_x, \theta_y, \theta_z) = \boldsymbol{C}_x(\theta_x)\boldsymbol{C}_y(\theta_y)\boldsymbol{C}_z(\theta_z).$$

After using the basic rotation matrices given in Eq. (3.2.1, 3.2.2, 3.2.3) we get

$$\boldsymbol{C} = \begin{bmatrix} \cos\theta_y\cos\theta_z & \cos\theta_y\sin\theta_z & -\sin\theta_y \\ \sin\theta_x\sin\theta_y\cos\theta_z - \cos\theta_x\sin\theta_z & \sin\theta_x\sin\theta_y\sin\theta_z + \cos\theta_x\cos\theta_z & \sin\theta_x\cos\theta_y \\ \cos\theta_x\sin\theta_y\cos\theta_z + \sin\theta_x\sin\theta_z & \cos\theta_x\sin\theta_y\sin\theta_z - \sin\theta_x\cos\theta_z & \cos\theta_x\cos\theta_y \end{bmatrix}$$

There are two distinct types of Euler angle rotations. In first type successive rotations are about each of three axes whereas in second type first and third rotations are about same axis with the second rotation about one of the two remaining axes. The first type of rotation has six possible orders of successive rotations each corresponding to a distinct set of Euler angles: $x \rightarrow y \rightarrow z$, $x \rightarrow z \rightarrow y$, $y \rightarrow x \rightarrow z$, $y \rightarrow z \rightarrow x$, $z \rightarrow x \rightarrow y$ and $z \rightarrow y \rightarrow x$. Similarly second type of rotation also has six possible orders of successive rotations: $x \rightarrow y \rightarrow x$, $x \rightarrow z \rightarrow x$, $y \rightarrow x \rightarrow y$, $y \rightarrow z \rightarrow y$, $z \rightarrow x \rightarrow z$ and $z \rightarrow y \rightarrow z$. Therefore, there are in total twelve distinct sets of Euler angles. Each set forms a distinct transformation matrix C. The choice of a set of Euler angles depends on the application. One can find a detailed description of attitude transformation using these distinct sets

of Euler angles in text books like one by Hughes [48].

We shall see later that attitude kinematics based on Euler angles can become singular for certain orientations. The four parameters attitude representation or quaternion can solve this problem of singularity.

3.2.2 Quaternion

The quaternion representation of attitude of a rigid body is based on Euler's eigenaxis theorem, which states that a general rotation in space is a rotation about some fixed axis. This fixed axis is also called eigenaxis as it is an eigenvector of direction cosine matrix C with eigenvalue of unity. Therefore, to represent attitude by quaternion we need to know a rotation angle θ and direction cosines of the fixed axis or eigenaxis $\boldsymbol{e}$. We have

$$\boldsymbol{C}\boldsymbol{e} = \boldsymbol{e}.$$

If e_x, e_y and e_z are direction cosines of the eigenaxis $\boldsymbol{e}$ then these direction cosines are identical both in inertial frame $\mathcal{F}_A = \{\hat{\boldsymbol{a}}_x, \hat{\boldsymbol{a}}_y, \hat{\boldsymbol{a}}_z\}$ and in body frame $\mathcal{F}_B = \{\hat{\boldsymbol{b}}_x, \hat{\boldsymbol{b}}_y, \hat{\boldsymbol{b}}_z\}$ i.e.

$$\begin{aligned} \boldsymbol{e} &= e_x\hat{\boldsymbol{a}}_x + e_y\hat{\boldsymbol{a}}_y + e_z\hat{\boldsymbol{a}}_z \\ &= e_x\hat{\boldsymbol{b}}_x + e_y\hat{\boldsymbol{b}}_y + e_z\hat{\boldsymbol{b}}_z. \end{aligned}$$

The quaternion or Euler parameters for a rotation angle θ about the Euler axis $\boldsymbol{e}$ can be defined as

$$\begin{aligned} q_0 &= \cos\frac{\theta}{2} \\ q_1 &= e_x \sin\frac{\theta}{2} \\ q_2 &= e_y \sin\frac{\theta}{2} \\ q_3 &= e_z \sin\frac{\theta}{2}. \end{aligned} \tag{3.2.4}$$

The four elements of quaternion satisfy a simple normalization constraint

$$q_0^2 + q_1^2 + q_2^2 + q_3^2 = 1.$$

This equation defines a four dimensional unit sphere. The quaternion trajectories on this sphere completely describe any possible rotational motion without any singularity. The transformation or direction cosine matrix in terms of quaternion can be parameterized as

$$C = \begin{bmatrix} 1-2(q_2^2+q_3^2) & 2(q_1q_2+q_3q_0) & 2(q_1q_3-q_2q_0) \\ 2(q_1q_2-q_3q_0) & 1-2(q_1^2+q_3^2) & 2(q_2q_3+q_1q_0) \\ 2(q_1q_3+q_2q_0) & 2(q_3q_2+q_1q_0) & 1-2(q_1^2+q_2^2) \end{bmatrix}.$$

3.3 Rotational Kinematics

In this section, we present the formulation of rotational kinematics of spacecraft. The kinematic equation relates the angular velocity of the rigid body to the attitude variable rates. In general for a given direction cosine matrix C transforming vectors from frame $\mathcal{F}_A$ to frame $\mathcal{F}_B$ and angular velocity ω expressed in frame $\mathcal{F}_B$, we have

$$\dot{C} = -\omega^{\times} C. \tag{3.3.5}$$

In the following subsections, we shall present the kinematic equation specific to Euler angles and quaternion representations.

3.3.1 Euler Angles

Euler angular rates $\dot{\theta} = \begin{bmatrix} \dot{\theta}_x & \dot{\theta}_y & \dot{\theta}_z \end{bmatrix}^T$ are related to angular velocity ω expressed in frame $\mathcal{F}_B$ through a kinematic equation. In order to derive this equation for $z \rightarrow y \rightarrow x$ order of successive rotations, we write vector sum of angular velocity vectors of each rotation expressed in frame $\mathcal{F}_B$ as

$$\omega = \dot{\theta}_x \hat{\mathbf{i}} + C_x(\theta_x)\,\dot{\theta}_y \hat{\mathbf{j}} + C_x(\theta_x)\,C_y(\theta_y)\,\dot{\theta}_z \hat{\mathbf{k}}$$

where $\hat{\mathbf{i}} = \begin{bmatrix} 1 \\ 0 \\ 0 \end{bmatrix}, \hat{\mathbf{j}} = \begin{bmatrix} 0 \\ 1 \\ 0 \end{bmatrix}, \hat{\mathbf{k}} = \begin{bmatrix} 0 \\ 0 \\ 1 \end{bmatrix}$ are standard unit vectors of the rotation axes expressed in respective frames. Then the required kinematic equation is

$$\dot{\theta} = S(\theta)\,\omega, \tag{3.3.6}$$

where

$$\boldsymbol{S}(\boldsymbol{\theta}) = \begin{bmatrix} 1 & \tan\theta_y \sin\theta_x & \tan\theta_y \cos\theta_x \\ 0 & \cos\theta_x & -\sin\theta_x \\ 0 & \sin\theta_x \sec\theta_y & \cos\theta_x \sec\theta_y \end{bmatrix}$$

for $\theta_y \neq \pm\frac{\pi}{2}$. For any particular application the order of successive Euler rotation is chosen such that this singularity of matrix $\boldsymbol{S}$ does not appear in the operating range of angles.

In attitude control problem the orbital motion is usually ignored as both motions can easily be decoupled. However, in momentum management, inclusion of orbital motion becomes necessary. In more realistic cases, spacecraft's orientation is measured with respect to orbital reference frame. This is a non-inertial frame orbiting about earth with mean orbital rate η. Then angular velocity vector of body with respect to inertial frame is

$$\boldsymbol{\omega} = \boldsymbol{S}^{-1}(\boldsymbol{\theta})\,\dot{\boldsymbol{\theta}} - \boldsymbol{C}(\boldsymbol{\theta})\, n_o \hat{\mathbf{j}}$$

where n_o is mean orbital motion. Therefore, the kinematic equation incorporating the orbital motion of orbital reference frame is given by

$$\dot{\boldsymbol{\theta}} = \boldsymbol{S}(\boldsymbol{\theta})\left(\boldsymbol{\omega} + \boldsymbol{C}(\boldsymbol{\theta})\, n_o \hat{\mathbf{j}}\right).$$

3.3.2 Quaternion

The kinematic equation for a rigid spacecraft in terms of quaternion can be expressed as

$$\begin{aligned} \dot{q}_0 &= -\frac{1}{2}\boldsymbol{\omega}^T \boldsymbol{q} \\ \dot{\boldsymbol{q}} &= \frac{1}{2}\left(q_0\boldsymbol{\omega} - \boldsymbol{\omega} \times \boldsymbol{q}\right). \end{aligned} \tag{3.3.7}$$

where $\boldsymbol{q} = \begin{bmatrix} q_1 & q_2 & q_3 \end{bmatrix}^T$ is the vector part and q_o is the scalar part of the quaternion. The attitude error or relative orientation in terms of quaternion $(q_{oe}, \boldsymbol{q}_e)$ is defined as

$$\begin{bmatrix} q_{0e} \\ q_{1e} \\ q_{2e} \\ q_{3e} \end{bmatrix} = \begin{bmatrix} q_{0f} & q_{1f} & q_{2f} & q_{3f} \\ -q_{1f} & q_{0f} & q_{3f} & -q_{2f} \\ -q_{2f} & -q_{3f} & q_{0f} & q_{1f} \\ -q_{3f} & q_{2f} & -q_{1f} & q_{0f} \end{bmatrix} \begin{bmatrix} q_0 \\ q_1 \\ q_2 \\ q_3 \end{bmatrix}. \tag{3.3.8}$$

Here q_{if} (for $i = 0, \cdots, 3$) are commanded quaternion parameters representing the desired orientation of spacecraft. If $\boldsymbol{\omega}_f$ is desired angular velocity vector then quaternion error rate is defined as

$$\begin{aligned} \dot{q}_{oe} &= -\frac{1}{2}(\boldsymbol{\omega} - \boldsymbol{\omega}_f)^T \boldsymbol{q}_e \\ \dot{\boldsymbol{q}}_e &= \frac{1}{2}\left(q_{oe}(\boldsymbol{\omega} - \boldsymbol{\omega}_f) - (\boldsymbol{\omega} - \boldsymbol{\omega}_f) \times \boldsymbol{q}_e\right). \end{aligned} \tag{3.3.9}$$

3.4 Spacecraft Attitude Dynamics

In this section, we shall develop the equation of attitude motion of a rigid spacecraft equipped with an array of n momentum exchange devices. These devices are used as control actuators for manoeuvring spacecrafts. Momentum exchange devices include variable Speed CMGs, fixed speed CMGs, momentum wheels (MW), and gimballed momentum wheels (GMW). Such equations have been formulated by Oh and Vadali [88], Schaub and Junkins [101] and by many other researchers. They have discussed attitude dynamics/control of spacecraft equipped with CMGs. Some other researchers have used mixed CMGs and RW for development of attitude dynamic equation [109]. We shall generalise the work of Oh and Vadali [88] which presents mathematical model for fixed speed CMG clusters to a generic formulation for momentum exchange devices.

In the development of the equation of motion we shall consider three frames of reference. First is inertial frame $\mathcal{F}_A$, the angular velocity of the body is measured with respect to this frame. Second is body frame $\mathcal{F}_B$, fixed to body of the vehicle. And third is a reference frame $\mathcal{F}_{Gi}$ associated to ith device in the cluster. For a general case $\mathcal{F}_{Gi}$ is oriented with x-axis along wheel's spin axis, y-axis along gimbal axis and z-axis completes a right-handed axis system as shown in Fig. (3.1). It should be noted that this frame is fixed with respect to body frame for MWs but it can rotate about gimbal axis for gimballed devices. Now we shall discuss the kinematics involved in transforming device frame $\mathcal{F}_{Gi}$ to body frame $\mathcal{F}_B$. Let $\{\hat{\boldsymbol{g}}_{xi}, \hat{\boldsymbol{g}}_{yi}, \hat{\boldsymbol{g}}_{zi}\}$ be the unit basis of $\mathcal{F}_{Gi}$ expressed in $\mathcal{F}_B$ then we can define a transformation matrix from $\mathcal{F}_{Gi}$ to $\mathcal{F}_B$ as

$$\boldsymbol{C}_i^T = [\hat{\boldsymbol{g}}_{xi}\ \hat{\boldsymbol{g}}_{yi}\ \hat{\boldsymbol{g}}_{zi}]. \tag{3.4.10}$$

The orientation of $\mathcal{F}_{Gi}$ in body is determined by two angles the gimbal angle δ_i (in case of MWs it will be a fixed orientation angle) and a fixed configuration angle β_i. Then transformation matrix relating frame $\mathcal{F}_B$ to the frame $\mathcal{F}_{Gi}$ is defined as

$$\boldsymbol{C}_i(\delta_i, \beta_i) = \boldsymbol{C}_{gi}(\delta_i)\boldsymbol{C}_{ci}(\beta_i).$$

The matrix $\boldsymbol{C}_{ci}$ depends on particular configuration, whereas

$$\boldsymbol{C}_{gi}(\delta_i) = \begin{bmatrix} \cos\delta_i & 0 & -\sin\delta_i \\ 0 & 1 & 0 \\ \sin\delta_i & 0 & \cos\delta_i \end{bmatrix}.$$

In the frame $\mathcal{F}_{Gi}$

$$\dot{\boldsymbol{\delta}}_{\boldsymbol{i}} = \begin{bmatrix} 0 \\ \dot{\delta}_i \\ 0 \end{bmatrix} = \dot{\delta}_i \hat{\mathbf{j}}$$

and

$$\boldsymbol{\Omega}_{\boldsymbol{i}} = \begin{bmatrix} \Omega_i \\ 0 \\ 0 \end{bmatrix} = \Omega_i \hat{\mathbf{i}}$$

for $i = 1, \cdots, n$, where Ω_i is spin rate of the ith wheel. Here $\{\hat{\mathbf{i}}, \hat{\mathbf{j}}, \hat{\mathbf{k}}\}$ are standard unit basis of the frame $\mathcal{F}_{Gi}$ expressed in itself. The matrix $\boldsymbol{C}_i$ exhibits the following properties:

$$\dot{\boldsymbol{C}}_i^T = \boldsymbol{C}_i^T \dot{\boldsymbol{\delta}}_i^{\times}, \tag{3.4.11}$$

$$\dot{\boldsymbol{C}}_i = -\dot{\boldsymbol{\delta}}_i^{\times} \boldsymbol{C}_i, \tag{3.4.12}$$

$$\boldsymbol{C}_i \boldsymbol{u}^{\times} \boldsymbol{v} = (\boldsymbol{C}_i \boldsymbol{u})^{\times} \boldsymbol{C}_i \boldsymbol{v}, \tag{3.4.13}$$

where $\boldsymbol{u}$ and $\boldsymbol{v}$ are two arbitrary vectors.

Now we shall develop the dynamic equation. The Euler equation of the rigid body motion is

$$\dot{\boldsymbol{H}} + \boldsymbol{\omega} \times \boldsymbol{H} = \boldsymbol{T}_{ext}. \tag{3.4.14}$$

where $\boldsymbol{H}$ is the total angular momentum, $\boldsymbol{\omega}$ is angular velocity of the body and $\boldsymbol{T}_{ext}$ is external torque all expressed in the $\mathcal{F}_B$. The total angular momentum of the spacecraft

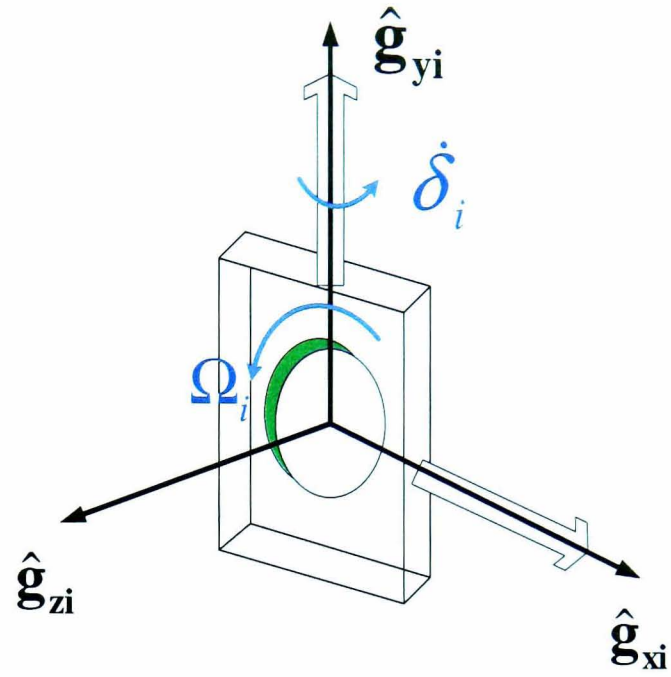

Figure 3.1: A single gimbal momentum exchange device.

equipped with a cluster of n momentum exchange devices expressed in $\mathcal{F}_B$ is

$$\boldsymbol{H} = \boldsymbol{I}\boldsymbol{\omega} + \sum_{i=1}^{n} \left(\boldsymbol{C}_i^T \boldsymbol{J}_i \dot{\boldsymbol{\delta}}_i + \boldsymbol{C}_i^T \boldsymbol{J}_i \boldsymbol{\Omega}_i \right). \tag{3.4.15}$$

Here $\boldsymbol{J}_i$ is the inertia matrix of the ith device expressed in $\mathcal{F}_{Gi}$ and $\boldsymbol{I}$ is total inertia matrix of the spacecraft expressed in $\mathcal{F}_B$. If $\boldsymbol{I}_s$ is inertia matrix of spacecraft without rotating devices then total inertia matrix of spacecraft is given by

$$\boldsymbol{I} = \boldsymbol{I}_s + \sum_{i=1}^{n} \boldsymbol{C}_i^T \boldsymbol{J}_i \boldsymbol{C}_i. \tag{3.4.16}$$

We can re-write total angular momentum equation (3.4.15) in a compact matrix form as

$$\boldsymbol{H} = \boldsymbol{I}\boldsymbol{\omega} + \boldsymbol{B}\dot{\boldsymbol{\delta}} + \boldsymbol{D}_o\boldsymbol{\Omega}. \tag{3.4.17}$$

Here $\boldsymbol{\Omega} = \begin{bmatrix} \Omega_1 \\ \Omega_2 \\ \vdots \\ \Omega_n \end{bmatrix}$ and $\dot{\boldsymbol{\delta}} = \begin{bmatrix} \dot{\delta}_1 \\ \dot{\delta}_2 \\ \vdots \\ \dot{\delta}_n \end{bmatrix}$ are n-dimensional vectors and

$$\boldsymbol{D}_o = [\boldsymbol{C}_1^T \boldsymbol{J}_1 \hat{\mathbf{i}} \;\; \boldsymbol{C}_2^T \boldsymbol{J}_2 \hat{\mathbf{i}} \;\; \ldots \;\; \boldsymbol{C}_n^T \boldsymbol{J}_n \hat{\mathbf{i}}], \tag{3.4.18}$$

$$\boldsymbol{B} = [\boldsymbol{C}_1^T \boldsymbol{J}_1 \hat{\mathbf{j}} \;\; \boldsymbol{C}_2^T \boldsymbol{J}_2 \hat{\mathbf{j}} \;\; \ldots \;\; \boldsymbol{C}_n^T \boldsymbol{J}_n \hat{\mathbf{j}}], \tag{3.4.19}$$

are matrices of order $3 \times n$. Substituting Eq. (3.4.17) in Eq. (3.4.14) we get

$$\begin{aligned} & \boldsymbol{I}\dot{\boldsymbol{\omega}} + \dot{\boldsymbol{I}}\boldsymbol{\omega} + \boldsymbol{B}\ddot{\boldsymbol{\delta}} + \dot{\boldsymbol{B}}\dot{\boldsymbol{\delta}} + \boldsymbol{D}_o\dot{\boldsymbol{\Omega}} \\ & + \dot{\boldsymbol{D}}_o\boldsymbol{\Omega} + \boldsymbol{\omega}^{\times}(\boldsymbol{I}\boldsymbol{\omega} + \boldsymbol{B}\dot{\boldsymbol{\delta}} + \boldsymbol{D}_o\boldsymbol{\Omega}) \;=\; \boldsymbol{T}_{ext}. \end{aligned} \tag{3.4.20}$$

In this equation some terms need further simplification and compactness. We shall explain the terms one by one and reduce them to some compact form.

1. Term $\boldsymbol{\omega}^{\times}\boldsymbol{D}_o\boldsymbol{\Omega}$

   Total angular momentum vector due to spinning wheels of momentum exchange devices is

   $$\boldsymbol{D}_o\boldsymbol{\Omega} = \sum_{i=1}^{n} \boldsymbol{C}_i^T \boldsymbol{J}_i \boldsymbol{\Omega}_i = \sum_{i=1}^{n} \boldsymbol{h}_i = \boldsymbol{h},$$

   where $\boldsymbol{h}_i$ is angular momentum of ith device. Rotation of the vehicle causes a rotation of the vector $\boldsymbol{h}$ with respect to inertial frame. It generates the torque $\boldsymbol{\omega}^{\times}\boldsymbol{h}$.

2. Term $\boldsymbol{\omega}^{\times}\boldsymbol{B}\dot{\boldsymbol{\delta}}$

   It is torque due to directional change of gimbal angular momentum caused by angular motion of vehicle. We define

   $$\boldsymbol{D}_2 = \boldsymbol{\omega}^{\times}\boldsymbol{B}$$

   to simplify the term.

3. Term $\dot{\boldsymbol{D}}_o\boldsymbol{\Omega}$

   It is torque due to directional change of angular momentum. We take

   $$\begin{aligned} \dot{\boldsymbol{D}}_o\boldsymbol{\Omega} &= \sum_{i=1}^{n} \dot{\boldsymbol{C}}_i^T \boldsymbol{J}_i \boldsymbol{\Omega}_i \\ &= \sum_{i=1}^{n} \boldsymbol{C}_i^T \dot{\boldsymbol{\delta}}_i^{\times} \boldsymbol{J}_i \boldsymbol{\Omega}_i \\ &= \sum_{i=1}^{n} \left(\boldsymbol{C}_i^T \hat{\mathbf{j}}\right)^{\times} \boldsymbol{C}_i^T \boldsymbol{J}_i \boldsymbol{\Omega}_i \dot{\delta}_i \\ &= \sum_{i=1}^{n} \hat{\boldsymbol{g}}_{yi}^{\times} \boldsymbol{h}_i \dot{\delta}_i \\ &= \boldsymbol{D}_1 \dot{\boldsymbol{\delta}}, \end{aligned}$$

where

$$\boldsymbol{D}_1 = [\hat{\boldsymbol{g}}_{y1}^{\times}\boldsymbol{h}_1 \;\; \hat{\boldsymbol{g}}_{y2}^{\times}\boldsymbol{h}_2 \;\; \ldots \;\; \hat{\boldsymbol{g}}_{yn}^{\times}\boldsymbol{h}_n]$$

4. Term $\dot{\boldsymbol{B}}\dot{\boldsymbol{\delta}}$

   This torque will only be generated when inertia matrix of devices $\boldsymbol{J}_i$ is not diagonal in $\mathcal{F}_{Gi}$. For a generic formulation we keep this term. We start with

$$\begin{aligned}
\dot{\boldsymbol{B}}\dot{\boldsymbol{\delta}} &= \sum_{i=1}^{n} \dot{\boldsymbol{C}}_i^T \boldsymbol{J}_i \dot{\boldsymbol{\delta}}_i \\
&= \sum_{i=1}^{n} \boldsymbol{C}_i^T \dot{\boldsymbol{\delta}}_i^{\times} \boldsymbol{J}_i \dot{\boldsymbol{\delta}}_i \\
&= \sum_{i=1}^{n} \left(\boldsymbol{C}_i^T \hat{\mathbf{j}}\right)^{\times} \boldsymbol{C}_i^T \boldsymbol{J}_i \hat{\mathbf{j}} \dot{\delta}_i^2 \\
&= \sum_{i=1}^{n} \hat{\boldsymbol{g}}_{yi}^{\times} \boldsymbol{b}_i \dot{\delta}_i^2 \\
&= \boldsymbol{D}_4 \mathrm{diag}(\dot{\delta}_1, \; \dot{\delta}_2, \ldots \; \dot{\delta}_n) \dot{\boldsymbol{\delta}}
\end{aligned}$$

   where

$$\boldsymbol{D}_4 = [\hat{\boldsymbol{g}}_{y1}^{\times}\boldsymbol{b}_1 \;\; \hat{\boldsymbol{g}}_{y2}^{\times}\boldsymbol{b}_2 \;\; \ldots \;\; \hat{\boldsymbol{g}}_{yn}^{\times}\boldsymbol{b}_n]$$

   and $\boldsymbol{b}_i = \boldsymbol{C}_i^T \boldsymbol{J}_i \hat{\mathbf{j}}$.

5. Term $\dot{\boldsymbol{I}}\boldsymbol{\omega}$

   It is torque due to variation of total inertia of spacecraft caused by internal moving parts. This term is given by

$$\begin{aligned}
\dot{\boldsymbol{I}}\boldsymbol{\omega} &= \sum_{i=1}^{n} \left(\dot{\boldsymbol{C}}_i^T \boldsymbol{J}_i \boldsymbol{C}_i \boldsymbol{\omega} + \boldsymbol{C}_i^T \boldsymbol{J}_i \dot{\boldsymbol{C}}_i \boldsymbol{\omega}\right) \\
&= \sum_{i=1}^{n} \left(\hat{\boldsymbol{g}}_{yi}^{\times} \boldsymbol{C}_i^T \boldsymbol{J}_i \boldsymbol{C}_i \boldsymbol{\omega} - \left(\boldsymbol{C}_i^T \boldsymbol{J}_i \hat{\mathbf{j}}\right)^{\times} \boldsymbol{\omega}\right) \dot{\delta}_i \\
&= \sum_{i=1}^{n} \left(\hat{\boldsymbol{g}}_{yi}^{\times} \boldsymbol{J}_i^b \boldsymbol{\omega} - \boldsymbol{b}_i^{\times} \boldsymbol{\omega}\right) \dot{\delta}_i \\
&= \boldsymbol{D}_3 \dot{\boldsymbol{\delta}},
\end{aligned}$$

   where $\boldsymbol{J}_i^b$ is inertia matrix of ith device expressed in $\mathcal{F}_B$ and

$$\boldsymbol{D}_3 = [\; \hat{\boldsymbol{g}}_{y1}^{\times} \boldsymbol{J}_1^b \boldsymbol{\omega} - \boldsymbol{b}_1^{\times} \boldsymbol{\omega}, \;\; \hat{\boldsymbol{g}}_{y2}^{\times} \boldsymbol{J}_2^b \boldsymbol{\omega} - \boldsymbol{b}_2^{\times} \boldsymbol{\omega}, \;\; \ldots \; \hat{\boldsymbol{g}}_{yn}^{\times} \boldsymbol{J}_n^b \boldsymbol{\omega} - \boldsymbol{b}_n^{\times} \boldsymbol{\omega} \;].$$

After substituting new forms of these terms in Eq. (3.4.20) we get

$$\begin{aligned} \boldsymbol{I}\dot{\boldsymbol{\omega}} &= -\boldsymbol{B}\ddot{\boldsymbol{\delta}} - (\boldsymbol{D}_1 + \boldsymbol{D}_2 + \boldsymbol{D}_3)\,\dot{\boldsymbol{\delta}} - \boldsymbol{D}_o\dot{\boldsymbol{\Omega}} - \boldsymbol{\omega}^{\times}(\boldsymbol{I}\boldsymbol{\omega} + \boldsymbol{h}) \\ &\quad -\boldsymbol{D}_4 \mathrm{diag}(\dot{\delta}_1,\ \dot{\delta}_2, \ldots\ \dot{\delta}_n)\dot{\boldsymbol{\delta}} + \boldsymbol{T}_{ext}. \end{aligned} \tag{3.4.21}$$

So far we have derived a generic dynamic equation of a spacecraft equipped with n momentum exchange devices. However, it is quite reasonable to assume that inertia matrix associated to each device is diagonal in respective $\mathcal{F}_{Gi}$ i.e.

$$\boldsymbol{J}_i = \mathrm{diag}\,(J_{xi}, J_{yi}, J_{zi})\,.$$

This would simplify the expressions for matrices $\boldsymbol{B}$, $\boldsymbol{D}_0$, $\boldsymbol{D}_1$, $\boldsymbol{D}_2$, $\boldsymbol{D}_3$,and $\boldsymbol{D}_4$ involved in Eq. (3.4.21). We explain this simplification in the following steps.

1. Matrix $\boldsymbol{B}$

   The ith column vector of matrix is

   $$\boldsymbol{b}_i = \boldsymbol{C}_i^T \boldsymbol{J}_i \hat{\mathbf{j}} = J_{yi}\hat{\boldsymbol{g}}_{yi}.$$

   Therefore,

   $$\boldsymbol{B} = [J_{y1}\hat{\boldsymbol{g}}_{y1}\ J_{y2}\hat{\boldsymbol{g}}_{y2}\ \ldots\ J_{yi}\hat{\boldsymbol{g}}_{yn}].$$

2. Matrix $\boldsymbol{D}_0$

   The ith column vector of matrix is

   $$\boldsymbol{C}_i^T \boldsymbol{J}_i \hat{\mathbf{i}} = J_{xi}\hat{\boldsymbol{g}}_{xi}.$$

   Therefore,

   $$\boldsymbol{D}_o = [J_{x1}\hat{\boldsymbol{g}}_{x1}\ J_{x2}\hat{\boldsymbol{g}}_{x2}\ \ldots\ J_{xn}\hat{\boldsymbol{g}}_{xn}].$$

3. Matrix $\boldsymbol{D}_1$

   The ith column vector of matrix is

   $$\hat{\boldsymbol{g}}_{yi}^{\times}\boldsymbol{h}_i = h_i\hat{\boldsymbol{g}}_{yi}^{\times}\hat{\boldsymbol{g}}_{xi} = -h_i\hat{\boldsymbol{g}}_{zi}.$$

   Therefore,

   $$\boldsymbol{D}_1 = [-h_1\hat{\boldsymbol{g}}_{z1}\ -h_2\hat{\boldsymbol{g}}_{z2}\ \ldots\ -h_n\hat{\boldsymbol{g}}_{zn}].$$

4. Matrix $\boldsymbol{D}_2$

   The ith column vector of matrix is

$$\begin{aligned}\boldsymbol{\omega}^{\times}\boldsymbol{b}_i &= J_{yi}\left(\omega_{xi}\hat{\boldsymbol{g}}_{xi}+\omega_{yi}\hat{\boldsymbol{g}}_{yi}+\omega_{zi}\hat{\boldsymbol{g}}_{zi}\right)^{\times}\hat{\boldsymbol{g}}_{yi}\\ &= -J_{yi}\omega_{zi}\hat{\boldsymbol{g}}_{xi}+J_{yi}\omega_{xi}\hat{\boldsymbol{g}}_{zi}\end{aligned}$$

   Here $(\omega_{xi},\omega_{yi},\omega_{zi})$ are components of $\boldsymbol{\omega}$ expressed in $\mathcal{F}_{Gi}$. Therefore,

$$\boldsymbol{D}_2=[-J_{y1}\omega_{z1}\hat{\boldsymbol{g}}_{x1}+J_{y1}\omega_{x1}\hat{\boldsymbol{g}}_{z1}\ -J_{y2}\omega_{z2}\hat{\boldsymbol{g}}_{x2}+J_{y2}\omega_{x2}\hat{\boldsymbol{g}}_{z2}\ \ldots\ -J_{yn}\omega_{zn}\hat{\boldsymbol{g}}_{xn}+J_{yn}\omega_{xn}\hat{\boldsymbol{g}}_{zn}]$$

5. Matrix $\boldsymbol{D}_3$

   The ith column vector of matrix is

$$\begin{aligned}\hat{\boldsymbol{g}}_{y1}^{\times}\boldsymbol{J}_1^{b}\boldsymbol{\omega}-\boldsymbol{b}_1^{\times}\boldsymbol{\omega} &= \hat{\boldsymbol{g}}_{yi}^{\times}\left(J_{xi}\omega_{xi}\hat{\boldsymbol{g}}_{xi}+J_{yi}\omega_{yi}\hat{\boldsymbol{g}}_{yi}+J_{zi}\omega_{zi}\hat{\boldsymbol{g}}_{zi}\right)-J_{yi}\omega_{zi}\hat{\boldsymbol{g}}_{xi}+J_{yi}\omega_{xi}\hat{\boldsymbol{g}}_{zi}\\ &= (J_{zi}-J_{yi})\omega_{zi}\hat{\boldsymbol{g}}_{xi}+(J_{yi}-J_{xi})\omega_{xi}\hat{\boldsymbol{g}}_{zi}\end{aligned}$$

   Therefore,

$$\begin{aligned}\boldsymbol{D}_3 &= [(J_{z1}-J_{y1})\omega_{z1}\hat{\boldsymbol{g}}_{x1}+(J_{y1}-J_{x1})\omega_{x1}\hat{\boldsymbol{g}}_{z1}\ \ (J_{z2}-J_{y2})\omega_{z2}\hat{\boldsymbol{g}}_{x2}+(J_{y2}-J_{x2})\omega_{x2}\\ &\quad \ldots\ (J_{zn}-J_{yn})\omega_{zn}\hat{\boldsymbol{g}}_{xn}+(J_{yn}-J_{xn})\omega_{xn}\hat{\boldsymbol{g}}_{zn}]\end{aligned}$$

6. Matrix $\boldsymbol{D}_4$

   The ith column vector of matrix is

$$\begin{aligned}\hat{\boldsymbol{g}}_{yi}^{\times}\boldsymbol{b}_i &= J_{yi}\hat{\boldsymbol{g}}_{yi}^{\times}\hat{\boldsymbol{g}}_{yi}\\ &= \boldsymbol{0}\end{aligned}$$

   Therefore, matrix $\boldsymbol{D}_4$ vanishes for diagonal inertia matrices $\boldsymbol{J}_i$.

In next section, we shall derive a feedback law for three-axis control of a spacecraft equipped with n momentum exchange devices.

3.5 Three-axis Feedback Control

In this section a state-feedback law is formulated for the attitude control of spacecraft with a cluster of n momentum exchange devices. Oh and Vadali [88] have used Liapunov stability theory in order to derive attitude feedback law for fixed speed CMG

clusters. Here we shall generalise their formulation for a cluster of momentum exchange devices. A detailed description of Liapunov theory can be found in Ref.[110]. If $(q_{of}, \boldsymbol{q}_f)$ is the desired quaternion and $\boldsymbol{\omega}_f$ is desired angular velocity then a candidate Liapunov function can be written as

$$V = \boldsymbol{q}_e^T \boldsymbol{q}_e + (q_{oe} - 1)^2 + \frac{1}{2}(\boldsymbol{\omega} - \boldsymbol{\omega}_f)^T K_1^{-1} I (\boldsymbol{\omega} - \boldsymbol{\omega}_f). \tag{3.5.22}$$

Where $\begin{bmatrix} q_{oe} \\ \boldsymbol{q}_e \end{bmatrix} = \tilde{\boldsymbol{q}}_e$ is error quaternion defined by Eq. (3.3.8) and $K_1^{-1} I > 0$.
The time derivative of Liapunov function is

$$\dot{V} = 2\boldsymbol{q}_e^T \dot{\boldsymbol{q}}_e + 2(q_{0e} - 1)\dot{q}_{0e} + (\boldsymbol{\omega} - \boldsymbol{\omega}_f)^T K_1^{-1} I (\dot{\boldsymbol{\omega}} - \dot{\boldsymbol{\omega}}_f) + \frac{1}{2}(\boldsymbol{\omega} - \boldsymbol{\omega}_f)^T K_1^{-1} \dot{I} (\boldsymbol{\omega} - \boldsymbol{\omega}_f). \tag{3.5.23}$$

We take

$$\begin{aligned} \dot{\boldsymbol{I}}\boldsymbol{\omega} &= \boldsymbol{D}_3 \dot{\boldsymbol{\delta}}, \\ \dot{\boldsymbol{I}}\boldsymbol{\omega}_f &= \boldsymbol{D}_5 \dot{\boldsymbol{\delta}}. \end{aligned}$$

By substituting $\dot{\boldsymbol{q}}_e$, $\dot{q}_{oe}$ from Equations (3.3.9) and $\dot{\boldsymbol{\omega}}$ from Eq. (3.4.21) and after simplifying we get

$$\dot{V} = -(\boldsymbol{\omega} - \boldsymbol{\omega}_f)^T \boldsymbol{K}_1^{-1} (-\boldsymbol{K}_1 \boldsymbol{q}_e + \boldsymbol{D}_0 \dot{\boldsymbol{\Omega}} + \boldsymbol{B}\ddot{\boldsymbol{\delta}} + \boldsymbol{D}\dot{\boldsymbol{\delta}} + \boldsymbol{\omega}^{\times}(\boldsymbol{I}\boldsymbol{\omega} + \boldsymbol{h}) - \boldsymbol{T}_{\boldsymbol{ext}} + \boldsymbol{I}\dot{\boldsymbol{\omega}}_f). \tag{3.5.24}$$

where

$$\boldsymbol{D} = \boldsymbol{D}_1 + \boldsymbol{D}_2 + 0.5(\boldsymbol{D}_3 + \boldsymbol{D}_5).$$

For $\dot{V}$ to be negative semi-definite we choose

$$-\boldsymbol{K}_1 \boldsymbol{q}_e + \boldsymbol{D}_0 \dot{\boldsymbol{\Omega}} + \boldsymbol{B}\ddot{\boldsymbol{\delta}} + \boldsymbol{D}\dot{\boldsymbol{\delta}} + \boldsymbol{\omega}^{\times}(\boldsymbol{I}\boldsymbol{\omega} + \boldsymbol{h}) - \boldsymbol{T}_{\boldsymbol{ext}} + \boldsymbol{I}\dot{\boldsymbol{\omega}}_f = \boldsymbol{K}_2(\boldsymbol{\omega} - \boldsymbol{\omega}_f). \tag{3.5.25}$$

where $\boldsymbol{K}_2 > 0$. Therefore,

$$\dot{V} = -(\boldsymbol{\omega} - \boldsymbol{\omega}_f)^T \boldsymbol{K}_1^{-1} \boldsymbol{K}_2 (\boldsymbol{\omega} - \boldsymbol{\omega}_f) < 0.$$

After rearranging Eq. (3.5.25) we get

$$\boldsymbol{D}_0 \dot{\boldsymbol{\Omega}} + \boldsymbol{B}\ddot{\boldsymbol{\delta}} + \boldsymbol{D}\dot{\boldsymbol{\delta}} = \boldsymbol{K}_1 \boldsymbol{q}_e + \boldsymbol{K}_2(\boldsymbol{\omega} - \boldsymbol{\omega}_f) - \boldsymbol{\omega}^{\times}(\boldsymbol{I}\boldsymbol{\omega} + \boldsymbol{h}) + \boldsymbol{T}_{\boldsymbol{ext}} - \boldsymbol{I}\dot{\boldsymbol{\omega}}_f. \tag{3.5.26}$$

The terms on right-hand-side of Eq. (3.5.26) constitute control torque $\boldsymbol{\tau}_c$ or required torque whereas terms on left-hand-side are output torque of exchange devices. Thus the equation

$$\boldsymbol{D}_0\dot{\boldsymbol{\Omega}} + \boldsymbol{B}\ddot{\boldsymbol{\delta}} + \boldsymbol{D}\dot{\boldsymbol{\delta}} = \boldsymbol{\tau}_c$$

is a general form of steering equation. If the gimbal commands $\ddot{\boldsymbol{\delta}}$, $\dot{\boldsymbol{\delta}}$ and rotor command $\dot{\boldsymbol{\Omega}}$ are such that the output torque and required torque satisfy the equation (3.5.26) then closed-loop system equation can be written as

$$I(\dot{\boldsymbol{\omega}} - \dot{\boldsymbol{\omega}}_f) = -\boldsymbol{K}_1\boldsymbol{q}_e - \boldsymbol{K}_2(\boldsymbol{\omega} - \boldsymbol{\omega}_f) - \frac{1}{2}(\boldsymbol{D}_3 - \boldsymbol{D}_5)\dot{\boldsymbol{\delta}}. \tag{3.5.27}$$

The $\dot{V}$ is apparently semi-negative definite as it is zero on trajectory defined by $\boldsymbol{\omega} = \boldsymbol{\omega}_f$. However, if we investigate using equation (3.5.27) $\boldsymbol{\omega} = \boldsymbol{\omega}_f$ results in $\boldsymbol{q}_e = 0$, which means $\dot{V}$ is negative definite. The key to this conclusion is the fact $\boldsymbol{D}_3 = \boldsymbol{D}_5$ and $\dot{\boldsymbol{\omega}} - \dot{\boldsymbol{\omega}}_f = 0$ for $\boldsymbol{\omega} = \boldsymbol{\omega}_f$. Therefore, closed loop system is globally asymptotically stable if gimbal commands $\ddot{\boldsymbol{\delta}}$, $\dot{\boldsymbol{\delta}}$ and rotor command $\dot{\boldsymbol{\Omega}}$ satisfy the equation (3.5.26) properly. Otherwise, asymptotic stability of closed loop system is not guaranteed. There are many possible choices for controller's gain guaranteeing the asymptotic stability of closed loop system but we choose gains of the form $\boldsymbol{K}_1 = k_1\boldsymbol{I}$ and $\boldsymbol{K}_2 = k_2\boldsymbol{I}$ where $k_1 > 0$ and $k_2 > 0$.

3.6 Momentum Wheels

The momentum/reaction wheels are the simplest form of momentum exchange devices. The direction of angular momentum of individual momentum wheel is fixed with respect to spacecraft body frame. Therefore, $\boldsymbol{D}_o$ is a fixed matrix. Obviously, there is no gimbal motion in this case i.e. $\ddot{\boldsymbol{\delta}} = \dot{\boldsymbol{\delta}} = 0$. After eliminating the gimbal motion from Eq. (3.4.21) it simplifies to the following form.

$$\boldsymbol{I}\dot{\boldsymbol{\omega}} = -\boldsymbol{\omega}^{\times}(\boldsymbol{I}\boldsymbol{\omega} + \boldsymbol{h}) - \boldsymbol{D}_0\dot{\boldsymbol{\Omega}} + \boldsymbol{T}_{ext} \tag{3.6.28}$$

In this case $\boldsymbol{D}_0\dot{\boldsymbol{\Omega}}$ is the output torque and $\boldsymbol{h}$ is the angular momentum of the wheels expressed in $\mathcal{F}_B$. In the previous section, we have derived a feedback law for a general three axis manoeuvre. For the momentum wheel based attitude control the general steering equation becomes

$$\boldsymbol{D}_0\dot{\boldsymbol{\Omega}} = \boldsymbol{\tau}_c.$$

The wheel acceleration command $\dot{\Omega}$ corresponding to a given commanded torque τ_c can be generated by inverting the matrix $\boldsymbol{D}_0$. Three reaction wheels, with each one's spin axis aligned to one of the satellite's body axis, makes up a simplest configuration for a three-axis control. The matrix $\boldsymbol{D}_0$ for this configuration is square and diagonal

$$\boldsymbol{D}_0 = \text{diag}(J_{x1}, J_{x2}, J_{x3}).$$

In this case control design can be carried out independently for each axis. In general more than three wheels are used in three-axis control for the purpose of redundancy. In that case the matrix $\boldsymbol{D}_0$ no longer remains square and its pseudo-inverse is used for generating wheel acceleration commands from torque command.

3.7 Control Moment Gyros

For a conventional single gimbal control moment gyro the spin rates of the wheels are kept constant i.e. $\dot{\Omega} = 0$. Usually wheel speed Ω_i of a CMG is much higher than slew rate so the term $\boldsymbol{D}_1\boldsymbol{\delta}$ dominates the output torque of CMGs and other terms involving matrices $\boldsymbol{B}_0$, $\boldsymbol{D}_2$ and $\boldsymbol{D}_3$ are comparatively negligible. To establish this fact we do a simple calculation of order of the magnitude of these terms for BILSAT-1 example. BILSAT-1 is a small earth-observation satellite equipped with a experimental payload of twin CMG system to control pitch axis attitude motion. The inertia matrix of satellite is

$$\boldsymbol{I}_s = \text{diag}\,(10, 10, 10)\,\text{kgm}^2.$$

The inertia matrix of ith CMG is

$$\boldsymbol{J}_i = \text{diag}\,(1.7, 1.2, 0.8) \times 10^{-4}\text{kgm}^2,$$

$i = 1, 2$. The angular momentum of ith CMG is $h_i = 0.28\text{Nms}$ for $i = 1, 2$. Maximum slew rate capability in pitch direction is

$$\begin{aligned} \omega_y^{max} &= 2h_i/I_y \\ &= 0.056\ \text{rad/s} \end{aligned}$$

In the Table (3.1) we compare the magnitudes of multiplying factors involved in the torque matrices. Therefore, it is clear that matrices $\boldsymbol{B}$, $\boldsymbol{D}_2$ and $\boldsymbol{D}_3$ are ignorable as

Table 3.1: Comparative magnitudes of matrices involved in Eq. (3.4.21).

Matrix	Multiplying factor	Magnitude
$\boldsymbol{D}_1$	h_i	0.28
$\boldsymbol{B}$	J_{yi}	1.2×10^{-4}
$\boldsymbol{D}_2$	$J_{yi}\omega^{max}$	6.72×10^{-6}
$\boldsymbol{D}_3$	$(J_{yi} - J_{zi})\omega^{max}$	2.24×10^{-6}

compared to $\boldsymbol{D}_1$. Here we have shown this comparison for a specific example. But this result is valid in general as h_i is much larger than $J_{yi}\omega^{max}$ for any CMG configuration. Therefore, after this simplification Eq. (3.4.17) and Eq. (3.4.21) can be re-written as

$$\boldsymbol{H} = \boldsymbol{I}\boldsymbol{\omega} + \boldsymbol{h}, \tag{3.7.29}$$

$$\boldsymbol{I}\dot{\boldsymbol{\omega}} = -\boldsymbol{\omega}^{\times}(\boldsymbol{I}\boldsymbol{\omega} + \boldsymbol{h}) - \boldsymbol{D}_1\dot{\boldsymbol{\delta}} + \boldsymbol{T}_{ext}. \tag{3.7.30}$$

For a cluster of fixed speed CMGs the output torque is given by

$$\boldsymbol{h} = \boldsymbol{D}_1\boldsymbol{\delta}. \tag{3.7.31}$$

In the absence of external torques $\boldsymbol{T}_{ext} = 0$ and after using Eq. (3.7.29) and Eq. (3.7.31) in Eq. (3.7.30) we get

$$\boldsymbol{I}\dot{\boldsymbol{\omega}} = -\boldsymbol{\omega}^{\times}\boldsymbol{H} - \dot{\boldsymbol{h}}. \tag{3.7.32}$$

The steering equation for a cluster of fixed speed CMGs is of the form

$$\boldsymbol{D}_1\dot{\boldsymbol{\delta}} = \boldsymbol{\tau}_c. \tag{3.7.33}$$

3.7.1 The Steering Problem

In general, steering problem seeks the solution of steering equation (3.7.33) by formulating a suitable steering law. Steering problem is an inverse kinematic problem. One may write a general form of steering law as

$$\dot{\boldsymbol{\delta}} = \boldsymbol{G}(\boldsymbol{\delta})\,\boldsymbol{\tau}_c. \tag{3.7.34}$$

Where matrix $\boldsymbol{G}(\boldsymbol{\delta})$ is supposed to be an inverse of matrix $\boldsymbol{D}_1$. If a steering law (3.7.34) exactly satisfy the steering equation (3.7.33) then Eq. (3.7.34) is termed as exact steering law. As a result of an exact gimbal steering the output torque exactly follows the

commanded torque. But we know that matrix $\boldsymbol{D}_1$ may become singular for certain gimbal angles, so in that case the inverse matrix $\boldsymbol{G}$ is not defined. Therefore, singularity is a major issue in gimbal steering problem. There are a number of situations where exact gimbal steering is not possible. For example, if gimbal angle trajectories generated by steering law (3.7.34) pass through singularity or vicinity of singularity then gimbal rate commands generated by the steering law have large excursions. If the torque requirement to follow these gimbal rate commands exceeds the torque capability of gimbal motors then exact steering is not possible. Alternatively, higher values of feedback gains may result in large value of commanded torque which may exceed the torque capability of CMG cluster. In that case also exact steering is not possible. In rest of the thesis, we have developed the methods for using exact steering in CMG clusters.

3.7.2 The Singularity Problem

The inverse kinematics of steering equation (3.7.33) for a cluster of n-CMGs involve the so-called singularity problem. The matrix $\boldsymbol{D}_1$ becomes singular for certain gimbal states for which output torque vectors (or matrix $\boldsymbol{D}_1$'s column vectors) $\boldsymbol{d}_i$ associated with $i = 1, 2, \cdots, n$ CMGs become co-planer. The normal to that plane gives singular direction vector $\hat{\boldsymbol{s}}$ as shown in Fig (3.2). Therefore, condition for singularity of matrix $\boldsymbol{D}_1$ is

$$\boldsymbol{D}_1^T \hat{\boldsymbol{s}} = \boldsymbol{0},$$

or

$$\boldsymbol{d}_i \left(\delta_i^s\right) . \hat{\boldsymbol{s}} = 0,$$

for $i = 1, 2, \cdots, n$ where δ_i^s is ith singular gimbal angle. As the vector $\boldsymbol{d}_i \left(\delta_i^s\right)$ is orthogonal to both gimbal axis $\hat{\boldsymbol{g}}_{yi}$ and singular direction vector $\hat{\boldsymbol{s}}$ so it can be written as

$$\boldsymbol{d}_i \left(\hat{\boldsymbol{s}}\right) = \sigma_i h_i \left|\hat{\boldsymbol{g}}_{yi} \times \hat{\boldsymbol{s}}\right|^{-1} \left(\hat{\boldsymbol{g}}_{yi} \times \hat{\boldsymbol{s}}\right) \tag{3.7.35}$$

provided $\hat{\boldsymbol{s}} \neq \pm \hat{\boldsymbol{g}}_{yi}$ and $\sigma_i = \pm 1$ for $i = 1, 2, \cdots, n$. Since $\boldsymbol{h}_i = \boldsymbol{d}_i \times \hat{\boldsymbol{g}}_{yi}$, the singularity condition for an ith angular momentum vector is given by

$$\boldsymbol{h}_i^s = \sigma_i h_i \left|\hat{\boldsymbol{g}}_{yi} \times \hat{\boldsymbol{s}}\right|^{-1} \left(\hat{\boldsymbol{g}}_{yi} \times \hat{\boldsymbol{s}}\right) \times \hat{\boldsymbol{g}}_{yi}. \tag{3.7.36}$$

The total singular momentum is the vector sum of the individual momenta $\boldsymbol{h}_i^s$ placed end-to-end in arbitrary order

$$\boldsymbol{h}^s = \sum_{i=1}^{n} \left(\sigma_i h_i \left| \hat{\boldsymbol{g}}_{yi} \times \hat{\boldsymbol{s}} \right|^{-1} \left(\hat{\boldsymbol{g}}_{yi} \times \hat{\boldsymbol{s}} \right) \times \hat{\boldsymbol{g}}_{yi} \right). \tag{3.7.37}$$

The projection of an ith angular momentum vector on singular direction is given by

$$\boldsymbol{h}_i^s . \hat{\boldsymbol{s}} = \sigma_i h_i \left| \hat{\boldsymbol{g}}_{yi} \times \hat{\boldsymbol{s}} \right|. \tag{3.7.38}$$

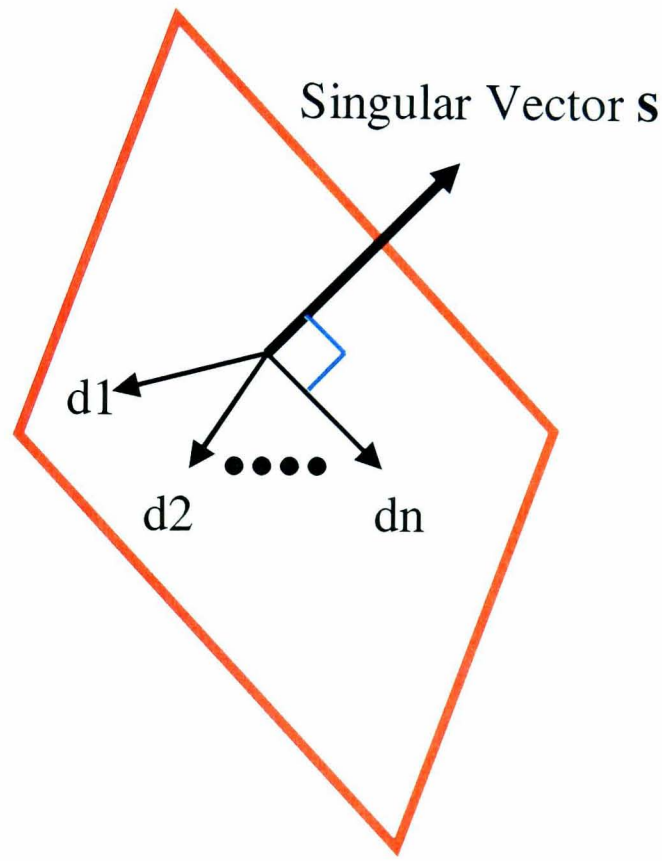

Figure 3.2: Singular direction vector.

If angular momentum vector associated with a cluster of CMGs is maximally (for all $\sigma_i > 0$) or minimally (for all $\sigma_i < 0$) projected along the singular direction then the singularity is called saturation singularity. It forms a saturation singular surface in momentum space or momentum envelope as shown in Fig. (3.3), representing the maximum momentum capability in a given direction. If the total angular momentum corresponding to a singular surface is inside the momentum envelope (with mixed sign

combinations of σ_i) then the singularity is called internal singularity. These singular surfaces of angular momentum are constructed by varying the unit vector $\hat{\boldsymbol{s}}$ in three-dimensional space with different combinations of signs of σ_i. For a cluster of n CMGs, there are 2^n possible combinations of signs of σ_i but there are only 2^{n-1} different singular surfaces. When $\hat{\boldsymbol{s}} = \pm\hat{\boldsymbol{g}}_{yi}$ then vector $\boldsymbol{h}_i$ rotates about gimbal direction $\hat{\boldsymbol{g}}_{yi}$ and which appears as a circular hole on the momentum envelope. There are $2n$ holes on the momentum envelope of a cluster of n CMGs. These holes can be seen in Fig. (3.3) for a four CMG cluster example.

Gimbal lock at a singular configuration may occur when the direction of required or commanded torque $\boldsymbol{\tau}_c$ is along singular direction $\hat{\boldsymbol{s}}$ of matrix $\boldsymbol{D}_1$ and no net torque is available in the required direction. In this case vector $\boldsymbol{\tau}_c$ lies in the null-space of matrix $\boldsymbol{D}_1$ and thus a CMG cluster is unable to produce any torque in desired direction.

In a redundant CMG cluster it is possible to change the gimbal configuration without changing the total angular momentum of the cluster. This motion of gimbals is called null motion as it produces no torque on spacecraft. In the redundant CMG clusters (with $n > 3$) there exist $n - 3$ degrees of null motion. Mathematically, it is the solution of homogeneous steering equation

$$\boldsymbol{D}_1\dot{\boldsymbol{\delta}} = 0.$$

The saturation singularities can not be escaped by null motion, whereas internal singularities are further classified as elliptic and hyperbolic singularities for being not escapable and escapable by null motion respectively. A detailed geometric description of the singularity problem of a CMG cluster can be found in the classic work by Margulies and Aubrun [83].

3.7.3 Overview of Some Pseudo-Inverse Based Steering Laws

The well-known steering law for obtaining the gimbal rates from Eq. (3.7.33) is based on pseudo-inverse of matrix $\boldsymbol{D}_1$ and it is also known as Moore-Penrose (MP) steering law. This steering law is given by

$$\dot{\boldsymbol{\delta}} = \boldsymbol{D}_1^T(\boldsymbol{D}_1\boldsymbol{D}_1^T)^{-1}\boldsymbol{\tau}_c. \tag{3.7.39}$$

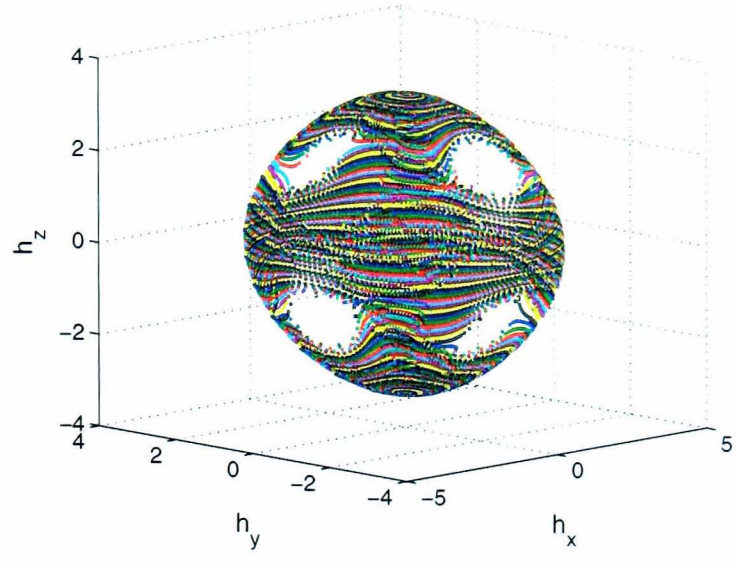

Figure 3.3: Momentum envelope of four CMG pyramid system.

This steering law minimizes the norm $\|\dot{\boldsymbol{\delta}}\|$ and it gives exact gimbal steering with acceptable gimbal rates provided $\boldsymbol{D}_1\boldsymbol{D}_1^T$ is not singular or $\boldsymbol{rank}(\boldsymbol{D}_1) = 3$. However, it generates excessively large gimbal rates $\dot{\boldsymbol{\delta}}$ in the vicinity of singularity and also it drives CMG cluster towards elliptic singularity.

The singularity robust (SR) inverse is obtained by minimizing a mixed norm of gimbal rate $\|\dot{\boldsymbol{\delta}}\|$ and torque error $\|\boldsymbol{D}_1\dot{\boldsymbol{\delta}} - \boldsymbol{\tau}_c\|$ with respect to $\dot{\boldsymbol{\delta}}$ [12, 88]

$$\dot{\boldsymbol{\delta}} = \boldsymbol{D}_1^T\left(\boldsymbol{D}_1\boldsymbol{D}_1^T + \lambda\mathbf{1}\right)^{-1}\boldsymbol{\tau}_c, \tag{3.7.40}$$

where λ is weighting factor and robustness measure of the solution. And $\mathbf{1}$ is a 3×3 identity matrix. It can be noted that SR inverse becomes the MP inverse for $\lambda = 0$. By introducing λ the solution becomes singularity robust but no longer remains exact. Thus λ can be chosen as

$$\lambda = \lambda_0 \exp(-\mu \det(\boldsymbol{D}_1\boldsymbol{D}_1^T)) \tag{3.7.41}$$

to provide a smooth transition from MP inverse ($\lambda = 0$) to SR inverse as system approaches to singularity ($\det(\boldsymbol{D}_1\boldsymbol{D}_1^T) \approx 0$). Therefore, in the vicinity of singularity, output torque produced by SR inverse deviates from commanded torque. When the commanded torque happens to lie in null-space i.e. $\boldsymbol{D}_1^T\boldsymbol{\tau}_c = 0$ then the gimbal rates generated by SR inverse become zero and gimbals are locked in singular configuration until commanded torque changes its direction. The SR logic often unnecessarily

constraint the operational envelope of CMG system by driving it to elliptic singularity. However, the Generalized Singularity Robust (GSR) logic proposed by Wie [134] can utilize the larger momentum envelope of a CMG cluster by introducing a pointing error. The GSR logic is

$$\dot{\boldsymbol{\delta}} = \boldsymbol{D}_1^T \left(\boldsymbol{D}_1 \boldsymbol{D}_1^T + \lambda \boldsymbol{E}\right)^{-1} \boldsymbol{\tau}_c = \boldsymbol{D}_1^{\#} \boldsymbol{\tau}_c, \tag{3.7.42}$$

with

$$\boldsymbol{E} = \begin{bmatrix} 1 & \epsilon_3 & \epsilon_2 \\ \epsilon_3 & 1 & \epsilon_1 \\ \epsilon_2 & \epsilon_1 & 1 \end{bmatrix} > 0$$

with $\epsilon_i = \epsilon_0 \sin(\nu t + \phi_i)$. And λ is defined as in Eq. (3.7.41). Here λ and ϵ_i are chosen properly such that $\boldsymbol{D}_1^{\#}\boldsymbol{\tau}_c \neq 0$ for any non-zero value of $\boldsymbol{\tau}_c$. The GSR steering logic passes the internal singularity quit rapidly but fail to pass saturation singularities for any choice of λ and ϵ_i. Therefore, Wie [134] developed a weighted GSR steering which was claimed to escape/pass saturation singularities for a proper choice of weight matrix.

$$\dot{\boldsymbol{\delta}} = \boldsymbol{W}\boldsymbol{D}_1^T \left(\boldsymbol{D}_1 \boldsymbol{W} \boldsymbol{D}_1^T + \lambda \boldsymbol{E}\right)^{-1} \boldsymbol{\tau}_c, \tag{3.7.43}$$

where $\boldsymbol{W} > 0$ is a weight matrix but its choice is not obvious.

3.8 Variable Speed CMGs

The variable speed CMGs have capability of operating in dual mode i.e MW and CMG mode simultaneously. Extra degrees of freedom available in this case are useful not only in attitude control but can also be used in power storage. A cluster of the variable speed CMGs is governed by the following dynamic equation

$$\boldsymbol{I}\dot{\boldsymbol{\omega}} = -\boldsymbol{\omega}^{\times}(\boldsymbol{I}\boldsymbol{\omega} + \boldsymbol{h}) - \boldsymbol{D}_0\dot{\boldsymbol{\Omega}} - \boldsymbol{D}_1\dot{\boldsymbol{\delta}} + \boldsymbol{T}_{ext}. \tag{3.8.44}$$

Thus the steering equation for a variable speed CMG cluster is

$$\boldsymbol{D}_o\dot{\boldsymbol{\Omega}} + \boldsymbol{D}_1\dot{\boldsymbol{\delta}} = \boldsymbol{\tau}_c.$$

This steering equation is solved to find the gimbal rate command and wheel acceleration commands from commanded torque. This equation can also be written in more compact form as

$$\boldsymbol{Q}\dot{\Gamma} = \boldsymbol{\tau}_c,$$

where $\Gamma = \begin{bmatrix} \Omega \\ \delta \end{bmatrix}$ and $\boldsymbol{Q} = \begin{bmatrix} \boldsymbol{D}_0 & \boldsymbol{D}_1 \end{bmatrix}$.

Schaub and Junkins [98, 100, 101, 102] developed singularity avoiding steering laws for attitude control of spacecraft using variable speed CMG cluster.

$$\dot{\Gamma} = \boldsymbol{W}\boldsymbol{Q}^T(\boldsymbol{Q}\boldsymbol{W}\boldsymbol{Q}^T)^{-1}\boldsymbol{\tau}_c, \tag{3.8.45}$$

where $\boldsymbol{W}$ is a $2n \times 2n$ diagonal weight matrix and it is defined as

$$\boldsymbol{W} = \begin{bmatrix} \boldsymbol{W}_\Omega^0 \exp\left(-\mu \det\left(\boldsymbol{D}_1\boldsymbol{D}_1^T\right)\right) & 0 \\ 0 & \boldsymbol{W}_\delta \end{bmatrix}.$$

Here $\boldsymbol{W}_\delta$ and $\boldsymbol{W}_\Omega^0$ are weight matrices of conventional CMG mode and RW mode respectively. The RW mode is used only when CMG mode approaches singularity. It is interesting to note that there is no modification in pseudo-inverse because the square matrix $\boldsymbol{Q}\boldsymbol{W}\boldsymbol{Q}^T$ is non-singular as long as the gimbal axes of at-least two or more CMGs are not parallel (or linearly independent). In this case CMGs are working in dual mode (RW and CMG) to avoid singularities, however, RW mode is used only when conventional CMG mode approaches singularity. They also developed null motion for variable speed CMG cluster to avoid wheel speed excursions generated by steering law (3.8.45)in Ref. [101].

We have attempted in Ref. [72] a combination of GSR steering law operating in CMG mode with MW mode of variable speed CMGs to get good pointing accuracy by compensating the attitude drift caused by GSR steering MW mode. If we allow the variation in wheel speed of CMGs in the Generalized Singularity Robust (GSR) law then the modified steering law termed as Generalized Variable Speed Singularity Robust (GVSSR) Steering law can be written as

$$\dot{\Gamma} = \boldsymbol{W}_1\boldsymbol{Q}^T\left(\boldsymbol{Q}\boldsymbol{W}_1\boldsymbol{Q}^T + \boldsymbol{\Lambda}\right)^{-1}\boldsymbol{\tau}_c + \boldsymbol{W}_2\boldsymbol{Q}^T(\boldsymbol{Q}\boldsymbol{W}_2\boldsymbol{Q}^T)^{-1}\boldsymbol{\tau}_{er}, \tag{3.8.46}$$

where

$$\boldsymbol{\Lambda} = \lambda \begin{bmatrix} 1 & l_3 & l_2 \\ l_3 & 1 & l_1 \\ l_2 & l_1 & 1 \end{bmatrix} > 0,$$

and

$$\lambda = \lambda_0 \exp\left(-\mu \det\left(\boldsymbol{D}_1\boldsymbol{D}_1^T\right)\right),$$

τ_{er} is error torque vector, W_1 and W_2 are suitably chosen weight matrices. These matrices are chosen such that CMG mode dominates in part one containing W_1 and RW dominates in part two containing W_2 of Eq. (3.8.46). The drift in attitude of satellite caused by GSR steering law of CMG mode is now corrected by RW mode against the error torque. Simulation results of this steering can be found in Ref. [72].

Combined attitude and power tracking using variable speed CMGs is studied by many researchers [93, 126, 139, 140]. Yoon and Tsiotras [139] have presented a combined steering approach of attitude and power control for spacecrafts using VSCMGs. They used an indirect adaptive control to account for uncertain inertia properties of a modular spacecraft. A systematic study of singularities associated with the VSCMG clusters employed for combined attitude and power tracking is presented in Ref. [140]. They managed to develop a criterion to determine usable momentum workspace based on singular surface argument.

The main focus of this thesis is to study the steering problem of fixed speed CMGs for attitude control only and this brief overview of variable speed CMGs is included to complete the discussion on momentum exchange devices.

Chapter 4

Exact Steering Law for Twin CMG Systems

4.1 Introduction

This chapter presents a detailed analysis of an exact steering problem for twin CMG systems for the case of single-axis rest-to-rest manoeuvre of a satellite. The analysis of twin CMG systems' exact steering is relatively simpler and provides deeper insights into a general CMG steering problem. Exact steering is possible when commanded torque matches the torque capability of a CMG cluster and also gimbal trajectories avoid singularities. Therefore, we can determine feedback gains for control law such that output torque exactly follows the commanded torque while avoiding the singularity and using the full momentum capability. In our approach analytical solutions of exact steering problem are used to determine the feedback gains. Various forms of Singularity Robust (SR) Steering Laws (Eq. (3.7.40), Eq. (3.7.42), Eq. (3.7.43)) have capability of passing or escaping the singularity at the cost of inaccuracy, but it has not been discussed that how one can avoid a singularity at first place (see Ref. [12, 88, 134]). As we know from experience singularities potentially degrade the performance of closed-loop system whether or not SR laws are used (see Fig. (4.9)). So first line of defence against singularity ought to be 'avoidance'. And in this chapter we have attempted to address singularity avoidance issue using exact CMG steering by selecting suitable feedback gains. Different features of singularity avoiding solution curves of exact steering prob-

lem have been studied for both with and without explicit gimbal rate constraint cases. The exact singularity avoiding solutions are near-optimal for the manoeuvres for which twin CMG systems have been designed. It is found that for the fixed values of singularity avoiding gains satellite's attitude phase-plane can be divided by a separatrix into two regions, one where singularity avoidance is possible and the other where it is not possible. It is observed that by gradually decreasing feedback gains the singularity avoiding region grows larger. This fact is used to develop variable gains for singularity avoidance using Exact Steering Law so that any manoeuvre could avoid singularity with faster rate. Finally, these techniques of finding singularity avoiding gains for Exact Steering Law are simulated for BILSAT-1 example. It has been shown to be an effective way of avoiding singularities while achieving the faster slew manoeuvres for twin CMG systems.

4.2 Twin CMG Systems

4.2.1 Mathematical Formulation

We consider a satellite equipped with two identical CMGs placed symmetrically with skew angle β as shown in Fig. (4.1). As CMGs are inertial actuators, so total angular momentum of satellite is conserved in absence of external torque. We can re-write Eq. (3.7.29) as

$$\boldsymbol{I\omega} + \boldsymbol{h} = \boldsymbol{H}_o.$$

Where $\boldsymbol{I}$ is inertia matrix of the satellite, $\boldsymbol{\omega}$ is the angular velocity vector of the satellite, $\boldsymbol{h}$ is the angular momentum vector of the CMGs and $\boldsymbol{H}_o$ is the momentum bias or total angular momentum expressed in satellite body co-ordinates. The dynamics of this system is governed by Eq. (3.7.32)

$$\boldsymbol{I\dot{\omega}} = -\dot{\boldsymbol{h}} - \boldsymbol{\omega} \times \boldsymbol{H}_o. \tag{4.2.1}$$

The vector $\boldsymbol{h}$ for the twin CMG system is given by

$$\boldsymbol{h} = h_{cmg} \begin{bmatrix} -\cos\delta_1 + \cos\delta_2 \\ \cos\beta\,(-\sin\delta_1 + \sin\delta_2) \\ \sin\beta\,(\sin\delta_1 + \sin\delta_2) \end{bmatrix}, \tag{4.2.2}$$

where $\delta_i, i = 1, 2$ is gimbal angle of the ith CMG and h_{cmg} is the angular momentum associated with each CMG. The output torque of the CMGs is governed by Eq. (3.7.31)

$$\dot{\boldsymbol{h}} = \boldsymbol{D_1}\dot{\boldsymbol{\delta}},$$

where $\boldsymbol{D_1}$ is the Jacobian matrix $\frac{\partial \boldsymbol{h}}{\partial \boldsymbol{\delta}}$, that is

$$\boldsymbol{D_1} = h_{cmg}\begin{bmatrix} \sin\delta_1 & -\sin\delta_2 \\ -\cos\beta\cos\delta_1 & \cos\beta\cos\delta_2 \\ \sin\beta\cos\delta_1 & \sin\beta\cos\delta_2 \end{bmatrix}. \tag{4.2.3}$$

Single axis manoeuvres can be achieved by moving the two gimbals symmetrically or anti-symmetrically. A pitch manoeuvre is achieved if we choose $\dot{\delta}_1 = -\dot{\delta}_2$ (and so $\delta_1 = -\delta_2$, provided the gimbal angles are initially at zero). Similarly a yaw manoeuvre is achieved by $\dot{\delta}_1 = \dot{\delta}_2$. As the direction of the torque is always perpendicular to the x-axis for symmetric (anti-symmetric) gimbal motion, so single axis roll manoeuvres can not be achieved in this configuration of two CMGs.

In this chapter, we consider a rest-to-rest pitch axis manoeuvre. Thus we choose $\delta_1 = -\delta_2$, in Eq. (4.2.2) and Eq. (4.2.3) to get simplified forms for $\boldsymbol{h}$ and $\boldsymbol{D_1}$ respectively, and then substitute in Eq. (4.2.1). Moreover, for a rest-to-rest manoeuvre, $\boldsymbol{\omega(0)} = \boldsymbol{0}$ and $\boldsymbol{\delta(0)} = \boldsymbol{0}$, so we get $\boldsymbol{H}_o = \boldsymbol{0}$. Hence Eq. (4.2.1) is simplified to a set of component equations as

$$\begin{aligned} I_x\dot{\omega}_x &= 0, \\ I_y\dot{\omega}_y &= -2h_{cmg}\cos\beta\cos\delta_2\dot{\delta}_2, \\ I_z\dot{\omega}_z &= 0. \end{aligned} \tag{4.2.4}$$

Thus motion is purely about y-axis and the configuration of two CMGs locked in anti-symmetric motion can be represented by a single gimbal angle variable δ in Eq. (4.2.4). We can ignore the x and z components and omit the subscripts y. As a result the equation for single axis attitude dynamics of a satellite with twin CMGs takes the form

$$I\dot{\omega} = -2h_{cmg}\cos\beta\cos\delta\dot{\delta}. \tag{4.2.5}$$

The right hand side of Eq. (4.2.5) is the output torque generated by the CMGs and is governed by the gimbal steering law. The satellite attitude kinematics is represented by

an angle variable θ with

$$\dot{\theta} = \omega. \tag{4.2.6}$$

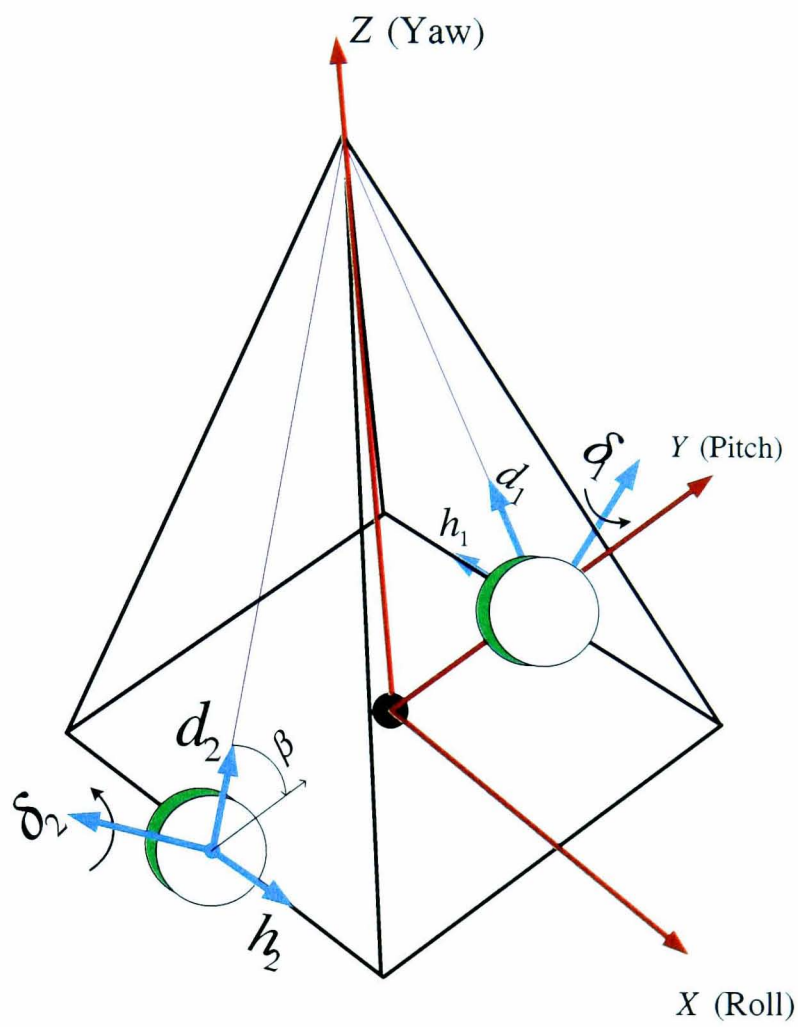

Figure 4.1: Twin CMG arrangement.

4.2.2 Feedback Law and CMG Steering

A steering law determines the gimbal dynamics from the control torque. A Liapunov approach is used to determine the control torque needed to stabilize the equilibrium point $(0, 0)$ in the (θ, ω) plane asymptotically. The Liapunov function V can be chosen to be

$$V = \frac{1}{2}k_\theta I\theta^2 + \frac{1}{2}I\omega^2, \tag{4.2.7}$$

where k_θ is a positive constant. The time derivative of the Liapunov function is

$$\dot{V} = k_\theta I\theta\dot{\theta} + I\omega\dot{\omega}.$$

Using Eq. (4.2.5) and Eq. (4.2.6) gives

$$\dot{V} = \omega \left(k_\theta I\theta - 2h_{cmg} \cos\beta \cos\delta\dot{\delta} \right).$$

Now, if

$$2h_{cmg} \cos\beta \cos\delta\dot{\delta} = k_\theta I\theta + k_\omega I\omega, \tag{4.2.8}$$

then

$$\dot{V} = -k_\omega I\omega^2 \leq 0,$$

where k_ω is a positive constant. Thus the feedback control torque required to manoeuvre the satellite comes out to be a PD controller in Eq. (4.2.8), and then the steering law is

$$\dot{\delta} = \frac{k_\theta\theta + k_\omega\omega}{\omega_m \cos\delta}, \tag{4.2.9}$$

where

$$\omega_m = \frac{2h_{cmg}\cos\beta}{I}.$$

If we integrate Eq. (4.2.5) for initial conditions $\omega(0) = 0$ and $\delta(0) = 0$ then we get

$$\omega = -\omega_m \sin\delta, \tag{4.2.10}$$

so ω_m is the maximum slew rate of the satellite.

Moreover, the output torque (the LHS of Eq. (4.2.8)) follows the control torque provided the CMG system is away from the singularity at $\delta = \pm\frac{\pi}{2}$ and its odd multiples.

4.2.3 Harmonic Oscillator Equations

The variables ω and δ depend on each other through Eq. (4.2.10)and only two independent state variables are needed to represent the system i.e. either (θ, ω) or, equivalently, (δ, θ).

The equations in the (δ, θ) plane are obtained by eliminating the ω in Eq. (4.2.9) and Eq. (4.2.10)

$$\begin{aligned} \dot{\delta} &= \frac{k_1\theta - k_\omega \sin\delta}{\cos\delta}, \\ \dot{\theta} &= -\omega_m \sin\delta. \end{aligned} \tag{4.2.11}$$

Here $k_1 = k_\theta/\omega_m$ is a positive constant. This model is nonlinear and also it is singular for $\delta = \pm\frac{\pi}{2}$.

On the other hand the equations in the (θ, ω) plane are linear

$$\begin{aligned} \dot{\omega} &= -k_\theta\theta - k_\omega\omega, \\ \dot{\theta} &= \omega. \end{aligned} \tag{4.2.12}$$

These are equations for a damped harmonic oscillator and have a well-known closed-form solution. Note however that ω must satisfy the constraint $|\omega| \leq \omega_m$. Since the satellite-CMG dynamic interaction and singular states are more explicit in the (δ, θ) plane (or nonlinear model (4.2.11)), the singularity avoiding trajectories are designed in this plane. These trajectories are then transformed to the (θ, ω) plane to study the closed-loop response of the satellite.

4.2.4 Incorporating the Gimbal Rate Constraint

In practice a gimbal motor has a gimbal rate saturation limit and so the gimbal rate requested by a steering law is not always executable. This fact is incorporated in the model to get more realistic solutions. Assume $|\dot{\delta}| \leq \alpha$, where α is a positive constant. Then the model (4.2.11) can be replaced by

$$\begin{aligned} \dot{\delta} &= \begin{cases} \alpha & , \quad \dot{\delta} \geq \alpha \\ \frac{k_1\theta - k_\omega \sin\delta}{\cos\delta} & , \quad |\dot{\delta}| < \alpha \\ -\alpha & , \quad \dot{\delta} \leq -\alpha \end{cases} \\ \dot{\theta} &= -\omega_m \sin\delta. \end{aligned} \tag{4.2.13}$$

In the (θ, ω) plane the gimbal rate constraint is transformed into an angular acceleration constraint by using the relation

$$\dot{\delta} = \frac{-\dot{\omega}}{\sqrt{\omega_m^2 - \omega^2}}.$$

The modified closed-loop model is

$$\begin{aligned} \dot{\omega} &= \begin{cases} \alpha\sqrt{\omega_m^2 - \omega^2} & , \quad \dot{\omega} \geq \alpha\sqrt{\omega_m^2 - \omega^2} \\ -k_\theta\theta - k_\omega\omega & , \quad |\dot{\omega}| < \alpha\sqrt{\omega_m^2 - \omega^2} \\ -\alpha\sqrt{\omega_m^2 - \omega^2} & , \quad \dot{\omega} \leq -\alpha\sqrt{\omega_m^2 - \omega^2} \end{cases} \\ \dot{\theta} &= \omega \quad , \quad |\omega| \leq \omega_m. \end{aligned} \tag{4.2.14}$$

We shall discuss in detail the effect of this gimbal rate saturation on solutions in the following sections.

4.3 Study of the Exact Steering Law

4.3.1 Phase Plane Representation

In this subsection, we will discuss the qualitative features of the nonlinear system (4.2.11) in the (δ, θ) plane. The system (4.2.11) has equilibrium points at $(\pm n\pi, 0)$, where $n = 0, 1, 2, \cdots$. It can be shown that these are all stable equilibria. The gimbal dynamics is singular at $\delta = \frac{(2n+1)\pi}{2}$, defining singularity manifolds (with undefined $\dot{\delta}$) in the phase plane represented by the solid vertical lines in Fig. (4.2). The nullcline defined by $\dot{\delta} = 0$ is a curve

$$\theta = \frac{k_\omega}{k_1} \sin \delta,$$

which is represented by the dashed sinusoidal curve in Fig. (4.2). The nullcline intersects the singularity manifolds at points $A(\frac{(4n+1)\pi}{2}, \frac{k_\omega}{k_1})$ and $A'(\frac{(4n-1)\pi}{2}, -\frac{k_\omega}{k_1})$, which are termed as critical points because of their special significance as $\dot{\delta}$ has a finite value at these points. In Fig. (4.2) the phase plane is divided into several regions by the nullcline and singularity manifolds. The control torque and $\cos\delta$, change sign at the boundaries of these regions. In region R_1 (and R_1') the $\cos\delta$ term in the denominator of the steering law in Eq. (4.2.11) has the opposite sign to that of the control torque (numerator), so the singularity behaves like an attractor and as a result traps the dynamics in its neighbourhood. On the other hand, the singularity behaves like a repeller in region R_2 (and R_2') where the numerator and the denominator of the steering law have the same signs. Therefore, the singularity can only be avoided if a trajectory starting in region R_1 enters region R_2 before hitting the singularity manifold. Otherwise a trajectory hits the singularity attractor in region R_1 and remains bounded in its neighbourhood until the critical point A is approached. Here trajectory enters region R_2 and is repelled by the singularity. The trajectory passing through the critical point A defines a separatrix between the inner trajectories (entering region R_2 without hitting the singularity) and the outer trajectories (hitting the singularity). The intercept of the separatrix trajectory with the $\delta = 0$ axis defines a critical value for the initial attitude angle θ_o such that

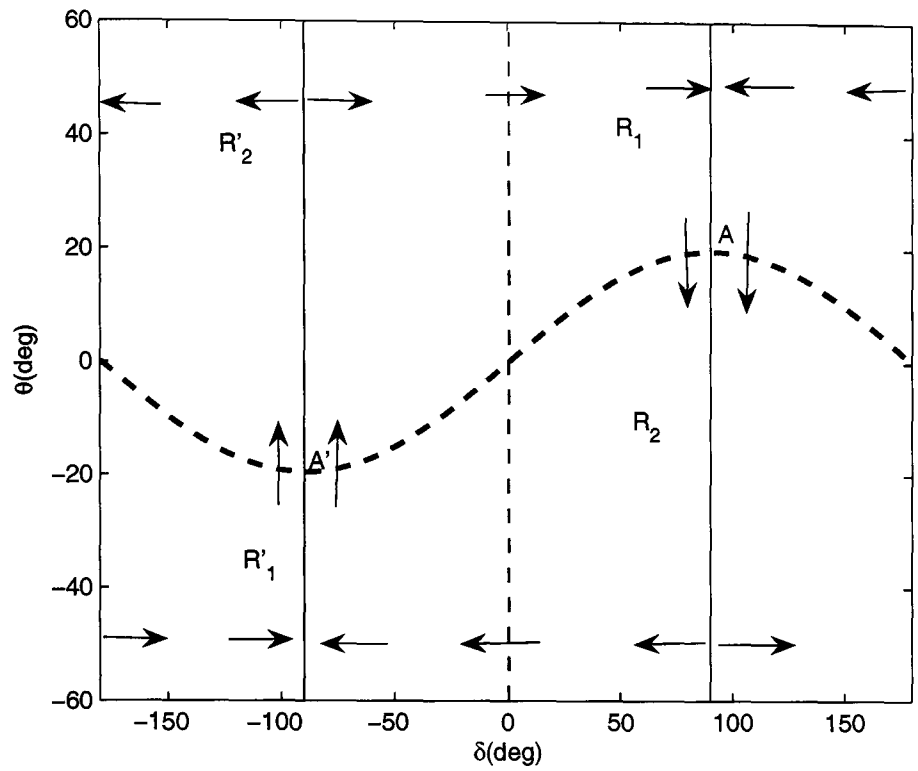

Figure 4.2: The singularity and nullcline in the (δ, θ) plane.

any trajectory starting above this limit is bound to hit the singularity. The separatrix trajectory is used to determine the feedback gains k_θ and k_ω needed to obtain a required agility while avoiding the singularity. Figure (4.3) shows a complete (δ, θ) phase portrait of the Eq. (4.2.11). One can see that a separatrix trajectory passes through the critical point A. The trajectories inside separatrix are singularity avoiding ones while those outside it hit the singularity. One can see jittering on the singularity attractor because $\dot{\delta}$ is undefined at $\delta = \frac{\pi}{2}$.

In the next subsection, we will solve the system in the (θ, ω) plane to obtain the exact analytic solutions which will then be used to calculate singularity avoiding feedback gains.

4.3.2 Time-Domain Behaviour

The closed-loop system (4.2.12) is a standard linear damped harmonic oscillator with bounded slew rate. However, for singularity avoiding trajectories the slew rate does not saturate at its maximum value during the course of manoeuvre. Therefore, the problem

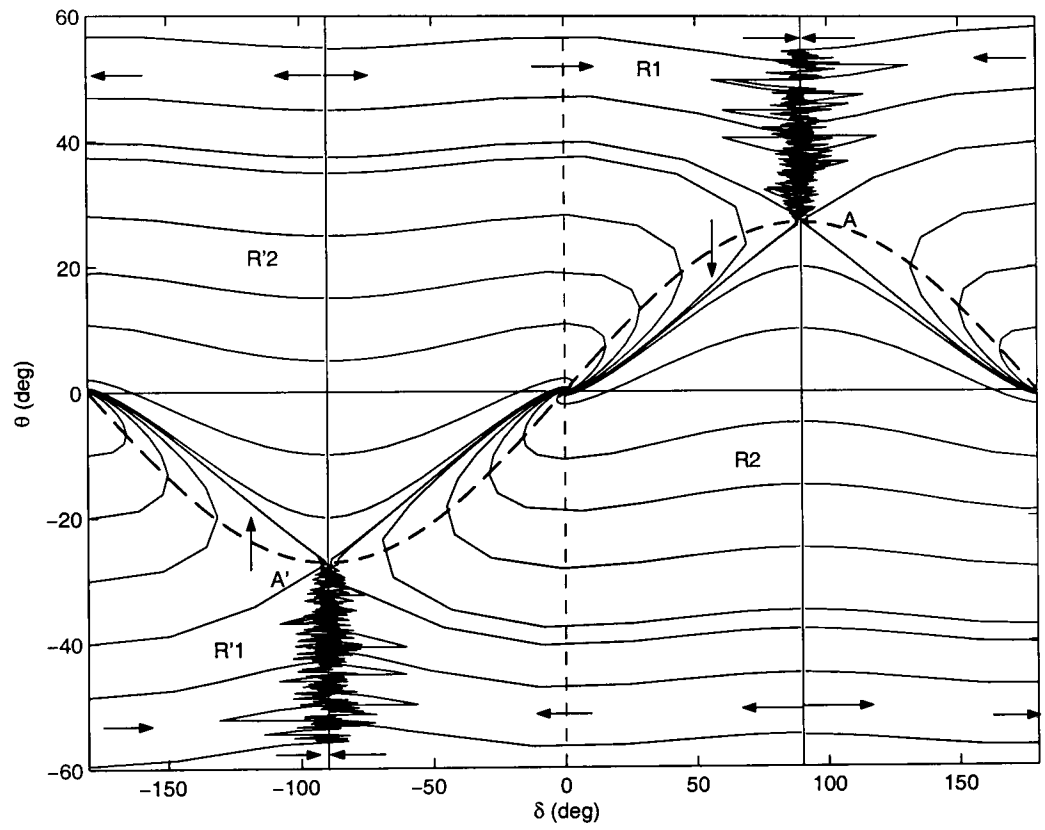

Figure 4.3: Phase portrait of the satellite-CMG system with the exact steering law in the (δ, θ) plane.

remains linear. We write system (4.2.12) in the form of the second order equation

$$\ddot{\theta} + k_\omega \dot{\theta} + k_\theta \theta = 0, \tag{4.3.15}$$

with $|\omega| \leq \omega_m$. The feedback gains k_θ and k_ω can be expressed in terms of a desired damping ratio ζ and the natural frequency ω_n of the closed-loop system as

$$\begin{aligned} k_\theta &= \omega_n^2, \\ k_\omega &= 2\zeta\omega_n. \end{aligned} \tag{4.3.16}$$

The resulting characteristic equation

$$s^2 + 2\zeta\omega_n s + \omega_n^2 = 0$$

has roots

$$s = \left(-\zeta \pm i\sqrt{1-\zeta^2}\right)\omega_n.$$

For an under-damped system ($\zeta < 1$) the solution with initial conditions $\theta(0) = \theta_o$ and $\dot{\theta}(0) = 0$ is

$$\begin{aligned} \theta &= \frac{\theta_o e^{-\zeta\omega_n t}}{\sin\phi} \sin(\omega_n t \sin\phi + \phi), \\ \omega &= -\frac{\theta_o \omega_n e^{-\zeta\omega_n t}}{\sin\phi} \sin(\omega_n t \sin\phi). \end{aligned} \tag{4.3.17}$$

where $\phi = \cos^{-1}\zeta$ and $|\omega| \leq \omega_m$. These equations always give a solution of Eq. (4.2.12), however, they are a solution of Eq. (4.2.11) provided it avoids the singularity. This solution can also be used to determine a number of interesting quantities like the maximum slew angle, maximum output torque, gimbal angle and gimbal rate profiles, and maximum gimbal rate etc. corresponding to the separatrix trajectory. Note that the critical point in the (θ, ω) plane is $A(\frac{k_\omega \omega_m}{k_\theta}, -\omega_m)$.

4.3.3 Feedback Gains

At the critical point A the output torque is zero i.e. $\dot{\omega} = 0$. We differentiate Eq. (4.3.17) w.r.t time t and then set its derivative to zero to find the time taken to get to the critical point from the initial condition, which is $t_A = \frac{\phi}{\omega_n \sin\phi}$. Substituting $\omega = -\omega_m$ and $t = t_A$ in Eq. (4.3.17) yields the initial condition for the separatrix trajectory as

$$\theta_o = \frac{\omega_m}{\omega_n} \exp\left(\frac{\phi}{\tan\phi}\right).$$

Therefore ω_n for separatrix trajectory is

$$\omega_n = \frac{\omega_m}{\theta_o} \exp\left(\frac{\phi}{\tan\phi}\right). \tag{4.3.18}$$

This value of ω_n is used for calculating the corresponding feedback gains given in Eq. (4.3.16). Conversely, this relation determines a maximum possible slew angle for a given set of gains and CMG capability without hitting the singularity.

4.3.4 Torque and Gimbal Dynamics

The advantage of exact steering formulation for twin CMG system presented in this chapter is that we can write explicit expressions for some useful dynamic variables such as output torque, gimbal angle and gimbal rate. We can also find maximum gimbal rate.

Output Torque Profile. The output torque profile for a twin CMG cluster can be derived by using the solution for θ and ω from Eq. (4.3.17) in Eq. (4.2.12) and after simplification we get

$$\tau_o = I\dot{\omega} = \omega_m I \omega_n \exp\left(-\frac{\omega_n t \sin\phi - \phi}{\tan\phi}\right) \frac{\sin(\omega_n t \sin\phi - \phi)}{\sin\phi}. \tag{4.3.19}$$

This expression of torque corresponds to the separatrix trajectory. As the torque has a damped harmonic profile so it is interesting to find the value of maximum overshoot and its time. The overshoot time is found by setting $\ddot{\omega} = 0$ and it results in

$$t = \frac{2\phi}{\omega_n \sin\phi}.$$

By substituting this expression for time in torque equation we get value of maximum overshoot in torque to be

$$\tau_o = I\omega_m\omega_n \exp\left(-\frac{\phi}{\tan\phi}\right).$$

For this reorientation manoeuvre case the output torque has its maximum value at $t = 0$ which is

$$\tau_o = -I\omega_m\omega_n \exp\left(\frac{\phi}{\tan\phi}\right).$$

Gimbal Angle Profile. Gimbal angle profile as a function of time is derived for separatrix trajectory. Comparing Eq. (4.2.13) with Eq. (4.3.17) yields

$$\sin\delta = \exp\left(-\frac{\omega_n t\sin\phi - \phi}{\tan\phi}\right)\frac{\sin\left(\omega_n t\sin\phi\right)}{\sin\phi}.$$

It can be checked that the function on the RHS of above equation has a value less than or equal to one for all times t. The function is equal to zero at $t = 0$ and for large values of t (i.e at the end of the manoeuvre) whereas its value is one at critical point with $t_A = \frac{\phi}{\omega_n \sin\phi}$.

Gimbal Rate Profile. The gimbal rate profile can be computed by using the following equation

$$\dot{\delta} = \frac{-\dot{\omega}}{\sqrt{\omega_m^2 - \omega^2}}.$$

After substituting expressions for ω and $\dot{\omega}$ from Eq. (4.3.17) and Eq. (4.3.19) respectively we get

$$\dot{\delta} = -\frac{\omega_n \exp\left(-\frac{\omega_n t\sin\phi-\phi}{\tan\phi}\right)\sin(\omega_n t\sin\phi - \phi)}{\sqrt{\sin^2\phi - \exp\left(-\frac{2\omega_n t\sin\phi-2\phi}{\tan\phi}\right)\sin^2(\omega_n t\sin\phi)}}.$$

It can be noted that gimbal rate is positive for $t < t_A$ and negative for $t > t_A$ and sign change occurs at $t = t_A$ where $\dot{\delta}$ is indeterminate. However, indeterminate forms generally have finite value, which in this case is found to be zero. Gimbal rate has its maximum value at $t = 0$ which is given by

$$\dot{\delta} = \omega_n \exp(\frac{\phi}{\tan\phi}). \tag{4.3.20}$$

Therefore, we are able to solve the single axis manoeuvre with twin CMGs analytically while avoiding the singularity. This approach determines the feedback gains needed to obtain the separatrix trajectory which optimizes the performance of the closed-loop system. However, there are some other factors which could also affect the performance of closed loop system adversely if not addressed properly. This includes hardware limits on gimbal rate and time-optimality for a rapid slew. In next section, we shall deal with these issues in detail.

4.4 Incorporating the Gimbal Rate Constraint

Here we shall study the effect of gimbal rate saturation on feedback gain synthesis and the time-optimality of Exact Steering Laws.

4.4.1 Phase Plane Representation

The (δ, θ) phase portrait of the system (4.2.14) is shown in Fig. (4.4) to Fig. (4.6). It contains the singularity manifold (solid vertical lines at $\delta = \pm\frac{\pi}{2}$) and nullcline (dashed sinusoidal curve) as in Fig. (4.3). The additional features in this phase portrait are the family of gimbal rate saturation curves ($\dot{\delta} = \pm\alpha$) given by

$$\theta(\delta) = \theta_o \mp \frac{\omega_m}{\alpha}\left(1 - \cos\delta\right), \tag{4.4.21}$$

corresponding to different values of the initial attitude angle θ_o. These are solution of bang-bang control problem. The feedback region around the nullcline is bounded by the switching curves

$$|\dot{\delta}| = \left|\frac{k_1\theta - k_\omega \sin\delta}{\cos\delta}\right| = \alpha,$$

or

$$\begin{aligned}\theta &= \frac{k_\omega}{k_1}\sin\delta \pm \frac{\alpha}{k_1}\cos\delta \\ &= \frac{\sqrt{{k_\omega}^2 + \alpha^2}}{k_1}\sin(\delta \pm \arctan(\alpha/k_\omega)).\end{aligned} \tag{4.4.22}$$

These switching curves are sinusoidal with phase lead or lag with respect to the nullcline. A state-trajectory starting from an initial point $(0, \theta_o)$ outside the feedback region follows the corresponding saturation curve until it enters the feedback region and then follows the harmonic oscillator solution. The separatrix trajectory (marked with a bold line in Fig. (4.6) starting from $\theta_o > 0$ (or $\theta_o < 0$) is on the α (or $-\alpha$) saturation curve before it switches to the $-\alpha$ (or α) saturation curve at the critical point A (or A') and finally switches to the feedback region. It is worth noting that the singularity is not passable even in this case as feedback function becomes singular.

4.4.2 Feedback Gains

Here we calculate the feedback gains corresponding to the separatrix trajectory, which is the desired closed-loop trajectory. This trajectory passes through the critical point

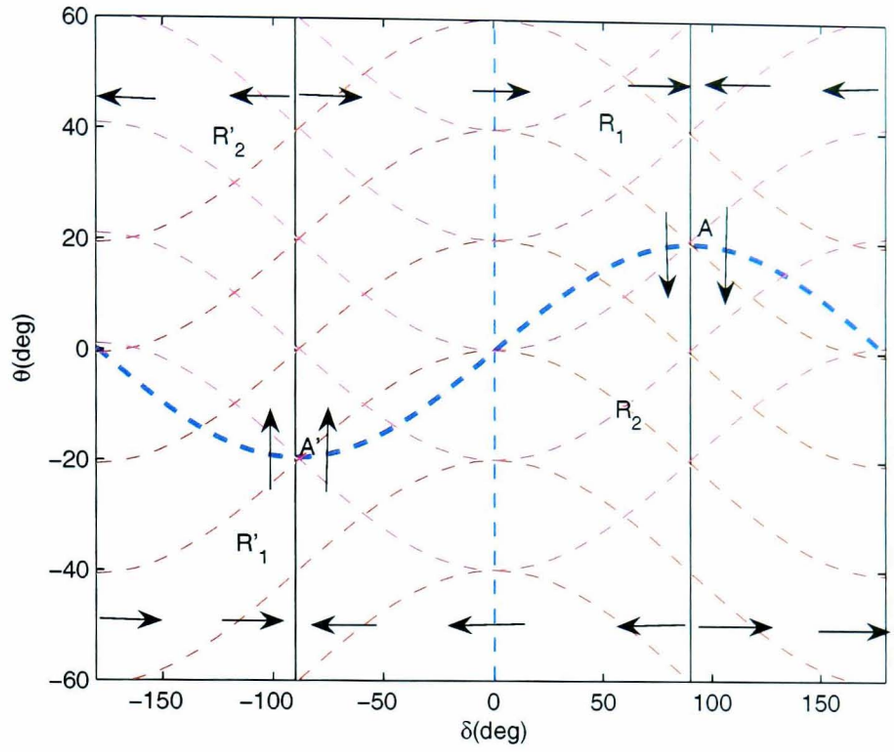

Figure 4.4: Gimbal rate saturation curves in the (δ, θ) plane.

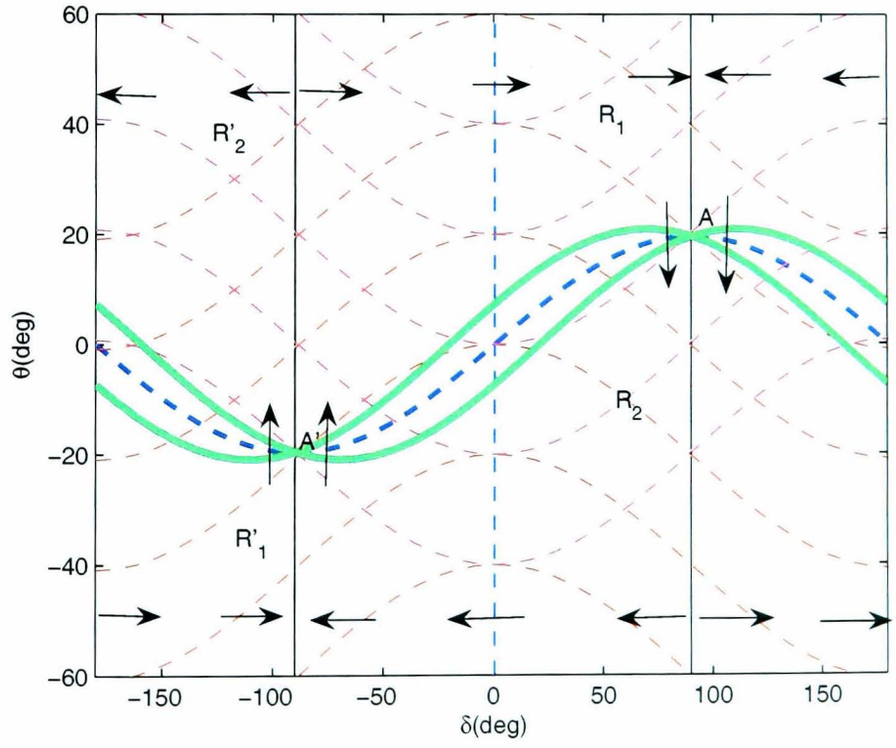

Figure 4.5: Plot of the feedback region in the (δ, θ) plane.

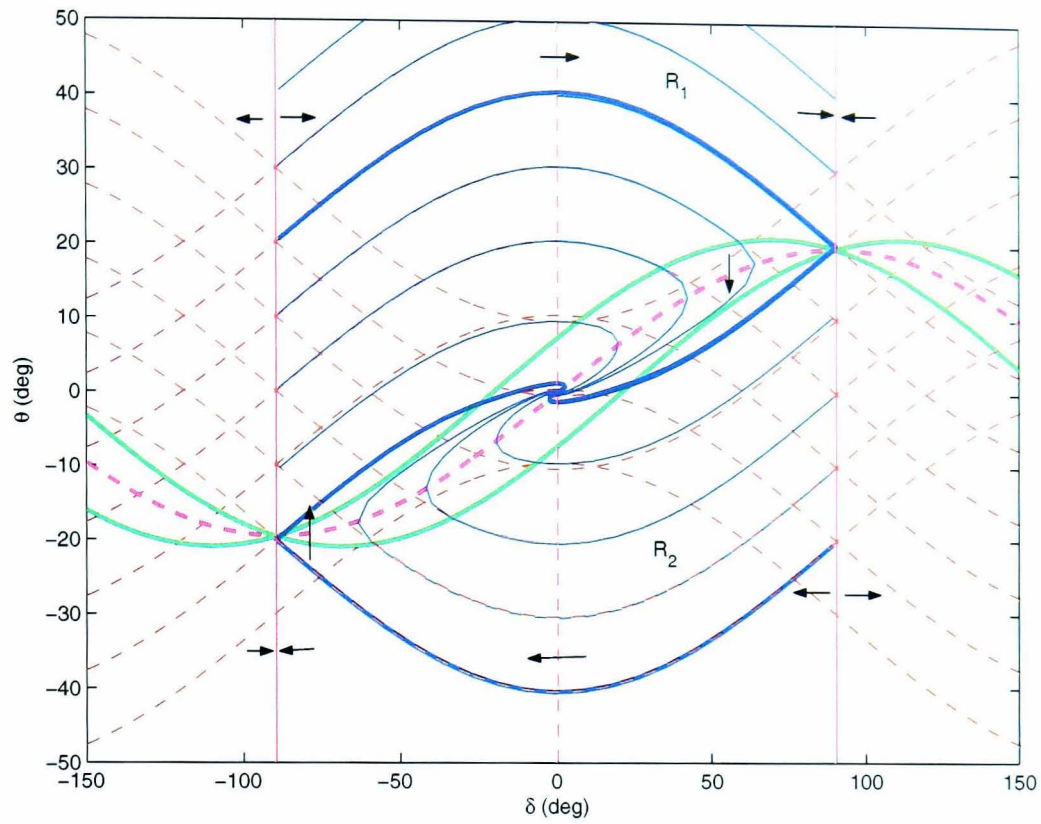

Figure 4.6: Phase portrait of satellite-CMG system with gimbal rate saturation (δ, θ) plane.

$A(\frac{\pi}{2}, \frac{k_\omega}{k_1})$ and follows the gimbal rate saturation or open-loop curve (4.4.21) outside the feedback region. The open-loop curve starting from θ_o reaches point A at $(\pi/2, \theta_o - \frac{\omega_m}{\alpha})$. Thus

$$\frac{k_\omega}{k_1} = \theta_o - \frac{\omega_m}{\alpha}.$$

But

$$\frac{k_\omega}{k_1} = \frac{2\zeta\omega_m}{\omega_n}.$$

Therefore, the natural frequency corresponding to the separatrix trajectory is

$$\omega_n = \frac{2\zeta\alpha\omega_m}{\theta_o\alpha - \omega_m}, \tag{4.4.23}$$

where $\theta_o > \frac{\omega_m}{\alpha}$. The damping ratio ζ is calculated from the overshoot requirement of the output response. The feedback gains k_θ and k_ω are then calculated from ω_n and ζ. In the next section, we derive the closed-form solution for separatrix trajectory and discuss its time-optimality.

4.4.3 Time Optimality

Time optimal single-axis manoeuvres with gimbal rate constraints can be obtained by bang-bang control. However, this classical solution is not preferred in practice because of the chattering problem. It can be observed in Fig. (4.6) that the separatrix trajectory follows the bang-bang solution or gimbal rate saturation curves outside the feedback region and a damped harmonic solution inside the feedback region in the vicinity of equilibrium point. So it can be a good candidate for a practical near-time-optimal solution. However, the choice of feedback gains affects the switching time and performance in the feedback region. So here we discuss time-optimality of the separatrix trajectory. As we know that the separatrix trajectory starting from an initial point $(0, \theta_o)$ follows the $+\alpha$-saturation curve and then switches to the $-\alpha$-saturation curve at the critical point $A\left(\frac{\pi}{2}, \theta_o - \frac{\omega_m}{\alpha}\right)$ at time instant $t = \frac{\pi}{2\alpha}$ before eventually switching to the feedback region at time instant $t = T_1$ with $\theta(T_1) = \theta_1$ and $\dot{\theta}(T_1) = \dot{\theta}_1$. The damped harmonic solution inside the feedback region is

$$\theta = M(t)\cos(N(t-L)), \tag{4.4.24}$$

$$\omega = -\omega_n M(t)\cos(N(t-L)-\phi), \tag{4.4.25}$$

where

$$\begin{aligned} B &= \frac{\zeta}{\sqrt{1-\zeta^2}}\left(\theta_1 + \frac{\dot{\theta}_1}{\zeta\omega_n}\right), \\ M_o &= \sqrt{B^2 + {\theta_1}^2}, \\ M(t) &= M_o \exp(-\zeta\omega_n(t-T_1)), \\ N &= \sin\phi\omega_n, \\ L &= \frac{1}{N}\arctan\frac{B}{\theta_1} + T_1, \\ \phi &= \cos^{-1}\zeta. \end{aligned}$$

The damping ratio ζ can be calculated from the maximum overshoot and settling time requirements using the explicit solution given in Eq. (4.4.24) and Eq. (4.4.25). We can find the explicit expression for switching time T_1 using the following open-loop

expressions at the boundary of feedback region:

$$\begin{aligned}\theta_1 &= \theta_o - \frac{\omega_m}{\alpha}\left(1-\cos\alpha T_1\right),\\ \dot{\theta}_1 &= -\omega_m \sin\alpha T_1,\\ \ddot{\theta}_1 &= -\omega_m \alpha\cos\alpha T_1.\end{aligned}$$

By substituting these expressions in the damped harmonic Eq. (4.3.15), we can get the following expression for T_1:

$$T_1 = \begin{cases} \frac{1}{\alpha}\arcsin\left(\frac{\omega_n}{2\zeta}\frac{\theta_o\alpha-\omega_m}{\omega_m\alpha}\cos\Phi_2\right)+\frac{1}{\alpha}\Phi_2, \\ \frac{\pi}{\alpha}-\frac{1}{\alpha}\arcsin\left(\frac{\omega_n}{2\zeta}\frac{\theta_o\alpha-\omega_m}{\omega_m\alpha}\cos\Phi_2\right)+\frac{1}{\alpha}\Phi_2, \end{cases} \tag{4.4.26}$$

where

$$\Phi_2 = \arctan\left(\frac{{\omega_n}^2-\alpha^2}{2\zeta\alpha\omega_n}\right).$$

These two switching times correspond to the intersection points of separatrix trajectory with the boundary of feedback region. One of these points corresponds to the critical point A and the other point corresponds to switching point of the feedback region. We can simplify these expressions for T_1 by using

$$\omega_n = \frac{2\zeta\alpha\omega_m}{\theta_o\alpha-\omega_m}$$

and

$$\theta_o = \frac{2\omega_m}{\alpha}$$

for the seperatrix trajectory in Eq. (4.4.26) to get

$$T_1 = \begin{cases} \frac{\pi}{2\alpha}, \\ \frac{3\pi}{2\alpha}-\frac{2}{\alpha}\arctan\left(1-\frac{1}{4\zeta^2}\right), \end{cases} \tag{4.4.27}$$

Thus for a separatrix trajectory the given choice of ω_n is optimal one and switching time depends only on tunable parameter ζ as rest of the parameters are design parameters.

The manoeuvre time t_f is defined by the requirement that $|\theta(t)| \leq \epsilon$ for all $t \geq t_f$, where ϵ is a small positive number. An approximate formula for t_f can be obtained by ignoring the cos-term in the solution $\theta(t)$ presented in Eq. (4.4.24). This gives

$$t_f = T_1 + \frac{1}{\zeta\omega_n}\left(\log(M_o(T_1)) - \log(\epsilon)\right). \tag{4.4.28}$$

We find extremum points of the function $t_f(T_1)$ as

$$\frac{dt_f}{dT_1} = 1 + \frac{1}{\zeta\omega_n M}\frac{dM_o}{dT_1} = 0.$$

But

$$\frac{dM_o}{dT_1} = \frac{B\dot{B} + \theta_1\dot{\theta}_1}{M_o}.$$

After simplifying we get

$$\sqrt{1-\zeta^2}B\left(\ddot{\theta}_1 + 2\zeta\omega_n\dot{\theta}_1 + {\omega_n}^2\theta_1\right) = 0.$$

This leads to two conditions for the switching time T_1

$$\ddot{\theta}_1 + 2\zeta\omega_n\dot{\theta}_1 + {\omega_n}^2\theta_1 = 0, \tag{4.4.29}$$

$$\theta_1 + \frac{\dot{\theta}_1}{\zeta\omega_n} = 0. \tag{4.4.30}$$

The switching condition in Eq. (4.4.29) satisfies the damped harmonic solution at the boundary of feedback region. We have already found an explicit expression for such switching time T_1 in Eq. (4.4.26). However, the second condition (4.4.30) does not satisfy damped harmonic solution which means that it switches to feedback control at the following instances.

$$T_1 = \begin{cases} \frac{1}{\alpha}\arcsin\left(\frac{\theta_o\alpha-\omega_m}{\omega_m}\sin\Phi_1\right) + \frac{1}{\alpha}\Phi_1, \\ \frac{\pi}{\alpha} - \frac{1}{\alpha}\arcsin\left(\frac{\theta_o\alpha-\omega_m}{\omega_m}\sin\Phi_1\right) + \frac{1}{\alpha}\Phi_1, \end{cases} \tag{4.4.31}$$

where

$$\Phi_1 = \arctan\frac{\zeta\omega_n}{\alpha},$$

and

$$\left|\frac{\theta_o\alpha - \omega_m}{\omega_m}\right| \leq 1.$$

For separatrix trajectory with

$$\omega_n = \frac{2\zeta\alpha\omega_m}{\theta_o\alpha - \omega_m}$$

and

$$\theta_o = \frac{2\omega_m}{\alpha}$$

we get

$$T_1 = \begin{cases} \frac{2}{\alpha}\arctan\left(2\zeta^2\right), \\ \frac{\pi}{\alpha}, \end{cases} \tag{4.4.32}$$

In this case final switching time of feedback control happened to be bang-bang manoeuvre time $\frac{\pi}{\alpha}$. This solution demands that switching is not made to feedback control before origin. It means that this solution brings us to classical bang-bang control, which does not require feedback control. Therefore, we drop this condition (4.4.30)and choose the condition (4.4.29), which uses the feedback control near origin.

4.5 Singularity Robust Steering Law Revisited

The singularity robust (SR) steering law given in Eq. (3.7.40) can be simplified for twin CMG system with anti-symmetric gimbal motion as

$$\dot{\delta} = \frac{\tau_c \cos\delta}{\omega_m \left(\cos^2\delta + \lambda_o \exp\left(-\cos^2\delta\right)\right)}, \tag{4.5.33}$$

where

$$\tau_c = k_\theta \theta + k_\omega \omega.$$

In this case feedback gains k_θ and k_ω are chosen using linear control system theory. The denominator in this case is never zero due to singularity robustness term $\lambda_o \exp\left(-\cos^2\delta\right)$ for positive values of λ_o. As system approaches to singularity the singularity robustness term grows larger. Therefore, faster gains in feedback law appear to have no problem. We have used this simplified form of SR logic in our simulations.

4.6 Variable Gains Steering Law

In this section, we study the Exact Steering Law with variable gains controller for a twin CMG system. The Exact Steering Law with fixed controller gains developed in previous sections gives near-optimal control for singularity avoiding trajectories with initial attitude $\theta_o \leq \omega_m(1/\alpha + 2\zeta/\omega_n)$, where ω_n is defined in Eq. (4.4.23). Any trajectory starting from $\theta_o > \omega_m(1/\alpha + 2\zeta/\omega_n)$ is bound to hit singularity and therefore is not permissible in that scheme. This may be deemed limitation of exact steering because we have to lower ω_n if θ_o happens to be outside separatrix which would result in slower response. We use the fact that singularity avoidance region grows larger as ω_n is lowered to propose the use of variable gains instead of fixed ones in Exact Steering Law. In this scheme feedback gains are made to vary along the trajectory such that

gains are zero at singularity, thus making the torque zero, and continuously vary along the trajectory. This can be done by introducing a singularity index $\sqrt{|\cos\delta|}$ in the gains. In the following subsections, we shall define variable feedback gains and shall also represent this system in (δ, θ) and (θ, ω) phase-planes for further analysis.

4.6.1 Variable Gains

The overall structure of Exact Steering Law (4.2.9) is kept unchanged, however, the feedback gains are re-defined as

$$\begin{aligned} k_\theta &= \omega_n^2 |\cos\delta|, \\ k_\omega &= 2\zeta\omega_n\sqrt{|\cos\delta|}. \end{aligned} \tag{4.6.34}$$

To justify the choice of the gains in Eq. (4.6.34) we rewrite Eq. (4.2.11) in matrix form

$$\begin{bmatrix} \dot{\delta} \\ \dot{\theta} \end{bmatrix} = \begin{bmatrix} -\frac{k_\omega}{\cos\delta} & \frac{k_\theta}{\omega_m \cos\delta} \\ -\omega_m & 0 \end{bmatrix} \begin{bmatrix} \sin\delta \\ \theta \end{bmatrix}. \tag{4.6.35}$$

Here determinant of the matrix involved is

$$\begin{vmatrix} -\frac{k_\omega}{\cos\delta} & \frac{k_\theta}{\omega_m \cos\delta} \\ -\omega_m & 0 \end{vmatrix} = \frac{k_\theta}{\cos\delta}.$$

Therefore, the choice of gains made in Eq. (4.6.34) makes determinant of the matrix $\omega_n^2 \text{sgn}(\cos\delta)$, where $\text{sgn}(x) = 1$ if $x > 0$ and $\text{sgn}(x) = -1$ if $x < 0$. This choice of gains makes the matrix invertible to a non-singular matrix. The properties of the solution trajectories of such a system are studied in the next subsection.

4.6.2 Phase Plane Representation

In this subsection, we represent the Exact Steering Law with variable gains defined in Eq. (4.6.34) in phase-plane. The phase-portrait of this system in (δ, θ) plane is shown in Fig. (4.7). The key features in this phase-portrait are singularity manifold ($\delta = \pm\pi/2$), gimbal rate saturation curves ($\dot{\delta} = \pm\alpha$), nullcline ($\dot{\delta} = 0$), feedback region $|\dot{\delta}| < \alpha$ and phase-plane trajectories (or solution curves). Many features in this phase-portrait are similar to those of Exact Steering with fixed gains in Fig. (4.6), like singularity manifolds are represented by solid vertical lines at ($\delta = \pm\frac{\pi}{2}$) and gimbal rate saturation

trajectories defined in Eq. (4.4.21) are represented by dashed lines. However, nullcline in this case is very different from the fixed gains case. Here it is defined by an equation

$$\begin{aligned}\theta &= \frac{k_\omega \omega_m}{k_\theta} \sin\delta \\ &= \frac{2\zeta\omega_m}{\omega_n} \frac{\sin\delta}{\sqrt{|\cos\delta|}}.\end{aligned} \tag{4.6.36}$$

In $\delta \in (-\pi/2, \pi/2)$ we have $\cos\delta > 0$ and it is nearly a tangent curve. A solution curve or trajectory initiated at point $(0, \theta_o)$ is bound to follow the gimbal rate saturation curve until it switches to feedback region around nullcline. The nullcline would never intersect the singularity manifold for the finite value of θ but has asymptotic behaviour near singularity as shown in Fig. (4.7). In fixed gain case controller's bandwidth ω_n is calculated by using the phase-portrait to find the critical point which is defined as the intersection point of singularity manifold and nullcline. However, in variable gain case such a point does not exist in the finite range of θ. Moreover, the boundary of feedback region merges with nullcline as $\delta \to \pi/2$. To get a fastest possible maneuver we synthesis ω_n such that a trajectory starting from θ_o would switch to feedback region and crosses nullcline in close proximity of the singularity to get maximum possible slew rate.

The ω_n's calculation for variable gains case uses the fact that a trajectory starting from an initial condition

$$\theta_o = (m+1)\frac{\omega_m}{\alpha}, \tag{4.6.37}$$

where m is a real number, crosses the nullcline at some $\delta = \delta_s$ before settling to the origin of (δ, θ) plane. For a given θ_o, δ_s is made as closer as possible to $\frac{\pi}{2}$ by properly choosing ω_n. One may notice in the phase-portraits Fig. (4.7) and Fig. (4.8) that the boundaries of feedback region merge in nullcline with the increasing value of δ. Therefore, if the switching point $(\delta_s, \theta(\delta_s))$ is closer to singularity then the gimbal rate saturation curves Eq. (4.4.21) directly intersect the nullcline Eq. (4.6.36). Therefore,

$$\theta_o - \frac{\omega_m}{\alpha}(1 - \cos\delta_s) = \frac{2\zeta\omega_m}{\omega_n} \frac{\sqrt{1-\cos^2\delta_s}}{\sqrt{|\cos\delta_s|}}.$$

Using the definition of θ_o given in Eq. (4.6.37) and after simplifying we get

$$\omega_n = 2n\zeta\alpha,$$

where n is a real number defined as

$$n = \frac{\sqrt{1 - \cos^2 \delta_s}}{\sqrt{|\cos \delta_s|}(m + \cos \delta_s)}. \tag{4.6.38}$$

The choice of n could be further simplified if $\cos \delta_s \ll 1$ and $\cos \delta_s \ll m$ then

$$n = \frac{1}{m\sqrt{|\cos \delta_s|}}.$$

Typically for $\cos \delta_s \leq 0.25$ a satellite can achieve more than $0.968\omega_m$ slew rate which is reasonably close to ω_m and this corresponds to $n \geq 2$ for $m = 1$ i.e. $\theta_o = 2\omega_m/\alpha$. However, shifting δ_s closer to singularity increases n excessively which may result in large overshoot in closed-loop response. So there has to be a trade-off in choice of n to achieve an optimal performance of the closed-loop system. A criterion for choosing a near-optimal value of n shall be discussed later.

The issue of stability of closed-loop system is also clearly evident in phase-portraits as all the trajectories starting in the given region converge to origin as $t \to \infty$. Another point to be noticed is that all trajectories with finite value of θ_o avoid singularity. The reason for this is that the nullcline asymptotically approaches the singularity line so a trajectory hits the nullcline and gimbal rate becomes $\dot{\delta} \leq 0$. It means that after passing nullcline δ starts decreasing and trajectory never hits singularity. It is important for good performance of the closed-loop system that the desired trajectory finally switches to gimbal rate saturation curve which passes through the origin. This can be ensured by proper choice of n or ω_n. So with the proper choice of variable gains the Exact Steering Law guarantees singularity avoidance.

4.7 Simulations and Results

In this section, we shall demonstrate the effectiveness of the Exact Steering Law together with the proposed singularity avoiding gains calculation technique. We consider a pitch axis manoeuvre of BILSAT. The BILSAT is equipped with a twin CMG system which is capable of performing 40^o manoeuvre in 20 seconds. The satellite and CMG data is summarized in Table (4.1). The damping ratio ζ is based on performance requirement such as desired maximum overshoot ($< 2\%$). For exact steering

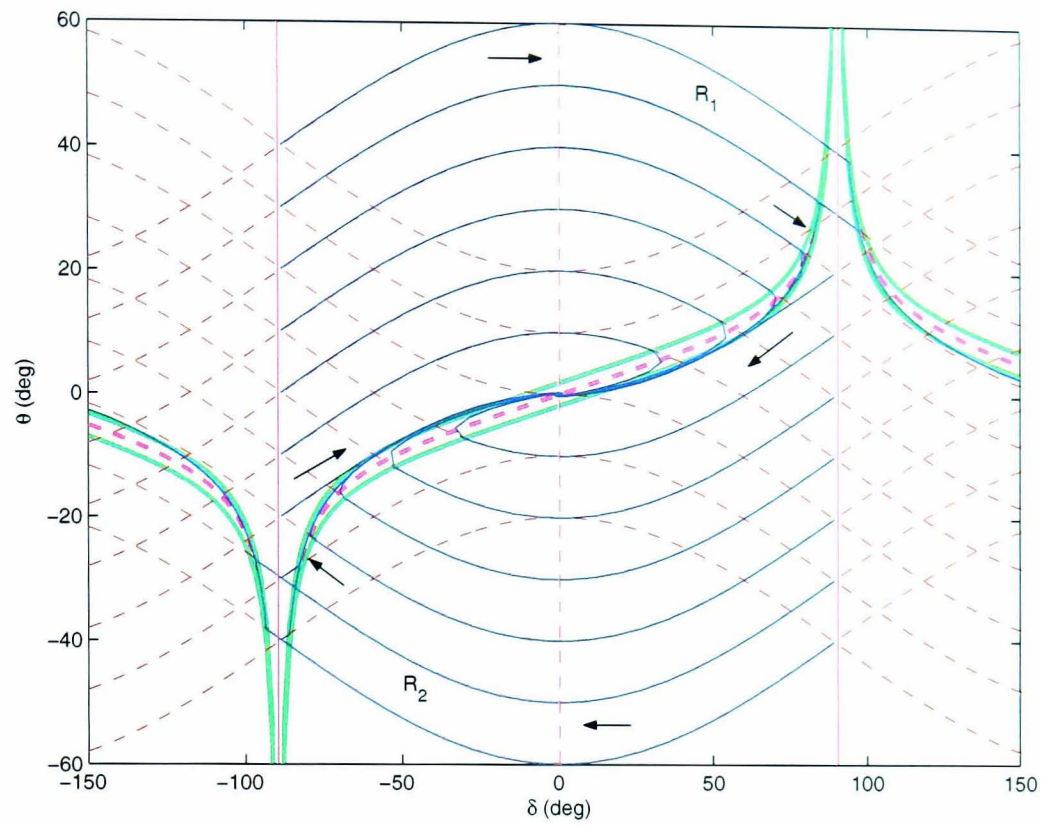

Figure 4.7: Phase portrait (δ, θ) for variable gain law.

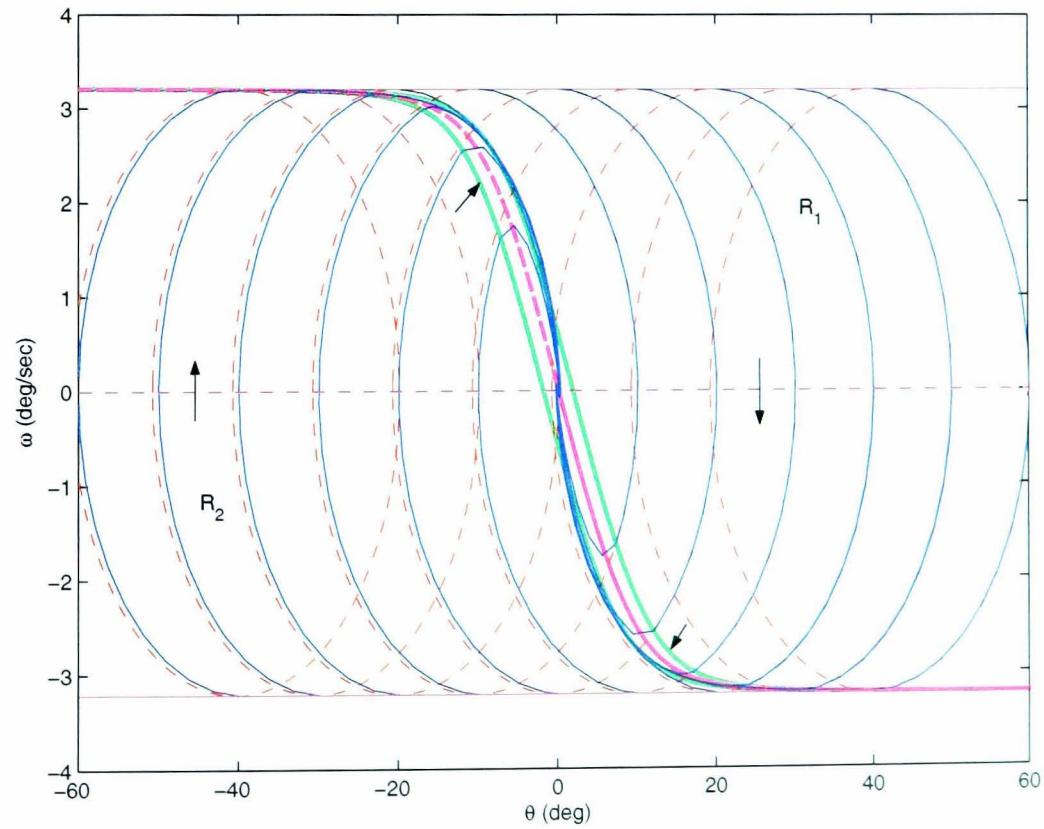

Figure 4.8: Phase portrait (θ, ω) for variable gain law.

Table 4.1: Satellite and CMG Data.

Parameter	Symbol	Value
CMG momentum	h_{cmg}	0.28 Nms
Moment of Inertia	$[I_x, I_y, I_z]$	$[10, 10, 10]$ kgm^2
Skew angle	β	0 deg
Maximum gimbal rate	α	9deg/s
Maximum slew rate	ω_m	3.2deg/s

Table 4.2: Feedback gains for the Exact Steering Law without Gimbal Rate Constraint (Exact without GRC), Exact Steering Law with Gimbal Rate Constraint (Exact with GRC) and Singularity Robust Steering Law (SR) for cases A and B.

Gains	Exact without GRC	Exact with GRC	SR in Case A	SR in Case B
ζ	0.8	0.8	0.8	0.8
ω_n	0.1887 rad/s	0.2608 rad/s	0.8 rad/s	0.5 rad/s
k_θ	0.0356	0.068	0.64	0.25
k_ω	0.3019	0.4173	1.28	0.8
λ_0	-	-	0.01	0.01

law without gimbal rate constraint case, the natural frequency ω_n is calculated by using Eq. (4.3.18), whereas for the exact steering with gimbal rate constraint case the ω_n is calculated by using Eq. (4.4.23). The calculation of feedback gains k_θ and k_ω is done by using Eq. (4.3.16). Here we consider a 40^o pitch manoeuvre i.e. $\theta_o = 40^o$ and summarize the calculated gain parameters for exact steering law without and with gimbal rate constraint cases in Table (4.2). Similarly, we also list the feedback gains for SR logic based on some performance criterion but independent of singularity avoiding consideration. The simulation results presented in next two subsections use feedback gains listed in Table (4.2).

4.7.1 Case A- Exact Steering Law

The Exact Steering Law is simulated for 40^o pitch manoeuvre corresponding to separatrix trajectory case. In this case no explicit gimbal rate limit is considered. So we use

feedback gain values from the column of Table (4.2) labeled as 'Exact without GRC'. The simulation results are shown in Fig. (4.9), which include plots of slew angle, slew rate, gimbal angle and gimbal rate all against time. In these results performance of Exact Steering law is compared with that of Singularity Robust (SR) steering logic. And feedback gains for SR steering logic are used from the column of Table (4.2) labeled as 'SR in Case A'. The choice of these gains is independent of the steering law which is a normal practice. Relatively large values of the feedback gains in case of SR logic drive the CMG system to the singular configuration where gimbal angles are locked for certain time and slew rate saturates at its maximum value in Fig. (4.9). However, this saturation causes an overshoot in the response. In this case slew rate saturates at its maximum value for quite a while but it does not help in reducing the manoeuvre time. It means that one has to consider slew rate saturation while choosing the values for feedback gains where as this slew rate saturation is directly related to singularity of the CMG cluster. Therefore, it seems prudent to consider slew rate saturation or gimbal lock at singularity while choosing feedback gains for SR logic to ensure good performance. One may use feedback gains calculated for exact steering in SR steering logic to obtain a better performance. Exact steering law with proper choice of feedback gains avoids singularity at first place and from results it is clear that settling time is almost the same for both cases. The maximum gimbal rate corresponding to the separatrix trajectory is calculated to be $25^o/\text{sec}$ by using Eq. (4.3.20).

4.7.2 Case B- Exact Steering Law with Gimbal Rate Constraint

BILSAT has a hardware gimbal rate saturation limit of $\pm 9\text{deg/s}$. Here we use the feedback gains from the column of Table (4.2) labeled as 'Exact with GRC' in simulation of 40^o pitch manoeuvre. These gains correspond to the separatrix trajectory of Fig. (4.6). We compare response of the Exact Steering Law with the response of bang-bang control in Fig. (4.10). The results show that the response of proposed method follows the bang-bang solution during most of the time and switches to closed-loop solution near the target point thus avoiding the chattering problem. Thus we see that this closed-loop solution with the chosen gains is near-optimal. In Fig. (4.11) we compare results of Exact Steering Law with results of SR logic with gimbal rate constraint. The feedback gains for SR logic are used from the column of Table (4.2) labeled as 'SR in Case B'.

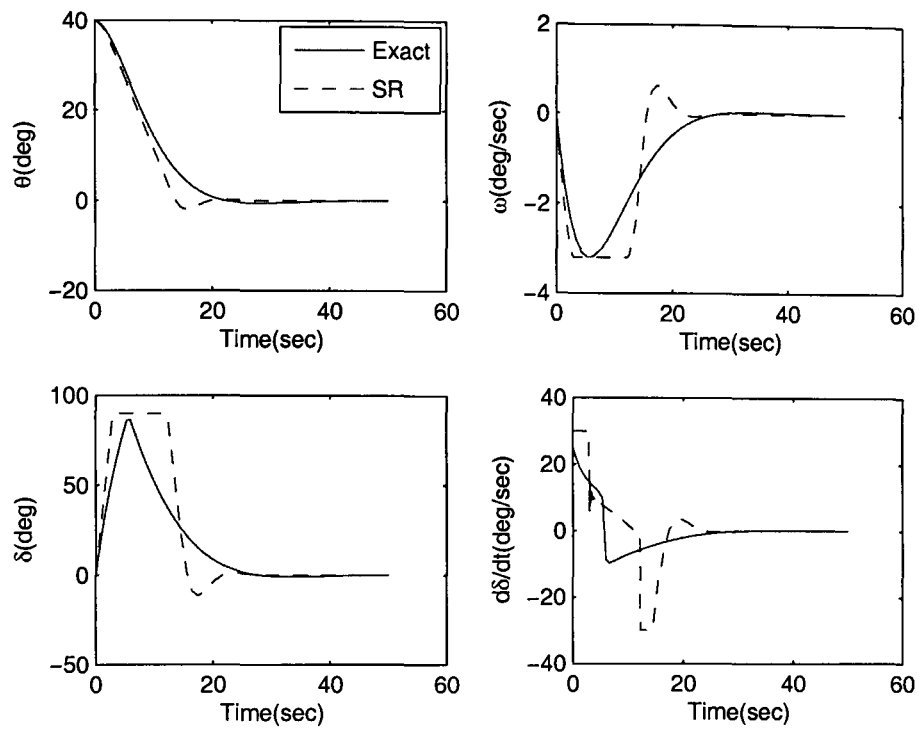

Figure 4.9: Exact steering vs. singularity robust logic.

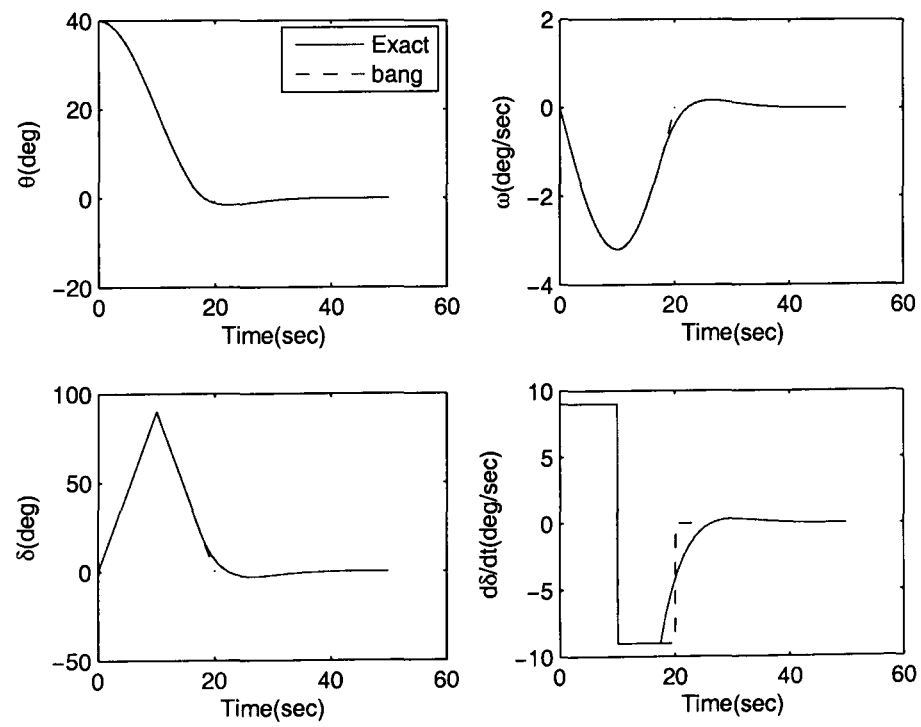

Figure 4.10: Exact steering vs. bang-bang control.

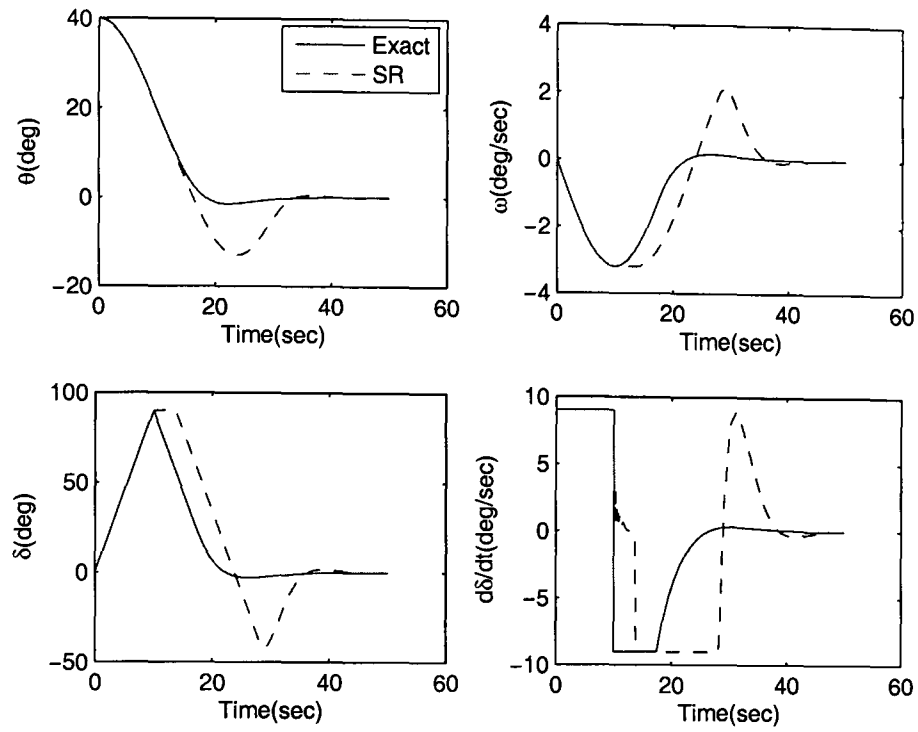

Figure 4.11: Exact steering vs. singularity robust logic.

One can note that in this case gains for SR logic are lowered from previous values in order to reduce possible overshoot. Even then SR logic suffers from gimbal lock at the singularity and its performance is deteriorated. The reason for this excessive overshoot in the response of SR is the combined effect of slew rate and gimbal rate saturation. As we have mentioned earlier the choice of higher gains for SR example is a deliberate attempt to emphasis a need for suitably selected feedback gains by considering the slew rate and gimbal rate saturation.

4.7.3 Case C- Exact Steering with Variable Gains

In this subsection, we find the near-optimal value of n defined in Eq. (4.6.38) for a pitch manoeuvre with an initial condition $\theta_o = \frac{2\omega_m}{\alpha}$ and then perform the manoeuvre using proposed Exact Steering Law with variable gains. Then we will show that a manoeuvre with $\theta_o > \frac{2\omega_m}{\alpha}$ by using the variable gains calculated for $\theta_o = \frac{2\omega_m}{\alpha}$ is not only possible but has a faster response than fixed gains case.

First we study the effect of variation of n on nullcline in (δ, θ) plane to find the optimal

value of n. In Fig. (4.12) nullcline is plotted for different values of n. It can be seen in Fig. (4.12) that the slope of the curve near origin decreases as n varies from 1 to 3. The gimbal rate saturation curve passing through the origin is also plotted. For minimal overshoot and smooth settling at origin a trajectory has to switch to this curve after passing through nullcline when gimbal rate saturates, and it is a desired switching curve. If a trajectory switches to a neighbouring saturation curve then this would result in overshoot or undershoot and a deteriorated performance. The equation of this desired switching curve passing through origin is

$$\theta(\delta) = \frac{\omega_m}{\alpha}(1 - \cos\delta)\,. \tag{4.7.39}$$

It is clear from Fig. (4.12) and its close-up view in Fig. (4.13) that higher values of n bring nullcline below this desired switching curve. So if nullcline is dropped below this curve then a trajectory can not switch to it after passing the nullcline. In Fig. (4.13) one can see that the critical value of n is around 2 where nullcline just avoids intersection with this curve. To further prove the point we have plotted the (δ, θ) trajectories all starting from $\theta_o = \frac{2\omega_m}{\alpha}$ with different values of n in Fig. (4.14). It is evident that only those trajectories which do not intersect nullcline have good performance i.e. minimal overshoot. On the other hand, small values of $n < 2$ would have slow response. Thus $n = 2$ gives fastest possible response with minimal overshoot. Generally speaking for a system with saturation limits higher values of gains result in large overshoots as we have already seen in Fig. (4.11).

In Fig. (4.15) we have compared a pitch manoeuvre for Exact Steering Law with variable gains and fixed gains. In both cases response time is almost the same but variable gain case have smoother response. Although in case of variable gains gimbal rate remained saturated for lesser amount of time. But in feedback region near origin gains are higher than the fixed gains case which results in faster and smoother response. Variation in gains along the trajectory are plotted in Fig. (4.16). The gains drop to their lowest values near singularity. Fixed gains are also plotted in the same figure. We have also plotted a trial Liapunov function for the system of the form given in Eq. (4.2.7) and its rate for both cases. System is stable with variable gains.

In the next experiment, we have simulated a 60^o pitch manoeuvre to highlight the ad-

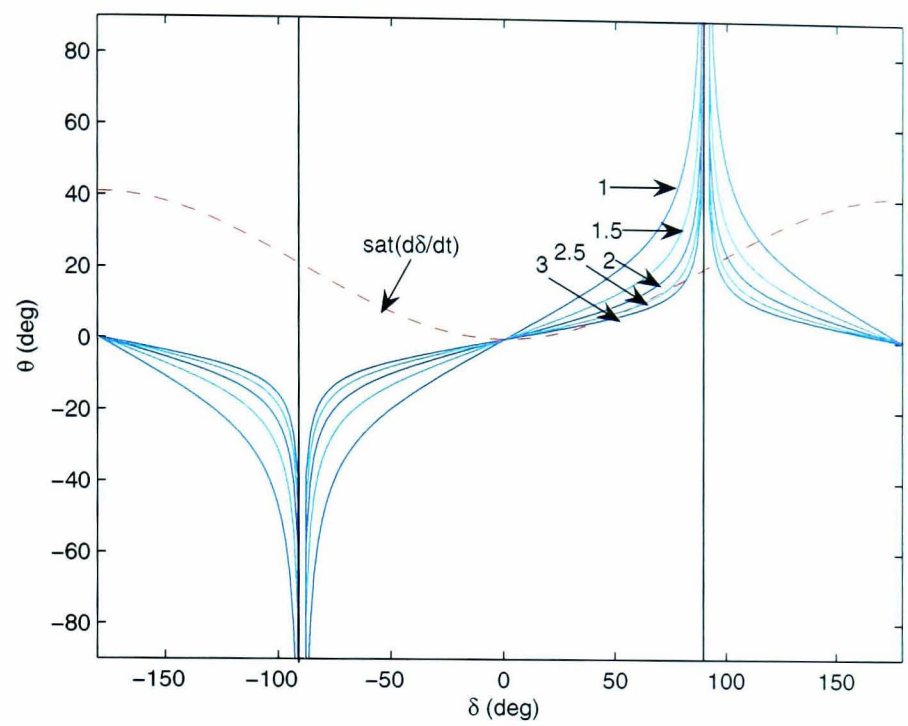

Figure 4.12: Variation in nullcline with n.

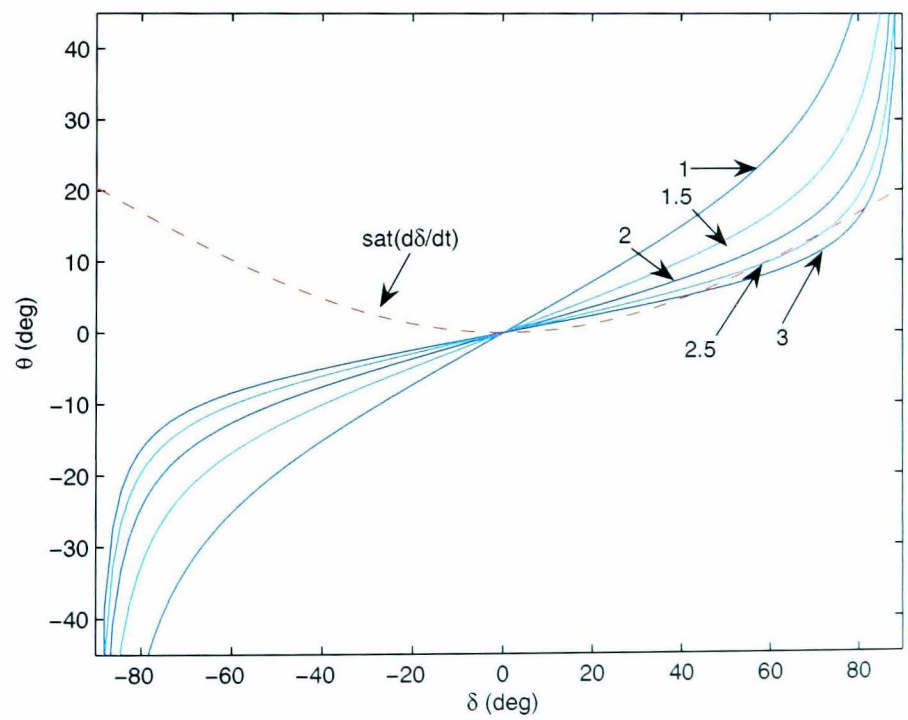

Figure 4.13: Close up view of nullcline variation diagram Fig. (4.12).

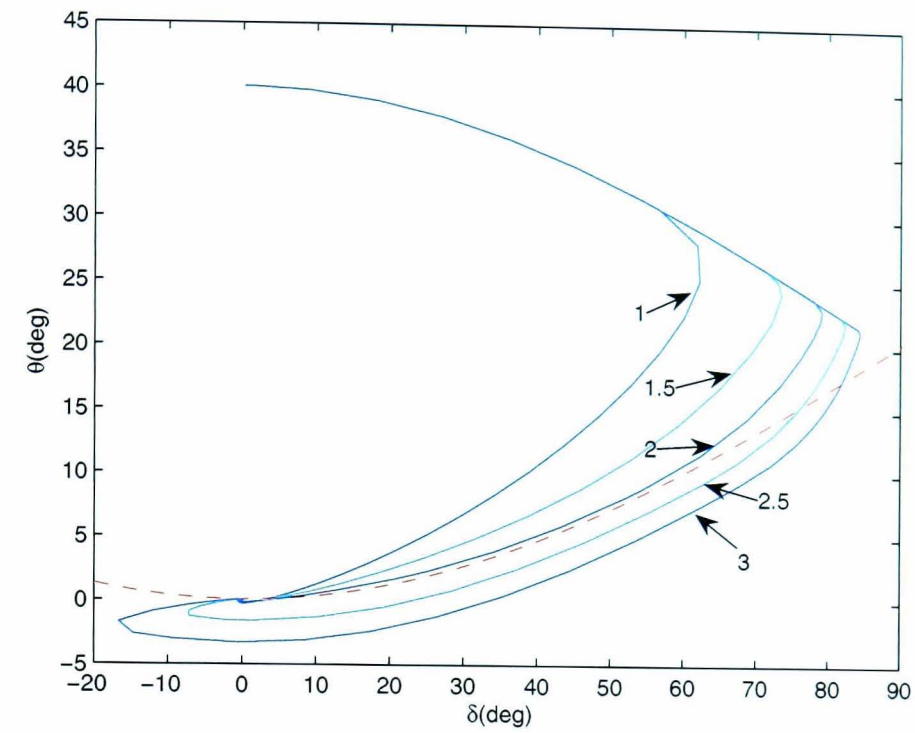

Figure 4.14: Variation in trajectory with n.

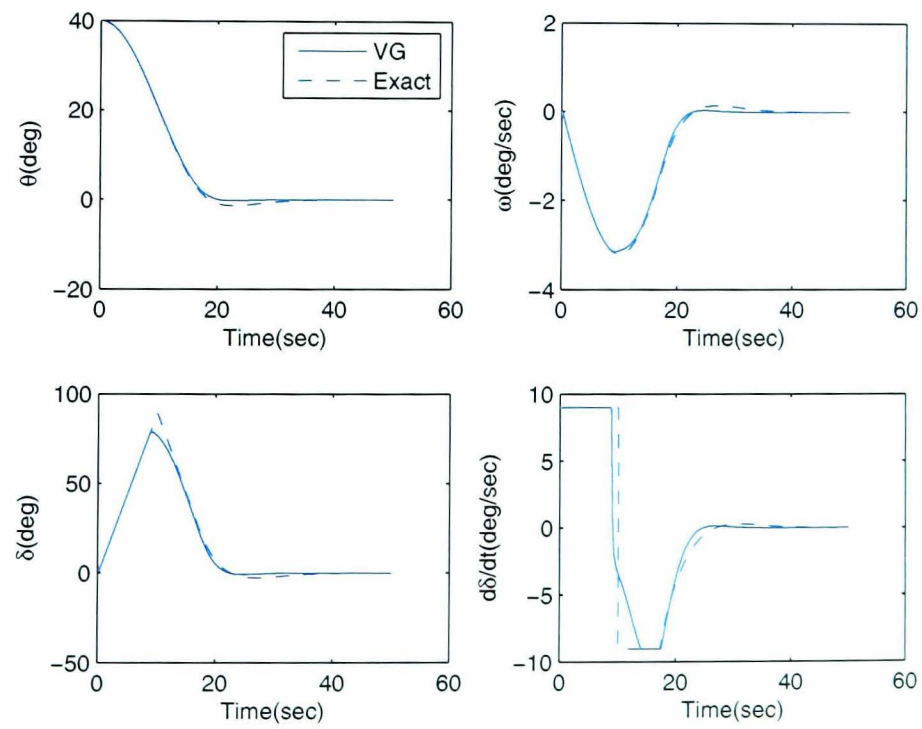

Figure 4.15: Simulation results for variable gain exact logic for $\theta_o = 40^o$.

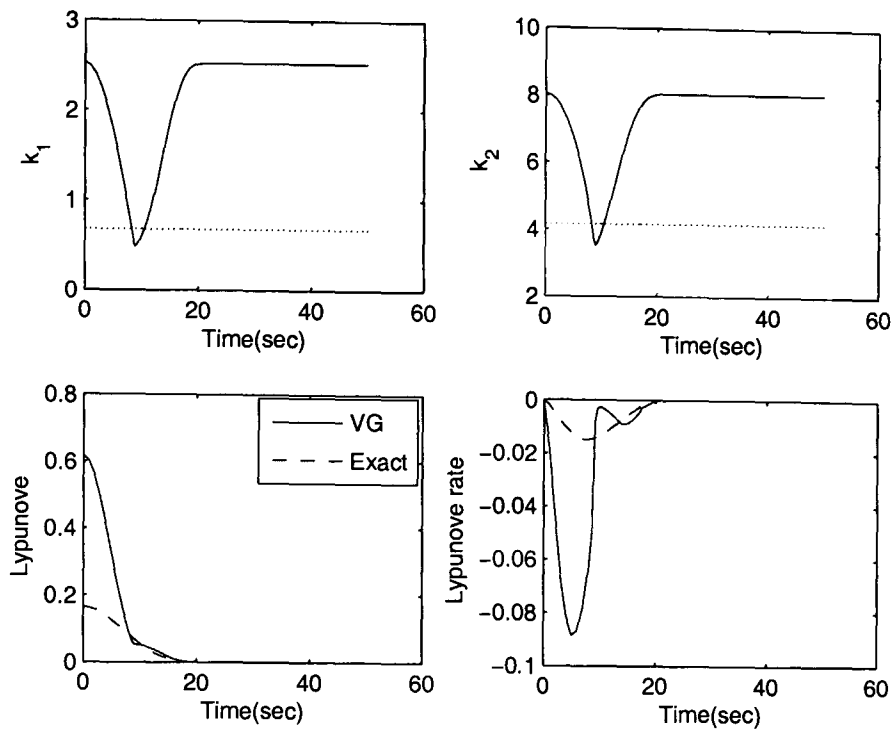

Figure 4.16: Simulation results for variable gain exact logic for $\theta_o = 40^o$.

vantage of variable gains over fixed gains in exact steering. In fixed gains case there is a separatrix trajectory starting from $\theta_o = \frac{2\omega_n}{\alpha}$ and all trajectories with $\theta_o > \frac{2\omega_n}{\alpha}$ are bound to hit singularity. Should we need a manoeuvre with $\theta_o > \frac{2\omega_n}{\alpha}$ then we need to update the gains using Eq. (4.4.23) to make that trajectory avoid singularity. For larger values of θ_o gains are slower. On the other hand, for variable gains Exact Steering the gains once calculated for $\theta_o = \frac{2\omega_n}{\alpha}$ can be used for a trajectory with $\theta_o > \frac{2\omega_n}{\alpha}$. To demonstrate this we perform a simulation for $\theta_o = \frac{3\omega_n}{\alpha}$ i.e.$(m = 2)$. In Fig. (4.17) results show a faster and smoother response for variable gains (solid lines) as compared to fixed gains (dashed lines) case of Exact Steering Law. Interestingly gimbal angle δ in this case approaches to singularity and slew rate ω saturates near to its maximum value. But as trajectory switches to desired switching curve so there is no overshoot in the response. In Fig. (4.18) we have presented the variation in gains, Liapunov function and its rate. In Fig. (4.19) the (δ, θ) trajectories for both cases have been plotted. It explains reason for the fast response of variable gain case. Initially both trajectories start from $\theta_o = \frac{3\omega_n}{\alpha}$ along the saturation curve to $(\frac{\pi}{2}, \frac{2\omega_n}{\alpha})$ which is critical point for fixed gains case. Beyond that point the fixed gains trajectory can not follow a gimbal rate saturation curve as that will bring it to $(0, \frac{\omega_n}{\alpha})$ rather than $(0, 0)$. On the other hand, in

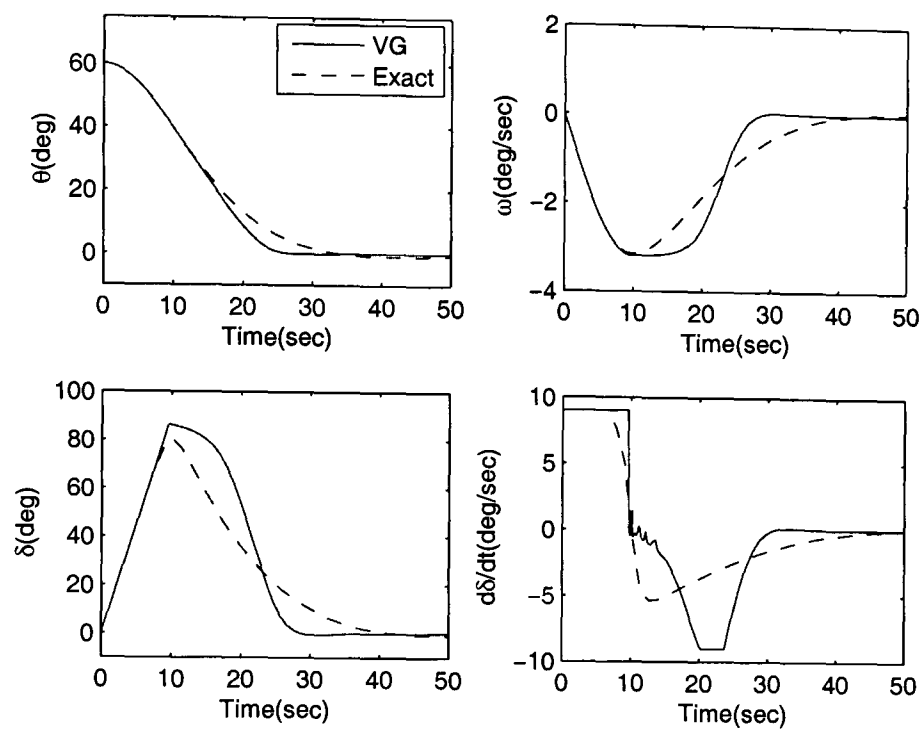

Figure 4.17: Simulation results for variable gain exact logic for $\theta_o = 60^o$.

variable gain's case trajectory stays near singularity and then come back to origin along the desired switching curve.

4.8 Summary

We have proposed an exact steering for twin CMG system and developed some techniques to calculate feedback gains such that exact solutions are possible without encountering any singularity. We have studied the feedback gains' calculation problem subjected to different restrictions imposed namely exactness, singularity avoidance, time-optimality and rate constraints like gimbal rate constraint and slew rate constraint. We have derived an exact expression for feedback gains in terms of constraints and have found a separatrix trajectory for singularity avoidance. Time-optimality of these solutions has been checked and it has shown to be very close to bang-bang solution. It has also been shown that SR solutions are not only not exact but can also exhibit performance degradation in form of large overshoots if we choose higher gains with no regard to saturation limits. However, the gains calculated for Exact Steering can also be used SR to get good performance. We have also proposed variable gains for Exact

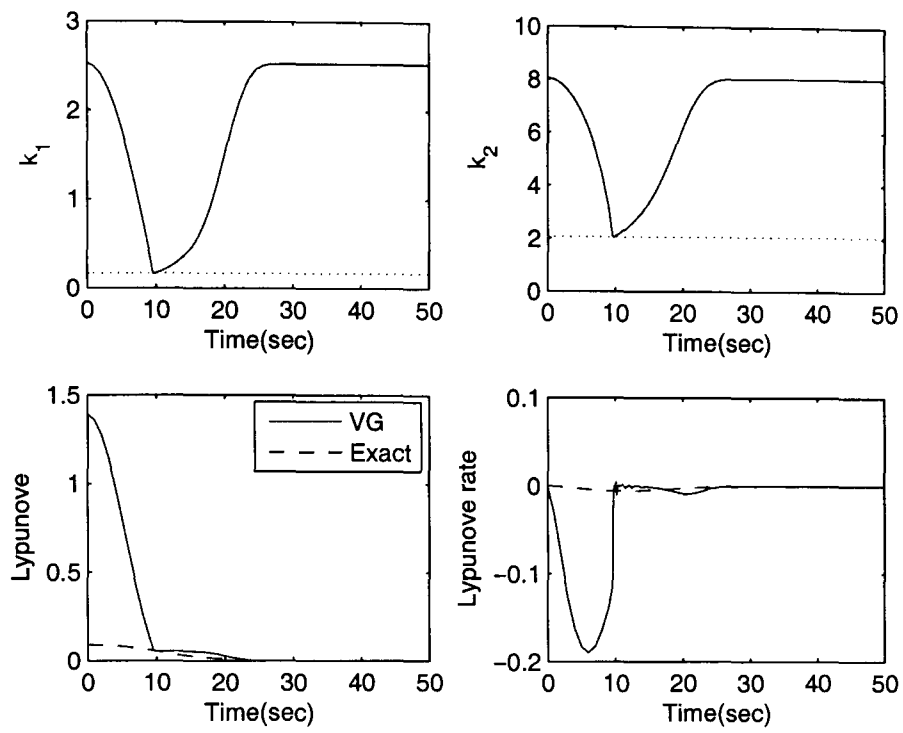

Figure 4.18: Simulation results for variable gain exact logic for $\theta_o = 60^o$.

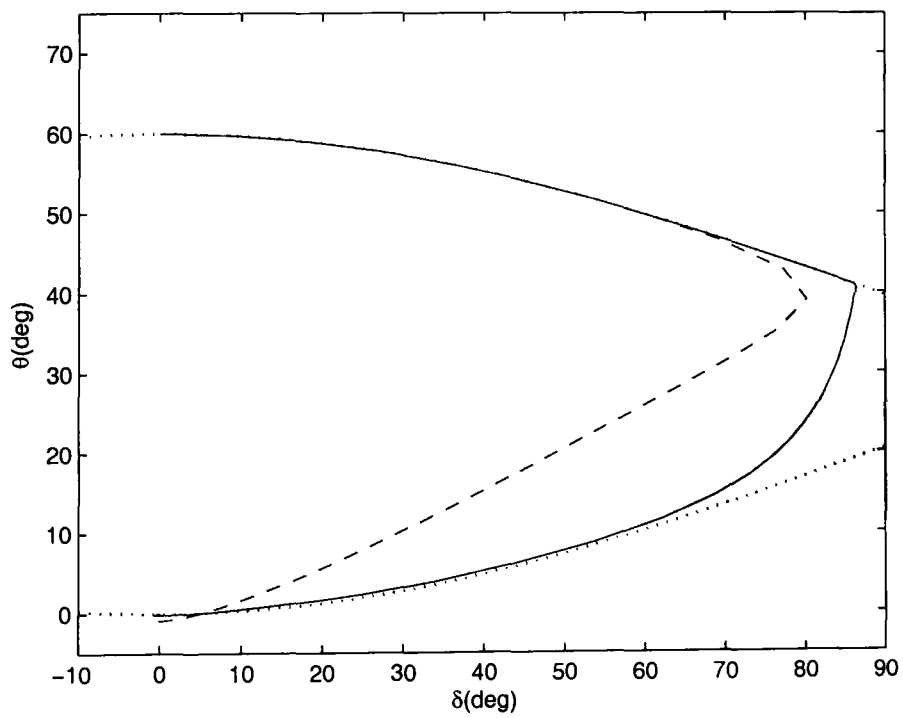

Figure 4.19: Simulation results for variable gain exact logic for $\theta_o = 60^o$.

Steering Law. A near-optimal choice of ω_n of variable gains case has been discussed. Variable gain steering has been shown to perform better than fixed gains steering.

In next chapter, this idea of exact steering with proper choice of gains will be extended to a four CMG pyramid system for three axis control.

Chapter 5

Exact Steering in Pyramid Type Four CMG Systems

5.1 Introduction

In this chapter, we shall develop an exact steering approach for four CMG pyramid systems. This new approach achieves an exact steering while using almost full momentum capability of CMG cluster by avoiding elliptic singularity. Moreover, this approach combines an extended version of feedback gains calculation technique proposed in Chapter 4 with a new steering law based on generalised inverse.

An exact steering law can use full momentum capability of a CMG cluster if it can effectively avoid elliptic singularity. Moore-Penrose steering law can not avoid elliptic singularity on its own, rather one has to add null motion to avoid internal singularities [8, 11, 12]. Steering laws with added null motion produce larger value of torque in order to avoid internal singularities. However, Margulies [83] has shown that mere existence of null motion does not guarantee the singularity avoidance. Similarly singularity robust (SR) steering law can not avoid elliptic singularity but it transits through singularity, therefore, this steering law is not able to use full momentum capability of CMG systems [11]. Generalised Singularity Robust (GSR) steering law is capable of escaping elliptic singularity and using larger angular momentum capability by causing pointing errors [128, 134]. Moreover, singularity robust techniques are not exact. Another approach to avoid elliptic singularity and using larger momentum envelope is

using preferred initial gimbal angles in MP or SR steering laws [124]. Preferred initial gimbal angles have non-zero values and they correspond to zero initial angular momentum of CMG cluster. Kurokawa [62] proposed an exact steering law which uses only a constrained momentum space.

The exact steering technique proposed in this chapter involves solving a three-axis attitude problem to generate an angular momentum path which uses full capability of the CMG cluster and then calculate corresponding feedback gains. This ensures a rapid slew rate matching the on-board CMGs capability. However, to realize this desired momentum path we need a steering law generating gimbal motion avoiding internal singularities. We have proposed a Generalised Inverse (GI) steering law to generate gimbal motion. GI steering law gives exact steering which avoids elliptic singularity, uses nearly full momentum capability of CMG cluster and returns gimbals to initial zero gimbal angle state.

5.2 Three-axis manoeuvres

In this section, a rest-rest three-axis manoeuvre of a satellite equipped with CMG cluster is described. The dynamic equation of such system is derived in Chapter 3 and it results in Eq. (3.7.32) which can be re-written as

$$\boldsymbol{I}\dot{\boldsymbol{\omega}} = -\dot{\boldsymbol{h}} - \boldsymbol{\omega} \times (\boldsymbol{I}\boldsymbol{\omega} + \boldsymbol{h}), \tag{5.2.1}$$

where $\boldsymbol{I}$ is inertia matrix of satellite, $\boldsymbol{\omega}$ is angular velocity vector of satellite, $\boldsymbol{h}$ is angular momentum vector associated with CMG cluster. A generalised three-axis manoeuvre of satellite equipped with four CMGs can be described as a single axis manoeuvre with angle θ about the eigen-axis $\boldsymbol{e}$. The quaternion representation of attitude of a satellite has been discussed in Chapter 3. A four parameter quaternion $\tilde{\boldsymbol{q}} = (q_o, q_1, q_2, q_3)$ has a scalar part q_o and a vector part $\boldsymbol{q} = [q_1, q_2, q_3]^T$. Quaternion $\tilde{\boldsymbol{q}}$ defined in Eq. (3.2.4) can be written in compact form as

$$\tilde{\boldsymbol{q}} = \cos\left(\frac{\theta}{2}\right) + \boldsymbol{e}\sin\left(\frac{\theta}{2}\right).$$

The quaternion kinematic equation (3.3.7) is also rewritten for the purpose of clarity

$$\begin{aligned} \dot{\boldsymbol{q}} &= \frac{1}{2}\left(q_o\boldsymbol{\omega} - \boldsymbol{\omega}\times\boldsymbol{q}\right), \\ \dot{q}_o &= -\frac{1}{2}\boldsymbol{\omega}^T\boldsymbol{q}. \end{aligned} \tag{5.2.2}$$

We consider a rest-to-rest eigen-axis manoeuvre about a given direction $\boldsymbol{e} = [e_1, e_2, e_3]^T$ with initial conditions $\boldsymbol{\omega}(0) = \mathbf{0}$, $\boldsymbol{h}(0) = \mathbf{0}$ and $\theta(0) = \theta_o$. Final conditions for the manoeuvre are $\boldsymbol{\omega}(t_f) = \mathbf{0}$, $\boldsymbol{h}(t_f) = \mathbf{0}$ and $\theta(t_f) = 0$, where t_f is the final time. Then the final condition for quaternion becomes $\tilde{\boldsymbol{q}}(t_f) = (1, 0, 0, 0)$ for $\theta(t_f) = 0$. Therefore, the error quaternion $\tilde{\boldsymbol{q}}_{\boldsymbol{e}}$ defined in Eq. (3.3.8) reduces to quaternion $\tilde{\boldsymbol{q}}$ at current time. The quaternion feedback control law is derived in Chapter 3 and it is given in Eq. (3.5.26). We assume that there is no external torque. Then the given control law reduces to the following form for rest-rest eigen-axis manoeuvre

$$\dot{\boldsymbol{h}} = \boldsymbol{K}_q\boldsymbol{q} + \boldsymbol{K}_\omega\boldsymbol{\omega} - \boldsymbol{\omega}\times(\boldsymbol{I}\boldsymbol{\omega} + \boldsymbol{h}), \tag{5.2.3}$$

where $\boldsymbol{K}_q = k_q\boldsymbol{I}$ and $\boldsymbol{K}_\omega = k_\omega\boldsymbol{I}$ are feedback gain matrices with k_q and k_ω as positive constants. For a manoeuvre about e-axis we can write

$$\boldsymbol{\omega} = \dot{\theta}\boldsymbol{e}, \tag{5.2.4}$$

$$\boldsymbol{q} = \sin\frac{\theta}{2}\boldsymbol{e}, \tag{5.2.5}$$

where $\dot{\theta}$ is slew rate of the body.

In the absence of external torque total angular momentum of the system remains conserved. Moreover with the given initial conditions $\boldsymbol{\omega}(0) = 0$, $\boldsymbol{h}(0) = 0$ the total angular momentum remains zero

$$\boldsymbol{I}\boldsymbol{\omega} + \boldsymbol{h} = 0.$$

Therefore, angular velocity of the vehicle is related to angular momentum of the CMG cluster as

$$\boldsymbol{\omega} = -\boldsymbol{I}^{-1}\boldsymbol{h}. \tag{5.2.6}$$

Vector $\boldsymbol{h}$ is parallel to vector $\boldsymbol{\omega}$ if later is about one of the principal axes of the vehicle or all three moment of inertia terms are equal i.e. vehicle has spherical symmetry. In

general for a given direction $\boldsymbol{e} = [e_1, e_2, e_3]^T$ of vector $\boldsymbol{\omega}$ there exist a direction $\boldsymbol{e_I}$ of vector $\boldsymbol{h}$ such that

$$\boldsymbol{Ie} = I_{ee}\boldsymbol{e_I}. \tag{5.2.7}$$

Where I_{ee} is effective moment of inertia in $\boldsymbol{e}$ direction and is defined as $I_{ee} = \sqrt{\boldsymbol{e}^T\boldsymbol{I}^T\boldsymbol{Ie}}$. Thus if manoeuvre is about $\boldsymbol{e}$ axis then $\boldsymbol{h}$ will vary about $\boldsymbol{e_I}$ axis.

A new variable $\eta \in [-\pi/2, \pi/2]$ is defined as a normalised measure of projection of vector $\boldsymbol{h}$ on direction $\boldsymbol{e_I}$. Thus we have

$$\boldsymbol{e_I}^T\boldsymbol{h} = h_e^{max} \sin\eta. \tag{5.2.8}$$

Here h_e^{max} is saturation value of angular momentum along $\boldsymbol{e_I}$ direction on momentum envelope. We also define the maximum slew rate capability about $\boldsymbol{e}$-axis as

$$\omega_e^{max} = h_e^{max}/\sqrt{\boldsymbol{e}^T\boldsymbol{II}^T\boldsymbol{e}}.$$

We substitute Eq. (5.2.8) and Eq. (5.2.4) in Eq. (5.2.3) and simplify it to get

$$\dot{\eta} = \frac{k_1 \sin\frac{\theta}{2} - k_\omega \sin\eta}{\cos\eta}, \tag{5.2.9}$$

where $k_1 = k_q/\omega_e^{max}$. Similarly, by using Eq. (5.2.8), Eq. (5.2.4) and Eq. (5.2.7) in Eq. (5.2.6) and after simplifying it we get

$$\dot{\theta} = -\omega_e^{max} \sin\eta. \tag{5.2.10}$$

These equations generate desired profile of normalised angular momentum variable η and vehicle's attitude θ. Thus we have reduced the problem to (η, θ) plane. The phase portrait in (η, θ) plane is similar to that of twin CMGs given in Chapter 4. Now we design feedback gains k_1 and k_ω such that momentum envelope is fully used (i. e. approach $\eta = \pi/2$) while avoiding singularity.

5.2.1 Feedback Gains

The Eq. (5.2.9) and Eq. (5.2.10) are reduced to the following form after eliminating η variable.

$$\ddot{\theta} + k_\omega\dot{\theta} + k_q \sin\frac{\theta}{2} = 0. \tag{5.2.11}$$

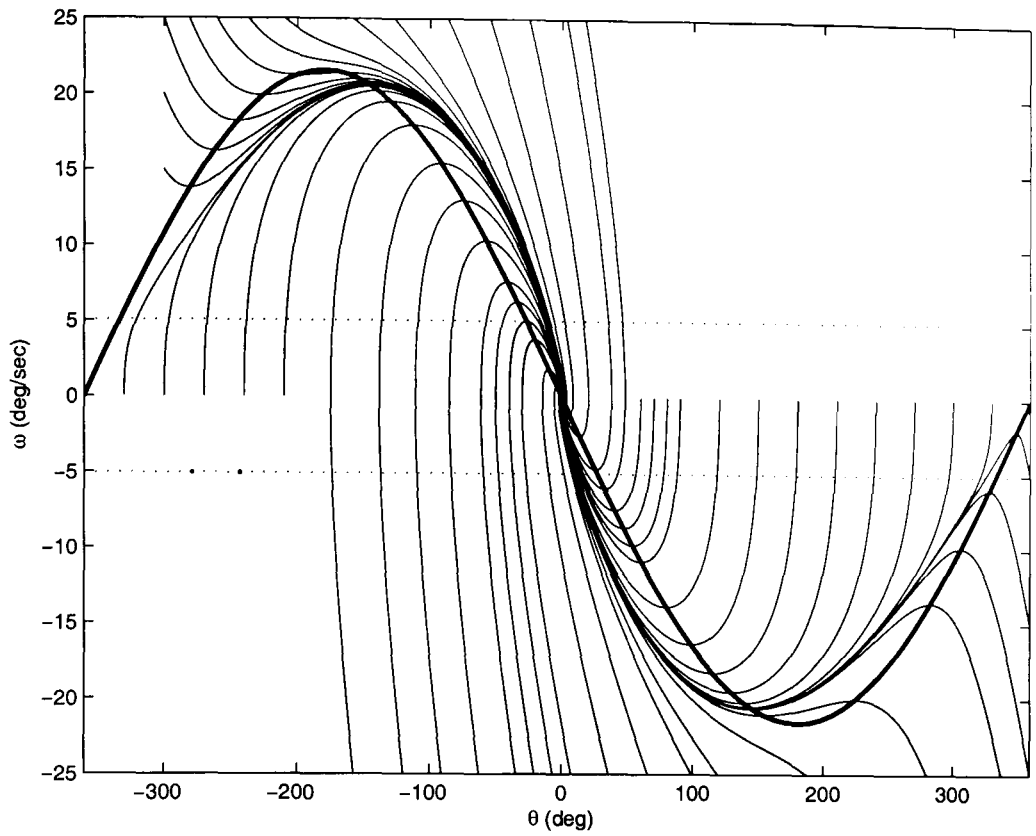

Figure 5.1: Phase portrait of damped non-linear pendulum model with $\zeta = 0.8$.

This is a damped pendulum equation. Feedback gains can be chosen as $k_q = 2\omega_n^2$ and $k_\omega = 2\zeta\omega_n$, where ω_n is natural frequency and ζ is damping ratio of closed-loop system. The factor of 2 is used in expression for k_q because here it is $\sin\frac{\theta}{2}$ rather than $\sin\theta$. The phase portrait of this nonlinear system is shown in Fig. (5.1). The natural frequency of linear closed-loop system calculated in Chapter 4 is given by

$$\omega_{nL} = \frac{\omega_e^{max} \exp\left(\frac{\phi}{\tan\phi}\right)}{\theta_o}, \tag{5.2.12}$$

where $\phi = \arccos\zeta$. If this frequency is used in the nonlinear system given by Eq. (5.2.11) then the corresponding trajectory starting from $(\theta_o, 0)$ does not pass through the critical point $(2\arcsin(\frac{\zeta\omega_e^{max}}{\omega_n}), -\omega_e^{max})$ as shown in Fig. (5.2). On the other hand, the nonlinear system (5.2.11) can not be solved analytically to calculate ω_n. However, we can find an approximate solution of Eq. (5.2.11) by using the fact that the trajectory of nonlinear system lies in the neighborhood of linear system's trajectory. The approximate solution will help to find the value of ω_n for which the desired trajectory passes through the critical point. We use the variational method to find an approximate solution of the

nonlinear equation. Eq. (5.2.11) is set up in the variational form as follows

$$\ddot{\theta} + 2\zeta\omega_n\dot{\theta} + \omega_n^2\theta = \omega_n^2(\theta_L - 2\sin\frac{\theta_L}{2}), \tag{5.2.13}$$

where θ_L is the solution of linear system and it is given by

$$\theta_L(t, \omega_{nL}) = \frac{\theta_o \exp(-\zeta\omega_{nL})}{\sin\phi}\sin(\omega_{nL}t\sin\phi + \phi).$$

The Eq.(5.2.13) can be re-arranged in the matrix form as

$$\begin{bmatrix} \dot{z}_1 \\ \dot{z}_2 \end{bmatrix} = \begin{bmatrix} 0 & 1 \\ -\omega_n^2 & -2\zeta\omega_n \end{bmatrix}\begin{bmatrix} z_1 \\ z_2 \end{bmatrix} + \begin{bmatrix} 0 \\ \omega_n^2 \end{bmatrix}(\theta_L - 2\sin\frac{\theta_L}{2}), \tag{5.2.14}$$

where $z_1 = \theta(t)$ and $z_2 = \dot{\theta}(t)$. The solution of this equation for the initial condition $[\theta_o, 0]^T$ is given by

$$\begin{aligned}\begin{bmatrix} z_1 \\ z_2 \end{bmatrix} &= \frac{\theta_o \exp(-\zeta\omega_n t)}{\sin\phi}\begin{bmatrix} \sin(\omega_n t\sin\phi + \phi) \\ -\omega_n\sin(\omega_n t\sin\phi) \end{bmatrix} \\ &+ \int_0^t \frac{\omega_n^2\exp(-\zeta\omega_n(t-s))}{\sin\phi}\begin{bmatrix} \sin(\omega_n(t-s)\sin\phi)/\omega_n \\ -\sin(\omega_n(t-s)\sin\phi - \phi) \end{bmatrix} \\ &\times\left(\theta_L(s) - 2\sin\frac{\theta_L(s)}{2}\right)ds. \end{aligned} \tag{5.2.15}$$

A trajectory starting from $[\theta_o, 0]^T$ will pass through the critical point if

$$\begin{bmatrix} \dot{z}_1 \\ \dot{z}_2 \end{bmatrix} = \begin{bmatrix} -\omega_e^{max} \\ 0 \end{bmatrix}.$$

By differentiating Eq. (5.2.15) we get

$$\begin{bmatrix} \dot{z}_1 \\ \dot{z}_2 \end{bmatrix} = \frac{\omega_n^2\theta_o\exp(-\zeta\omega_n t)}{\sin\phi}\left(1 - \frac{1}{\theta_o}\left(\theta_L(t) - 2\sin\frac{\theta_L(t)}{2}\right)\right)\begin{bmatrix} -\sin(\omega_n t\sin\phi)/\omega_n \\ \sin(\omega_n t\sin\phi - \phi) \end{bmatrix}.$$

Thus $\dot{z}_2 = 0$ implies that

$$\sin(\omega_n t\sin\phi - \phi) = 0$$

and this follows to the time at critical point

$$t^* = \frac{\phi}{\omega_n\sin\phi}.$$

We substitute t^* in $\dot{z}_1 = -\omega_e^{max}$ to get

$$\omega_n = \omega_{nL}/\alpha, \tag{5.2.16}$$

where

$$\alpha = 1 - \frac{1}{\theta_o}\left(\theta_L(t^*) - 2\sin\frac{\theta_L(t^*)}{2}\right). \tag{5.2.17}$$

Now Eq. (5.2.16) and Eq. (5.2.17) are solved numerically to find ω_n and α. We use Newton-Raphson method for numerical solution. Eq. (5.2.16) and Eq. (5.2.17) are re-arranged in the following form

$$\boldsymbol{F}(\omega_n, \alpha) = \begin{bmatrix} \alpha\omega_n - \omega_{nL} \\ \alpha\theta_o - \theta_o + \theta_L(t^*) - 2\sin\frac{\theta_L(t^*)}{2} \end{bmatrix} = 0. \tag{5.2.18}$$

The Jacobian of $\boldsymbol{F}$ is

$$\nabla\boldsymbol{F}(\omega_n, \alpha) = \begin{bmatrix} \alpha & \omega_n \\ (1 - \cos\frac{\theta_L}{2})\frac{\partial\theta_L}{\partial\omega_n} & \theta_o \end{bmatrix}, \tag{5.2.19}$$

where

$$\frac{\partial\theta_L}{\partial\omega_n} = \frac{\theta_o\omega_{nL}\phi\exp(-\frac{\omega_{nL}\phi}{\omega_n\tan\phi})}{\omega_n^2\sin^2\phi}\sin(\omega_{nL}\phi/\omega_n).$$

Now if

$$\boldsymbol{y} = \begin{bmatrix} \omega_n \\ \alpha \end{bmatrix}$$

then the Newton-Raphson formula for the ith iteration is

$$\boldsymbol{y}[i+1] = \boldsymbol{y}[i] - [\nabla\boldsymbol{F}(\boldsymbol{y}[i])]^{-1}\boldsymbol{F}(\boldsymbol{y}[i])$$

with

$$\boldsymbol{y}[0] = \begin{bmatrix} \omega_{nL} \\ 1 \end{bmatrix}.$$

This method gives us an approximate value of ω_n corresponding to trajectory which nearly passes through critical point. The difference is only 0.05% of maximum slew rate. In Table (5.1) we compare the natural frequencies for linear and nonlinear systems for different slew angles. It can be seen that for small angles the difference between linear and nonlinear frequencies is quite small and it grows with increasing slew angle.

Table 5.1: Comparison of natural frequencies ω_{nL} and ω_n for linear and non-linear systems respectively with different slew angles.

θ_o(deg)	ω_{nL}(rad/s)	ω_n(rad/s)	α
10	1.1940	1.1945	0.9996
20	0.5970	0.5979	0.9984
30	0.3980	0.3994	0.9964
40	0.2985	0.3004	0.9936
50	0.2388	0.2412	0.9899
60	0.1990	0.2019	0.9854
70	0.1706	0.1741	0.9800
80	0.1492	0.1533	0.9736

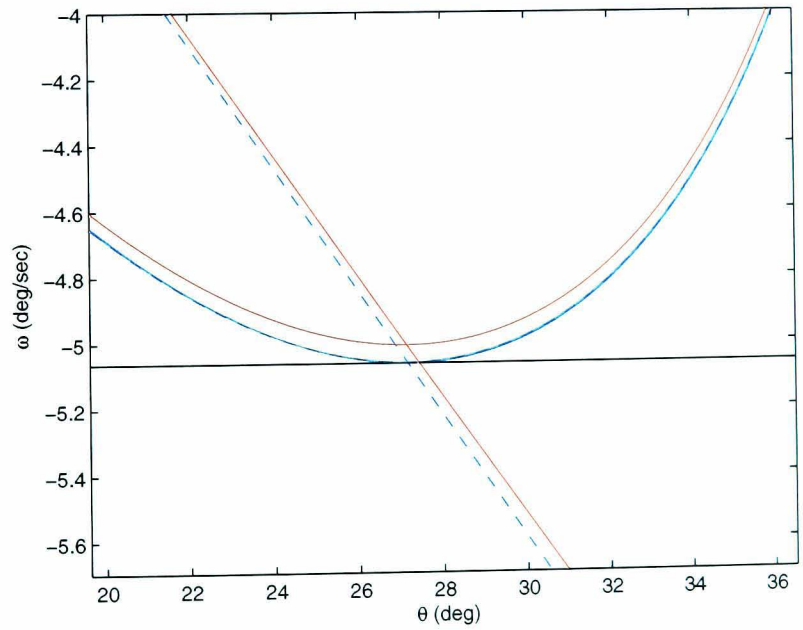

Figure 5.2: Nullcline for linear (dashed) and nonlinear (solid) systems; ω_{nL} used in linear system made trajectory to pass through critical point; ω_{nL} used in nonlinear system made trajectory to turn before critical point; ω_n used in nonlinear system made trajectory to pass through critical point.

5.3 Four CMG Pyramid Systems

In this section, mathematical model for CMG systems is used to define singularities and maximum slew capability in a particular direction. We consider a cluster of four identical CMGs placed symmetrically in a pyramid configuration with skew angle β as shown in Fig. (5.3). Here $\boldsymbol{h}_i$ is the angular momentum vector associated for ith CMG, $\hat{\boldsymbol{g}}_{yi}$ is fixed gimbal direction and $\boldsymbol{d}_i$ is torque vector as explained in Chapter 3. The vector $\boldsymbol{h}$ for four CMGs pyramid system is defined as

$$\boldsymbol{h} = h_{cmg} \begin{bmatrix} -c\beta \sin\delta_1 - \cos\delta_2 + c\beta \sin\delta_3 + \cos\delta_4 \\ \cos\delta_1 - c\beta \sin\delta_2 - \cos\delta_3 + c\beta \sin\delta_4 \\ s\beta \sin\delta_1 + s\beta \sin\delta_2 + s\beta \sin\delta_3 + s\beta \sin\delta_4 \end{bmatrix}, \tag{5.3.20}$$

where $\delta_i, i = 1,2,3,4$ is gimbal angle of ith CMG, (h_{cmg}) is magnitude of angular momentum and $c\beta = \cos\beta$ and $s\beta = \sin\beta$. The output torque of CMGs is

$$\dot{\boldsymbol{h}} = \boldsymbol{D_1}\dot{\boldsymbol{\delta}}$$

where $\boldsymbol{D_1}$ is Jacobian matrix defined as $\frac{\partial \boldsymbol{h}}{\partial \boldsymbol{\delta}}$ or

$$\boldsymbol{D_1} = h_{cmg} \begin{bmatrix} -c\beta\cos\delta_1 & \sin\delta_2 & c\beta\cos\delta_3 & -\sin\delta_4 \\ -\sin\delta_1 & -c\beta\cos\delta_2 & \sin\delta_3 & c\beta\cos\delta_4 \\ s\beta\cos\delta_1 & s\beta\cos\delta_2 & s\beta\cos\delta_3 & s\beta\cos\delta_4 \end{bmatrix}. \tag{5.3.21}$$

We have defined the singularity of a CMG cluster in Chapter 3. A CMG cluster is said to be singular in a given direction $\boldsymbol{e}_I$ if torque vectors $\boldsymbol{d}_i$ (ith column of matrix $\boldsymbol{D}_1$) associated with all four CMGs become co-planner. Mathematically $\boldsymbol{e}_I^T \boldsymbol{d}_i = 0$ for all i. Where $\boldsymbol{e}_I$ is a unit vector normal to that plane. Note that the direction $\boldsymbol{e}_I$ is related to the direction of required manoeuvre $\boldsymbol{e}$ through relation (5.2.7). A singular torque vector $\boldsymbol{d}_i^s$ is defined in Eq. (3.7.35) which can be rewritten for singular direction $\boldsymbol{e}_I$ as

$$\boldsymbol{d}_i^s = \sigma_i h_{cmg} \frac{\hat{\boldsymbol{g}}_{yi} \times \boldsymbol{e}_I}{|\hat{\boldsymbol{g}}_{yi} \times \boldsymbol{e}_I|},$$

where $\sigma_i = \pm 1$. Similarly a singular angular momentum vector can be defined by using Eq. (3.7.37) as

$$\boldsymbol{h}^s = h_{cmg} \sum_{i=1}^{4} \sigma_i \frac{(\hat{\boldsymbol{g}}_{yi} \times \boldsymbol{e}_I) \times \hat{\boldsymbol{g}}_{yi}}{|\hat{\boldsymbol{g}}_{yi} \times \boldsymbol{e}_I|}.$$

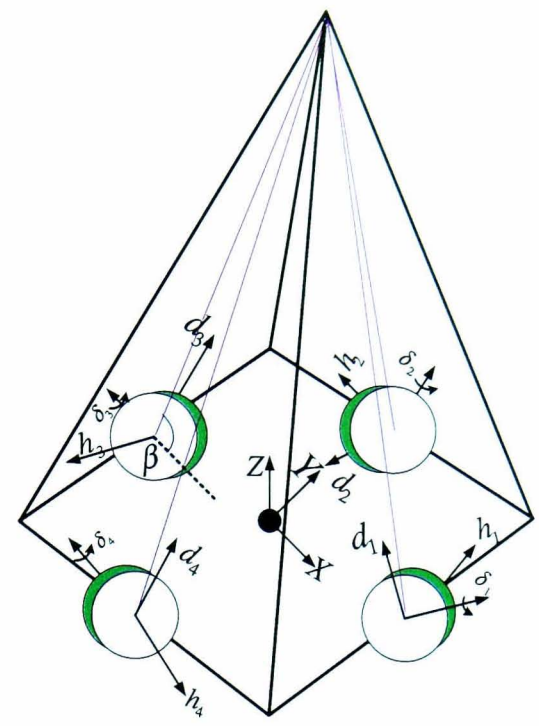

Figure 5.3: Four CMG pyramid system.

The projection of angular momentum vector on direction $\boldsymbol{e}_I$ is given by

$$\begin{aligned} \boldsymbol{e}_I^T \boldsymbol{h}^s &= h_{cmg} \sum_{i=1}^{4} \sigma_i \frac{\boldsymbol{e}_I^T (\hat{\boldsymbol{g}}_{yi} \times \boldsymbol{e}_I) \times \hat{\boldsymbol{g}}_{yi}}{|\hat{\boldsymbol{g}}_{yi} \times \boldsymbol{e}_I|} \\ &= h_{cmg} \sum_{i=1}^{4} \sigma_i |\hat{\boldsymbol{g}}_{yi} \times \boldsymbol{e}_I|. \end{aligned} \tag{5.3.22}$$

For saturation singularity we choose $\sigma_i = +1$ for all CMGs. Therefore, full momentum capacity in a given direction $\boldsymbol{e}_I$ is found to be

$$h_e^{max} = h_{cmg} \sum_{i=1}^{4} |\hat{\boldsymbol{g}}_{yi} \times \boldsymbol{e}_I|. \tag{5.3.23}$$

The maximum slew rate capability of the vehicle about $\boldsymbol{e}$-axis ω_e^{max} can be defined as

$$\begin{aligned} \omega_e^{max} &= \frac{h_e^{max}}{I_{ee}} \\ &= \frac{h_{cmg}}{I_{ee}} \sum_{i=1}^{4} |\hat{\boldsymbol{g}}_{yi} \times \boldsymbol{e}_I|. \end{aligned} \tag{5.3.24}$$

5.4 Generalised Inverse Steering Law

In previous sections, we have formulated an approach to compute feedback gains for a three-axis reorientation manoeuvre such that full momentum capacity of CMG cluster

could be used. And we can also generate a desired momentum profile for a given manoeuvre as

$$\boldsymbol{h}(\boldsymbol{\delta}) = h_e^{max} \sin \eta \boldsymbol{e}_I.$$

It can be noted that angular momentum of CMGs is nonlinear function of gimbal angles as given in Eqn. (5.3.20). Because of non-linearity of angular momentum function it is not easy to solve for gimbal angles directly from a given angular momentum profile. However, it can be noted that the differential $d\boldsymbol{h}$ is a linear function of differential $d\boldsymbol{\delta}$. Therefore, pseudo-inverse based approach and its singularity robust variants are used to find gimbal rates and then gimbal angles. However, the internal singularities associated with pseudo-inverse can affect the ability of CMGs to follow the desired momentum profile. To overcome this problem we introduce a new approach based on generalised inverse rather than pseudo-inverse in order to avoid encounter with elliptic singularity and to be able to follow desired momentum profile as close as possible. Margulies [83] has defined the three rows of $\boldsymbol{D_1}$ as basis of torque producing gimbal rate space to obtain Moore-Penrose inverse. We can define a new 3×4 matrix $\boldsymbol{A}(\boldsymbol{\delta})$ such that

$$\dot{\boldsymbol{\delta}} = \boldsymbol{A^T v}. \tag{5.4.25}$$

Here three rows of matrix $\boldsymbol{A}$ are defined as basis of gimbal rate space with $\boldsymbol{v} = [v_x, v_y, v_z]^T$ be the components in these basis. We know that

$$\begin{aligned} \dot{\boldsymbol{h}} &= \boldsymbol{D_1}\dot{\boldsymbol{\delta}} \\ &= \boldsymbol{D_1 A^T v}. \end{aligned}$$

If $\boldsymbol{D_1 A^T}$ is not singular then

$$\boldsymbol{v} = (\boldsymbol{D_1 A^T})^{-1}\dot{\boldsymbol{h}}. \tag{5.4.26}$$

This leads to a generalised inverse steering law

$$\dot{\boldsymbol{\delta}} = \boldsymbol{A^T}(\boldsymbol{D_1 A^T})^{-1}\dot{\boldsymbol{h}}. \tag{5.4.27}$$

One can note that Moore-Penrose inverse is just a special case of this generalised inverse when $\boldsymbol{A} = \boldsymbol{D_1}$. The detailed discussion about generalised inverse of matrices can be found in Ref. [7, 17]. The fundamental properties of generalised matrices, such

that two matrices $\boldsymbol{X}$ and $\boldsymbol{Y}$ are generalised inverse of each other, can be defined as

$$\begin{aligned} \boldsymbol{YXY} &= \boldsymbol{Y}, \\ \boldsymbol{XYX} &= \boldsymbol{X}, \\ (\boldsymbol{XY})^T &= \boldsymbol{XY}, \\ (\boldsymbol{YX})^T &= \boldsymbol{YX}. \end{aligned}$$

The proposed generalised inverse based on matrix $\boldsymbol{A}$ satisfy all except third property whereas Moore-Penrose inverse uniquely satisfy all four properties. Now we need to find the matrix $\boldsymbol{A}$ such that elliptic singularity could be avoided. Moreover, in this case singularities of the matrix $\boldsymbol{D}_1\boldsymbol{A}^T$ are also very important. Therefore, we try to choose matrix $\boldsymbol{A}$ such that its singularities are not encountered in the momentum workspace of the CMG cluster. If singularity of matrix $\boldsymbol{A}$ is encountered inside the momentum workspace defined by feedback (which were designed to maximise the workspace) then we need to reduce feedback gains to exclude the singularity of matrix $\boldsymbol{A}$. The choice of matrix $\boldsymbol{A}$ is explained in next section.

5.5 Elliptic Singularity Avoidance through Choice of the Matrix $\boldsymbol{A}$

There are many possible choices of matrix $\boldsymbol{A}$. But the choice of $\boldsymbol{A}$ is made such that the elliptic singularity could be avoided and momentum capability of CMG cluster could fully be used. We have made the following choice

$$\boldsymbol{A} = \boldsymbol{D}_1 + \boldsymbol{D}_o. \tag{5.5.28}$$

Here matrix $\boldsymbol{D}_o$ for four identical CMG system is given by

$$\boldsymbol{D_o} = h_{cmg} \begin{bmatrix} -c\beta \sin\delta_1 & -\cos\delta_2 & c\beta \sin\delta_3 & \cos\delta_4 \\ \cos\delta_1 & -c\beta \sin\delta_2 & -\cos\delta_3 & c\beta \sin\delta_4 \\ s\beta \sin\delta_1 & s\beta \sin\delta_2 & s\beta \sin\delta_3 & s\beta \sin\delta_4 \end{bmatrix}. \tag{5.5.29}$$

For this choice of matrix $\boldsymbol{A}$ the gimbal rate command $\dot{\boldsymbol{\delta}}$ will be different from those of Moore-Penrose case or its singularity robust variants. As a result gimbal angles will follow a different path and hence a different angular momentum profile. Ideally we should

be able to find a matrix $\boldsymbol{A}$ which could enable us to use full momentum envelope or workspace by avoiding elliptic singularity. For example in pyramid type CMG system with four units the elliptic singularity in roll direction is $[-\pi/2, 0, \pi/2, 0]$. MP-inverse solution and its singularity robust variant uses only two CMGs (1 and 3 in this case) for roll direction control if initial gimbal angles are set at zero. That is why gimbal angle trajectories hit elliptic singularity. In this situation elliptic singularity can only be avoided by using all four CMGs which is achieved by given choice of matrix $\boldsymbol{A}$ as shown in Fig. (5.8). In this figure generalised singularity robust (GSR) steering law initially uses only two CMGs as it is based on a modified MP inverse and then hit elliptic singularity and start using all four CMGs to escape singularity. On the other hand, proposed steering law uses all four CMGs from start and avoids elliptic singularity. Therefore, for the given choice of matrix $\boldsymbol{A}$ we can avoid elliptic singularity of matrix $\boldsymbol{D}_1$ which enables us to use much larger percentage of the momentum workspace (see Fig. (5.11)). In the roll direction singularity of matrix $\boldsymbol{A}$ is encountered near the boundary of workspace. To exclude this singularity we need to slightly reduce the workspace by reducing the feedback gains. Here we explain how to reduce the feedback gains to reduce the workspace. We calculate the $\det\left(\boldsymbol{D}_1\boldsymbol{A}^T\right)$ as function of variable η and plot it as shown in Fig. (5.4). It can be seen that matrix $\boldsymbol{D}_1\boldsymbol{A}^T$ becomes singular at $\eta^s = 74^o$. As generalised-inverse steering law is not singularity robust so we need to avoid this singularity by reducing feedback gains. To exclude this singularity from workspace we need to reduce the natural frequency ω_n by factor $\sin\eta^s$

$$\omega_n^s = \omega_n \sin\eta^s.$$

The reduction in feedback gains will shift the turning point of the trajectory in (η, θ) phase-plane from $(\pi/2, 2\arcsin(\zeta\omega_e^{max}/\omega_n))$ to a new point $(\eta^s, 2\arcsin(\zeta\omega_e^{max}/\omega_n^s))$. The reduced work space is $\sin\eta^s \times 100$ percent of the maximum available momentum space h_e^{max}. For example when $\eta^s = 74^o$ then available work space is 96 percent of full momentum space.

Another feature of generalised-inverse steering law is return of gimbal angles to zero at the end of the manoeuvre provided singularity has not been encountered (see Fig. (5.8)). This is a very useful feature.

This choice of matrix $\boldsymbol{A}$ has a disadvantage of being not able to start at preferred gimbal angles. These are non-zero initial gimbal angles corresponding to zero initial angular momentum. The advantage of using preferred gimbal angles in MP-inverse based steering laws is that they help in avoiding elliptic singularity. A detailed discussion on preferred gimbal angles can be found in Ref. [124]. The preferred gimbal angles for roll manoeuvre are $[\pi/4, -\pi/4, \pi/4, -\pi/4]$. The matrix $\boldsymbol{A}$ is singular for these preferred gimbal angles.

$$\boldsymbol{A} = \sqrt{2}h_{cmg}\begin{bmatrix} -c\beta & -1 & c\beta & 1 \\ 0 & 0 & 0 & 0 \\ s\beta & 0 & s\beta & 0 \end{bmatrix}$$

Thus proposed steering law cannot start from this singularity. The preferred gimbal angles are good initial conditions for MP-inverse based steering laws whereas for the proposed steering law $[0, 0, 0, 0]$ can be considered preferred gimbal initial condition.

In this thesis, we do not study the singularities of matrix $\boldsymbol{A}$. We have seen that for roll manoeuvre with initial gimbal angles at zero the singularity is encountered near the outer envelope of the momentum.

In next subsection, we introduce a variant of proposed steering law which uses a modified form of matrix $\boldsymbol{A}$. This steering law will be able to use even larger momentum space. Moreover, modified law will also be able to start from preferred gimbal angles.

5.5.1 A Modified Form of the Matrix A

We introduce a modified form of matrix $\boldsymbol{A}$ as

$$\boldsymbol{A} = \boldsymbol{D}_1 + \lambda \boldsymbol{D}_o. \tag{5.5.30}$$

Here choice of parameter λ is crucial in extending the workspace to its maximum limit. We choose

$$\lambda = \lambda_o \exp(-\mu \det(\boldsymbol{D}_1 \boldsymbol{D}_1^{\mathrm{T}})),$$

where λ_o and μ are the constants to be fixed. The value of λ increases as system approaches towards singularity. The matrix $\boldsymbol{A}$ causes all four CMGs to move to avoid elliptic singularity. In Fig. (5.5) we plot $\det\left(\boldsymbol{D}_1 \boldsymbol{A}^T\right)$ with variable η. The singularity of

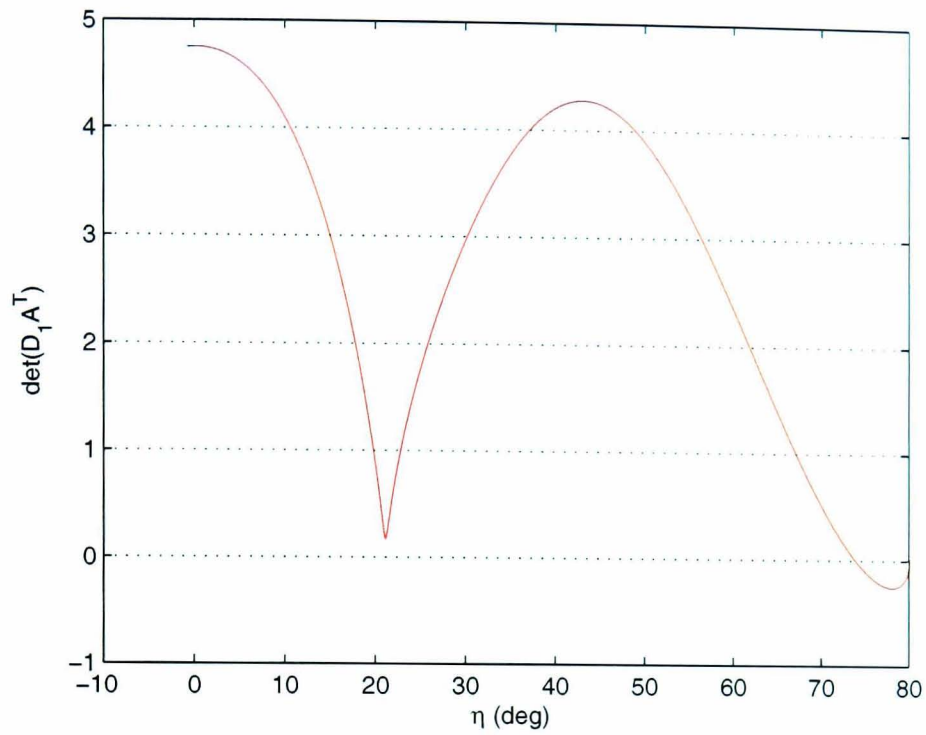

Figure 5.4: Plot of $\det\left(\boldsymbol{D}_1\boldsymbol{A}^T\right)$ vs. η; this plot is used to reduce the workspace.

matrix $\boldsymbol{A}$ is now encountered at $\eta^s = 80^o$ which corresponds to 98 percent of maximum envelope. Therefore, feedback gains are slightly reduced to exclude this singularity. If matrix $\boldsymbol{A}$ does not encounter singularity within the workspace then gimbal angle profiles return back to zero (see Fig. (5.15)). This is an advantage of using this GI approach with prescribed choice of matrix $\boldsymbol{A}$. Moreover, with this modified form of $\boldsymbol{A}$ the generalised inverse based steering law can start from preferred gimbal angles (see Fig. (5.16)).

5.5.2 Matrix A for an Arbitrary Direction of Manoeuvre

Here we generalise the procedure of finding a suitable matrix $\boldsymbol{A}$ for an arbitrary direction of manoeuvre. A search for an optimal choice of λ_o and μ is performed such that η^s (singularity of matrix $\boldsymbol{A}$) is as close to 90^o (saturation singularity) as possible. This can be achieved by maximizing the minimum value of $\det(\boldsymbol{D}_1\boldsymbol{A}^T)$ with respect to λ_o and μ. As we need to search these parameters over η space, so it is convenient to re-arrange the Generalised Inverse steering law (5.4.27) in order to make η as an

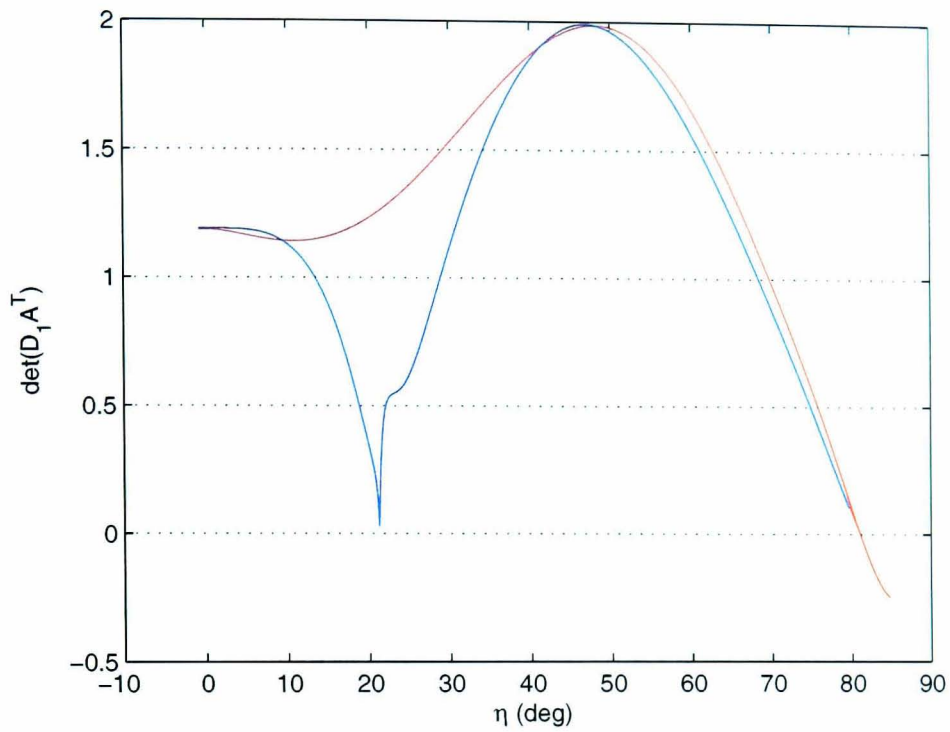

Figure 5.5: Plot of $\det\left(\boldsymbol{D}_1\boldsymbol{A}^T\right)$ vs. η for modified $\boldsymbol{A}$.

independent variable rather than time. Differentiating Eq. (5.2.8) yields

$$\dot{\boldsymbol{h}} = h_e^{max}\cos\eta\dot{\eta}\boldsymbol{e_I}.$$

Now we can replace $\boldsymbol{e_I}$ and h_e^{max} by using Eq. (5.2.7) and

$$h_e^{max} = \omega_e^{max} I_{ee}.$$

Therefore,

$$\dot{\boldsymbol{h}} = \omega_e^{max}\cos\eta\dot{\eta}\boldsymbol{I}\boldsymbol{e}.$$

By substituting $\dot{\boldsymbol{h}}$ from this equation in Eq. (5.4.27) we get

$$\dot{\boldsymbol{\delta}} = \boldsymbol{A^T}(\boldsymbol{D_1}\boldsymbol{A^T})^{-1}\omega_e^{max}\cos\eta\dot{\eta}\boldsymbol{I}\boldsymbol{e}.$$

Now this equation can be re-arranged to get the following form

$$\frac{\mathrm{d}\boldsymbol{\delta}}{\mathrm{d}\eta} = \boldsymbol{A^T}(\boldsymbol{D_1}\boldsymbol{A^T})^{-1}\cos\eta\omega_e^{max}\boldsymbol{I}\boldsymbol{e}. \tag{5.5.31}$$

This equation can be used to determine the workspace excluding the singularity of matrix $\boldsymbol{A}$ characterized by variable η^s in all directions. Then feedback gains are found

Table 5.2: Simulation Data.

Parameter	Value
h_{cmg}	0.28 Nms
$[I_x, I_y, I_z]$	$[10, 10, 10]$ kgm^2
ζ	0.8
ω^{max}	5.06 deg/s
β	54.7 deg

for reduced workspace by reducing ω_n by the factor of $\sin \eta^s$. The constants λ_o and μ are tuned to maximize the value of η^s for a given direction $\boldsymbol{e}$. This procedure is used to find $\lambda_o = 1.2$ and $\mu = 5.0$ with $\eta^s = 80^o$ in roll direction $\boldsymbol{e} = [1, 0, 0]^T$. These values of λ_o and μ are used while simulating modified GI steering law in examples 2 and 3 of the next section, where we shall present and discuss the simulation result of the proposed steering techniques for roll manoeuvre examples.

5.6 Simulation and Results

In this section, we shall simulate the Generalized Inverse Steering Law (GISL) for different rest-to-rest manoeuvre examples. The satellite and CMGs data used in these simulations is summarized in Table (5.2). Here BILSAT-1 data values (satellite/CMG sizes) are used except it uses four CMGs pyramid system. To test the performance of GISL for the given two choices of matrix $\boldsymbol{A}$ we have selected the roll manoeuvre example with initial values of gimbal angles to be zero. We know that in pyramid arrangement of four CMG systems roll and pitch directions have elliptic singularity problem. For this reason we have chosen the roll manoeuvre example. We have compared the performance of the proposed method with Generalised Singularity Robust (GSR) method given in Eq. (3.7.42), which is known to be best to pass/escape elliptic singularity by introducing a small de-tour in angular momentum direction. In another example proposed method is tested for a roll manoeuvre with a set of preferred initial gimbal angles.

In example 1 we perform a 40 deg roll manoeuvre to demonstrate that the proposed

logic can exploit almost full momentum envelope. We know that the Singularity Robust logic can access only a restricted momentum space due to elliptic singularity and this issue of larger momentum usage by avoiding elliptic singularity has been addressed in GSR to large extent. However, issues like exactness of control action, attitude error and return of gimbal angles at the end of the manoeuvre are better addressed in proposed steering law than GSR while exploiting almost full momentum capability. We compare the performance of proposed method with GSR while choosing same feedback gains for both methods. Figure (5.6) shows that proposed law generates angular rate only in roll direction whereas GSR causes small motions in other two directions also. Moreover, roll rate, in the case of GSR, saturates at elliptic singularity for some time then it increases as system escapes the singularity. As a result roll angle, in the case of proposed law, settles in shorter time and has no attitude errors in pitch and yaw directions as shown in Fig. (5.7). To explain the reason for this improved performance we plot gimbal angle profiles in Fig. (5.8). Pseudo-inverse based steering laws (which include GSR) lead CMG system towards elliptic singularity $[-\pi/0, 0, \pi/2, 0]$ due to symmetric motion of only two gimbals (1 and 3). The GSR escapes singularity by then moving all four gimbals and breaking the symmetric motion of gimbals 1 and 3. This leaves gimbals in non-zero gimbal state at the completion of manoeuvre. Whereas proposed steering law uses motion of all four gimbals from the start of the manoeuvre and becomes able to avoid elliptic singularity at first place. Moreover, it brings back gimbals to initial zero state at the end of manoeuvre. In Fig. (5.9) we have compared the gimbal rate profiles. For proposed steering law the gimbal rates are not significantly larger than those of GSR law. In Fig. (5.10) we have plotted the singularity indices and norm of angular momentum vector. For the same feedback gains and control structure GI exploits larger angular momentum than GSR. The same fact can be seen in Fig. (5.11). However, due to singularity of matrix $\boldsymbol{A}$ we can not exploit momentum to full extent.

In example 2 we compare the modified GI steering law with GSR steering law. The constants $\lambda_o = 1.2$ and $\mu = 5.0$ are used in modified GI simulation. The results are shown in Fig. (5.12), Fig. (5.13), Fig. (5.14) and Fig. (5.15). The improvement of using modified form can only be seen in phase-portrait where it exploits even larger momen-

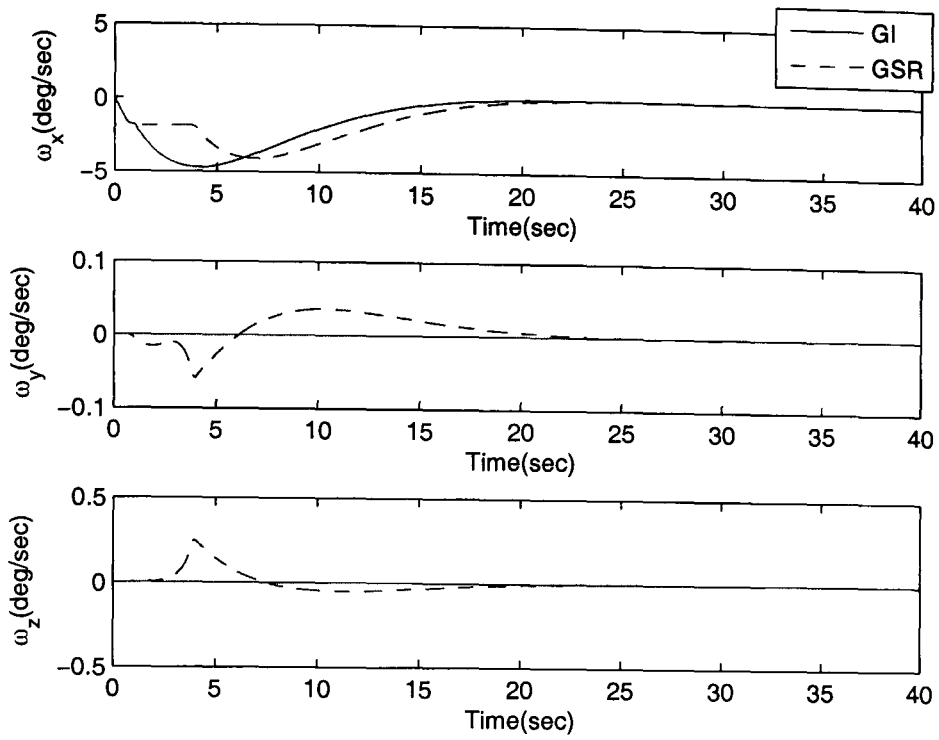

Figure 5.6: Roll manoeuvre example 1: angular velocity components of satellite in body coordinates for proposed Generalised-Inverse (GI) steering law and GSR steering law.

tum.

In example 3 we have simulated a roll manoeuvre with initial preferred gimbal angles $[\pi/4, -\pi/4, \pi/4, -\pi/4]$. Pseudo-inverse based steering methods use motion of all four gimbal to avoid elliptic singularity if they start from preferred gimbal angles. We have compared the proposed GI with GSR. In both cases gimbal angles follow similar path and return back to initial condition of gimbal angles whereas for GSR case they do not come back as shown in Fig. (5.16). This close following of the gimbal angles by two methods could be explained on the following basis. GSR law is based on pseudo-inverse for which given gimbal condition is preferred initial condition. Therefore, gimbal angles remain well away from singularity as seen in Fig. (5.18). Similarly proposed GI method with modified matrix $\boldsymbol{A}$ will have a very small value of parameter $\lambda = \lambda_o \exp(-\mu \det(\boldsymbol{D}_1 \boldsymbol{D}_1^{\mathrm{T}}))$ as system remains away from singularity for preferred initial gimbal angles. Therefore it generates solution close to pseudo-inverse. However, a small difference in gimbal angle trajectories generated by two methods is captured in Fig. (5.17). As GSR has not encounter singularity in this example, therefore, induced

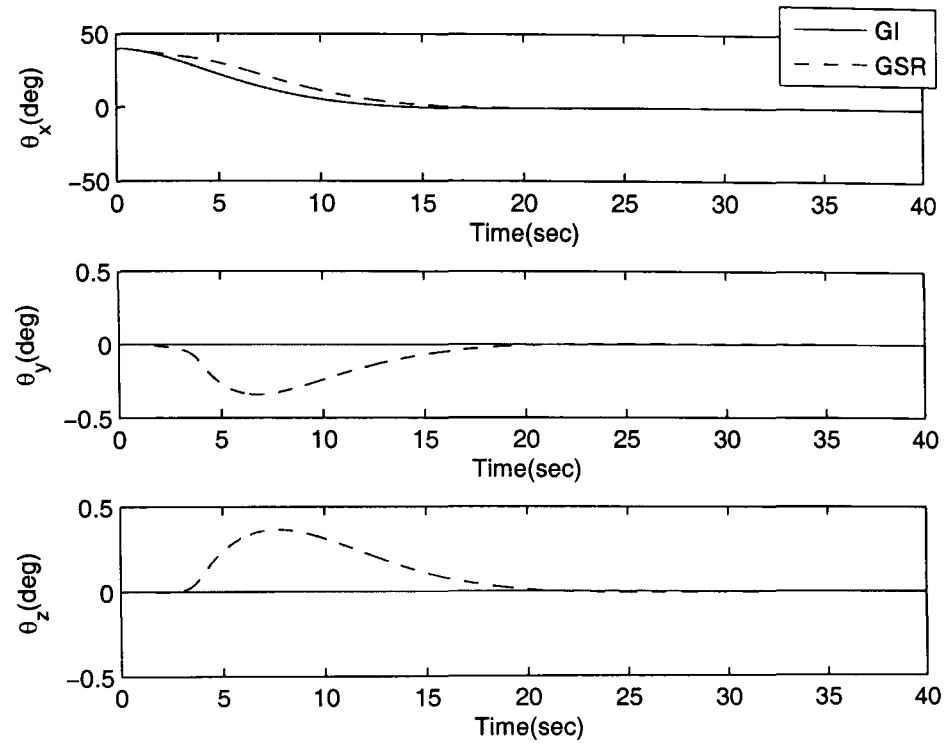

Figure 5.7: Roll manoeuvre example 1: attitude angles of satellite for proposed Generalised-Inverse (GI) steering law and GSR steering law.

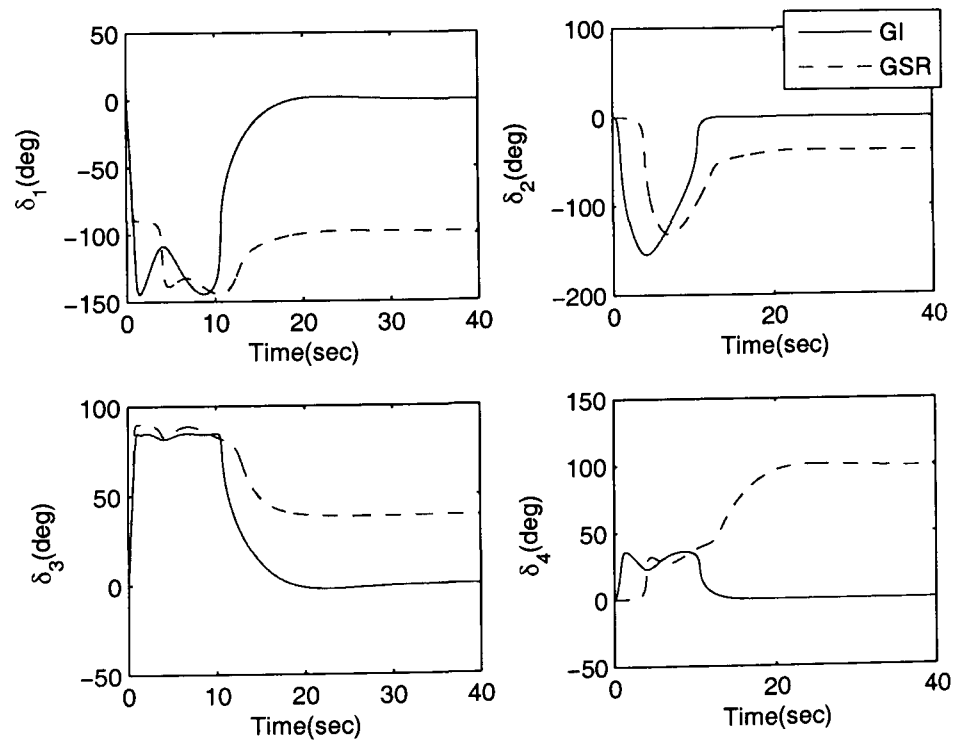

Figure 5.8: Roll manoeuvre example 1: gimbal angle profile for proposed Generalised-Inverse (GI) steering law and GSR steering law.

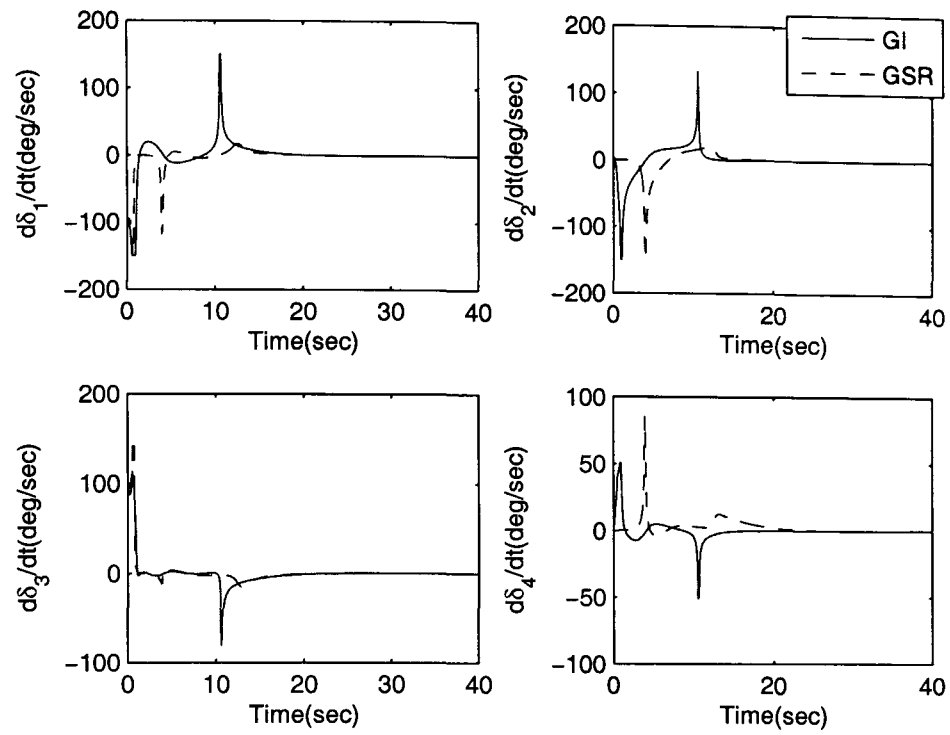

Figure 5.9: Roll manoeuvre example 1: gimbal rate profile for proposed Generalised-Inverse (GI) steering law and GSR steering law.

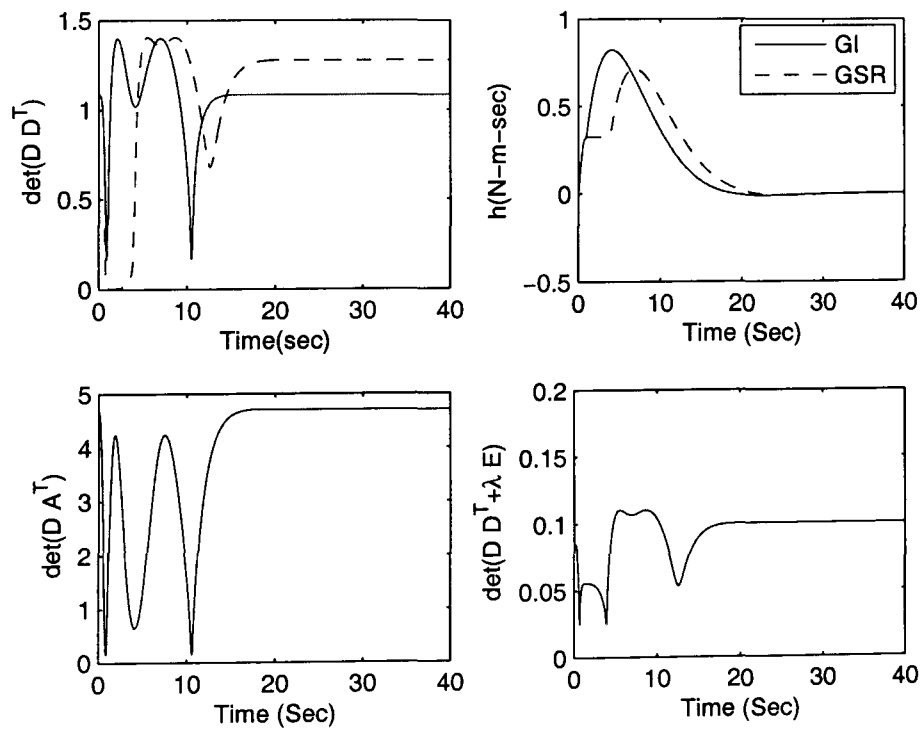

Figure 5.10: Roll manoeuvre example 1:(a) singularity index (b) angular momentum profile for proposed Generalised-Inverse (GI) steering law and GSR steering law (c) singularity index of GI and (d) singularity index of GSR.

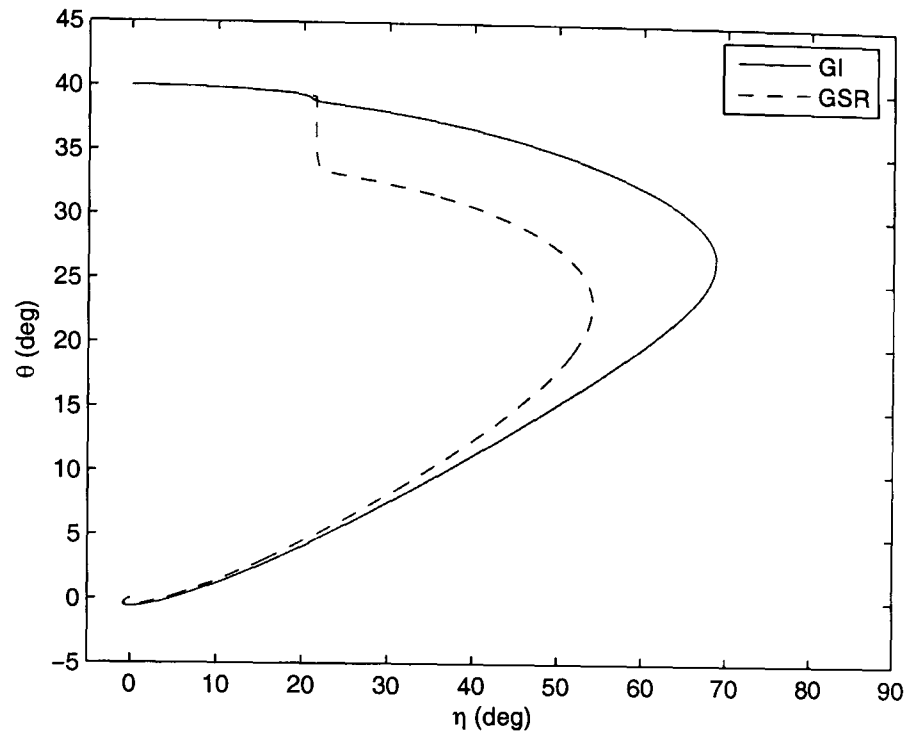

Figure 5.11: Roll manoeuvre example 1:the phase portrait comparison of proposed Generalised-Inverse (GI) steering law and GSR steering law.

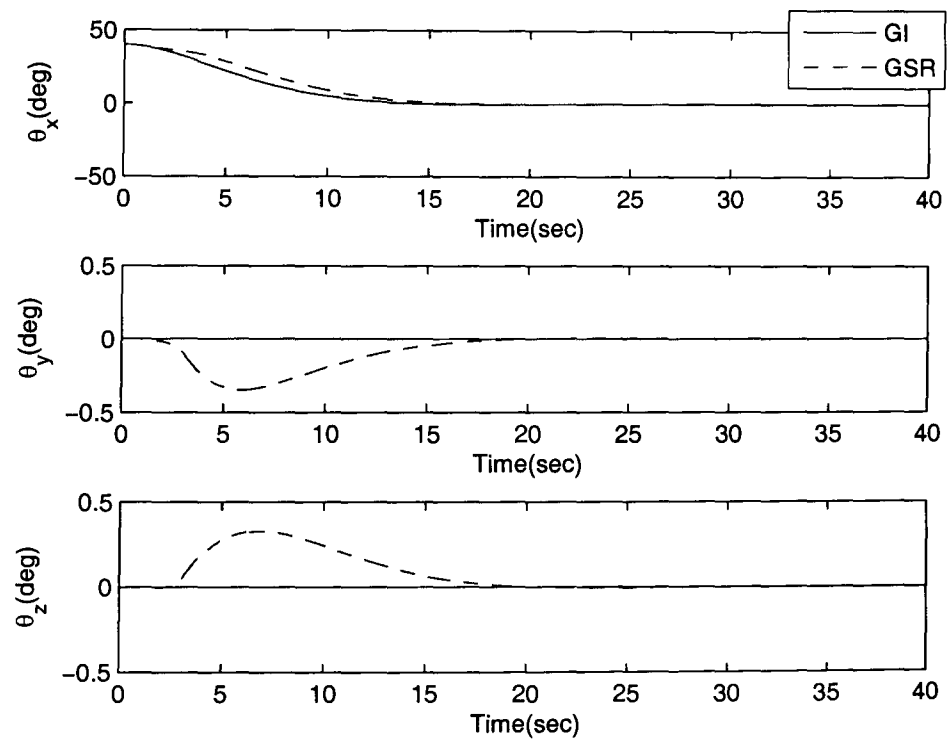

Figure 5.12: Roll manoeuvre example 2: attitude angles of satellites for modified GI steering law and GSR steering law.

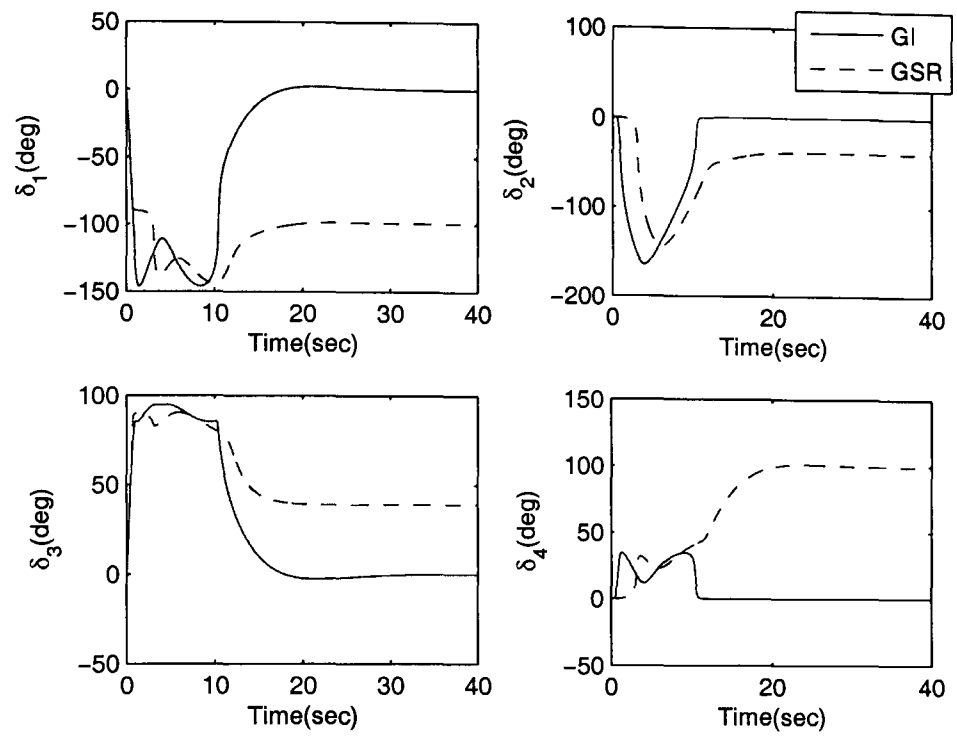

Figure 5.13: Roll manoeuvre example 2: gimbal angle profiles for modified GI steering law and GSR steering law.

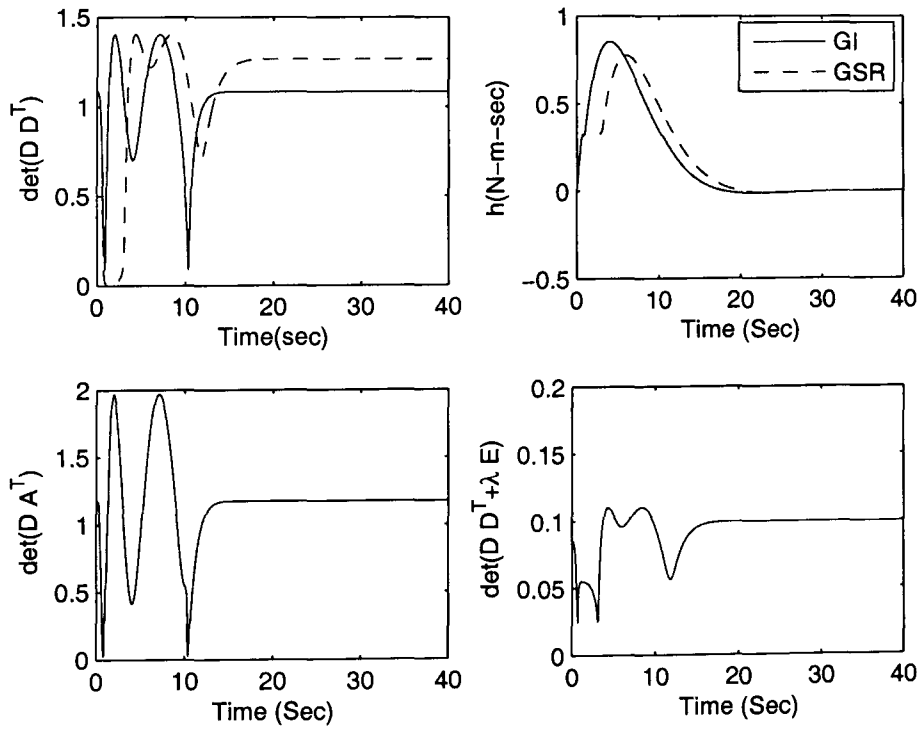

Figure 5.14: Roll manoeuvre example 2: singularity indices for modified GI steering law and GSR steering law.

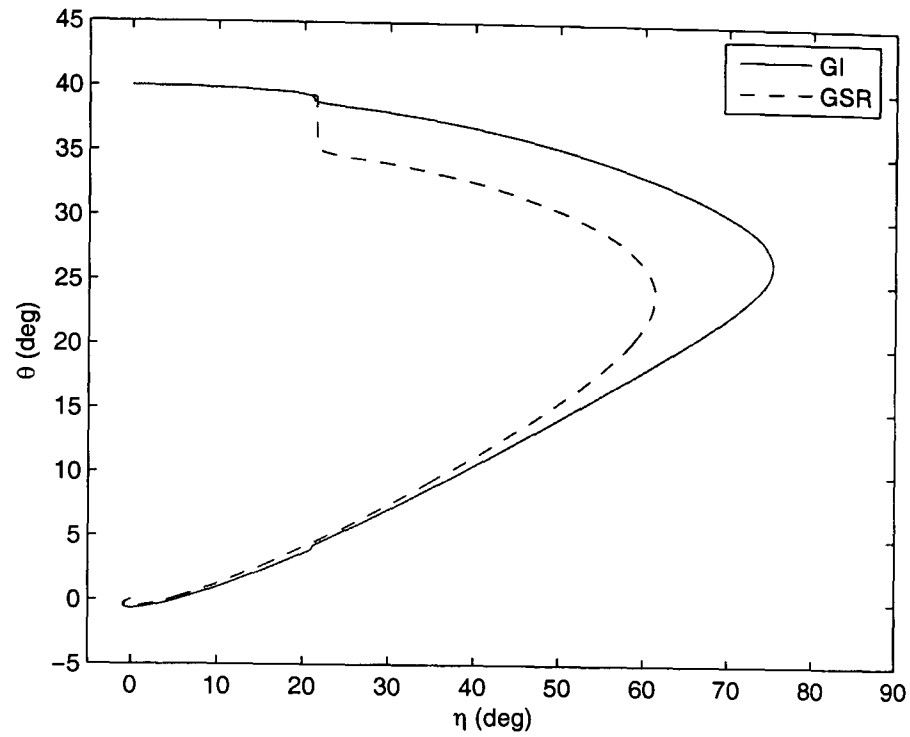

Figure 5.15: Roll manoeuvre example 2: phase plots for modified GI steering law and GSR steering law.

attitude error is negligible. It can be seen in Fig. (5.19).

5.7 Summary

A three axis reorientation manoeuvre of a satellite equipped with four CMGs pyramid cluster has been studied. The proposed Generalised-Inverse Steering Law gives an exact control, uses almost full momentum capability and avoids elliptic singularity. The commanded torque in the proposed steering law uses calculated feedback gains which together with generalised-inverse make system to use almost full momentum capability. Numerical simulations demonstrated that the proposed method gives exact control with higher agility as compared to Generalised Singularity Robust Law as former avoids elliptic singularity altogether. The proposed steering law brings the gimbal angles to zero on completion of manoeuvre provided initial condition of gimbal angles was zero. Whereas this is not the case in Generalised Singularity Robust Law. However, the proposed law is not suitable for a manoeuvre started from a singular configuration. In next chapter, we shall propose a singularity escaping steering law.

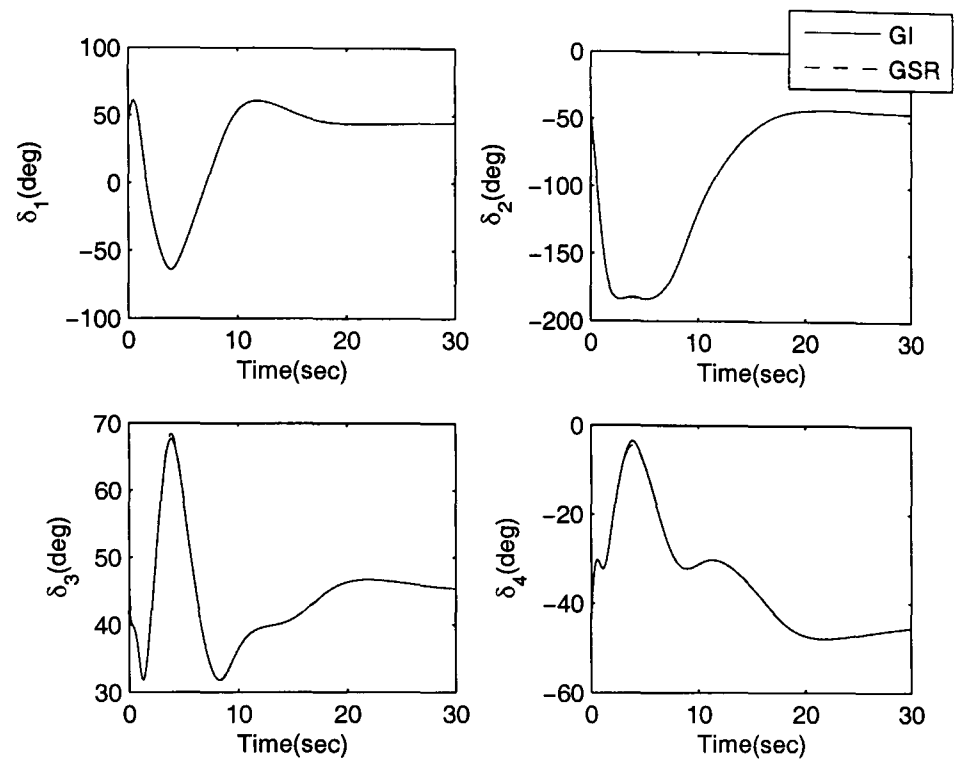

Figure 5.16: Roll manoeuvre example 3: gimbal angles for modified GI steering law and GSR steering law.

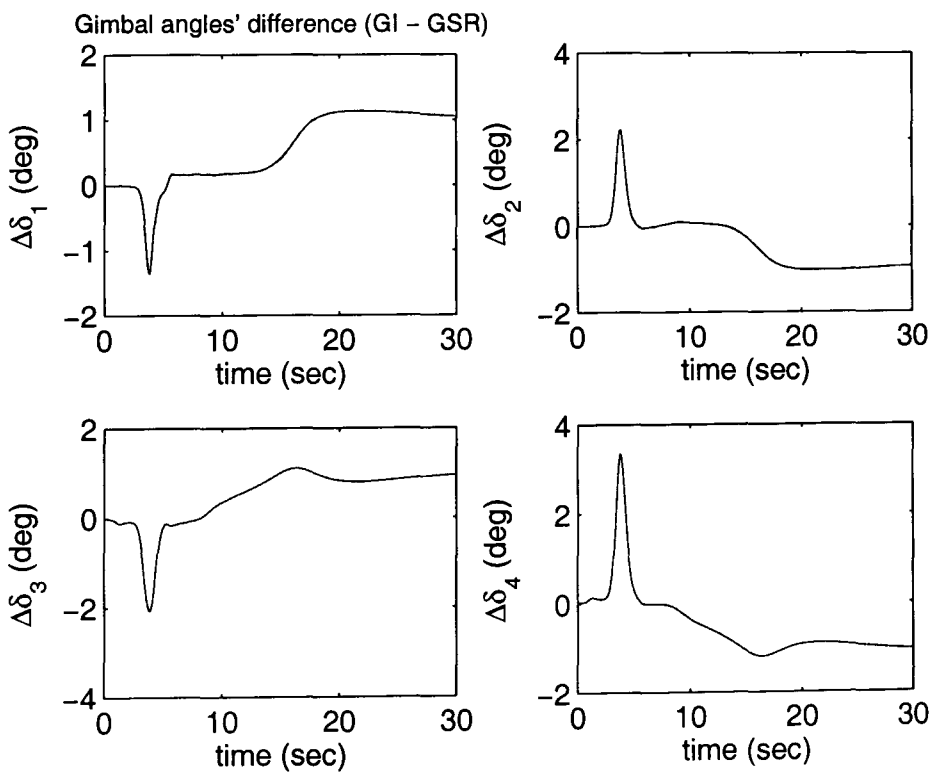

Figure 5.17: Roll manoeuvre example 3: gimbal angles' difference in modified GI steering law and GSR steering law.

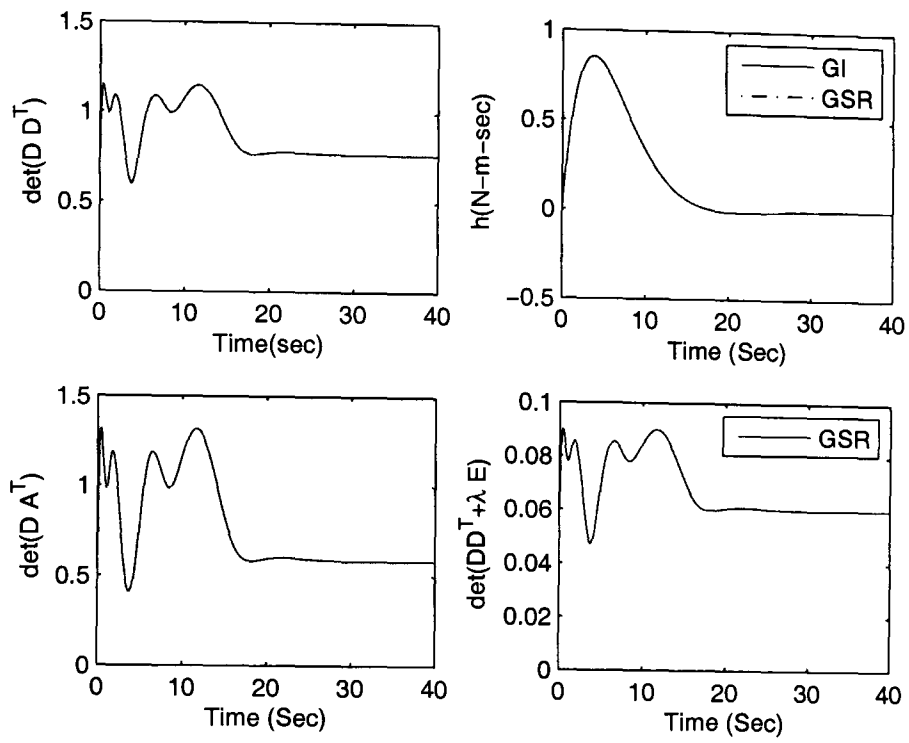

Figure 5.18: Roll manoeuvre example 3: singularity indices for modified GI steering law and GSR steering law.

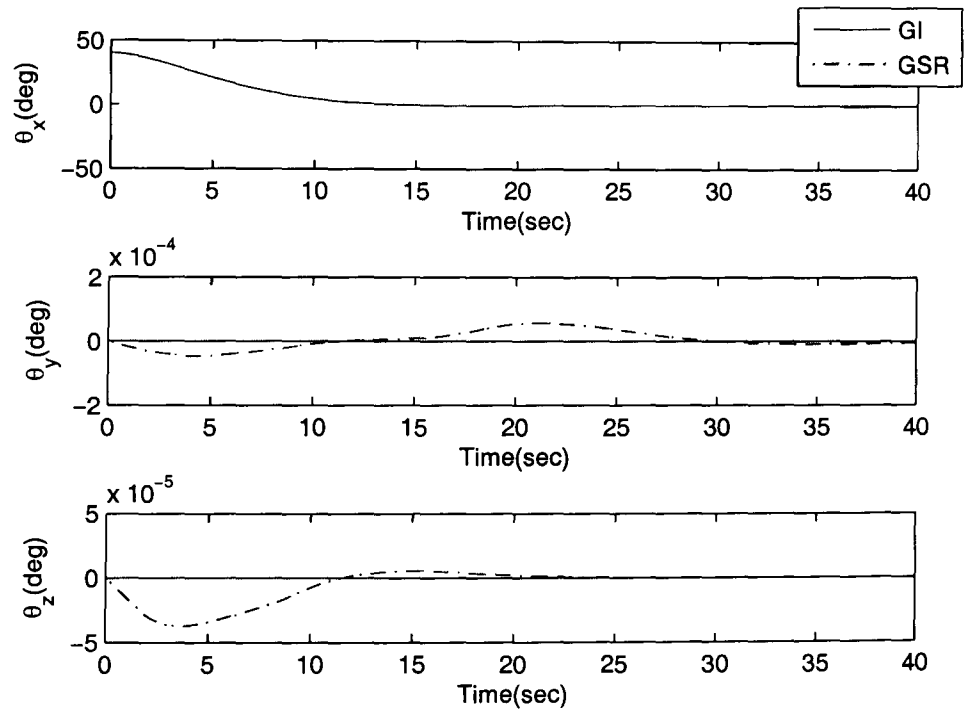

Figure 5.19: Roll manoeuvre example 3: attitude angles for modified GI steering law and GSR steering law.

Chapter 6

Singularity Escaping Steering Law

6.1 Introduction

In this chapter, we propose and analyze a new singularity escaping steering law. The so-called impassable elliptic singularities (see Section 3.7.2) can potentially degrade the performance of attitude control system of a satellite in number of ways e.g. gimbal lock and inability to attain full momentum capability. Generalised Singularity Robust (GSR) method can escape elliptic singularity by introducing a deterministic dither which in turn causes a tumble [128, 134]. This attitude error makes it not suitable for tracking manoeuvre. Therefore, there is a need for a steering law which could avoid or escape or transit elliptic singularity to use full momentum capability without causing attitude error. The Generalised-Inverse (GI) steering law (5.4.27) introduced in previous chapter can avoid elliptic singularity while using almost full momentum envelope. But it can not escape (or start from) elliptic singularity because the matrix $\boldsymbol{D_1 A}^T$ in Eq. (5.4.27) is not invertible at singularity. Therefore, singularity robustness in this steering law is needed to make it able to start from singularity. So here we proposed a new singularity escaping steering law which is obtained by introducing singularity robustness in GI-inverse steering law. Singularity robustness is achieved by minimal addition of error term in singular direction only. It will be seen later in simulation results that proposed steering law has many advantages over GSR steering law like proposed method gives quicker escape from singularity, produces no pointing errors and brings back the gimbal angles to their zero initial condition at the end of a rest-rest manoeuvre. In the rest of

the chapter this new singularity escaping law will be formally presented and developed. Finally it is compared with GSR steering law.

6.2 The Proposed Singularity Escaping Steering Law

In this section, we present the proposed Singularity Escaping (SE) steering law. A SE law can be obtained by making Generalised-Inverse (GI) steering law (Eq. 5.4.27), proposed in previous chapter, singularity robust. Moore-Penrose steering law was made singularity robust in Ref. [12] which tackled numerical aspect of the CMG steering by making matrix inversion possible on encounter with singularity. However, numerical robustness of an inverse based steering law is not sufficient to guarantee the closed-loop performance in the face of singularity. In the case of singularity robust (SR) steering law gimbal lock at elliptic singularity can potentially degrade the performance of attitude control system. Moreover, it is not able to use full momentum capability of CMGs and can not escape elliptic singularity. These shortcomings of singularity robust were address by generalised singularity robust law (GSR) which adds deterministic dither to escape singularity and can use larger momentum of CMGs if and when faced with singularity. On the other hand, the price paid is attitude tumbling (see Fig. 6.18) and error torques (see Fig. 6.20). Moreover, a single-axis manoeuvre starting with zero gimbal angles does not end up at zero gimbal angle state in case of GSR (see Fig. 6.19), which may cause momentum build up in CMG devices and it is not good if a repeatability of manoeuvre is required. Similarly tumbling effect or pointing inaccuracy as a result of singularity escape makes it not a good candidate for attitude tracking as well.

In proposing new singularity escaping steering law we have tried to address aforementioned problems associated with simple SR and GSR. The GI steering law is made singularity robust by adding an minimal matrix spanning the complementary sub-space of the singular matrix to make matrix as a full rank matrix. For a singular direction vector $\boldsymbol{e}$ the outer product matrix

$$\boldsymbol{E} = \boldsymbol{e}\boldsymbol{e}^T \tag{6.2.1}$$

is defined on the complementary sub-space of the singular matrix $\boldsymbol{D_1 D_1}^T$ if $\boldsymbol{e}^T \boldsymbol{D}_1 = 0$. Therefore, the proposed steering law is

$$\dot{\boldsymbol{\delta}} = \boldsymbol{A^T}(\boldsymbol{D_1 A^T} + \lambda_s \boldsymbol{E})^{-1} \boldsymbol{\tau}_c. \tag{6.2.2}$$

Where λ_s is singularity escaping parameter (SEP) defined as

$$\lambda_s = \kappa_s \exp\left(-\frac{m^2}{2\sigma_s^2}\right),$$

here κ_s and σ_s are positive constants and

$$m = \sqrt{\det\left(\boldsymbol{D_1 D_1^T}\right)}/h_{cmg}.$$

$\boldsymbol{\tau_c}$ is commanded torque. Here the matrix $\boldsymbol{A}$ has same definition as in Eq. (5.5.30)

$$\boldsymbol{A} = \boldsymbol{D}_1 + \lambda \boldsymbol{D_0},$$

where λ is singularity avoiding parameter (SAP) defined as

$$\lambda = \kappa \exp\left(-\frac{m^2}{2\sigma^2}\right),$$

where κ and σ are positive constants. The parameters involved in SAP and SEP are selected such that the performance of the closed-loop system is enhanced, and it is dealt in detail in the next section. It is important to note that this particular choice of matrix $\boldsymbol{E}$ defined in Eq. (6.2.1) is not sufficient in singularity escape unless the generalised inverse (i. e. with matrix $\boldsymbol{A}$) is used. For example in the case of SR steering law (Eq. 3.7.40) the matrix $\left(\boldsymbol{D}_1 \boldsymbol{D}_1^T + \lambda \mathbf{1}\right)$ to be inverted has a full rank even then it is not able to escape elliptic singularity. It means that a combined effect of using matrices $\boldsymbol{A}$ and $\boldsymbol{E}$ helps proposed steering law in escaping from the elliptic singularity.

6.3 SAP and SEP

This section is about optimising singularity avoiding parameter (SAP) $\lambda(\kappa, \sigma, m)$ and singularity escaping parameter (SEP) $\lambda_s(\kappa_s, \sigma_s, m)$. This section will also help in understanding the competing effect of SAP and SEP on control accuracy and gimbal rates. Strategy used here is simple and very clear. We change the values of four parameters σ, κ, κ_s and σ_s one by one and see the effect on output torque and maximum gimbal rate.

We apply a constant command torque in roll direction $\dot{\boldsymbol{h}} = [1, 0, 0]^T$ and also we take $h_{cmg} = 1\text{Nms}$. It should be noted that in roll and pitch axes the elliptic singularity is more pronounced and troublesome. In an exact steering/control output torque closely follows the commanded torque. However, when system passes nearby the singularity the output torque deviates from commanded torque profile, whereas maximum gimbal rate value rises. Now the optimal values of those four parameters are selected such that the torque error is minimum possible with gimbal rate not exceeding a preset limit which in this case is chosen to be 3rad/s.

6.3.1 Effect of σ

It measures spread of SAP λ over singularity index m. The value of m varies between 0 and 1.5 for a pyramid system with skew angle $\beta = 54.7\text{deg}$. We vary the value of σ from .6 to 1.2 while keeping the other parameters fixed at $\kappa = 1$,$\kappa_s = 0.5$ and $\sigma_s = 0.4$. The larger value of σ means wide spread of SAP over singularity index. As a result λ would have larger values even when system is away from singularity configuration. Therefore, it means less torque error but higher gimbal rates as larger value of SAP not only helps system avoid singularity but it take system away from Moore-Penrose solution which is a least gimbal rate solution (see section 3.7.3). The Fig.(6.1) shows the output torque for different values of σ. It can be seen that torque error (a dip below 1) reduces (becomes narrower and shallower) with increasing value of σ. On the other hand, gimbal rate rises as seen in Fig.(6.2).

6.3.2 Effect of κ

The parameter κ is value of SAP λ at singularity ($m = 0$). So larger value of κ means strong singularity avoidance, smaller torque error as seen in Fig. (6.3) and higher gimbal rate as seen in Fig. (6.4). Although increasing both κ and σ have similar effect on torque error and gimbal rate but there is a key difference which is increasing σ raises the value of λ at far points whereas increasing κ raises λ overall especially near singularity. So torque error reduces more rapidly by increasing κ than by σ at the cost of higher gimbal rates.

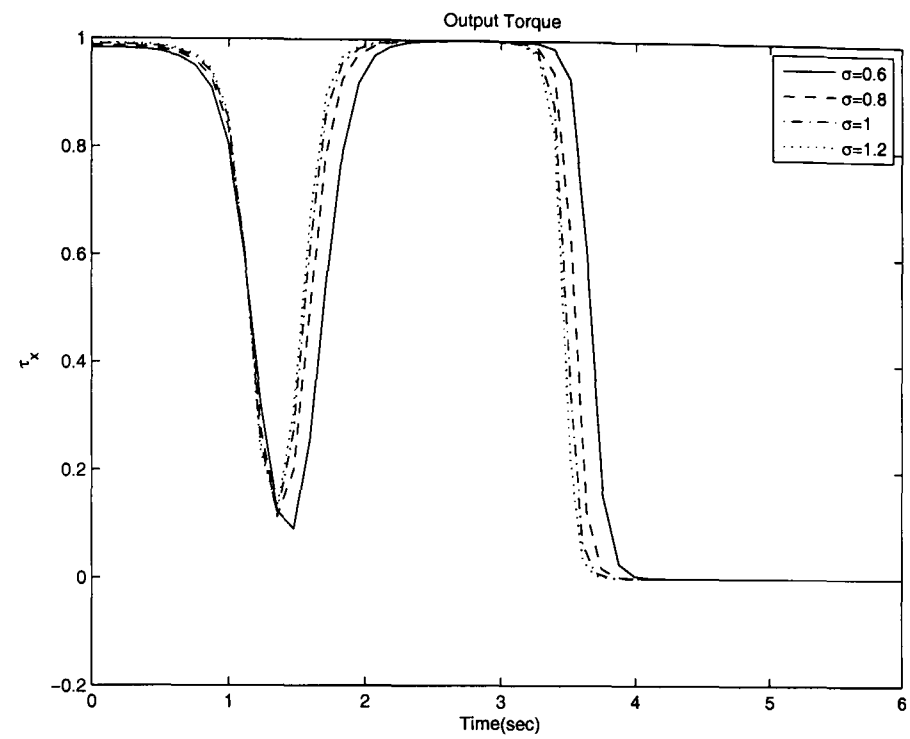

Figure 6.1: Output torque for various values of σ at fixed values $\kappa = 1$,$\kappa_s = 0.5$ and $\sigma_s = 0.4$.

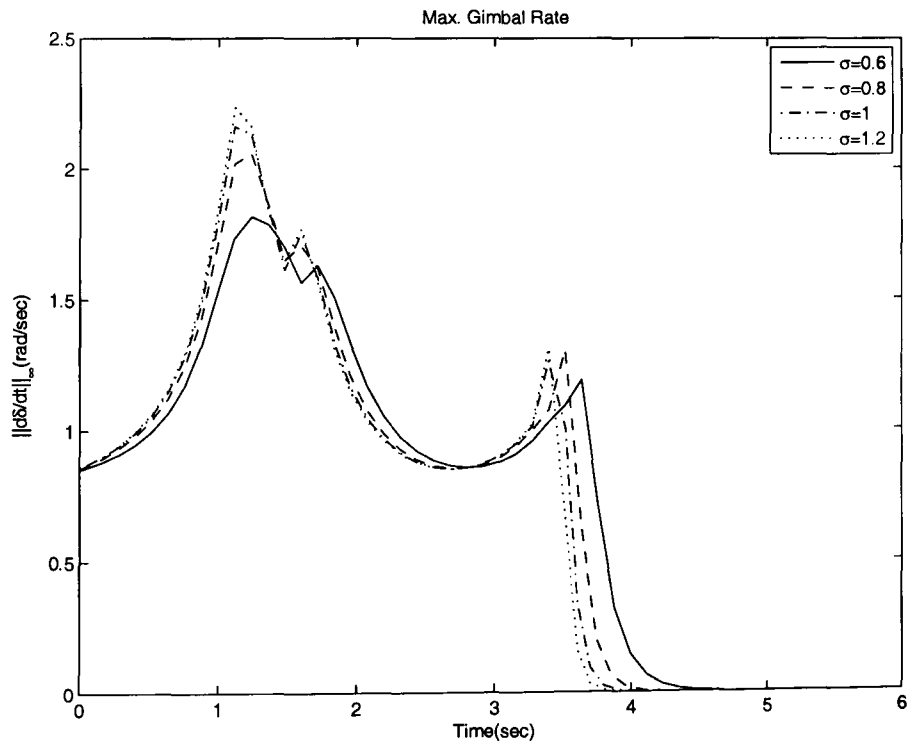

Figure 6.2: Max. Gimbal rate for various values of σ at fixed values $\kappa = 1$,$\kappa_s = 0.5$ and $\sigma_s = 0.4$.

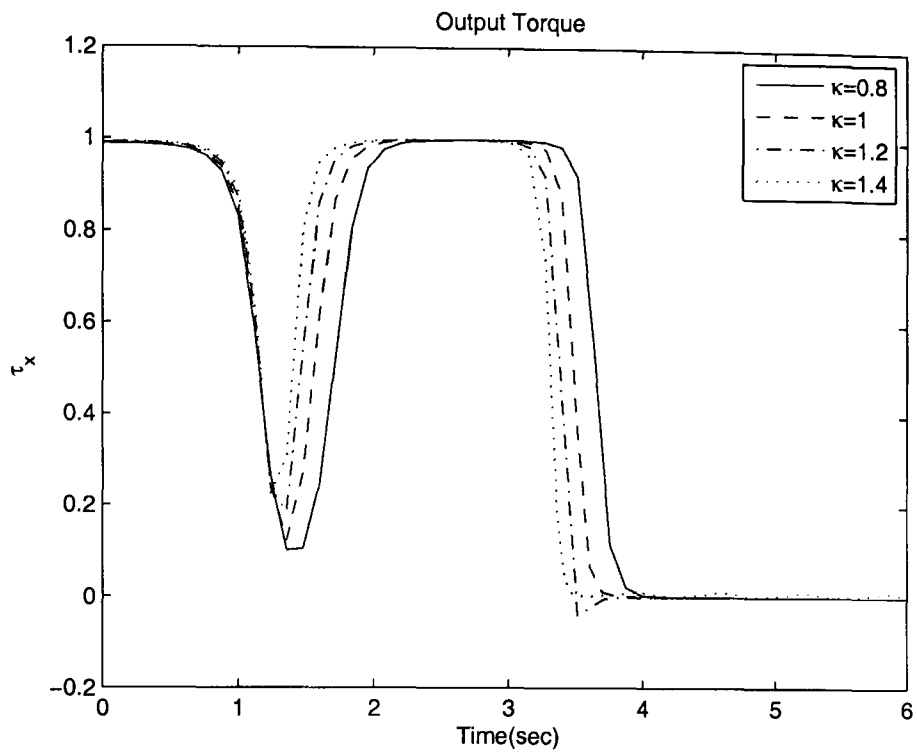

Figure 6.3: Output torque for various values of κ at fixed values $\sigma = 1$,$\kappa_s = 0.5$ and $\sigma_s = 0.4$.

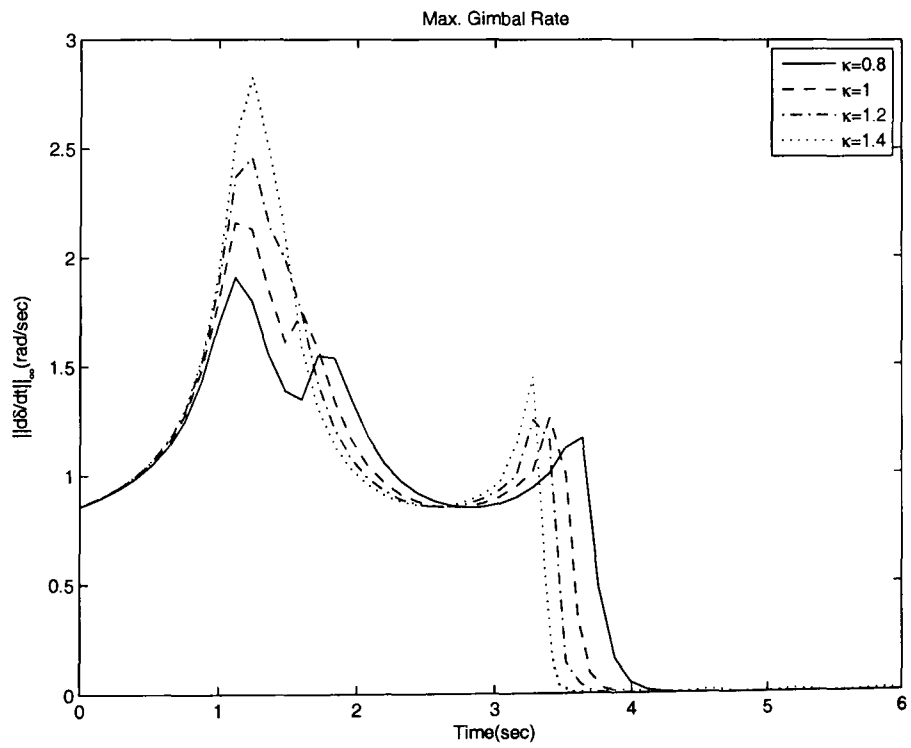

Figure 6.4: Max. Gimbal rate for various values of κ at fixed values $\sigma = 1$,$\kappa_s = 0.5$ and $\sigma_s = 0.4$.

6.3.3 Effect of σ_s

The SEP provides both singularity robustness and singularity escaping properties to the steering law. On the other hand, SEP also causes torque error so it is highly desirable that SEP has small amplitude and small spread. The effect of σ_s on torque error can be seen in Fig. (6.5). With the decreasing values of σ_s the error torque decreases both in magnitude and in spread and gimbal rate increases as seen in Fig. (6.6).

6.3.4 Effect of κ_s

The variation in κ_s has direct effect on torque error. By reducing κ_s one can reduce the magnitude of the error torque significantly, however, at the price of higher gimbal rates as seen in Fig. (6.7) and (6.8). It can be noted that λ is significant for larger values of m when system is away from singularity whereas λ_s is more significant near singularity.

6.3.5 Selection of Parameters

After studying the effect of these parameters we select the suitable values based on certain criterion. The maximum gimbal rate is thought to be useful criterion as it is constraint by a hardware limit. The $3\mathrm{rad/s}$ limit is usually found in the literature which is achievable by current technology. We choose $\sigma = 1$ although for $\sigma = 1.2$ gimbal rate is less than 2.5 but we have to have margin for adjustment of κ_s and σ_s for which gimbal rate is more sensitive. Then we choose κ to be 1.2 as it is maximum value for which gimbal rate is just $2.5\mathrm{rad/s}$. Then come the selection of σ_s. Again choice is simple because for $\sigma_s = 0.4$ the gimbal rate remains below the $2.5\mathrm{rad/s}$. Finally with choice of $\kappa_s = 0.4$ we can get gimbal rate less than $3\mathrm{rad/s}$. In the beginning we kept margin for κ_s because magnitude of torque error can be drastically controlled by κ_s so by reducing the κ_s we can reduce the torque significantly. We have not used any advanced search method to find these parameters. But the advantage of technique used by us is its clarity which helps in understanding the sensitivities of gimbal rate with respect to these parameters.

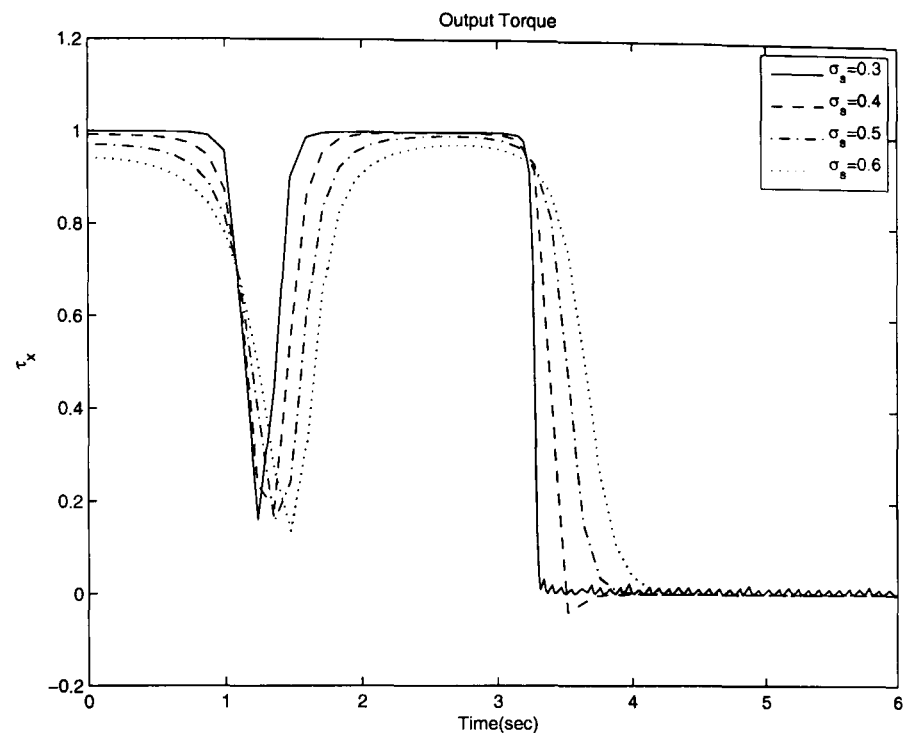

Figure 6.5: Output torque for various values of σ_s at fixed values $\kappa = 1.2$,$\kappa_s = 0.5$ and $\sigma = 1$.

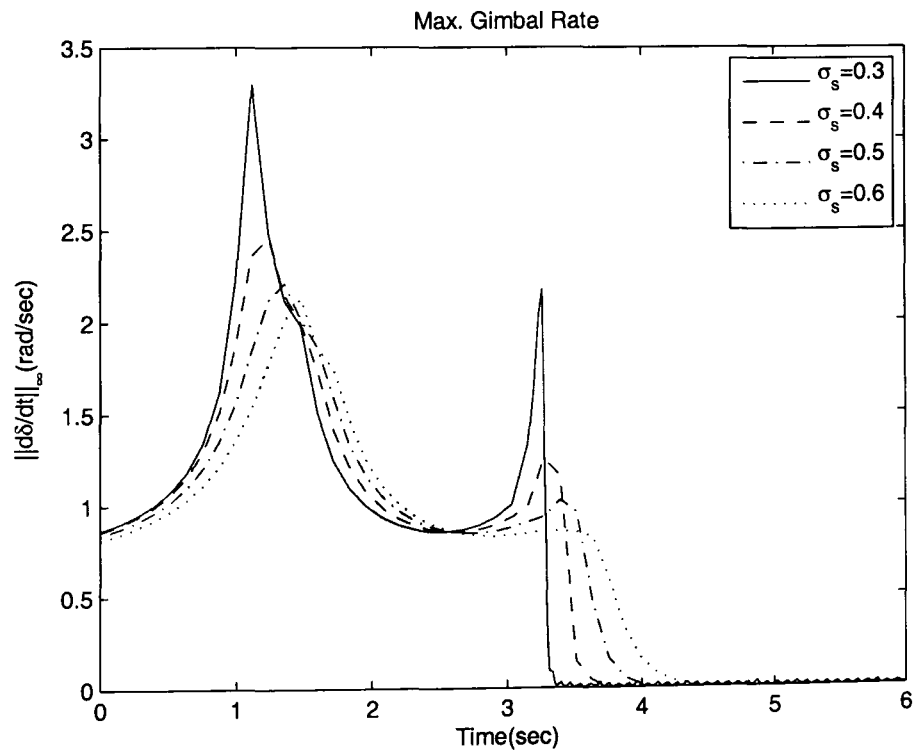

Figure 6.6: Max. Gimbal rate for various values of σ_s at fixed values $\kappa = 1.2$,$\kappa_s = 0.5$ and $\sigma = 1$.

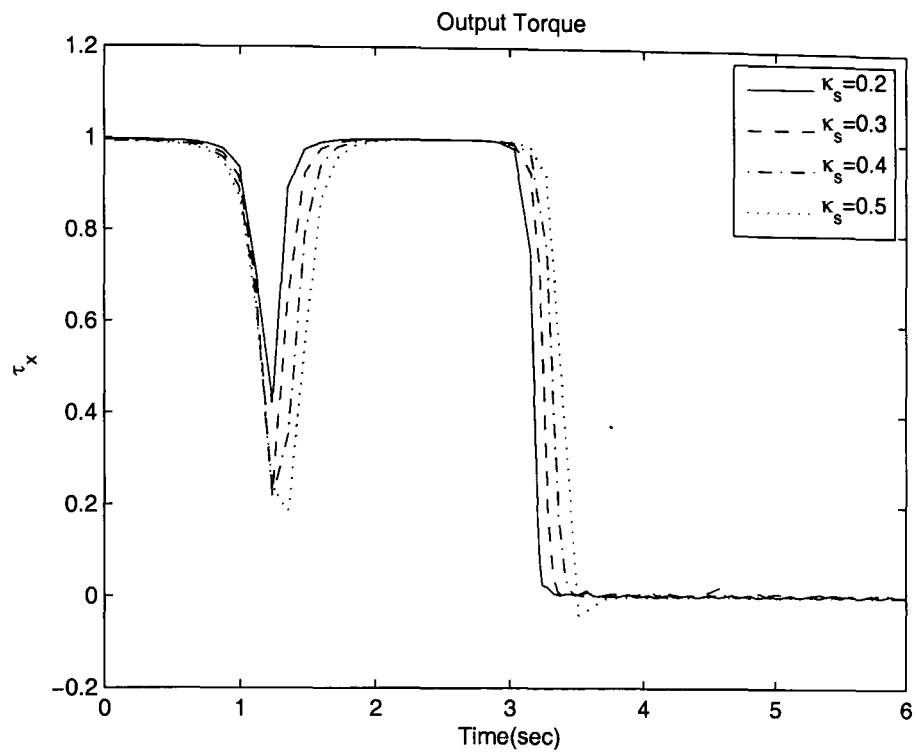

Figure 6.7: Output torque for various values of κ_s at fixed values $\sigma = 1$,$\kappa = 1$ and $\sigma_s = 0.4$.

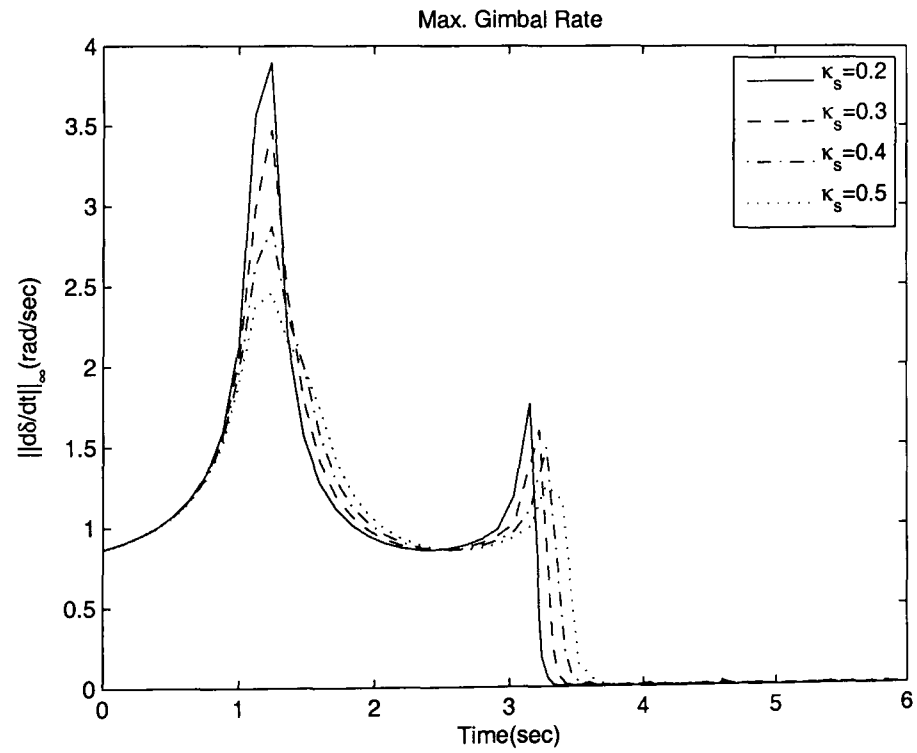

Figure 6.8: Max. Gimbal rate for various values of κ_s at fixed values $\sigma = 1$,$\kappa = 1$ and $\sigma_s = 0.4$.

6.4 Simulation Tests

In this section, we shall compare the performance of our SE steering law with that of GSR in a non-dimensional simulation to preserve the generality. In these cases commanded torque $[1, 0, 0]^T$ is applied over a four CMG pyramid system. The angular momentum of each CMG is suppose to be 1Nms. Here we study two cases one starting from zero gimbal angles, other starting from elliptic singularity $[-90^o, 0^o, 90^o, 0^o]$. In Fig. (6.9) to Fig. (6.16) solid line represents simulation results of SE steering law whereas dashed line represents the results of GSR steering law.

6.4.1 Case I: Starting from Zero Gimbal Condition

In Fig. (6.9) a comparison of gimbal angle profiles generated by SE and GSR steering laws is presented. In case of GSR only two CMGs odd pair (1 and 3) operates for first few seconds until the system reaches the singular configuration whereupon even pair (2 and 4) starts moving to break the symmetry of pseudo-inverse based logic. Whereas SE logic uses all four CMGs from the beginning. It chooses such gimbal angles path for which manoeuvre remains single axis. The Fig. (6.10(a),(b),(c)) show the output torque components. The proposed method produces torque only in the desired direction and there is virtually no torque in other two directions. Whereas in GSR case output torque is not unidirectional due to the effect of elliptic singularity. As a matter of fact the GSR method uses these torque errors in order to escape from singularity. The maximum gimbal rate is plotted in Fig. (6.10(d)). The gimbal rate generated by SE steering law is reasonably smooth and within limits whereas gimbal rate generated by GSR has very high value. Although it can be corrected by adjusting the parameters involved in GSR but at the cost of increased errors in the output torque. We compare the angular momentum profiles generated by two methods in Fig. (6.11). The error generated by GSR to escape elliptic singularity can also be seen in angular momentum plots. Whereas SE steering law gives purely a single axis manoeuvre and escapes elliptic singularity. However, for the given choice of matrix $\boldsymbol{A}$ the x-component of angular momentum saturates at slightly different value than the saturation value. The singularity index in Fig. (6.11(d)) shows SE law encounters no singularity of D_1 but it encounters a saturation singularity of matrix $\boldsymbol{A}$ as shown in Fig. (6.12(a)). The profile

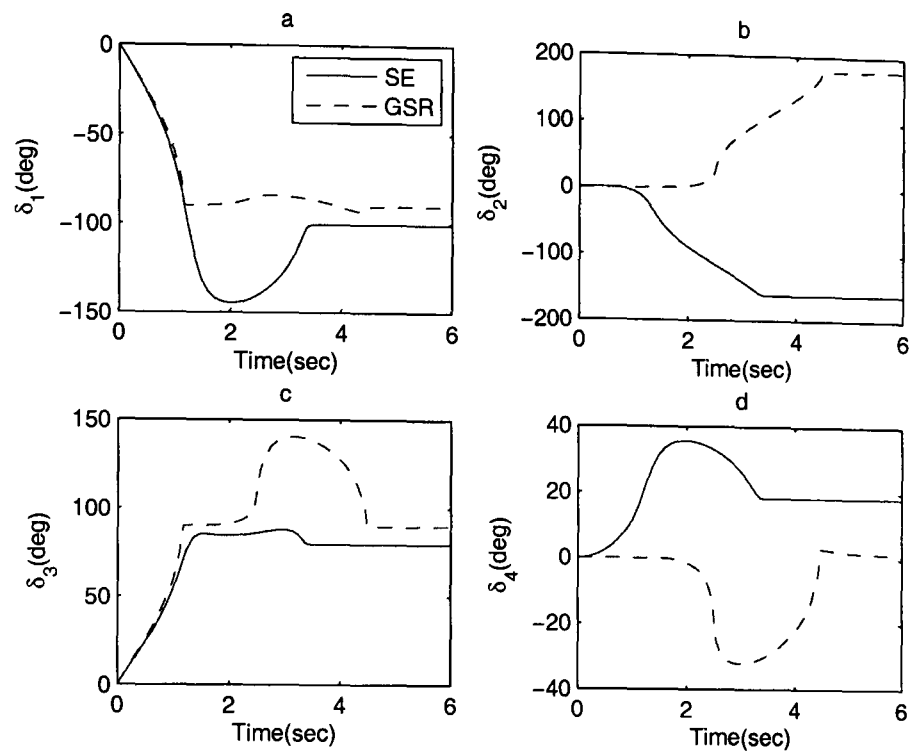

Figure 6.9: Simulation Test Case I: comparison of gimbal angles profile.

of SAP and SEP are given in Fig. (6.12(c),(d)).

6.4.2 Case II: Starting from Elliptic Singularity

Elliptic singularity is most troublesome singularity as it restricts the available momentum. This singularity can not be escaped with null motion or singularity robust law. However, the GSR can escape it with some error torques and pointing inaccuracy. The following simulation experiment shows that the proposed logic can escape the elliptic singularity with high pointing accuracy. In Fig. (6.13) gimbal angles are plotted to compare the results of the GSR and SE steering law. It is clear in this figure that proposed method very quickly escapes the singularity quicker than GSR. All four CMGs are used in this escape mechanism. In case of GSR gimbal finally settles at saturation singularity whereas in proposed method it settles at singularity of matrix A. In Fig. (6.14(a)) it can be observed that x-component of torque generated by GSR logic remains zero for 1sec and GSR logic generates other two components of torque (see in Fig. (6.14(b),(c))) in order to escape singularity. On the other hand, x-component of torque generated by SE logic has a very small negative value for a small fraction

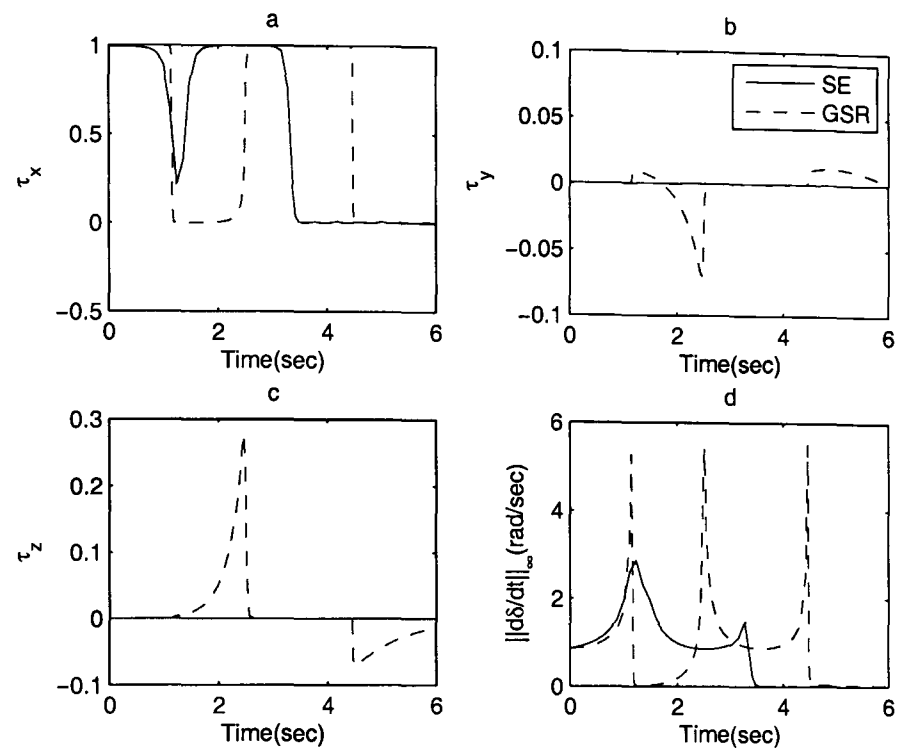

Figure 6.10: Simulation Test Case I: comparison of output torque components (a), (b), (c) and maximum gimbal rate (d).

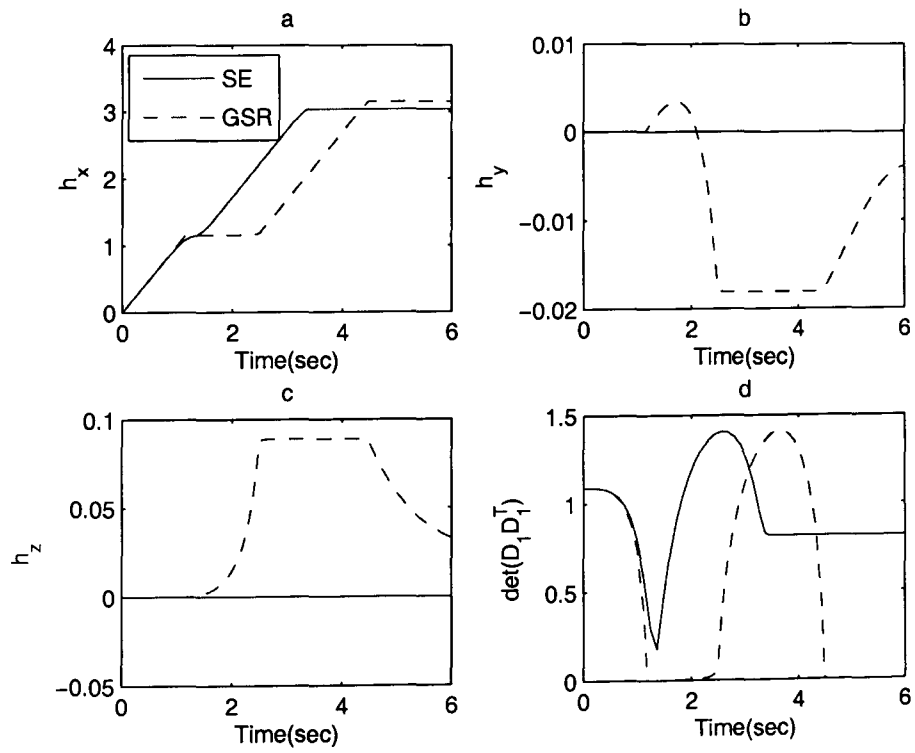

Figure 6.11: Simulation Test Case I: comparison of angular momentum components (a), (b), (c) and singularity index (d).

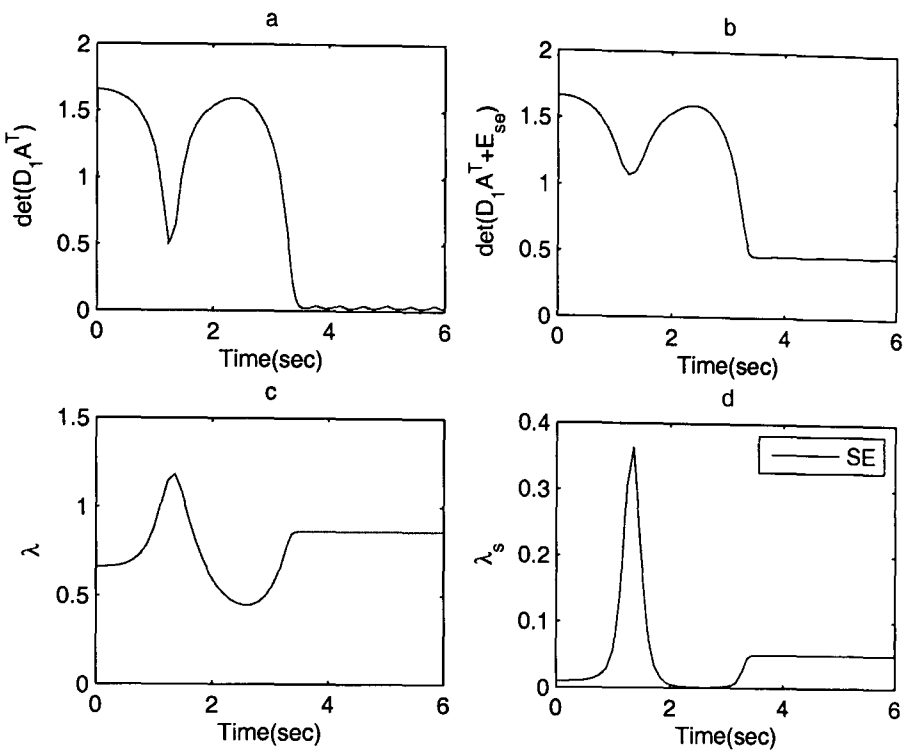

Figure 6.12: Simulation Test Case I: Singularity measures (a), (b), SAP (c) and SEP (d).

of a second (see in Fig. (6.14(a))) whereas other two components in Fig. (6.14(b),(c)) remain zero. Therefore, SE logic can escape singularity much faster than GSR logic. Maximum gimbal rate remains within the limit of 2.5rad/s as shown in Fig. (6.14(d)). The higher gimbal rate of GSR could be reduced by changing the parameters involved in it but that would result in higher torque error and pointing inaccuracy. The proposed method gives strictly single axis manoeuvre so angular momentum develops only in roll axis for proposed logic contrary to GSR as shown in Fig. (6.15(a),(b),(c)). We have plotted different singularity indices in Fig. (6.15(d)) and Fig. (6.16(a),(b)). The singularity index in Fig. (6.16(b)) has reasonable value throughout the manoeuvre. Beyond 2.5sec the matrix $\boldsymbol{A}$ nearly becomes singular as $\det(\boldsymbol{D}_1\boldsymbol{A}^T) \approx 0$ but $\det(\boldsymbol{D}_1\boldsymbol{D}_1^T) \neq 0$. The SAP λ reduces in its value as the system moves away from singularity but rises again as system moves toward saturation singularity as shown in Fig. (6.16(c)). The SEP λ_s has highest value at elliptic singularity and it quickly falls to zero and after 2sec when system reaches near saturation singularity it rises again as shown in Fig. (6.16(d)).

We have seen in these simulation tests that the proposed method gives effective, faster and accurate way of escaping the so-called elliptic singularity. In next sections, we shall

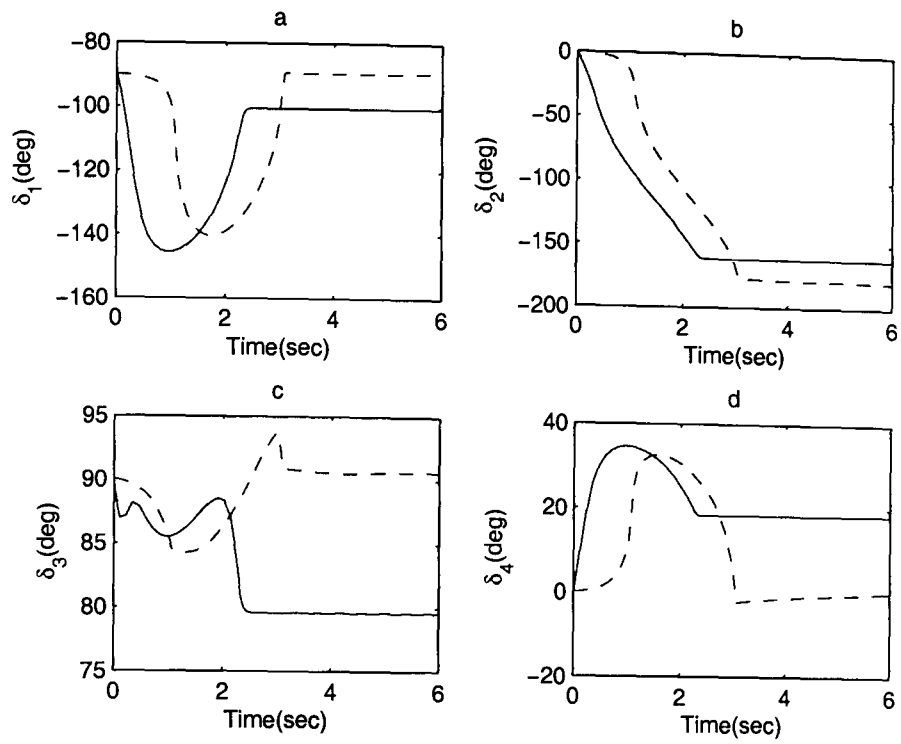

Figure 6.13: Simulation Test Case II: comparison of gimbal angles profile.

simulate this method for reorientation manoeuvre for a particular satellite example.

6.5 Reorientation Manoeuvre Examples

In this section, we shall simulate the proposed method for a rest-rest roll manoeuvre. The satellite data is given in Table (6.1). In these simulations we shall compare the performance of proposed method with the GSR method. A 40deg roll manoeuvre is performed for two sets of initial gimbal condition. In case-I initial gimbal angles are assumed to be at zero. The advantages of the proposed law over GSR are demonstrated in the following results. The singularity avoiding aspect of proposed steering law via matrix $\boldsymbol{A}$ prevent system from the effect of elliptic singularity so it can use larger momentum envelope. Figure (6.17) gives a comparison of angular velocity profiles generated by GSR and proposed logic. It can clearly be seen that proposed method makes system attain larger slew rates without being affected by elliptic singularity. And manoeuvre is purely single axis unlike GSR case. The higher angular rate gives the advantage of faster manoeuvre which can be seen by plotting attitude profiles in Fig. (6.18). Clearly GSR generates pointing error. The gimbal angle profile given in Fig. (6.19) shows that

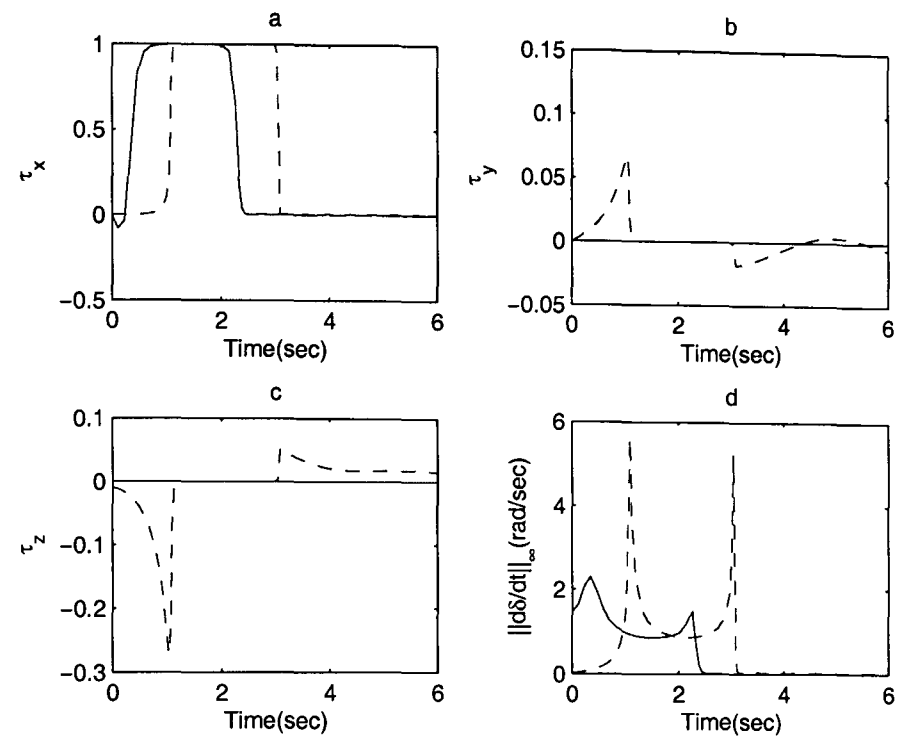

Figure 6.14: Simulation Test Case II: comparison of output torque components (a), (b), (c) and maximum gimbal rate (d).

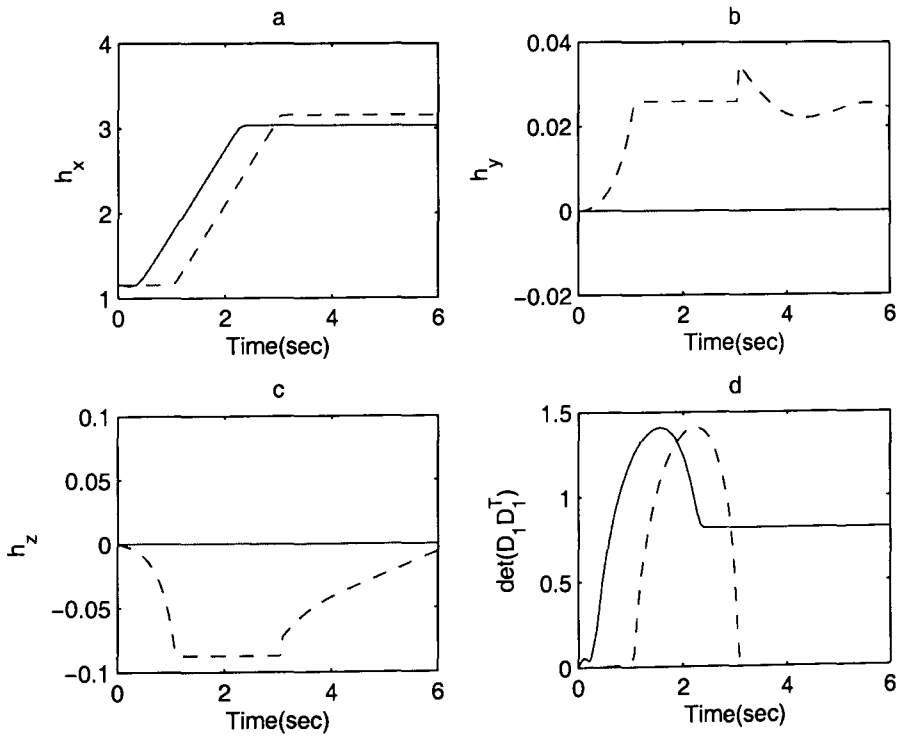

Figure 6.15: Simulation Test Case II: comparison of angular momentum components (a), (b), (c) and singularity index (d).

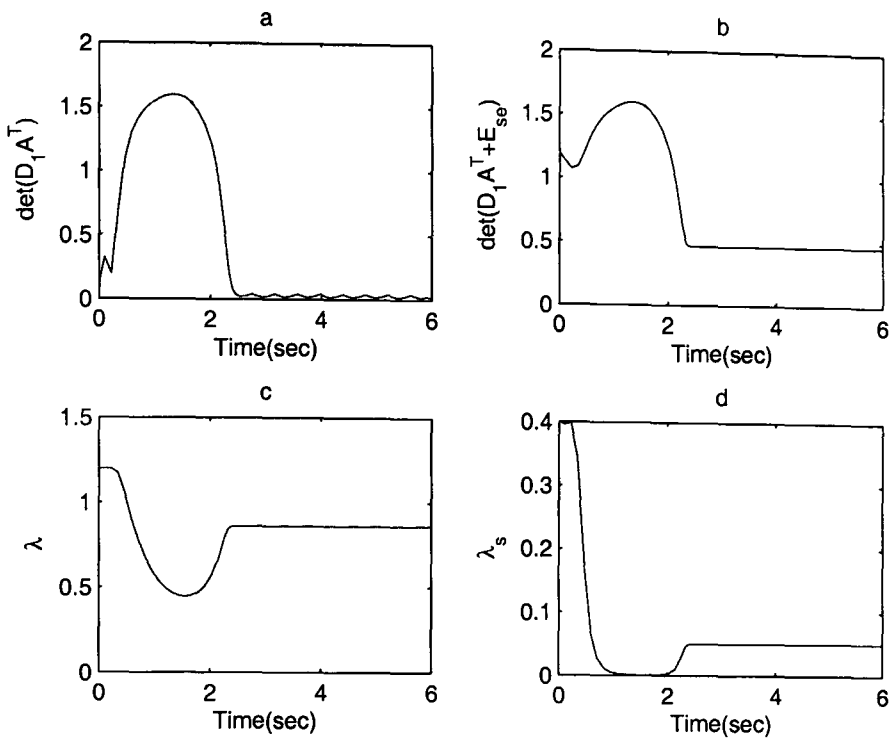

Figure 6.16: Simulation Test Case II: Singularity measures (a), (b), SAP (c) and SEP (d).

the proposed method uses all four CMGs from the beginning which helps in avoiding the elliptic singularity. And at the end of the manoeuvre all four CMGs are brought back to zero. Whereas the GSR initially uses only two CMGs until it hits the singularity. It passes through it by using gimbal motion of all four CMGs. But it can not bring all four CMGs back to zero. Figure. (6.20(a), (b), (c)) show the plots of output torque components. It is clear that output torque for proposed steering law is strictly in desired direction with no errors in the other directions unlike the GSR case. However, singularity slightly affects the output torque because of restricted gimbal rate limit. The maximum gimbal rates in Fig. (6.21(d)) are comparable for both logics. Again in angular momentum profiles shown in Fig. (6.21 (a), (b), (c)) the proposed method has generated manoeuvre in the desired direction. Whereas GSR produces momentum in other directions to escape elliptic singularity thus reducing the momentum capability in desired direction. The singularity index in Fig. (6.21(d)) shows that proposed method has avoided elliptic singularity unlike GSR. In Fig. (6.22(a),(b)) we have plotted singularity measures of generalised inverse and singularity robust generalised inverse, both are far from singularity. The SAP and SEP are plotted in Fig. (6.22(c),(d)). The SEP is very small throughout except near singularity.

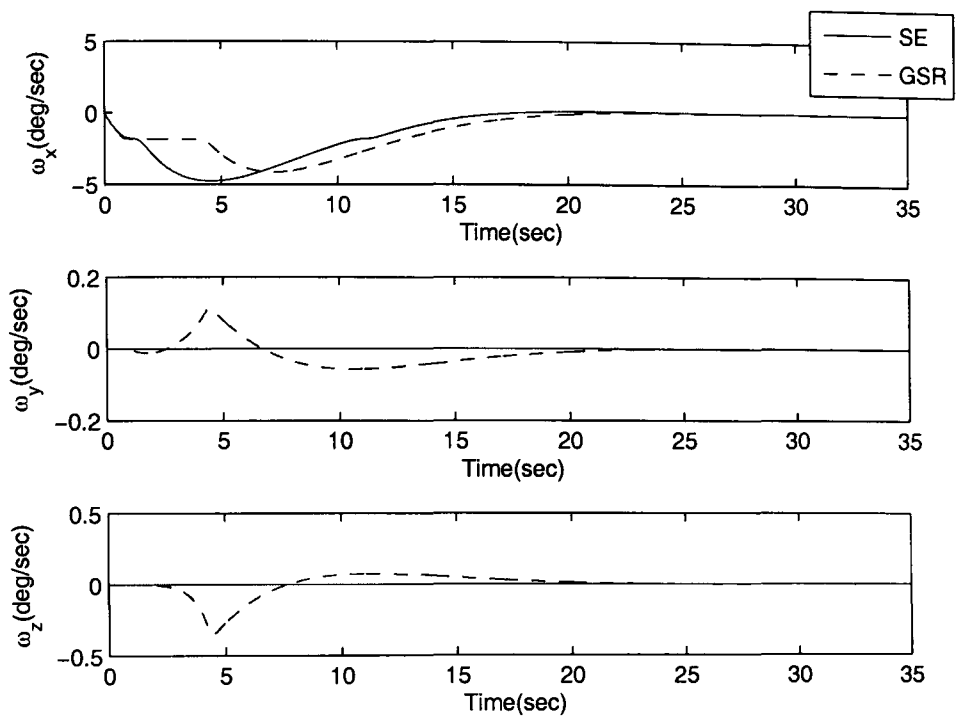

Figure 6.17: Reorientation Manoeuvre Case I: comparison of angular velocity components of satellite.

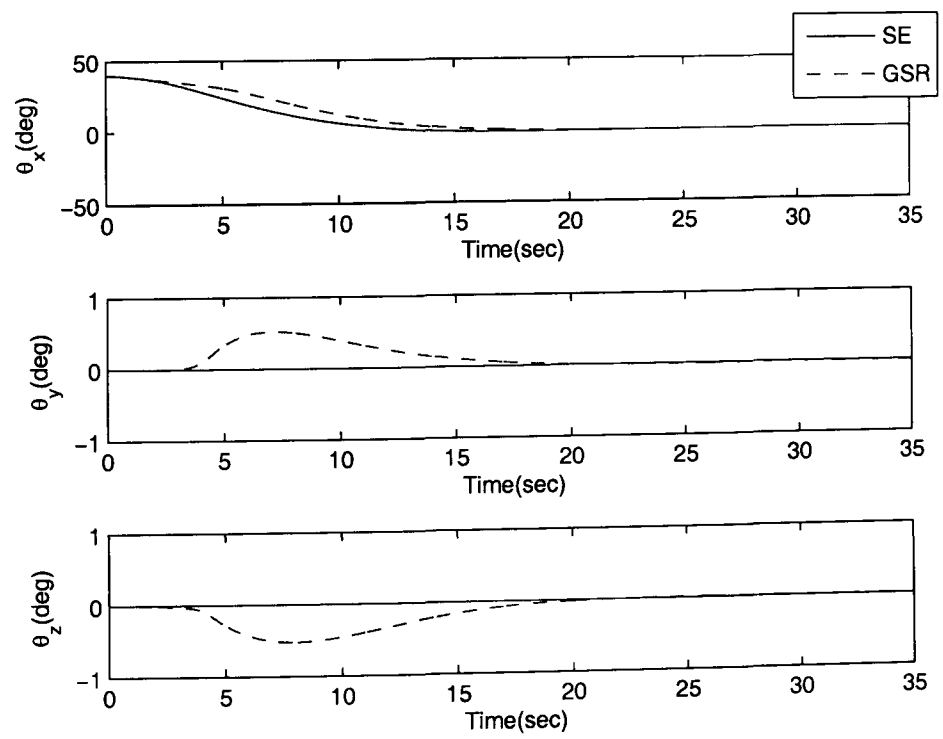

Figure 6.18: Reorientation Manoeuvre Case I: comparison of attitude angles.

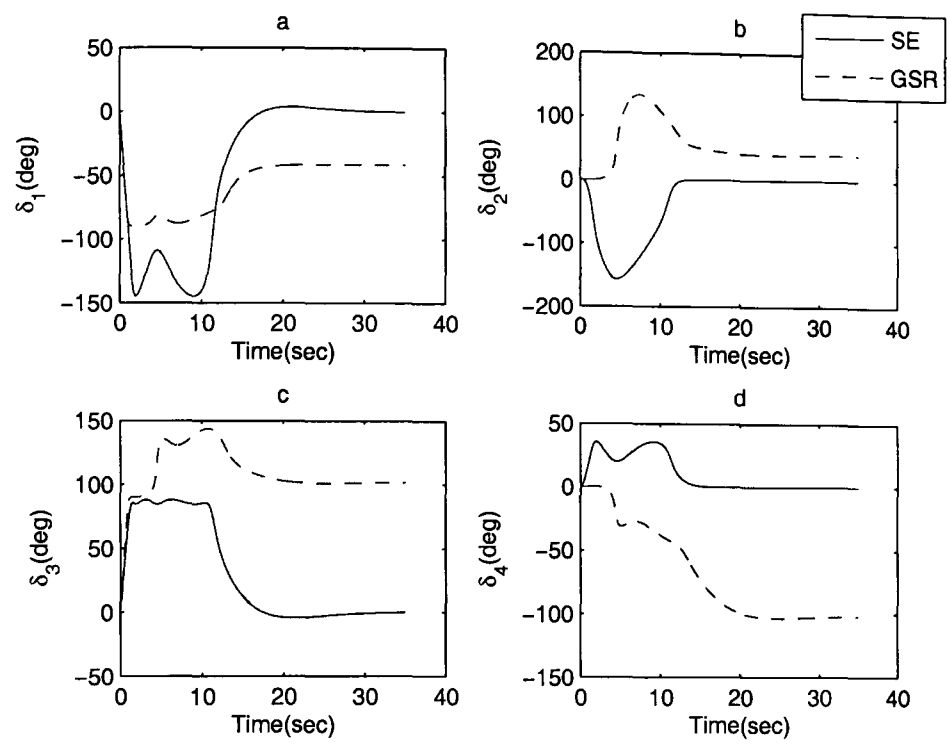

Figure 6.19: Reorientation Manoeuvre Case I: comparison of gimbal angle profiles.

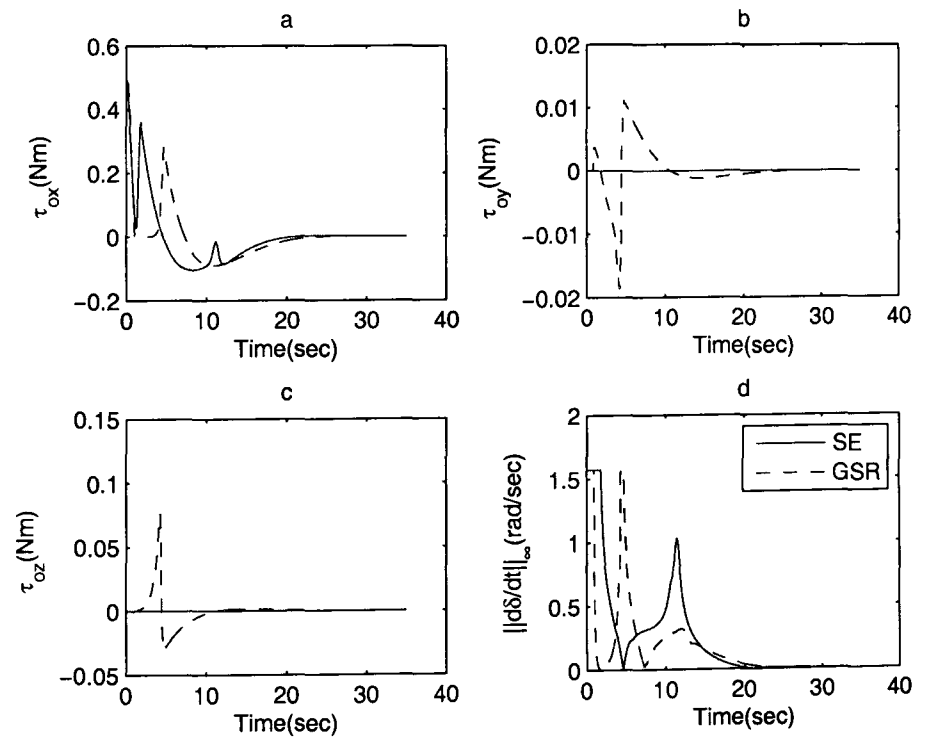

Figure 6.20: Reorientation Manoeuvre Case I: comparison of output torque components (a), (b), (c) and maximum gimbal rate (d).

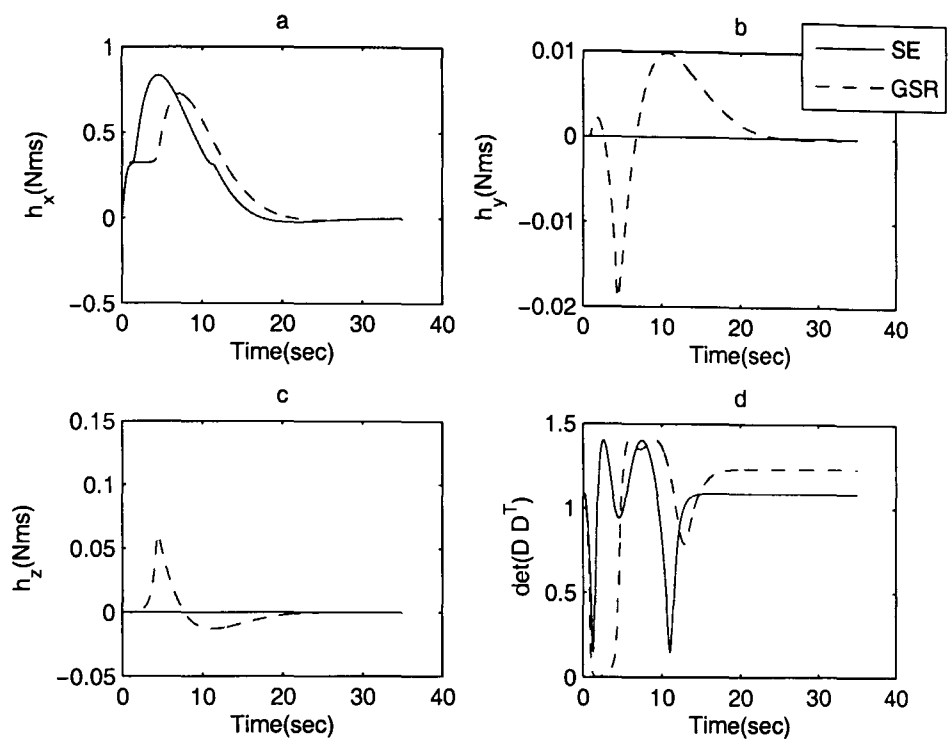

Figure 6.21: Reorientation Manoeuvre Case I: comparison of angular momentum components (a), (b), (c) and singularity index (d).

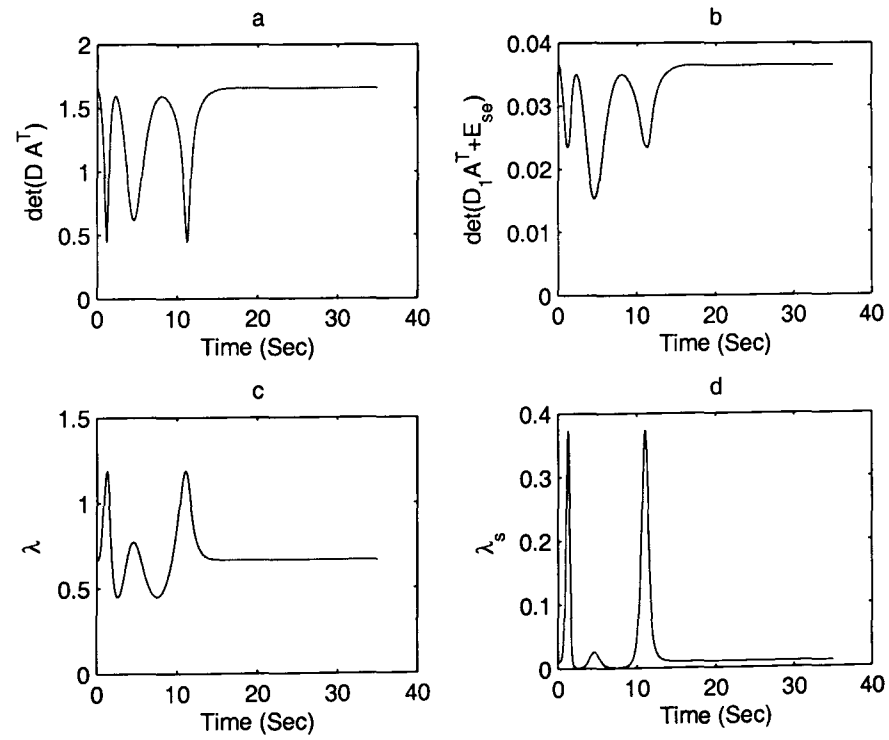

Figure 6.22: Reorientation Manoeuvre Case I: Singularity indices (a), (b), SAP (c), SEP (d).

Table 6.1: Simulation Parameters.

Parameter	Value
h_{cmg}	0.28 Nms
$[I_x, I_y, I_z]$	$[10, 10, 10]$ kgm^2
β	54.7 deg
ω_e^{max}	5 deg/s
k_1	$1Nm/rad$
K_2	$2\sqrt{k_1 I}$
$[\theta_x, \theta_y, \theta_z]_0$	$[40^O, 0, 0]$
$[\theta_x, \theta_y, \theta_z]_f$	$[0, 0, 0]$

In case-II the system start from elliptic singularity. As expected the GSR produces attitude errors, whereas proposed method can perform an attitude manoeuvre without any error as shown in Fig. (6.23) and Fig. (6.24). It can be observed in Fig. (6.25) that all four CMGs start moving quickly to escape elliptic singularity and singularity escape for the proposed method is much faster than GSR method. Gimbal angle profiles generated by GSR method escape elliptic singularity and then pass through a saturation singularity before settling to some final condition. In Fig. (6.27(a)) x-component of angular momentum generated by GSR logic saturates at some value for which singularity index in Fig. (6.27(d)) is zero so it is saturation singularity. On the other hand, gimbal angle profiles generated by proposed logic escapes elliptic singularity and then pass through a different saturation singularity for which singularity index in Fig. (6.27(d)) is not zero but singularity index of generalised inverse in Fig. (6.28(a)) is zero. So clearly it is singularity of matrix $\boldsymbol{A}$. Again one can see that torque in Fig. (6.26(a),(b),(c)) and angular momentum in Fig. (6.27(a),(b),(c)) generated by proposed logic are strictly in desired direction contrary to GSR case. Maximum gimbal rate is almost same for both cases (see Fig. (6.26(d))). Variation in SAP and SEP during the course of manoeuvre are plotted in Fig. (6.28(c),(d)). SEP has large values at singularity escape points.

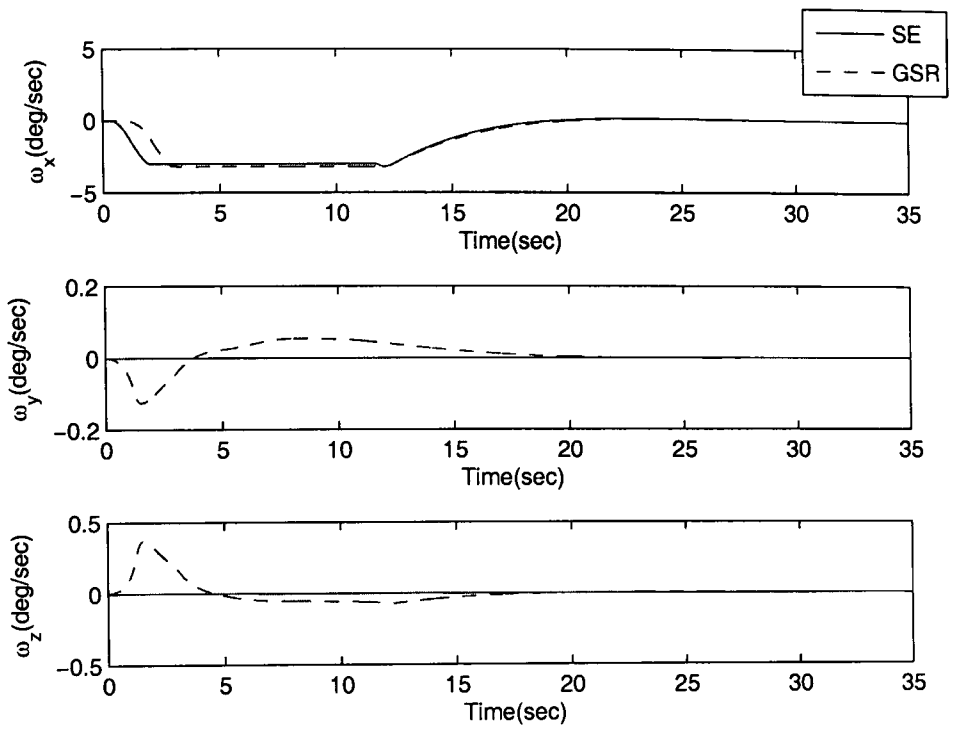

Figure 6.23: Reorientation Manoeuvre Case II: comparison of angular velocity components of satellite.

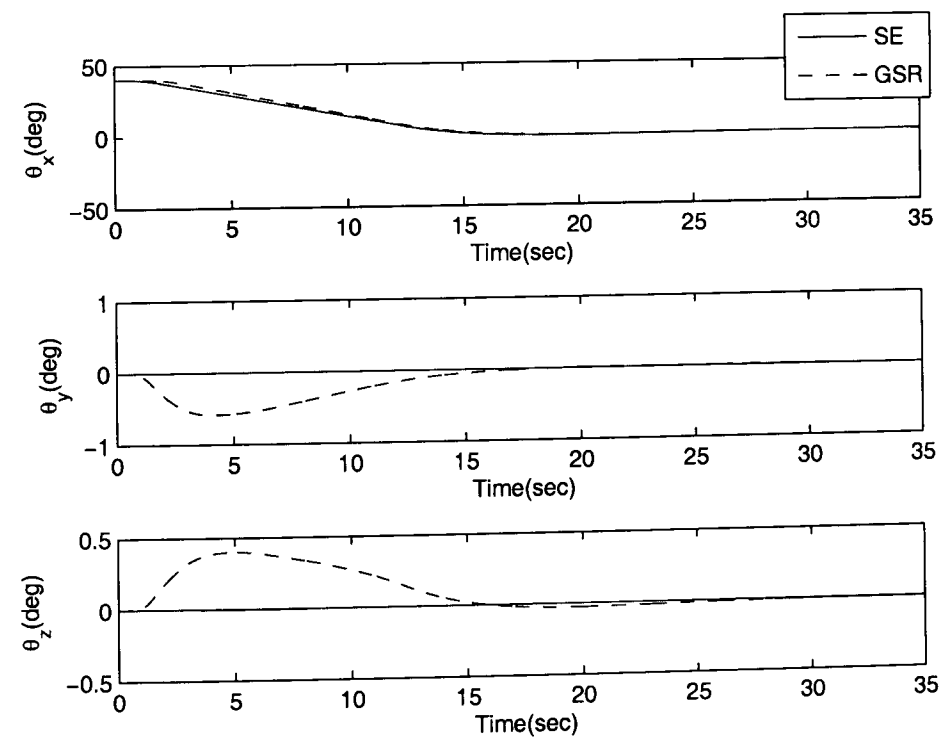

Figure 6.24: Reorientation Manoeuvre Case II: comparison of attitude angle profiles.

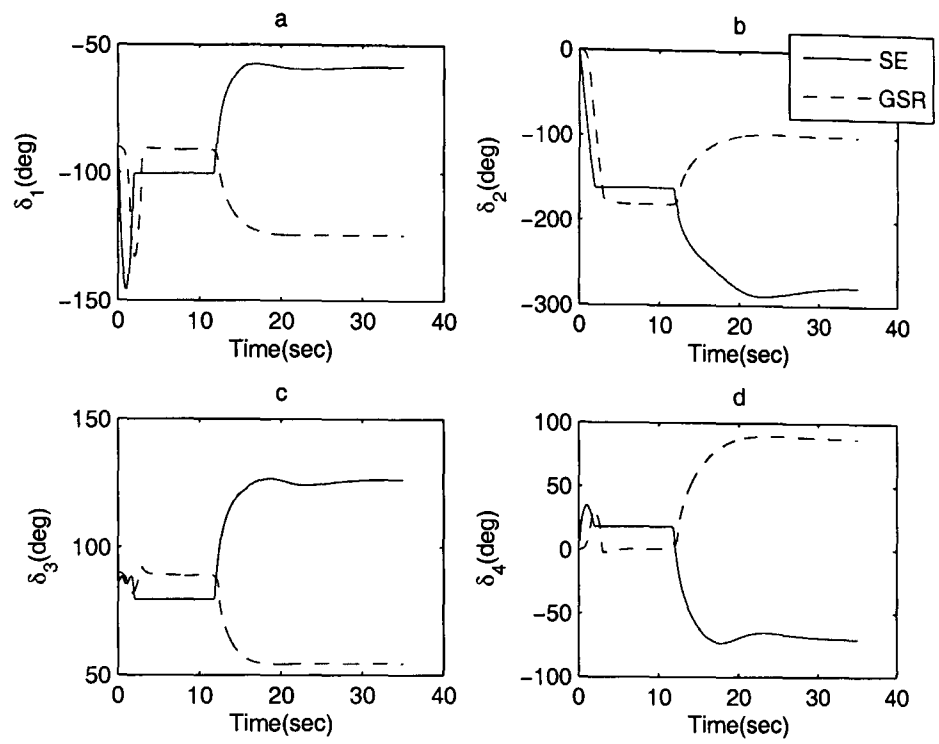

Figure 6.25: Reorientation Manoeuvre Case II: comparison of gimbal angle profiles.

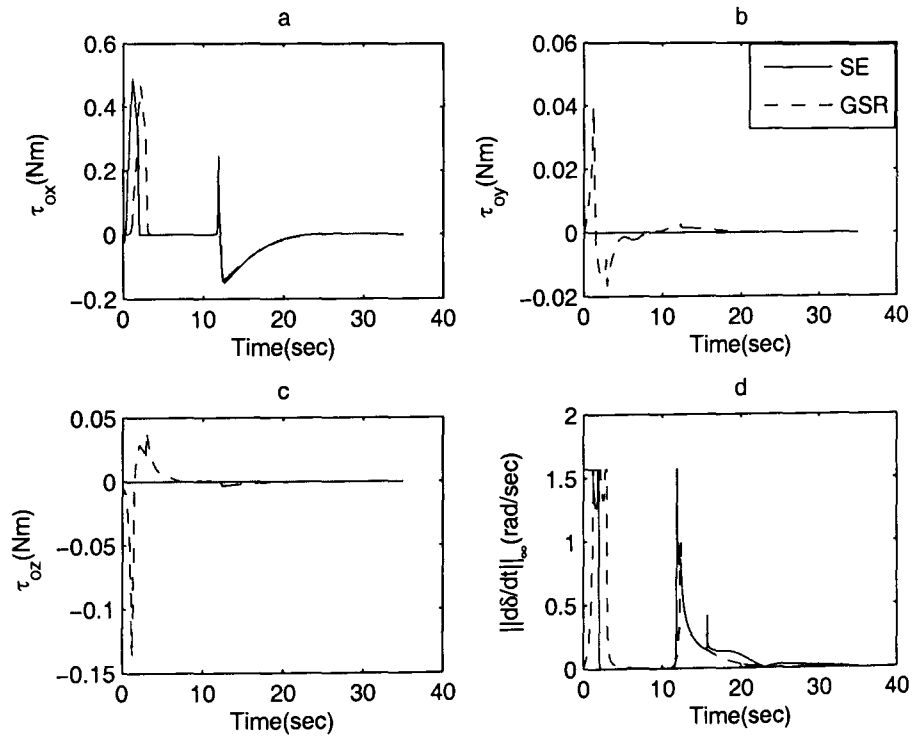

Figure 6.26: Reorientation Manoeuvre Case II: comparison of output torque components (a), (b), (c) and maximum gimbal rate (d).

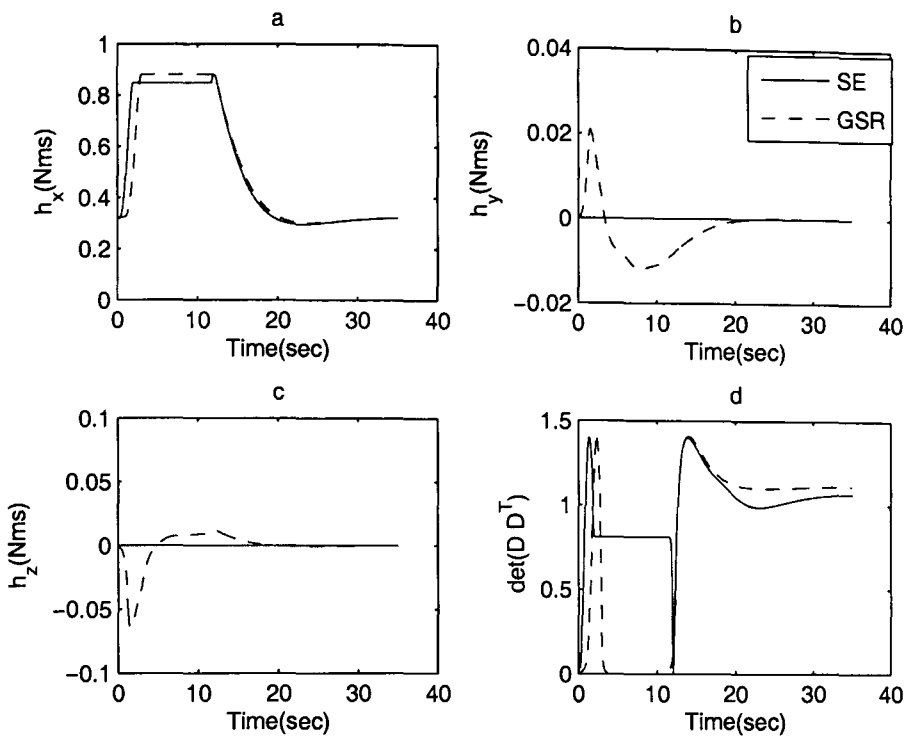

Figure 6.27: Reorientation Manoeuvre Case II: comparison of angular momentum components (a), (b), (c) and singularity index (d).

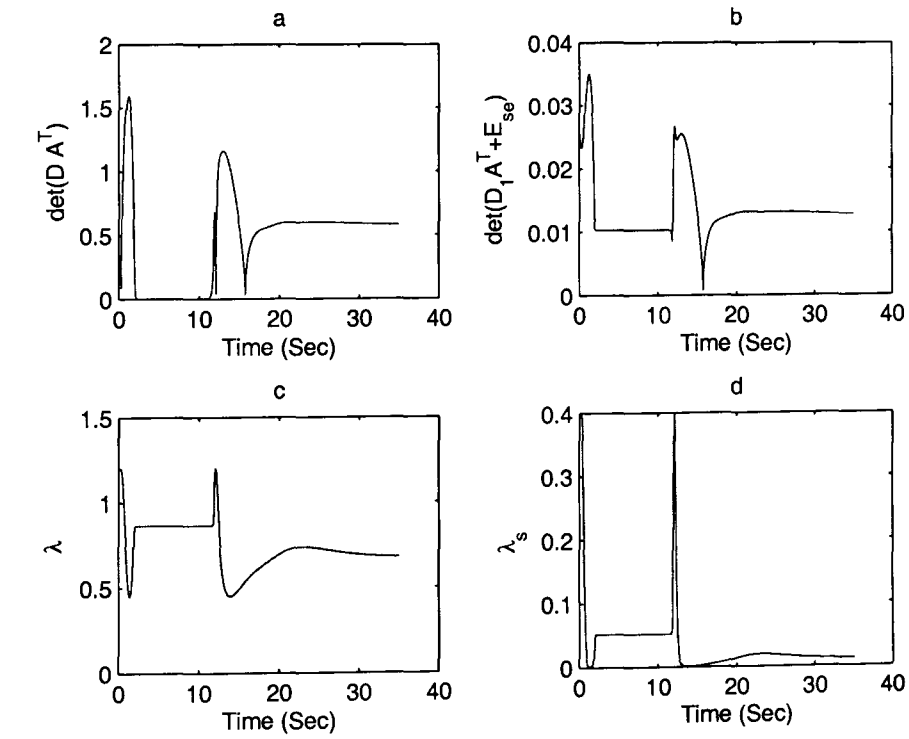

Figure 6.28: Reorientation Manoeuvre Case II: Singularity indices (a), (b), SAP (c) and SEP (d).

6.6 Summary

The Generalised-Inverse based steering law proposed in Chapter 5 is made singularity robust in order to make it able to escape elliptic singularity. This is done by adding singular matrix defined in the complementary space to make sum matrix of the full rank. The singularity avoiding (SAP) and singularity escaping parameters (SEP) are chosen such that the overall performance is enhanced. Typically SAP has a broad spread and SEP has a narrow spread around singularity. The performance of the proposed method is tested and compared with GSR. It has been shown that the proposed method is much quicker to escape elliptic singularity, it produces no pointing errors. The proposed method has been shown to outperform the GSR method in a reorientation manoeuvre.

Chapter 7

Inverse-Free Steering Law

7.1 Introduction

In last two chapters, we have developed a novel technique to steer the four CMG cluster which is based on generalised-inverse of Jacobian matrix. We have shown in Chapter 6 that generalised-inverse based singularity robust law can effectively escape elliptic singularity with high pointing accuracy. However, we still need to compute the inverse of the Jacobian matrix. In present chapter, we shall develop a technique for CMG steering which does not involve the computation of inverse of Jacobian matrix. We have termed this steering technique as inverse-free steering law. There is no concern of singularity in inverse-free steering. Therefore, an inverse-free steering can be thought as a singularity free steering but strictly in computational sense. However, the physical effect of singularity like slew rate saturation can be seen even in some forms of inverse-free steering law. This effect will be explained later in this chapter. The idea of inverse-free steering law was originally proposed by Krishnan et. al [59]. Their steering law uses transpose of the Jacobian matrix rather than its inverse. And it also uses the radial basis function networks to parameterize the nonlinear controller. However, its obvious disadvantage is that it requires learning of networks which can be computationally burdensome. Avanzini [4] has proposed a steering law that uses gimbal angle commands rather than gimbal rate commands to derive the CMG cluster. In this sense it becomes an inverse free steering law. Gimbal angle commands are computed by static inversion of the kinematic relation between gimbal angles and angular velocity of satellite. This

kinematic relation is given in Eq. (5.2.6) as $\boldsymbol{I}^{-1}\boldsymbol{h}(\boldsymbol{\delta}) = -\boldsymbol{\omega}$. In static inversion of Eq. (5.2.6) an approximate linear solution for gimbal angles is found in the neighborhood of the static position $\boldsymbol{\delta} = \mathbf{0}$. Such solution is valid only for small values of gimbal angles which means slow manoeuvres. They have also found approximate nonlinear solution to allow fast manoeuvres. In this technique the issue of singularity is said to be removed apparently but there are issues of exactness and its ability to use larger momentum space.

In this chapter, we shall develop a generic form of steering law which does not involve any matrix inversion, therefore, it is singularity free. Moreover, we have provided stability proof of such steering law through Liapunov theorem. Here we have studied two forms of inverse free steering law one which involves the transpose of the Jacobian matrix and the other involves transpose of a generic matrix function of gimbal angles (matrix $\boldsymbol{A}$ introduced in Chapter 5). The first form of proposed steering law is not able to start from elliptic singularity while satellite is rotationally at rest. Although this law is inverse free still there is momentum saturation near a gimbal configuration corresponding to zero value of commanded torque for some interval of time. Then the steering law breaks the symmetry of gimbal motion to exploit the larger momentum of CMG system. The other form or modified form of steering law which involves transpose of matrix $\boldsymbol{A}$ rather than Jacobian matrix $\boldsymbol{D}_1$ is able to start from elliptic singularity and it can use the larger momentum space. The inverse-free steering law produces motion of satellite in all three axes. Therefore, it is not suitable for tracking manoeuvre. Moreover, in this case gimbal angles do not return to zero gimbal condition on completion of the manoeuvre. All these features of this steering law are demonstrated through simulations.

7.2 Development of Inverse-Free Steering Law

In this section, we shall develop an inverse-free approach to steer CMG cluster. We use the Liapunov's stability theorem to find a stablising control which then results in an inverse-free steering law. We take the following Liapunov function for rest-rest

reorientation manoeuvre

$$V = k_1 \boldsymbol{q}_e^T \boldsymbol{q}_e + k_1 (q_{oe} - 1)^2 + \frac{1}{2} \boldsymbol{\omega}^T \boldsymbol{M}^{-2}(\boldsymbol{\delta}) \boldsymbol{I} \boldsymbol{\omega}. \tag{7.2.1}$$

Where $\begin{bmatrix} q_{oe} \\ \boldsymbol{q}_e \end{bmatrix} = \tilde{\boldsymbol{q}}_e$ is error quaternion defined by Eq. (3.3.8), $\boldsymbol{\omega}$ is angular velocity vector, $\boldsymbol{I}$ is inertia matrix and $\boldsymbol{M}(\boldsymbol{\delta})$ is positive definite non-singular matrix function of gimbal angle vector. And k_1 is a positive feedback gain.

By taking the time derivative of Liapunov function we get

$$\dot{V} = k_1 \boldsymbol{\omega}^T \boldsymbol{q}_e + \boldsymbol{\omega}^T (\boldsymbol{M}^{-2}(\boldsymbol{\delta}) \boldsymbol{I} \dot{\boldsymbol{\omega}} - \boldsymbol{M}^{-3}(\boldsymbol{\delta}) \dot{\boldsymbol{M}} \boldsymbol{I} \boldsymbol{\omega}) \tag{7.2.2}$$

But Eq. (3.7.32) can be rewritten as

$$\boldsymbol{I} \dot{\boldsymbol{\omega}} = -\boldsymbol{D}_1 \dot{\boldsymbol{\delta}}$$

for rest-rest manoeuvre $\boldsymbol{H} = \boldsymbol{I}\boldsymbol{\omega} + \boldsymbol{h} = 0$. We get

$$\dot{V} = -\boldsymbol{\omega}^T \left(-k_1 \boldsymbol{q}_e + \boldsymbol{M}^{-2}(\boldsymbol{\delta}) \boldsymbol{D}_1 \dot{\boldsymbol{\delta}} \right) - \boldsymbol{\omega}^T \boldsymbol{M}^{-3}(\boldsymbol{\delta}) \dot{\boldsymbol{M}} \boldsymbol{I} \boldsymbol{\omega}$$

Here we choose

$$\boldsymbol{M}^{-2}(\boldsymbol{\delta}) \boldsymbol{D}_1 \dot{\boldsymbol{\delta}} = k_1 \boldsymbol{q}_e + k_2 \boldsymbol{M}^{-1}(\boldsymbol{\delta}) \boldsymbol{\omega} \tag{7.2.3}$$

such that $\dot{V}$ becomes negative semi-definite, where $k_2 > 0$. Therefore, after rearrangement we get

$$\dot{V} = -\boldsymbol{\omega}^T \left(k_2 \boldsymbol{M}^{-1}(\boldsymbol{\delta}) + \boldsymbol{M}^{-3}(\boldsymbol{\delta}) \dot{\boldsymbol{M}} \boldsymbol{I} \right) \boldsymbol{\omega}.$$

Here $\dot{V}$ is negative semi-definite only if

$$k_2 \boldsymbol{M}^2(\boldsymbol{\delta}) + \dot{\boldsymbol{M}}(\boldsymbol{\delta}) \boldsymbol{I} \geq \boldsymbol{0} \tag{7.2.4}$$

This condition puts constraints on gimbal rates and gimbal path. We can formulate inverse-free steering law from the following steering equation.

$$\boldsymbol{D}_1 \dot{\boldsymbol{\delta}} = k_1 \boldsymbol{M}^2(\boldsymbol{\delta}) \boldsymbol{q}_e + k_2 \boldsymbol{M}(\boldsymbol{\delta}) \boldsymbol{\omega}. \tag{7.2.5}$$

Matrix $\boldsymbol{M}(\boldsymbol{\delta})$ is chosen such that constraint given in Eq. (7.2.4) is satisfied and inverse free steering is possible. One of the obvious choice is

$$\boldsymbol{M} = \boldsymbol{D}_1 \boldsymbol{D}_1^T \tag{7.2.6}$$

which gives the following inverse free steering law

$$\dot{\boldsymbol{\delta}} = \boldsymbol{D_1^T}\left(k_1 \boldsymbol{D_1 D_1^T q}_e + k_2 \boldsymbol{\omega}\right). \tag{7.2.7}$$

This steering law clearly does not require an inversion of Jacobian matrix rather it needs transpose of the said matrix. The nonlinear control function now has dependence on gimbal angles through much simpler relation than that of neural network based approximation of nonlinear function given in Ref. [59]. Therefore, it offers a simpler but effective approach for inverse free steering. Its simplicity and effectiveness would be demonstrated through simulations. The choice discussed in this section can not steer a CMG cluster out of the elliptic singularity due to symmetric gimbal motion generated by $\boldsymbol{D}_1^T$ matrix in the steering law. It may be noted that there can be many other choices for matrix $\boldsymbol{M}(\boldsymbol{\delta})$ subjected to Liapunov based condition. In next section, we shall study another choice of matrix $\boldsymbol{M}(\boldsymbol{\delta})$ which will result in a modified singularity escaping inverse-free steering law.

7.3 An Inverse-Free Singularity Escape

The inverse-free steering law developed in previous section is not capable of escaping elliptic singularity while satellite is rotationally at rest. At elliptic singularity Jacobian matrix $\boldsymbol{D}_1$ is singular and direction of required torque lies in the null-space of the matrix $\boldsymbol{D}_1$. Therefore, we choose a different matrix function $\boldsymbol{M}(\boldsymbol{\delta})$ in the steering equation (7.2.5) to develop a singularity escaping inverse-free law. One may choose

$$\boldsymbol{M} = \boldsymbol{D_1 A^T} \tag{7.3.8}$$

where

$$\boldsymbol{A} = \boldsymbol{D}_1 + \lambda \boldsymbol{D_o}$$

and

$$\lambda = \lambda_o \exp\left(-\mu \det(\boldsymbol{D_1 D_1^T})\right)$$

with λ_o and μ as positive constants as defined in Eq. (5.5.30). The resulting steering law is

$$\dot{\boldsymbol{\delta}} = \boldsymbol{A^T}\left(k_1 \boldsymbol{D_1 A^T q}_e + k_2 \boldsymbol{\omega}\right). \tag{7.3.9}$$

This is clearly inverse-free steering law and it involves the transpose of matrix $\boldsymbol{A}$ rather than Jacobian matrix $\boldsymbol{D_1}$. We have seen the advantage of using the matrix $\boldsymbol{A}$ in generalised-inverse based steering laws in previous chapters. A CMG steering law using this matrix tends to use larger momentum space and avoid/escape singularities. We shall see, in next section, a similar advantage of using matrix $\boldsymbol{A}$ in inverse-free steering law. We shall simulate both forms of the proposed inverse-free steering law to demonstrate their effectiveness.

7.4 Simulation Results and Discussion

In this section, we shall simulate proposed steering laws to perform a 40^o roll manoeuvre of a small satellite using four CMG pyramid system. The satellite and CMG data is similar to that of used in Chapter 5 and 6 given in Table (5.2). We run simulations for three cases namely inverse-free steering law with initial gimbal angles at zero, exploiting larger momentum space and singularity escape with modified inverse-free steering law.

7.4.1 Case-I: Simulating Inverse-Free Steering Law

Here we simulate inverse-free steering law given in Eq. (7.2.7) for a 40^o roll manoeuvre. Initial gimbal angles are considered to be zero. Results are given in the following figures. It is clear from the Fig. (7.1) that the resulting motion of satellite is not constraint to purely roll direction but it also produces small motions in other two directions. For this reason such method is not suitable for tracking manoeuvres, however, we can use it for reorientation manoeuvre. One can see in Fig. (7.1(a)) that ω_x saturates at some smaller value for more than 5 seconds of the time. During this time other two components of angular velocity vector are zero. This means that satellite manoeuvres purely about roll axis for some time and then roll speed increases and motion in other two directions is started. This can be explained through gimbal motion given in Fig. (7.3) and Fig. (7.4), where δ_1 and δ_3 move symmetrically whereas δ_2 and δ_4 remain at zero for first few seconds of manoeuvre. This pure roll manoeuvre was possible due to matrix $\boldsymbol{D_1}$ and direction of commanded torque. As commanded torque is function of gimbal configuration through $\boldsymbol{M(\delta)}$, so there are some configurations of the gimbal angles where

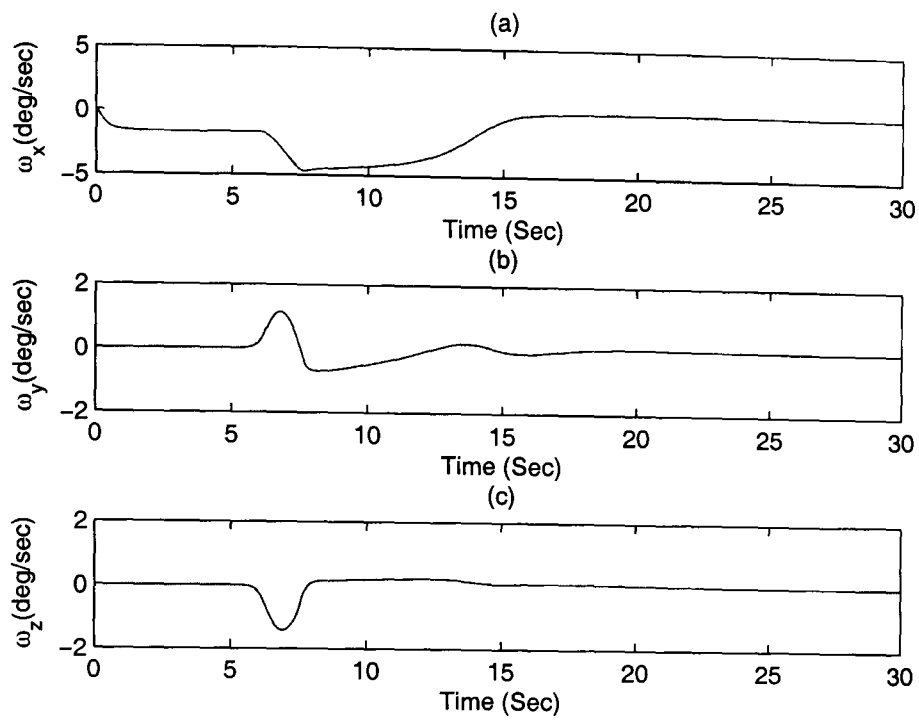

Figure 7.1: Roll manoeuvre case I: angular velocity components of satellite in body coordinates for proposed Inverse-Free steering law.

commanded torque is zero without achieving the control objective. In this example proposed steering law leads to a gimbal configuration where commanded torque becomes zero for sometime. During this time ω_x is constant and q_{ex} decreases with a constant rate. The decreasing value of q_{ex} will make torque slightly negative which will result in making $\dot{\delta}_3 < 0$ and $\dot{\delta}_1 = -\dot{\delta}_3$. When $|\dot{\delta}_3|$ exceeds $|\omega_x|$ this makes torque positive again and breaks the symmetry of δ_1 and δ_3. Therefore, all four gimbals start moving to access a higher value in momentum space, which can be seen in Fig. (7.6(a)). Final condition of gimbal angles is not zero in this case as shown in Fig. (7.3). But this final condition of gimbal angles corresponds to a zero angular momentum state as shown in Fig. (7.6(a),(b),(c)). The output torque follows the commanded torque except where gimbal rates saturate as shown in Fig. (7.5(a),(b),(c)). The Liapunov function rate is negative as it can be seen in Fig. (7.5(d)) which ensures the stability of the system with proposed steering law. The attitude angles in pitch and yaw directions remain less than 2^o as shown in Fig. (7.2(b),(c)). Singularity index in Fig. (7.6(d)) shows that CMG system remains far from singularity during the course of the manoeuvre.

7.4.2 Case-II: Simulating Modified Inverse-Free Steering Law

Now we shall simulate the modified form of the Inverse-Free Steering Law to perform a 40^o roll manoeuvre. It will be seen that by changing the matrix M we can improve the performance of attitude control system in terms of maximum utilization of available resources. In this case we simulate the steering law given in Eq. (7.3.9). The use of matrix A in steering law has improved the speed of manoeuvre. It can be noticed in Fig. (7.7) that angular rate in roll direction can reach larger value from start. This in turn shortens the time to complete the manoeuvre. However, this law also generates small motions in pitch and yaw directions as seen in Fig. (7.7(b),(c)). Attitude angles of satellite are given in Fig. (7.8). The pointing error is less than 2 degrees. The gimbal angles follow a different path and all four CMGs start moving from the very beginning (see Fig. (7.9) which makes system to use larger momentum space as seen in Fig. (7.12(a),(b),(c)). Moreover, final condition of gimbal angles is non-zero but it corresponds to zero angular momentum as shown in Fig. (7.12(a),(b),(c)). This law generates higher gimbal rate commands initially in all four CMGs as shown in Fig. (7.10). The output torque follows the commanded torque with exception of gimbal rate saturation regions as shown in Figures (7.11(a), (b), (c)). The Liapunov rate plot given in Fig. (7.11(d)) is negative definite which manifests the stability of the method. In this method system remains well away from singularity as it can be seen in Fig. (7.12(d)).

7.4.3 Case-III: Escaping Elliptic Singularity with Inverse-Free Steering Law

In inverse-free steering, escape from the elliptic singularity is not possible for the choice $M = D_1 D_1^T$ as in this case commanded torque lies in the null space of matrix D_1. However, with modified inverse-free steering law we can escape elliptic singularity. In this example we again consider a 40^o roll manoeuvre with gimbals held at elliptic singularity $[-90^o, 0, 90^o, 0]$ initially. Simulation results are shown in the following figures. Angular velocity components given in Fig. (7.13) show that the proposed method is able to escape the elliptic singularity. The maximum angular speed achieved in this case is smaller as initial angular momentum of CMGs in this case is not zero. Therefore, momentum imparted by CMG cluster to satellite in this case is smaller. Manoeuvre is

completed quickly as shown in Fig. (7.14) and attitude angles in other two directions remain within 3^o. Gimbal angle profile is given in Fig. (7.15). Gimbal angles have escaped singularity very quickly. Finally gimbal angles settle to a state whose angular momentum is equal to initial angular momentum (corresponding to elliptic singularity). But this final gimbal configuration is not singular as final value of singularity index in Fig. (7.18(d)) is far from zero. Output torque follows the input torque except in the case when gimbal rate command saturates as shown in Fig. (7.17(a), (b), (c)). The plot of Liapunov rate in Fig. (7.17(d)) shows the stability of steering logic. Finally angular momentum profile is given in Fig. (7.18(a), (b), (c)) and singularity index is given in Fig. (7.18(d)). This shows that system remains away from singularity during the course of manoeuvre.

7.5 Summary

In this chapter, we have presented a new technique of CMG steering which does not involve inverse of Jacobian matrix. We have termed resulting steering law as Inverse-Free Steering Law. Proposed steering law just uses the transpose of the Jacobian matrix or another matrix $\boldsymbol{A}$. Liapunov's stability theorem is used to derive the control law in some generic settings which then yields a generic form of inverse free steering law. The proposed steering logic is a good candidate for situations where tracking is not required as it can produce motion in other directions. In this case singularity is not of particular concern as even at singularity gimbal rate commands are finite due to exclusion of inverse from the logic. Steering law with transpose of Jacobian matrix cannot escape elliptic singularity, however, its generic form with matrix $\boldsymbol{A}$ has ability to escape the elliptic singularity. The effectiveness of Inverse-Free steering law is demonstrated through simulations. It has advantage of using higher momentum capacity of CMG cluster, escaping elliptic singularity and manoeuvring satellite efficiently. The obvious disadvantage is a slight tumbling of satellite and settling of gimbal angles to a non-zero condition.

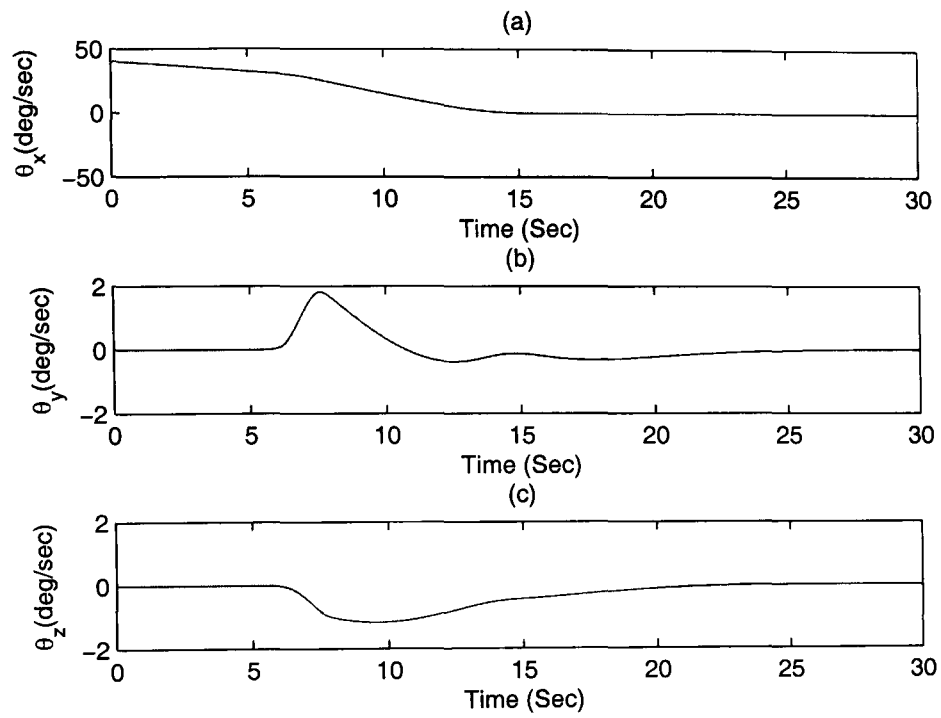

Figure 7.2: Roll manoeuvre case I: attitude angles of satellite for proposed Inverse-Free steering law.

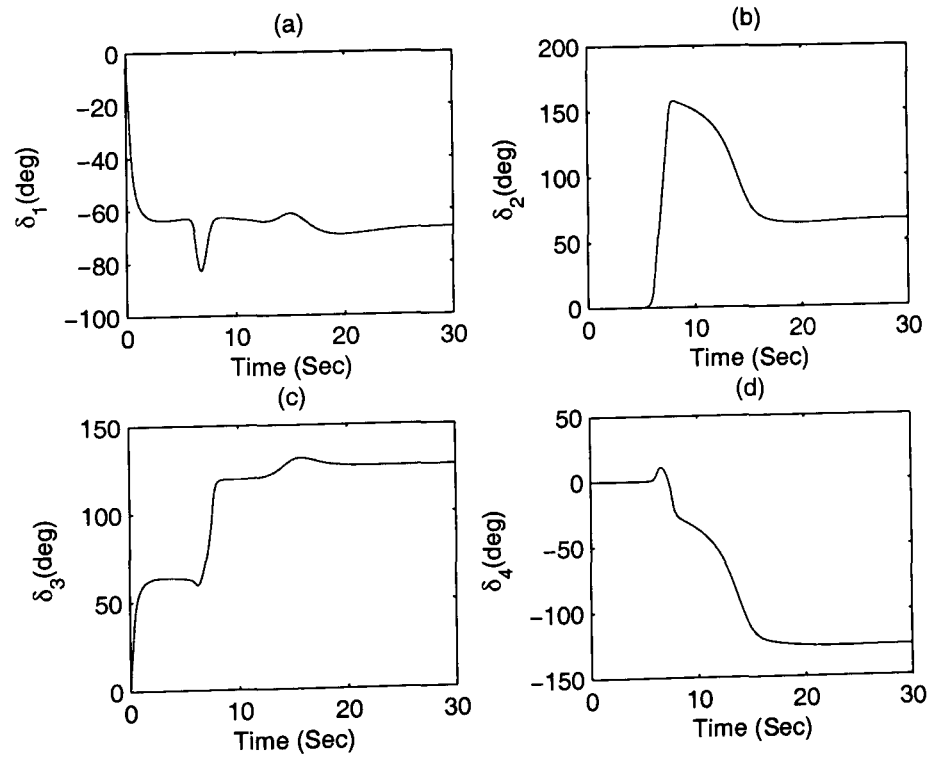

Figure 7.3: Roll manoeuvre case I: gimbal angle profiles for proposed Inverse-Free steering law.

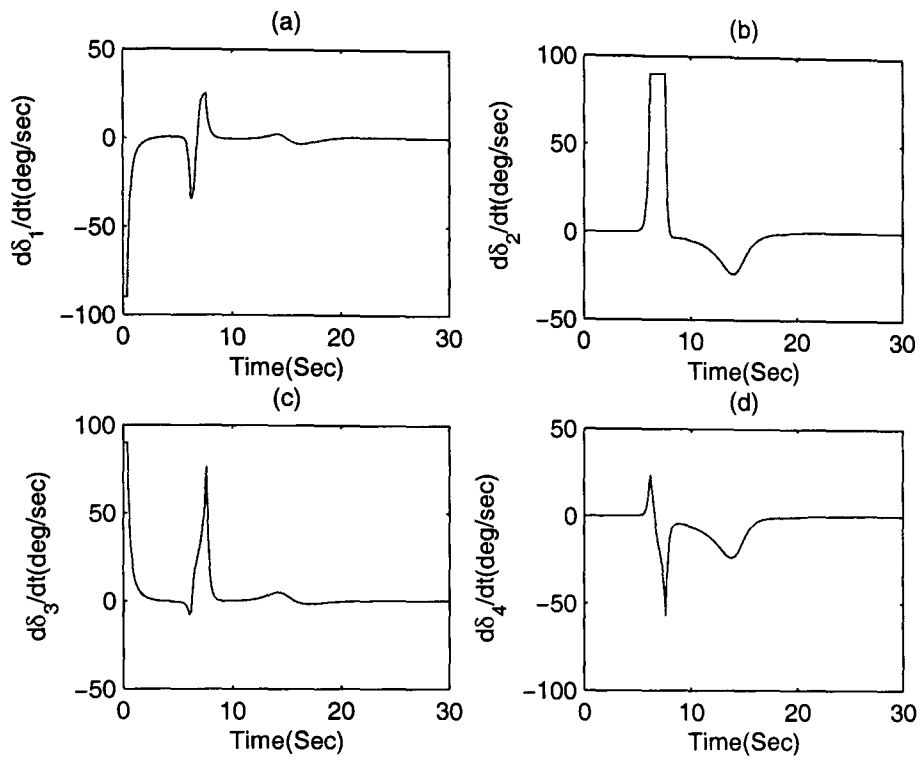

Figure 7.4: Roll manoeuvre case I: gimbal rate profiles for proposed Inverse-Free steering law.

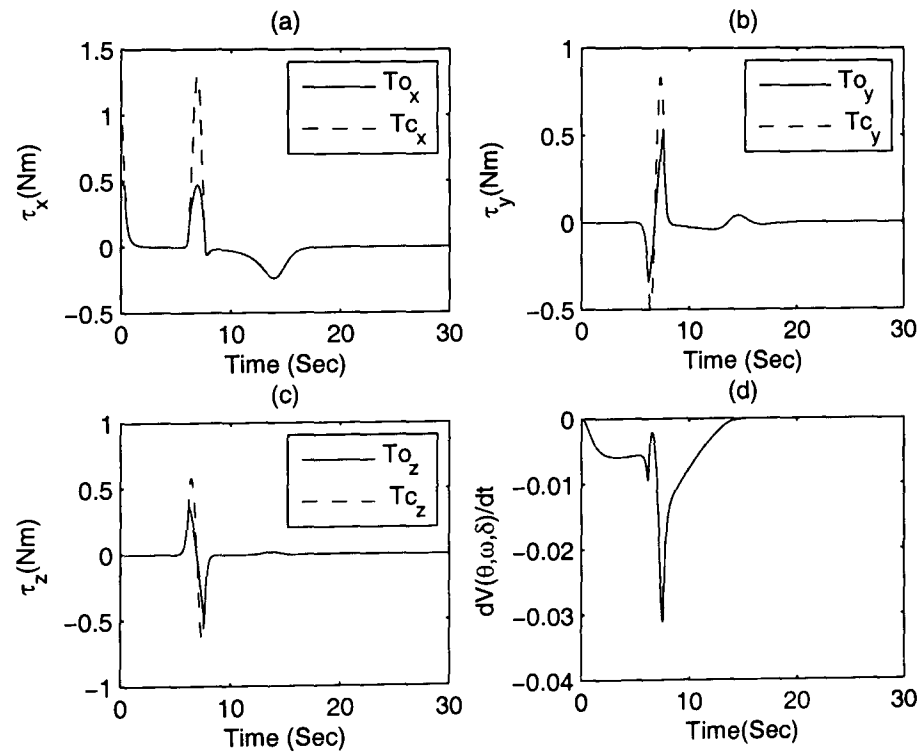

Figure 7.5: Roll manoeuvre case I: output and commanded torques (a),(b),(c)and Liapunov rate(d)for proposed Inverse-Free steering law.

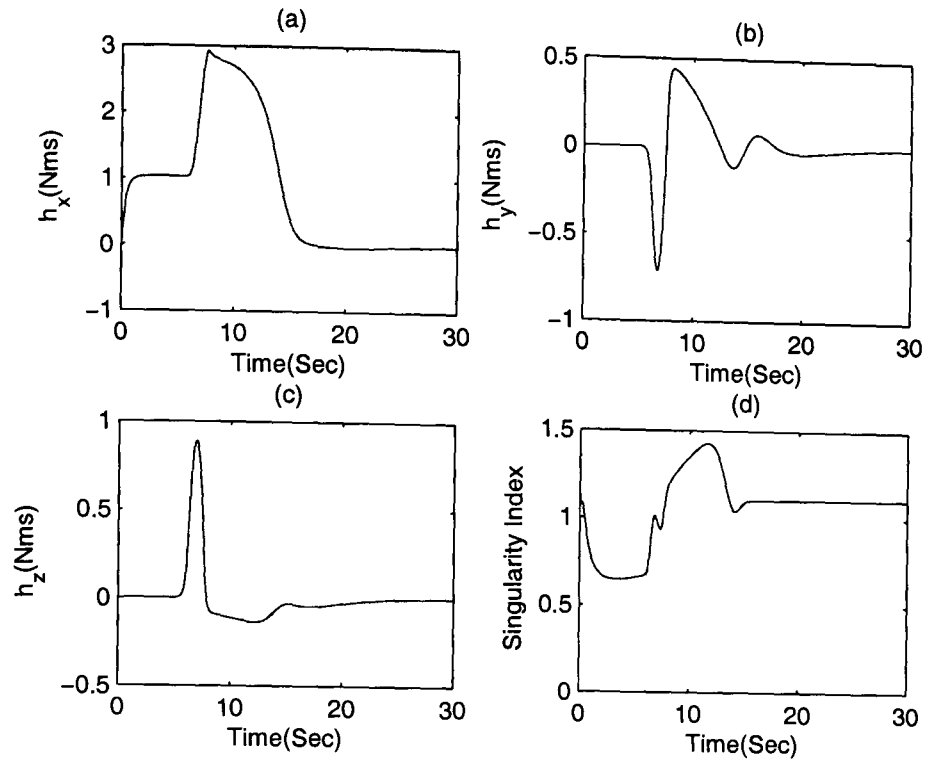

Figure 7.6: Roll manoeuvre case I: angular momentum components (a),(b),(c)and singularity index(d) for proposed Inverse-Free steering law.

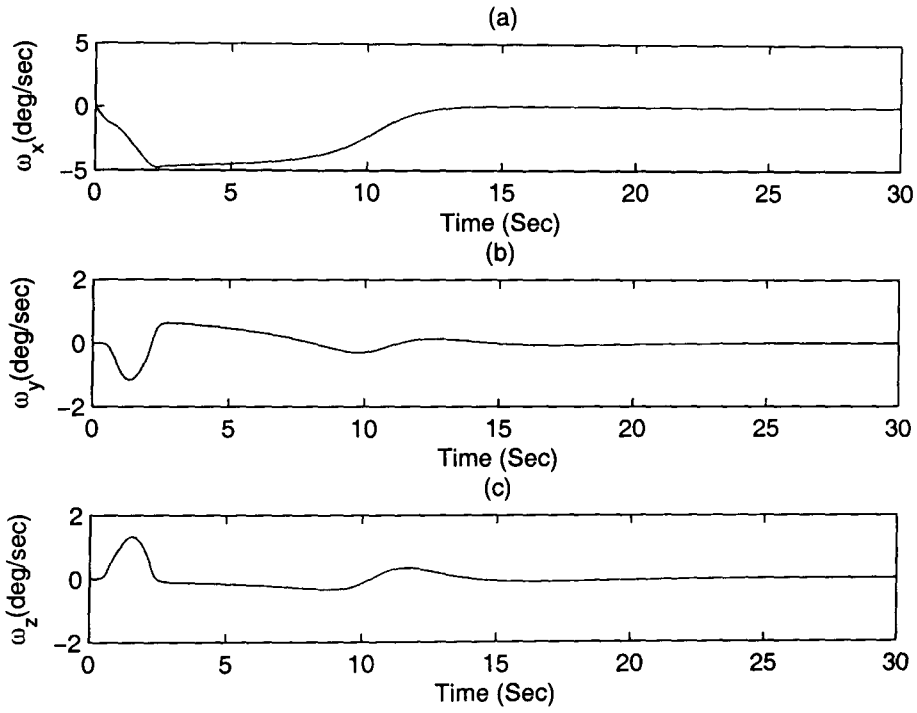

Figure 7.7: Roll manoeuvre case II: angular velocity components of satellite in body coordinates for proposed Modified Inverse-Free steering law.

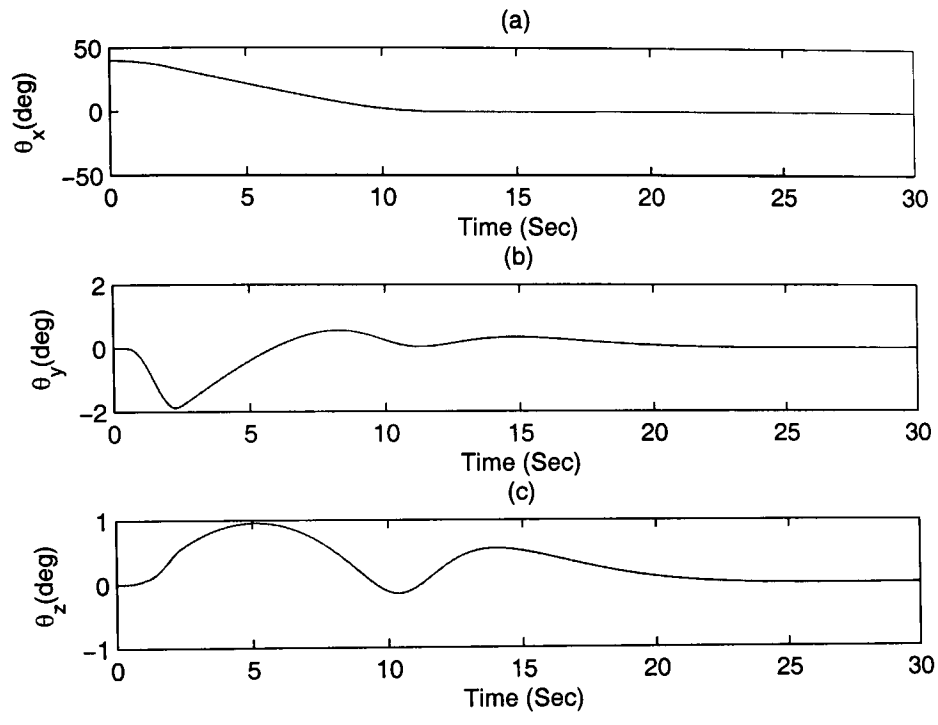

Figure 7.8: Roll manoeuvre case II: attitude angles of satellite for proposed Modified Inverse-Free steering law.

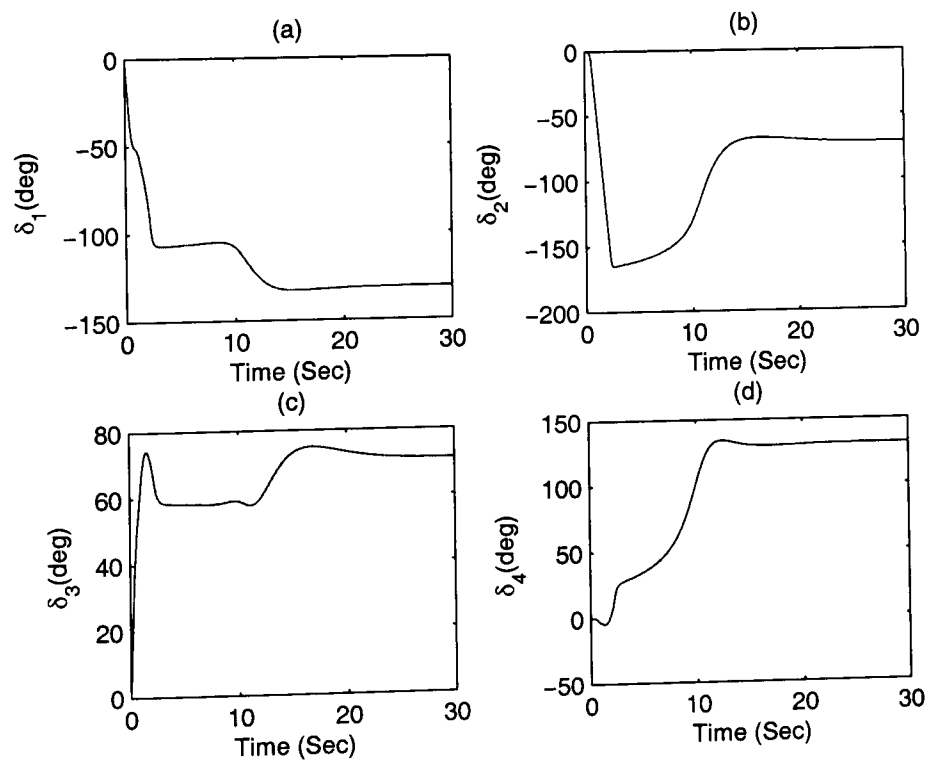

Figure 7.9: Roll manoeuvre case II: gimbal angle profiles for proposed Modified Inverse-Free steering law.

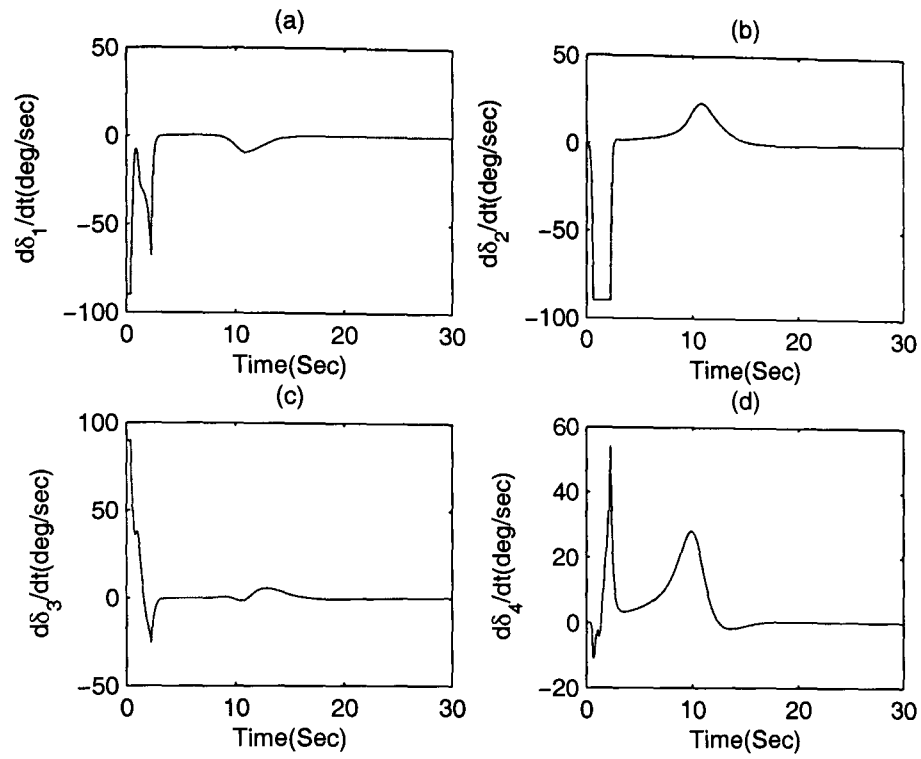

Figure 7.10: Roll manoeuvre case II: gimbal rate profiles for proposed Modified Inverse-Free steering law.

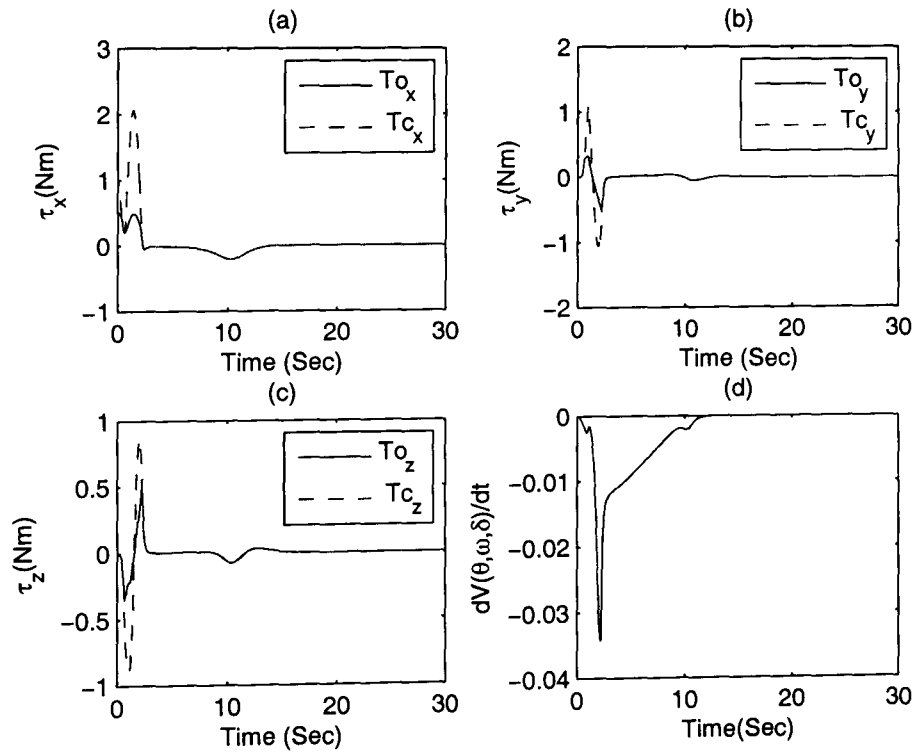

Figure 7.11: Roll manoeuvre case II: output and commanded torques (a),(b),(c)and Liapunov rate(d)for proposed Modified Inverse-Free steering law.

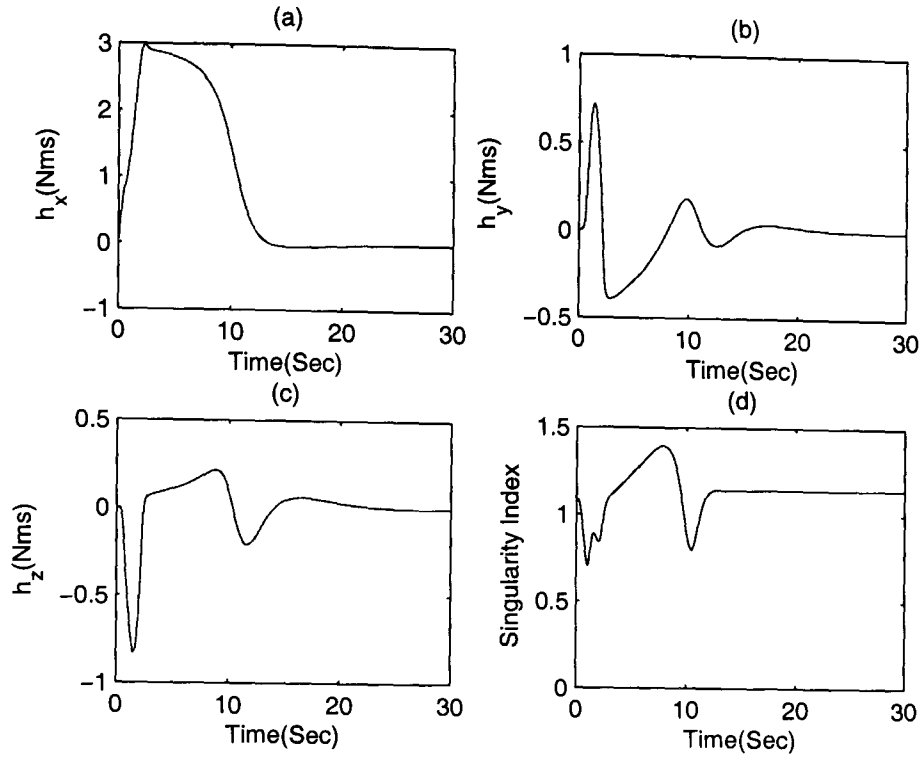

Figure 7.12: Roll manoeuvre case II: angular momentum components (a),(b),(c)and singularity index(d) for proposed Modified Inverse-Free steering law.

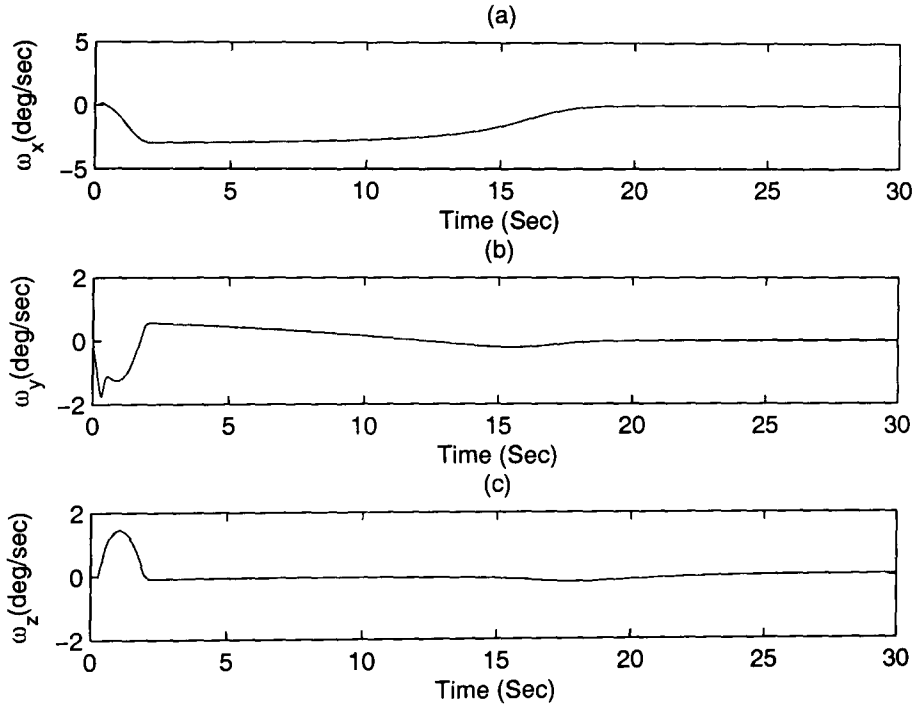

Figure 7.13: Roll manoeuvre case III: angular velocity components of satellite in body coordinates for proposed Modified Inverse-Free steering law.

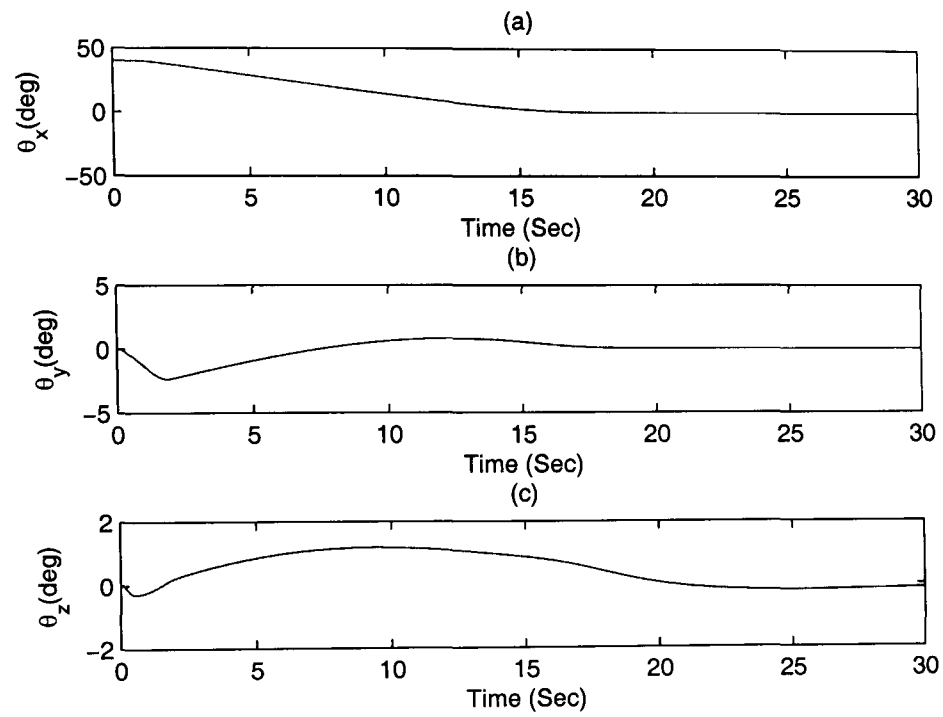

Figure 7.14: Roll manoeuvre case III: attitude angles of satellite for proposed Modified Inverse-Free steering law.

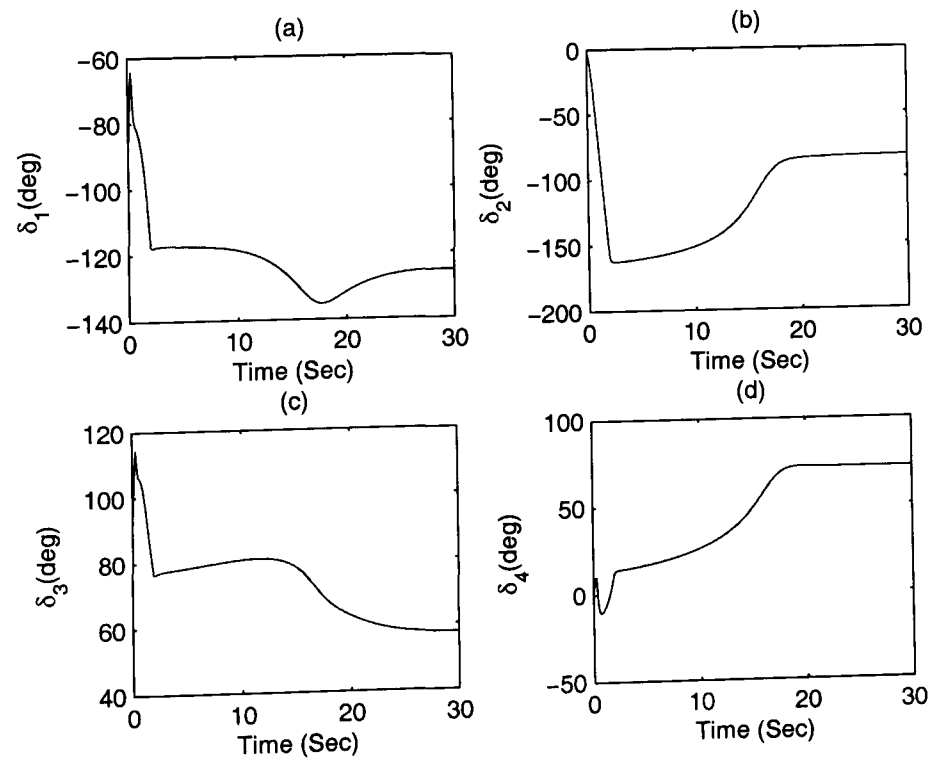

Figure 7.15: Roll manoeuvre case III: gimbal angle profiles for proposed Modified Inverse-Free steering law.

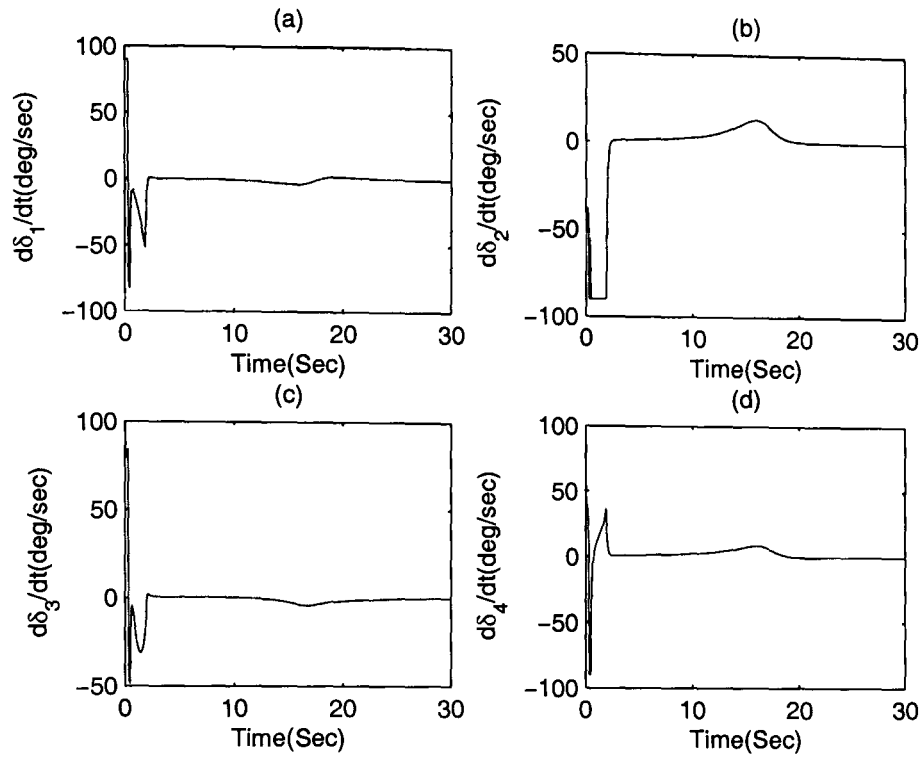

Figure 7.16: Roll manoeuvre case III: gimbal rate profiles for proposed Modified Inverse-Free steering law.

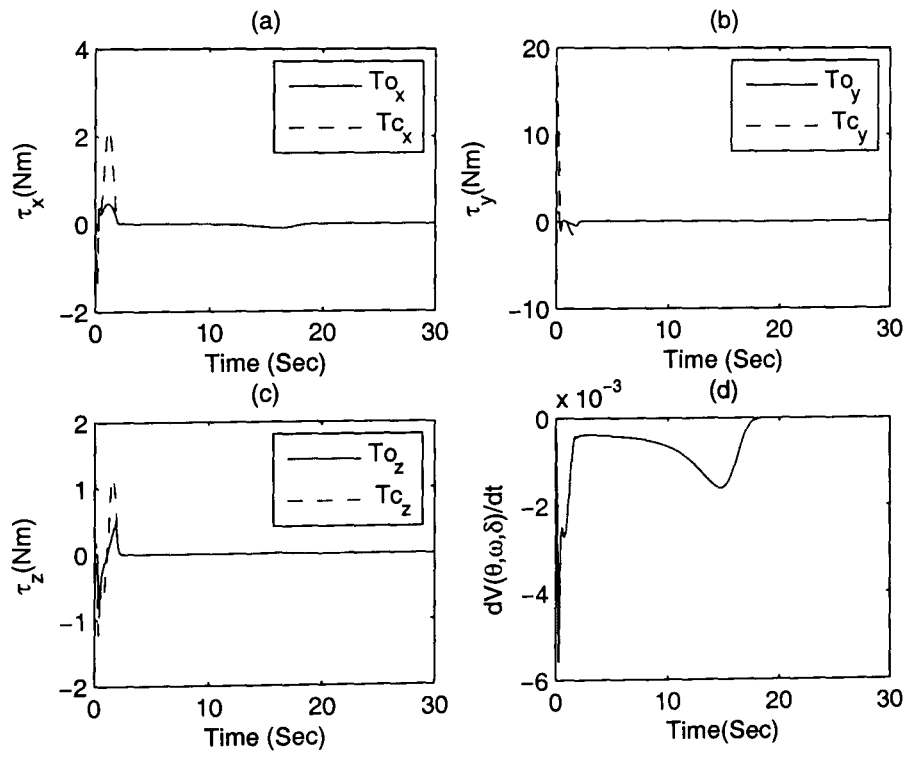

Figure 7.17: Roll manoeuvre case III: output and commanded torques (a),(b),(c)and Liapunov rate(d)for proposed Modified Inverse-Free steering law.

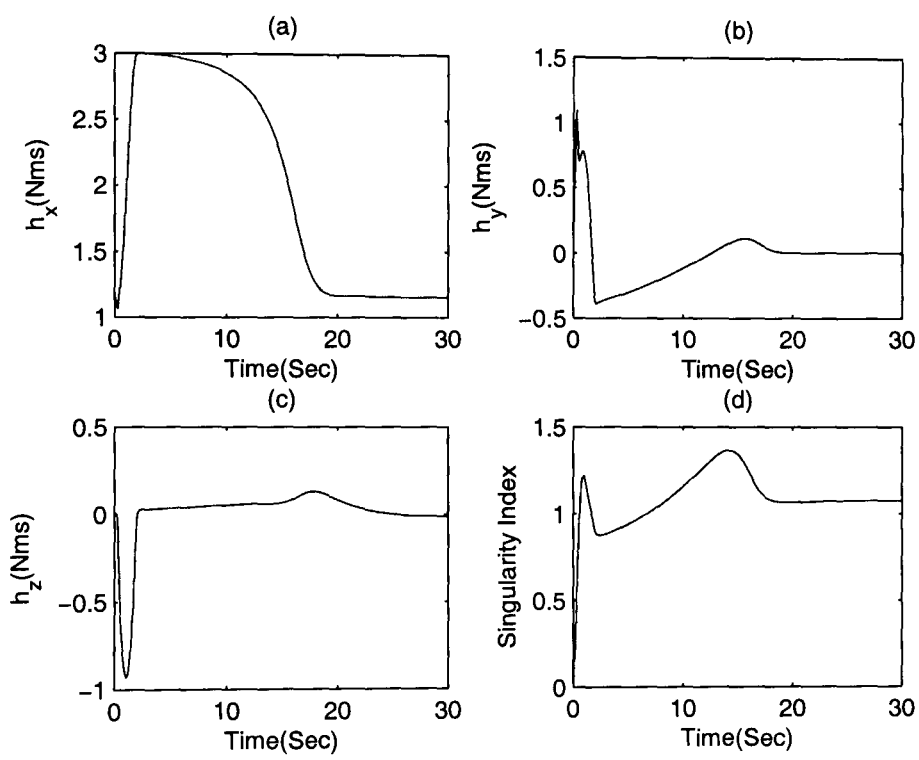

Figure 7.18: Roll manoeuvre case III: angular momentum components (a),(b),(c)and singularity index(d) for proposed Modified Inverse-Free steering law.

Chapter 8

Conclusion and Further Work

This chapter summarizes the main conclusions drawn from this thesis and points out some areas of further research.

8.1 Conclusions

With advent of new mini CMGs for modern attitude control systems of new generation of small agile satellites with high Earth observation capability the need for new accurate and efficient CMG steering laws has been felt more than ever. In spite of torque amplification property of CMGs, dealing with singularities is the most difficult part of the CMG steering problem. Singularities can deteriorate the performance of overall system if the implemented steering law is not efficient enough. Some designers overdesign the CMG cluster to counter the possible effects of the internal singularities. But an efficient use of onboard resources for new generation of satellites will rule out such oversizing. Variant forms of Singularity Robust Steering Laws based on pseudo-inverse are usually used, but they lead toward elliptic singularity and as a result either restrict the available momentum space or cause the pointing error. We have carried out this study in the quest of accurate and efficient steering laws for CMG clusters. Here we shall present key conclusions drawn from core chapters of this thesis.

8.1.1 Mathematical Model of a Satellite Equipped with Momentum Exchange Devices

Chapter 3 presents the development of mathematical model of attitude dynamics and control of a satellite equipped with momentum exchange devices. These devices include reaction wheels, momentum wheels, single gimbal CMGs and variable speed CMGs. This chapter also presents a brief review of mathematical formulation of CMG singularity problem and some of the existing steering laws. The following conclusions can be drawn from this chapter:

- Development of a generic mathematical model for attitude dynamics and control of satellites without specifying the type or inertia properties of momentum exchange devices is proved to be very useful. It provides a framework for deduction of equations for particular type or inertia properties of devices.

- In the deduction and further simplification of the dynamic equation for satellite equipped with CMG systems certain terms are ignored for being comparatively very small. It has been shown to be a valid assumption by comparing the magnitudes of these terms for a typical example.

- The exact steering problem has been defined. Exact steering in the CMG systems is possible if the systems remain well away from the singularity and feedback gains are chosen such that commanded torque can match the torque capability of the CMG systems.

8.1.2 Exact Steering in Twin CMG Systems

In Chapter 4 new exact steering techniques are developed for twin CMG systems employed for single axis control. These techniques use phase-plane analysis to find analytical expressions for feedback gains such that exact steering can use full momentum capacity of CMG cluster without hitting the singularity. We have developed three techniques of achieving exact steering in twin CMG systems: exact steering with no knowledge of explicit Gimbal Rate Constraint (Exact without GRC); exact steering with explicit Gimbal Rate Constraint (Exact with GRC); exact steering with explicit

Gimbal Rate Constraint and Variable Gains structure (Exact with GRC and VG). Table (8.1) summarizes the key features of these steering laws. We have demonstrated the effectiveness of these proposed exact steering laws through computer simulations developed in MATLAB/SIMULINK for BILSAT-1 example. A part of this work has been published as a conference paper [1]. The outcomes of this chapter are as follows:

- The phase-plane analysis of the twin CMG system has established that the separatrix trajectory, separating the singularity avoiding trajectories from those which encounter singularity, is the desired trajectory for the closed-loop system's output. This trajectory uses full momentum capacity without hitting the singularity. The feedback gains corresponding to this trajectory are formulated analytically.

- Exact steering problem with no gimbal rate constraint reduces to damped harmonic oscillator equation with well-known solution. Therefore, this problem is solved analytically to find expressions for feedback gains, slew angle, slew rate, gimbal angle, gimbal rate and output torque for a given pitch manoeuvre.

- Incorporation of gimbal rate limit in exact steering scheme of twin CMG systems produces near-optimal solutions. Phase-plane analysis shows that the separatrix trajectory for rest-rest single axis manoeuvre follows the bang-bang trajectory before entering the feedback region (where gimbal rate is not saturated) near equilibrium point (which in this case is origin). Feedback gains are calculated analytically for this choice of trajectory.

- We have shown that exact steering is also possible with variable or adaptive feedback gains. In this logic gains are gradually decreased as system approaches toward singularity and they are increased as system moves away form the singularity. The main advantage of variable gain method over fixed gains method is that rapid large angle slew manoeuvres can be performed relatively easily and effectively.

- The formulation developed here for twin CMGs can be used to design a twin CMG cluster for the given mission requirements.

Table 8.1: Comparison of Proposed Exact Steering Laws for Twin CMG Systems

Exact without GRC	Exact with GRC	Exact with GRC and VG
Fixed feedback gains	Fixed feedback gains	Variable feedback gains
Phase-plane analysis	Phase-plane analysis	Phase-plane analysis
Separatrix trajectory	Separatrix trajectory	No separatrix trajectory
Avoids singularity	Avoids singularity	Avoids singularity
Optimality is not shown	Near time-optimal	Near time-optimal
Small gains for large slew	Small gains for large slew	Large gains for large slew

8.1.3 Exact Steering in Four CMG Systems

In Chapter 5, the exact steering treatment of twin CMGs used for single axis control is generalised for four CMG cluster employed for three axis control. We use the quaternion feedback law which holds the direction of manoeuvre fixed in the inertial space. As the Exact Steering Law based on Moore-Penrose inverse of Jacobian matrix can not avoid elliptic singularity so it can not use full extent of momentum capacity. Therefore, we have proposed an Exact Steering Law based on generalised inverse. We have published a conference paper [2] proposing the use of generalised-inverse for exact steering of the four CMG pyramid system. The outcomes of this chapter are as follows:

- Angular momentum vector of the CMG cluster has a fixed direction during the eigen-axis manoeuvre. So a new angle variable can be defined to represent norm of the momentum vector. Therefore, this new angle variable and slew angle are then used for phase-plane analysis of four CMG system employed for three-axis manoeuvre.

- For large slew angles the equation of closed-loop system reduces to equation of damped pendulum.

- Due to non-linearity of problem, numerical method such as Newton-Raphson method can be used to determine the feedback gains corresponding to desired trajectory using full momentum capability of CMG cluster.

- Singularity structure is much more complex in four CMG systems due to pres-

ence of internal singularities. Therefore, knowing gains does not solve the problem completely unless an exact steering law is developed which can avoid elliptic singularity in order to use full extent of angular momentum.

- We have shown that the proposed Generalised-Inverse (GI) steering law can avoid elliptic singularity and can use 95 percent of full momentum capacity of CMG cluster for the given choice of feedback gains.

- Simulation results show that GI steering law outperforms the Generalised Singularity Robust (GSR) steering law in number of ways. GI avoids elliptic singularity by moving all four gimbals from start whereas GSR encounters elliptic singularity due to symmetric motion of only two (odd) gimbals and then escapes singularity by moving all four gimbals. Thus GSR causes a pointing error whereas GI causes no pointing error. For the same choice of feedback gains GI exploits larger momentum space than GSR, therefore, GI causes a faster slew manoeuvre than GSR. GI brings gimbals back to initial zero state after the completion of manoeuvre whereas GSR can not bring gimbals back to initial zero state.

- The singularity of GI lies at 95 percent of outer envelope of the CMG cluster for roll axis. It has been shown that by using a modified form of proposed GI steering law this singularity can move out from 95 to 99 percent of full momentum capability. A method of obtaining the modified form of GI steering law is also discussed.

- Modified form of GI steering law can start from preferred initial gimbal angles whereas GI can not start from this set of gimbal angles.

- Simulation results for modified GI also outperform the GSR as GI's results did except modified GI exploits even larger momentum space.

- Exact steering methods for CMG systems based on GI or modified GI can avoid elliptic singularity but they can not escape this singularity.

8.1.4 Singularity Escaping Steering

In Chapter 6, we have shown that exact steering law based on generalised inverse can be made singularity robust by adding a disturbance in the singular direction only. We have tested this scheme in open-loop analysis and compared with GSR method. We have also tested this scheme for some reorientation manoeuvre examples. Main conclusions drawn from this chapter are as follows:

- Proposed GI steering law can be made singularity robust by adding a small dither in singular direction only. The resulting steering law can escape elliptic singularity in a very effective way. This new steering law is called Singularity Escaping (SE) steering law.

- In SE steering law the choice of two parameters namely Singularity Avoiding Parameter (SAP) and Singularity Escaping Parameter (SEP) affects the output torque profile and maximum gimbal rate excursions. A careful study reveals that by increasing the value SAP and its spread over singularity index improves the singularity avoidance property of SE steering law, which means that output torque accuracy is improved at the cost of increased gimbal rates. On the other hand, increase in the value and spread of SEP improves the singularity escaping property of SE steering law but it degrades the output torque accuracy with decreased gimbal rates. Therefore, SAP and SEP are selected on the basis of a criterion of maximum allowable gimbal rate limit taken to be $2.5\mathrm{rad/s}$.

- Open-loop simulation tests comparing the performance of SE steering law and GSR law show some interesting results. Two tests are performed. In first test, simulation starts from initial zero gimbal angles. Results shown that SE moves all four gimbals from start whereas GSR moves only two gimbals initially and encounter elliptic singularity. GSR stays in elliptic singularity for $1\mathrm{sec}$ before it recovers from singularity by causing pointing error. SE has a very brief encounter with an internal singularity (but not elliptic one) but output torque recovers quickly and no pointing error is caused. In second test, simulation starts from elliptic singularity. SE moves all four gimbals immediately and recovers from singularity within $1/4\mathrm{sec}$ whereas GSR still takes $1\mathrm{sec}$ and causes pointing error.

SE has caused a very small negative torque in order to escape the singularity with no pointing error.

- In a reorientation manoeuvre example SE steering law exhibits the following merits over GSR: it has no pointing error; it has faster escape from singularity; and it brings gimbal angles back to initial zero state at the end of the manoeuvre.
- The SE steering law is suitable fast tracking manoeuvres.

8.1.5 Inverse Free Steering

In Chapter 7, an Inverse Free (IF) steering law has been proposed to generate another class of exact steering which does not involve inverse of Jacobian matrix. It involves transpose of Jacobian matrix. We have derived a generic form of inverse free law from Liapunov stability theory. The following conclusions can be drawn from this chapter:

- We have seen that inverse free steering law does not mean singularity free steering law.
- The inverse free steering law which involves transpose of Jacobian matrix passes/transit through a gimbal angle state corresponding to zero commanded torque. This gimbal state manifests itself through the saturation of angular momentum at nearly one-third of maximum available value.
- Although IF steering is numerically robust as it does not involve inverse of a matrix. But it involves transpose of Jacobian matrix so it can not escape elliptic singularity.
- In modified IF steering law, Jacobian matrix is replaced by another suitably chosen matrix A such that modified IF can escape elliptic singularity and can also avoid zero commanded toque gimbal state of IF steering law.
- The main disadvantages of this scheme are as follows: it produces small motions in other directions; gimbal angles do not return to initial zero state after completion of the manoeuvre.
- IF steering law or its modified form are not suitable tracking manoeuvres. But they are quite effective and simple for reorientation manoeuvres.

Table 8.2: Comparison of Proposed Steering Laws for Four CMG Systems

GI Steering Law	SE Steering Law	IF Steering Law
Exact steering	Singularity robust steering	Exact steering
Avoids elliptic singularity	Avoids elliptic singularity	Avoids elliptic singularity
No escape	Escapes elliptic singularity	Escapes elliptic singularity
High pointing accuracy	High pointing accuracy	No pointing accuracy
Gimbals return back to zero	Gimbals return back to zero	No return back
Computes inverse of matrix	Computes inverse of matrix	Inverse-free computation

In Table (8.2), we have summarized different features of our newly proposed steering laws.

8.2 Further Work

We have proposed and developed novel ideas about Exact Steering in twin and four CMG systems, Singularity Escaping Steering and Inverse Free Steering in this thesis. The following ideas can be taken as new streams of further research work.

1. Some optimization scheme has to be developed to find matrix $\boldsymbol{A}$ which can extend the available momentum to its full capacity. Geometric view of steering law based on this matrix $\boldsymbol{A}$ has not yet been developed so any further work on this exact steering law should address its geometric features.

2. Some optimum search method can be developed to find parameters involved in Singularity Escaping Steering Law which minimizes output torque error subjected to gimbal rate constraint.

3. Inverse free steering law can be improved to reduce the motion in undesired direction or pointing error.

4. One may study the application of proposed generalised-inverse steering law and inverse-free steering law to combined power and attitude control problem for variable-speed CMG systems.

Bibliography

[1] S. Asghar, P. L. Palmer, and M. Roberts. An exact steering law for twin control moment gyro systems. In *Proceedings of the 6th International ESA Conference on Guidance, Navigation and Control Systems*, Loutraki, Greece, October 2005.

[2] S. Asghar, P. L. Palmer, and M. Roberts. Exact steering law for pyramid-type four control moment gyro systems. In *AIAA/AAS Astrodynamics Specialist Conference*, Keystone, CO, August 2006.

[3] G. F. Auclair and R. C. Wells. Control moment gyro selection and design criteria. In *AIAA Guidance, Control and Flight Dynamics Conference*, number 70-976, 1970.

[4] G. Avanzini. Gimbal-position command generation for a cluster of control moment gyroscopes. In *AAS/AIAA Astrodynamics Specialists Conference*, number AAS 05-418, Lake Tohoe, CA, August 2005.

[5] G. Avanzini and G. de Matteis. A local optimization technique for attitude motion tracking using control moment gyroscopes. *The Journal of Astronautical Sciences*, 50(2):213–229, 2002.

[6] D. R. Baker and C. W. Wampler. Some facts concerning the inverse kinematics of redundant manipulators. In *Proceedings of the IEEE International Conference on Robotics and Automation*, volume 2, pages 604–609, Raleigh, NC, 1987.

[7] S. Barnett. *Matrices in Control Theory*. Van Nostrand Reinhold Company, 1971.

[8] N. S. Bedrossian. Steering law design for redundant single gimbal control moment gyro systems. Master's thesis, Mechanical Engineering, MIT, Cambridge, MA, 1987.

[9] N. S. Bedrossian. Characterizing spatial redundant manipulator singularities. In *Proceedings of IEEE International Conference on Robotics and Automation*, number 1, pages 714–719, 1990.

[10] N. S. Bedrossian. Classification of singular configurations for redundant manipulators. In *Proceedings of IEEE International Conference on Robotics and Automation*, number 2, pages 818–823, 1990.

[11] N. S. Bedrossian, J. Paradiso, E. V. Bergmann, and D. Rowell. Redundant single gimbal control moment gyroscope singularity analysis. *Journal of Guidance, Control and Dynamics*, 13(6):1096–1101, 1990.

[12] N. S. Bedrossian, J. Paradiso, E. V. Bergmann, and D. Rowell. Steering law design for redundant single gimbal control moment gyroscope. *Journal of Guidance, Control and Dynamics*, 13(6):1083–1089, 1990.

[13] A. Behal, D. Dawson, E. Zeregoglu, and Y. Fang. Nonlinear tracking control of an underactuated spacecraft. In *Proceedings of the American Control Conference*, pages 4684–4689, Anchorage, AK, May 2002.

[14] K. D. Bilimoria and B. Wie. Time-optimal three-axis reorientation of a rigid spacecraft. *Journal of Guidance, Control and Dynamics*, 16(3):446–452, 1993.

[15] R. H. Bishop, S. J. Paynter, and J. W. Sunkel. Adaptive control of space station with control moment gyros. *IEEE Control Systems Magazines*, 12(5), 1992.

[16] J. C. Blondin. Small-CMG's: Needs, capabilities, trade and implementation. In *AAS/AIAA GNC Rocky-Mountain Conference*, 1996.

[17] T. L. Boullion and P. L. Odell. *Generalized Inverse Matrices*. John Wiley and Sons, Inc, 1971.

[18] A. Bradford. BILSAT-1: A low cost, agile, earth observation micro-satellite for Turkey. In *IAF*, Houston, TX, October 2002.

[19] J. Busseuil, M. Llibre, and X. Roser. High precision mini-CMGs and their spacecraft applications. In *AAS Guidance and Control Advances in Astronautical Sciences*, number AAS 98-006, Breckenridge, Colorado, 1998.

[20] R. Byers, S. Vadali, and T. Pollock. Feedforward/feedback control law for near time optimal spacecraft reorientation. In *AAS/AIAA Astrodynamics Specialist Conference*, Durango, CO, 1991.

[21] R. M. Byers and S. R. Vadali. Quasi-closed-form solution to the time-optimal rigid spacecraft reorientation problem. *Journal of Guidance, Control and Dynamics*, 16(3):453–461, 1993.

[22] C. K. Carrington and J. L. Junkins. Nonlinear feedback control of spacecraft slew maneuvers. *Journal of Astronautical Sciences*, 32(1):29–45, 1984.

[23] C. Carroll, A. Hildebrand, D. Balam, and J. Matthews. NESS: Using a microsatellite to search for and track satellites and asteroids. In *6th ISU Annual International Symposium*, Strasbourg, May 2001.

[24] V. A. Chobotov. *Spacecraft Attitude Dynamics and Control.* Krieger Publishing Company, 1991.

[25] R. S. Chowdhry and E. M. Cliff. Optimal rigid body reorientation problem. In *Proceedings of AIAA Guidance, Navigation and Control Conference*, Portland, OR, 1990.

[26] R. S. Chowdhry, E. M. Cliff, and F. H. Lutze. On optimal rigid body motion. In *Proceedings of AIAA Guidance, Navigation and Control Conference*, pages 1560–1569, Boston, MA, 1989.

[27] W. B. Chubb, D. N. Schultz, and S. M. Seltzer. Attitude control and precision pointing of the apollo telescope mount. In *AIAA Guidance, Control and Flight Dynamics Conference*, 1967.

[28] B. K. Colburn and L. R. White. Computational considerations for a spacecraft attitude control system employing control moment gyro. *Journal of Spacecraft*, 14(1):40–53, 1977.

[29] T. R. Coon and J. E. Irby. Skylab attitude control system. *IBM Journal of Research Development*, pages 58–66, 1976.

[30] D. E. Cornick. Singularity avoidance control laws for single gimbal control moment gyros. In *Proceedings of AIAA Guidance and Control Conference*, pages 20–33, 1979.

[31] J. Crenshaw. 2-speed, a single-gimbal control moment gyro attitude control system. In *Proceedings of AIAA Guidance and Control Conference*, 1973.

[32] R. Cristi, J. Burl, and N. Russo. Adaptive quaternion feedback regulation for eigenaxis rotations. *Journal of Guidance, Control and Dynamics*, 17(6):1287–1291, 1994.

[33] A. Defendini and et al. Low cost CMG-based AOCS designs. In *Proceedings 4th ESA International Conference on Spacecraft Guidance, Navigation and Control Systems*, pages 393–398, Noordwijk, The Netherlands, October 1999.

[34] J. Dominguez and B. Wie. Computation and visualization of control moment gyroscope singularities. In *AIAA Guidance, Navigation and Control Conference*, Monterey, CA, August 2002.

[35] T. A. W. Dwyer. The control of angular momentum for asymmetric rigid bodies. *IEEE Transactions on Automatic Control*, 27(3):686–688, 1982.

[36] T. A. W. Dwyer. Exact nonlinear control of large angle rotational manoeuvre. *IEEE Transactions on Automatic Control*, 29(9):769–774, 1984.

[37] V. N. Branets et al. Development experience of the attitude control system using single-axis control moment gyros for long-term orbiting space stations. In *38th Congress of the Astronautical Federation*, 1987.

[38] J. R. Etter. A solution of the time optimal euler rotation problem. In *AIAA Guidance, Navigation and Control Conference*, Boston, MA, 1989.

[39] J. Fausz and D. Richie. Flywheel simultaneous attitude control and energy storage using VSCMGs. In *IEEE International Conference on Control Applications*, pages 991–995, Ancorage, AK, Sept. 2000.

[40] A. Fleming and I. M. Ross. Singularity-free optimal steering of control moment gyros. In *AAS/AIAA Astrodynamics Specialists Conference*, number AAS 05-419, Lake Tohoe, CA, August 2005.

[41] K. A. Ford. *Reorientation of flexible Spacecraft Using Momentum Exchange Devices*. Phd thesis, Air Force Institute of Technology, 1997.

[42] K. A. Ford and C. D. Hall. Singular direction avoidance steering for control moment gyros. *Journal of Guidance, Control and Dynamics*, 23(4):648–656, 2000.

[43] C. D. Hall. High-speed flywheels for integrated energy storage and attitude control. In *Proceedings of the American Conference*, pages 1894–1898, 1997.

[44] R. D. Hefner and C. H. McKenzie. A technique for maximizing the torque capability of control moment gyro systems. In *Proceedings of AAS/AIAA Astrodynamics Conference*, volume 2, pages 905–920, 1983.

[45] C. J. Heilberg. A practical approach to modeling single-gimbal control moment gyroscopes in agile spacecraft. In *Proceedings of the AIAA Guidance, Navigation, and Control Conference and Exhibit*, Denver, Colorado, 2000.

[46] C. J. Heilberg, D. Bailey, and B. Wie. Precision spacecraft pointing using single gimbal control moment gyros with disturbances. *Journal of Guidance, Control and Dynamics*, 23(1):77–85, 2000.

[47] B. R. Hoelscher and S. R. Vadali. Optimal open-loop and feedback control using single gimbal control moment gyroscopes. *Journal of Astronautical Sciences*, 42(2):189–206, 1994.

[48] P. C. Hughes. *Spacecraft Attitude Dynamics*. New York: Wiley Sons, 1986.

[49] R. Iwens. Quasi time-optimal spacecraft reorientation maneuvers using single gimbal control gyros. In *Proceedings of the 6th Asilomar Conference on Circuits and Systems*, pages 40–45, Asilomar, CA, Nov. 1972.

[50] A. D. Jacot and D. J. Liska. Control moment gyros in attitude control. *Journal of Spacecraft and Rockets*, 3(9):1313–1320, 1966.

[51] J. L. Junkins and Y. Kim. *Introduction to Dynamics and Control of Flexible Structures*. AIAA Education Series, 1993.

[52] J. L. Junkins and H. Schaub. *Analytical Mechanics of Aerospace Systems*. Texas, 2000.

[53] J. L. Junkins and J. D. Turner. Optimal spacecraft rotational maneuvers. *Elsevier*, 1986.

[54] J. J. Kalley and H. L. Mork. Development and air bearing test of a double gimbal momentum wheel attitude control system. In *Proceedings of AIAA 5th Communications Satellite Systems Conference*, 1974.

[55] T. R. Kane, P. W. Likins, and D. A. Levinson. *Spacecraft Dynamics*. McGraw-Hill Book Company, 1983.

[56] R. Kraft. CMG singularity avoidance in attitude control of a flexible spacecraft. In *Proceedings of American Control Conference*, pages 56–58, 1993.

[57] J. Kranton. Minimum-time attitude maneuvers with control moment gyroscopes. *AIAA Journal*, 8(8):1523–1525, 1970.

[58] H. Krishnan, N. H. McClamroch, and M. Reyhanoglu. Attitude stabilization of rigid spacecraft using two momentum wheel actuators. *Journal of Guidance, Control and Dynamics*, 18(2), 1995.

[59] S. Krishnan and S. R. Vadali. An inverse-free technique for attitude control of spacecraft using cmgs. *Acta Astronautica*, 39(6):431–438, 1996.

[60] H. Kurokawa. Geometrical view to steering of the pyramid type CMG system. In *Proceedings of 18th International Symposium on Space Technology and Science ISTS*, pages 1051–1057, 1992.

[61] H. Kurokawa. Exact singularity avoidance control of the pyramid type CMG system. In *AIAA Guidance, Navigation and Control Conference*, number AIAA-94-3559-CP, pages 170–180, Washington, 1994.

[62] H. Kurokawa. Constrained steering law of pyramid-type control moment gyros and ground tests. *Journal of Guidance, Control and Dynamics*, 20(3):445–449, 1997.

[63] H. Kurokawa. A geometric study of single gimbal control moment gyros- singularity problem and steering law. Technical Report 175, Mechanical Engineering Laboratory, Japan, June 1997.

[64] H. Kurokawa. Survey of theory and steering laws of single-gimbal control moment gyros. *Journal of Guidance, Control and Dynamics*, 30(5):1331–1340, 2007.

[65] H. Kurokawa and N. Yajima. A study of single gimbal CMG system. In *Proceedings of 15th International Symposium on Space Technology and Science ISTS*, pages 1219–1224, 1986.

[66] H. Kurokawa, N. Yajima, and S. Usui. A new steering law of a single gimbal CMG system of pyramid configuration. In *Proceedings of IFAC Automatic Control in Space*, 1985.

[67] V. Lappas and B. Wie. Robust CMG steering logic with gimbal angle constraints. In *AIAA/AAS Astrodynamics Specialist Conference and Exhibit*, number AIAA-2006-6651, Keystone, Colorado, August 2006.

[68] V. J. Lappas. *A Control Moment Gyro (CMG) Based Attitude Control System (ASC) for Agile Small Satellites*. PhD thesis, University of Surrey, 2002.

[69] V. J. Lappas and et al. Attitude control for small satellites using the control moment gyros. In *Proceedings of 52nd International Astronautical Federation Congress*, 2001.

[70] V. J. Lappas, W. H. Steyn, and C. Underwood. Design and testing of a control moment gyroscope cluster for small satellites. *Journal of Spacecraft and Rockets*, 41(6), 2004.

[71] V. J. Lappas, W. H. Steyn, and C. I. Underwood. Attitude control for small satellites using the control moment gyros. *Acta Astronautica*, 51:101–111, 2002.

[72] V.J. Lappas, S. Asghar, P.L. Palmer, and D. Fertin. Combined singularity avoidance for redundant control moment gyro clusters with accurate pointing constraints. In *AIAA Conf of Guidance, Navigation and Control*, number AIAA-2004-5131, Rhode Is, USA, August 2004.

[73] H. Lee, I. Lee, and H. Bang. Optimal steering laws for variable speed control moment gyros. In *AIAA Guidance, Navigation, and Control Conference and Exhibit*, San Francisco, California, August 2005.

[74] J. Lee, H. Bang, and H. Lee. Singularity avoidance by game theory for control moment gyros. In *AIAA Guidance, Navigation, and Control Conference and Exhibit*, San Francisco, California, August 2005.

[75] F. Li and P. M. Bainum. Minimum time attitude slewing maneuver of spacecraft. In *AIAA 26th Aerospace Sciences Meeting*, Reno, NV, 1988.

[76] F. Li and P. M. Bainum. Numerical approach for solving rigid spacecraft minimum time attitude maneuvers. *Journal of Guidance, Control and Dynamics*, 13(1):38–45, 1990.

[77] K. Lian, L. Wang, and L. Fu. Controllability of spacecraft systems in a central gravitational field. In *Proceedings of the 32nd conference on decision and control*, pages 3105–3110, San Antonio, Texas, December 1993.

[78] K. Lim and D. Moerder. A feasibility study on the control of a generic air vehicle using CMG. In *AIAA Guidance, Navigation, and Control Conference and Exhibit*, Keystone, Colorado, August 2006.

[79] S. P. Linden. Precision CMG control for high accuracy pointing. In *Proceedings of AIAA Guidance and Control Conference*, number 73-871, 1973.

[80] D. J. Liska. A two-degree-of-freedom control moment gyro for high accuracy attitude control. *Journal of Spacecraft*, pages 75–83, 1968.

[81] T. C. Liu and et al. Optimal control of a variable spin speed CMG system for space vehicle. In *Proceedings of IEEE Conference on Decision and Control*, pages 722–726, 1973.

[82] J. Longuski. Solution of euler equations of motion and eulerian angles for near symmetric rigid bodies subject to constant moments. In *Proceedings of AIAA/AAS Astrodynamics Conference*, Danvers, MA, 1980.

[83] G. Margulies and J. N. Aubrun. Geometric theory of single gimbal control moment gyro systems. *Journal of Astronautical Sciences*, 26(2):159–191, 1978.

[84] M. Meffe and G. Stocking. Momentum envelope topology of single-gimbal CMG arrays for space vehicle control. In *10th Annual AAS Guidance and Control Conference*, number ASS 87-002, Keystone, Colorado, 1987.

[85] Y. Nakamura and H. Hanafusa. Inverse kinematics solutions with singularity robustness for robot manipulator control. *Journal of Dynamic Systems, Measurement and Control*, 108:163–171, 1986.

[86] H. Nijmeijer and A. J. Van der Shaft. *Spacecraft Dynamics*. McGraw-Hill Book Company, 1983.

[87] B. J. Oconnor and L. A. Morine. A description of the CMG and its application to space vehicle control. *Journal of Spacecraft and Rockets*, 6(3):225–231, 1969.

[88] H. S. Oh and S. R. Vadali. Feedback control and steering laws for spacecraft using single gimbal control moment gyros. *Journal of Astronautical Sciences*, 39(2):183–203, 1991.

[89] J. A. Paradiso. A highly adaptable steering/selection procedure for combined CMG/RCS spacecraft control. In *AAS Guidance and Control Conference*, volume 61, Keystone, CO, Feb 1986.

[90] J. A. Paradiso. Global steering of single gimballed control moment gyroscopes using a direct search. *Journal of Guidance, Control and Dynamics*, 15(5):1236–1244, 1992.

[91] A. N. Pechev. Feedback-based steering law for control moment gyros. *Journal of Guidance, Control and Dynamics*, 30(3):848–855, 2007.

[92] D. J. Richie, V. J. Lappas, and P. L. Palmer. Sizing/optimization of a small satellite energy storage and attitude control system. *Journal of Spacecraft and Rockets*, 44(4):940–952, 2007.

[93] D. J. Richie, P. Tsiotras, and J. L. Fausz. Simultaneous attitude control and energy storage using VSCMGs: Theory and simulation. In *Proceedings of the American Control Conference*, pages 3973–3979, 2001.

[94] R. M. Rokui and S. Kalaycioglu. Control moment gyro (CMG) based spacecraft attitude control using feedback linearization control technique. In *Proceedings of the AAS Rocky Mountain Conference*, 1997.

[95] X. Roser and M. Sghedoni. Control moment gyroscopes (CMGs) and their application in future scientific missions. In *Proceedings of 3rd International Conference on Spacecraft Guidance, Navigation and Control Systems*, pages 523–528, 1997.

[96] S. C. Rybak and et al. Achieving ultrahigh accuracy with a body pointing CMG/RW control system. In *Proceedings of AIAA Guidance and Control Conference*, 1973.

[97] C. Salenc and X. Roser. AOCS for agile scientific spacecraft with mini-CMG's. In *Proceedings of 4th ESA International Conference on Spacecraft Guidance, Navigation and Control systems*, pages 379–384, Noordwijk, The Netherland, October 1999.

[98] H. Schaub. *Novel coordinates for nonlinear multi-body motion with applications to spacecraft dynamics and control.* Phd thesis, Texas AM University, 1998.

[99] H. Schaub and J. L. Junkins. Stereographic orientation parameters for attitude dynamics: A generalization of rodrigues parameters. *Journal of Astronautical Sciences*, 44(1):1–19, 1996.

[100] H. Schaub and J. L. Junkins. CMG singularity avoidance using VSCMG null motion. In *Proceedings of the AIAA Guidance, Navigation and Control Conference*, Boston, MA, 1998.

[101] H. Schaub and J.L. Junkins. Singularity avoidance using null motion and variable-speed control moment gyros. *Journal of Guidance, Control and Dynamics*, 23(1):11–16, 2000.

[102] H. Schaub, S. R. Vadali, and J. L. Junkins. Feedback control law for variable speed control moment gyros. *Journal of Astronautical Sciences*, 46(3):307–328, 1998.

[103] S. L. Scrivener and R. C. Thompson. Survey of time-optimal attitude maneuvers. *Journal of Guidance, Control and Dynamics*, 17(2):225–233, 1994.

[104] S. M. Seltzer. Large space telescope oscillations induced by CMG friction. *Journal of Spacecraft*, 12(2):96–105, 1975.

[105] M. D. Shuster. A survey of attitude representations. *Journal of Astronautical Sciences*, 41(4):439–517, 1993.

[106] M. J. Sidi. *Spacecraft Dynamics and Control: A Practical Engineering Approach*. Cambridge University Press, 1996.

[107] S. N. Singh and T. C. Bossart. Exact feedback linearization and control of space station using CMG. *IEEE Transactions on Automatic Control*, 38(1):184–87, 93.

[108] S. B. Skaar and L. G. Kraige. Large-angle spacecraft attitude maneuvers using an optimal reaction wheel power criterion. *Journal of Astronautical Sciences*, 32(1):47–61, 1984.

[109] C. E. Skelton and C. D. Hall. Mixed control moment gyro and momentum wheel attitude control strategies. In *Proceedings of AAS Conference*, number AAS 03-558, 2003.

[110] J-J. E. Slotine and W Li. *Applied Nonlinear Control*. Prentice Hall, Englewood Cliffs, New Jersey 07632, 1991.

[111] A. Suzuki, H. Kurokawa, and S. Kokaji. Robust attitude control using a CMG system and an experiment with simulation platform. In *Proceedings of 12th IFAC Automatic Control in Aerospace*, pages 197–202, 1992.

[112] A. Suzuki, H. Kurokawa, and S. Kokaji. Three axis control of an experimental platform using cmgs. In *Proceedings of 18th International Symposium on Space Technology and Science (ISTS)*, pages 1059–1066, 1992.

[113] B. Thornton, T. Ura, Y. Nose, and S. Turnock. Zero-G class underwater robots: Unrestricted attitude control using control moment gyros. *IEEE Journal of Oceanic Engineering*, 32(3):565–583, 2007.

[114] E. N. Tokar. Efficient design of powered gyro-stabilizer systems. *Cosmic Research*, pages 16–23, 1978.

[115] E. N. Tokar. Problems of gyroscopic stabilizer control. *Cosmic Research*, pages 141–147, 1978.

[116] E. N. Tokar and V. N. Platonov. Singular surfaces in unsupported gyrodyne systems. *Cosmic Research*, pages 675–685, 1979.

[117] P. Tsiotras. Stabilization and optimality results for the attitude control problem. *Journal of Guidance, Control and Dynamics*, 19(4):772–779, 1996.

[118] P. Tsiotras, H. Shen, and C. Hall. Satellite attitude control and power tracking with energy/momentum wheels. *Journal of Guidance, Control and Dynamics*, 24(1):23–34, 2002.

[119] S. R. Vadali. On the euler parameter constraint. *Journal of Astronautical Sciences*, 36(3):259–265, 1988.

[120] S. R. Vadali, M. T. Carter, T. Singh, and N. S. Abhyankar. Near-minimum-time maneuvers of large structure: Theory and experiments. *Journal of Guidance, Control and Dynamics*, 18(6):1380–1385, 1995.

[121] S. R. Vadali, L. G. Kraige, and J. L. Junkins. New results on the optimal spacecraft attitude manoeuvre problem. *Journal of Guidance, Control and Dynamics*, 7(3):378–380, 1984.

[122] S. R. Vadali and Junkins J. L. Spacecraft large angle rotational manoeuvres with optimal momentum transfer. *Journal of Astronautical Sciences*, 31(2):217–235, 1983.

[123] S. R. Vadali and Junkins J. L. Optimal open-loop and stable feedback control of rigid spacecraft attitude maneuvers. *Journal of Astronautical Sciences*, 32(2):105–122, 1984.

[124] S. R. Vadali, H. S. Oh, and S. R. Walker. Preferred gimbal angles for single gimbal control moment gyroscopes. *Journal of Guidance, Control and Dynamics*, 13(6):1090–1095, 1990.

[125] S. R. Valadi and S. Krishnan. Suboptimal command generation for control moment gyroscopes and feedback control of spacecraft. *Journal of Guidance, Control and Dynamics*, 18(6):1350–1354, 1995.

[126] R. Varatharajoo and S. Fasoulas. Methodology for the development of combined energy and attitude control systems for satellites. *Aerospace Science and Technology*, 6:303–311, 2002.

[127] J. R. Wertz. *Spacecraft Attitude Determination and Control*. Reidal Publishing Company, Dordrecht, Holland, 1978.

[128] B. Wie. *Space Vehicle Dynamics and Control*. AIAA Education series, Reston, VA, 1998.

[129] B. Wie. New singularity escape and avoidance steering logic for control moment gyro systems. In *Proceedings the AIAA Guidance, Navigation and Control Conference*, number 2003-5659, Austin, TX, August 2003.

[130] B. Wie. Singularity analysis and visualization for single-gimbal control moment gyro systems. In *AIAA Guidance, Navigation and Control Conference*, number 2003-5658, Austin, TX, August 2003.

[131] B. Wie, D. Bailey, and C. Heiberg. Rapid multitarget acquisition and pointing control of agile spacecraft. *Journal of Guidance, Control and Dynamics*, 25(1):96–104, 2002.

[132] B. Wie and P. M. Barba. Quaternion feedback for spacecraft large angle maneuvers. *Journal of Guidance, Control and Dynamics*, 8(3):360–365, 1985.

[133] B. Wie and P. M. Barba. Singularity analysis and visualization for single-gimbal control moment gyro systems. *Journal of Guidance, Control and Dynamics*, 27(2):271–282, 2004.

[134] B. Wie, C. J. Heilberg, and D. Bailey. Singularity robust steering logic for redundant single-gimbal control moment gyros. *Journal of Guidance, Control and Dynamics*, 24(5):865–872, 2001.

[135] B. Wie and J. Lu. Feedback control logic for spacecraft eigenaxis rotations under slew rate and control constraints. *Journal of Guidance, Control and Dynamics*, 18(6):1372–1379, 1995.

[136] B. Wie, H. Weiss, and A. Arapostathis. Quaternion feedback regulator for spacecraft eigenaxis rotations. *Journal of Guidance, Control and Dynamics*, 12(3):375–380, 1989.

[137] Z. Wu and W. Chou. Avoidability of singular states in redundant single gimbal control moment gyroscope systems. In *AIAA Guidance, Navigation and Control Conference*, Denver, Colorado, August 2000.

[138] Z. Wu and H. Wu. Existence of nonlinear steering in redundant single gimbal control moment gyroscope systems. In *AIAA Guidance, Navigation and Control Conference*, August 1998.

[139] H. Yoon and P. Tsiotras. Spacecraft adaptive attitude and power tracking with variable speed control moment gyroscopes. *Journal of Guidance, Control, and Dynamics*, 25(6):1081–1090, 2002.

[140] H. Yoon and P. Tsiotras. Singularity analysis of variable-speed control moment gyros. *Journal of Guidance, Control, and Dynamics*, 27(3):374–386, 2004.

[141] T. Yoshikawa. Steering law for roof type configuration control moment gyro system. *Automatica*, 13:359–368, 1979.